

**Synthesis and Testing of Inhibitors for
JumonjiC Domain-Containing Histone Demethylases**



Inauguraldissertation

zur Erlangung des akademischen Grades eines

Doctor rerum naturalium (Dr. rer. nat.)

der Fakultät für Chemie und Pharmazie

der Albert-Ludwigs-Universität Freiburg

vorgelegt von

Sandra Wenzler

geboren in Villingen-Schwenningen, Deutschland

2020

Eidesstattliche Versicherung

gemäß §7 Absatz 1 Satz 3 Nr. 8 der Promotionsordnung der Albert-Ludwigs-Universität für die Fakultät für Chemie und Pharmazie.

1. Bei der eingereichten Dissertation zu dem Thema
„Synthesis and Testing of Inhibitors for JumonjiC Domain-Containing Histone Demethylases“
handelt es sich um meine eigenständig erbrachte Leistung.
2. Ich habe nur die angegebenen Quellen und Hilfsmittel benutzt und mich keiner unzulässigen Hilfe Dritter bedient. Insbesondere habe ich wörtlich oder sinngemäß aus anderen Werken übernommene Inhalte als solche kenntlich gemacht.
3. Die Dissertation oder Teile davon habe ich bislang nicht an einer Hochschule des In- oder Auslands als Bestandteil einer Prüfungs- oder Qualifikationsleistung vorgelegt.
4. Die Richtigkeit der vorstehenden Erklärungen bestätige ich.
5. Die Bedeutung der eidesstattlichen Versicherung und die strafrechtlichen Folgen einer unrichtigen oder unvollständigen eidesstattlichen Versicherung sind mir bekannt.

Ich versichere an Eides statt, dass ich nach bestem Wissen die reine Wahrheit erklärt und nichts verschwiegen habe.

Freiburg, 02.02.2021

Ort und Datum



Unterschrift

Dekan der Fakultät: Prof. Dr. Oliver Einsle

Vorsitzender des Promotionsausschusses: Prof. Dr. Stefan Weber

Referent: Prof. Dr. Manfred Jung

Korreferent: Prof. Dr. Henning Jessen

Datum der mündlichen Prüfung: 02.02.2021

The experimental parts of this research project as well as the production of the present thesis were undertaken between February 2016 and November 2020 in the group of Prof. Dr. Manfred Jung at the Institute of Pharmaceutical Sciences, Albert-Ludwigs-University Freiburg.

Zusammenfassung

JumonjiC Domänen-enhaltende Histon-Demethylasen (JmjC-KDMs) sind epigenetische Enzyme, welche Methylgruppen von Histon- und Nicht-Histonproteinen in einem Eisen(II)- und 2-Oxoglutarat-abhängigen Mechanismus oxidativ entfernen können. Ihre Beteiligung an einer Vielzahl von Erkrankungen, insbesondere Krebs, wurde in zahlreichen Studien gezeigt.

Diverse auf bekannten Inhibitoren basierende Verbindungen wurden synthetisiert oder von Kollaborationspartnern bezogen und in dieser Arbeit bewertet. Die biochemische Testung erfolgte in zwei orthogonalen Assays. Diese Arbeitsweise ermöglichte die iterative Optimierung synthetisierter Verbindungen basierend auf Aktivitätsmessungen. Hierzu wurden zwei wesentliche Strategien angewendet, nämlich die Erzeugung von Bioisosteren publizierter Inhibitoren und die Synthese von Analoga des klinisch zugelassenen Eisenchelators Deferasirox. Der erste Ansatz lieferte zwei Grundgerüste mit IC₅₀-Werten im unteren mikromolaren Bereich, die jeweils Tetrazole als bioisosteren Ersatz für Carbonsäuren enthalten. Der zweite Ansatz resultierte in fünf verschiedenen zentralen Motiven – Triazolen, Thiazolen, Oxazolen, Pyrazolen und Imidazolen. Für zahlreiche Verbindungen wurde eine inhibitorische Potenz im einstellig mikromolaren Bereich erhalten und Struktur-Aktivitätsbeziehungen wurden aufgeklärt. Für eine Thiazol-Verbindung wurde eine schwache Selektivität für KDM4A gegenüber KDM5A und KDM6B erreicht. Mit einer ösophagealen Krebszelllinie wurden die zelluläre Aktivität und Zielstruktur-spezifische Effekte anhand von Immunfluoreszenz-Messungen für ausgewählte Verbindungen nachgewiesen. Die Synthese zweier Fluoreszenz-markierter und eines Biotin-markierten Derivates sowie deren hohe Aktivität gegenüber KDM4A liefern einen Startpunkt für weitere *In vitro*- und möglicherweise auch *In vivo*-Studien. Die neu entdeckten Inhibitoren, insbesondere die Deferasirox-basierten Verbindungen, können als wertvolle Werkzeuge zur Untersuchung der physiologischen und pathophysiologischen Funktionen von KDMs dienen und können eingesetzt werden um das therapeutische Potential dieser Enzymklasse näher zu charakterisieren.

Summary

JumonjiC domain-containing histone demethylases (JmjC-KDMs) are epigenetic enzymes capable of oxidatively removing methyl marks from histone and non-histone proteins in an iron(II)- and 2-oxoglutarate-dependent mechanism. Their involvement in various diseases, particularly cancer, has been shown in numerous studies.

Diverse compounds based on known KDM inhibitors were synthesized or acquired from collaboration partners and evaluated in this work. Biochemical testing was performed using two orthogonal KDM4A assays. This workflow allowed iterative compound optimization based on activity measurements. Two main strategies were employed in the inhibitor development, namely the generation of bioisosteres of published inhibitors and the synthesis of analogs of the clinically approved iron-chelator deferasirox. The first approach yielded two scaffolds with IC₅₀ values in the micromolar range, which both contain tetrazoles as bioisosteric replacement for carboxylic acids. The second approach resulted in five different core structures – triazoles, thiazoles, oxazoles, pyrazoles and imidazoles. An inhibitor potency in the single-digit micromolar range could be achieved for numerous compounds and distinctive structure activity relationships were uncovered. Weak selectivity for KDM4A over KDM5A and KDM6B was accomplished for a thiazole compound. Antiproliferative cellular activity on an oesophageal cancer cell line was shown and on-target effects on KDM4 were revealed using immunofluorescence measurements for selected compounds. The synthesis of two fluorescently and one biotin-labelled derivative and their high activity towards KDM4A provide a starting point for further *in vitro* and possibly also *in vivo* studies. The newly discovered inhibitors, particularly the deferasirox-based compounds, may serve as valuable tool compounds for the study of the physiological and pathophysiological roles of KDMs and may be used for the investigation of the therapeutic potential of this enzyme class.

Acknowledgements

I would like to express my gratitude to all the people who have enabled me to undertake this fascinating research project and who have enriched our time together. First and foremost, I want to thank my supervisor Prof. Dr. Manfred Jung for the opportunity to work in his group and for the constant support, inspiration and motivation during these years. I would also like to acknowledge my co-supervisor Prof. Dr. Henning Jessen for his time and dedication and the inspiring discussions of this project.

I am also very grateful to Dr. Nicolas P. F. Barthes for joining me in some projects, his useful advice as well as his enthusiasm and commitment to our collaboration and without whom this project would not have advanced so far. I would like to thank all present and former members of the Jung group for the great and helpful working atmosphere, their enthusiasm and their ceaseless support: Dr. Johannes Bacher, Arianna Colcerasa, Emina Cokljat, Viktor Hazai, Dr. Mirjam Hau, Dr. Alexander Hauser, Dr. Daniel Herp, Dr. Eva-Maria Herrlinger, Dr. Inga Hoffmann, Sebastian Klein, Andreas Kürner, Dr. Ludovica Morera, Dr. Martin Roatsch, Dr. Matthias Schiedel, Michael Schmidt, Karin Schmidtkunz, Dr. Johannes Schulz-Fincke, Ludwig Seifert, Johannes Seitz, Dr. Johanna Senger, Dr. Roman Simon, Maximilian Staudt, Dr. Sören Swyter, Pavlos Tzortzoglou, Anja Vogelmann, Dr. Tobias Wagner, Nathalie Woessner and Sarah Zähringer, Ph. D. Special thanks goes to Dr. Eva-Maria Herrlinger for being such an amazing supportive lab partner and to all members who proofread parts of my thesis. I am also thankful to all intern students who chose to join the Jung group and who contributed to this project: Elena Hättig, Philipp Mußler and Stephanie Schmidt.

My gratitude goes to all the members of the Department of Pharmaceutical and Medicinal Chemistry, in particular to Sascha Ferlaine for the recording of NMR-Spectra, as well as to Anne Behrens, Dr. David Conradt, Dr. Silke Foegen, Desirée Popadic, Dr. Matthias Schiedel and Marita Wagner for the pleasant time

supervising the “Arzneibuch-Praktikum”. I would also like to thank Christoph Warth from the Department of Chemistry for the recording of mass spectra.

I am thankful to the group of Prof. Dr. Wolfgang Sippl (MLU Halle-Wittenberg) and in particular Dr. Dina Robaa for their contributions in molecular docking and virtual screening, which have added valuable contributions to this project.

I would like to thank the team of Prof. Dr. Roland Schüle (University Medical Center Freiburg) for kindly providing the enzyme KDM4A required for *in vitro* experiments. I would like to extend my thanks to all collaborators who have contributed to this project either by synthesis of compounds or by conducting additional experiments, which were valuable to the advancement of the research project discussed in this thesis. This includes Dr. Georg Fassauer (Link group, EMAU Greifswald), Vivien Ngo (Hein group, Albert-Ludwigs-Universität Freiburg), Dr. Stefan Müller (Engelhardt group, Universitätsklinikum Freiburg) and Dr. Nenad Filipović (Department of Chemistry and Biochemistry, University of Belgrade).

Lastly, I would like to thank my family for their constant support and encouragement.

Contents

Zusammenfassung	v
Summary	vii
List of Figures	xv
List of Schemes	xvii
List of Tables	xviii
1 Introduction	1
1.1 Epigenetics	1
1.1.1 DNA Modifications	2
1.1.2 Histone Modifications	3
1.1.3 Epigenetics in Disease and Therapy	6
1.2 Histone Demethylases	7
1.2.1 FAD-dependent Lysine-specific Demethylases	7
1.2.2 JmjC Domain-containing Histone Demethylases	9
1.3 Assays for JmjC Domain-containing Histone Demethylases	21
1.3.1 Formaldehyde Dehydrogenase Assay	22
1.3.2 Other Assays based on Formaldehyde Quantification	24
1.3.3 Antibody-based Assays	25
1.3.4 Mass spectrometry-based Assays	29
1.3.5 Assays based on Radiometric Detection	30
1.3.6 Affinity-based Assays	30
1.4 Inhibitors	34
1.4.1 Concept of Prodrugs and Bioisosteres	35
1.4.2 Co-Substrate Analogs/Iron-binding Inhibitors	36
1.4.3 Diverse Small Molecule Inhibitors	50
1.4.4 Covalent Inhibitors	55
1.4.5 Peptidic Inhibitors	56
1.4.6 Zinc ejecting Inhibitors	57
1.4.7 Discussion	58
2 Aim of the Project	60
3 Assays	62
3.1 Activity Assays used in this Work	62
3.1.1 FDH-coupled Assay	62
3.1.2 LANCEUltra® assay	64

4 Development of novel Inhibitors for JmjC-containing histone demethylases	67
4.1 Lysine Mimics	67
4.2 Carboxylic Acid Bioisosteres based on known Inhibitors	69
4.2.1 Sulfoxides, Sulfones	69
4.2.2 Boronic acids	74
4.2.3 Tetrazoles.....	77
4.2.4 Tetrazolylhydrazides	84
4.2.5 Summary and Discussion	86
4.3 Deferasirox Derivatives	87
4.3.1 1,2,4-Triazoles	88
4.3.2 Thiazoles and Oxazoles	110
4.3.3 Pyrazoles and Imidazoles	127
4.3.4 Selectivity against other Jmj-KDMs.....	135
4.3.5 Cellular Activity	137
4.3.6 Summary and Discussion	142
4.4 2-Hydrazonylthiazoles and Selenazoles	143
4.4.1 Biochemical Activity	144
5 Conclusion and Outlook	147
6 Experimental	149
6.1 Biochemical Assays	149
6.1.1 General Remarks	149
6.1.1.1 Reagents and Chemicals	149
6.1.2 Peptides and Antibodies	151
6.1.3 Buffers	152
6.1.4 Enzymes.....	152
6.1.5 Equipment and Software	153
6.1.6 FDH-Coupled Enzyme Activity Assay	154
6.1.7 LANCEUltra® Assay	157
6.1.8 Fluorescence Polarization assay	160
6.2 Synthesis	163
6.2.1 General Remarks	163
6.2.2 Compound Purification.....	163
6.2.3 Nuclear Magnetic Resonance-Spectrometry	164
6.2.4 Mass Spectrometry	165
6.2.5 Analytical High-performance Liquid Chromatography	165
6.2.6 General Procedures	166

6.2.7 Sulfones and Sulfoxides	168
2-(Methylsulfonyl)isonicotinic acid (69a)	168
Methyl 2-(methylthio)isonicotinate (71a)	169
Methyl 2-(methylsulfinyl)isonicotinate (74a)	170
2-(Methylsulfinyl)isonicotinic acid (68a)	171
Methyl 2-(benzylthio)-6-chloroisonicotinate (71b)	172
Methyl 2-(benzylsulfinyl)-6-chloroisonicotinate (74a)	173
2-(Benzylthio)-6-chloroisonicotinic acid (68b)	173
Methyl 2-(benzylsulfonyl)-6-chloroisonicotinate (75)	174
2-(Benzylsulfonyl)-6-chloroisonicotinic acid (68b)	175
6.2.8 Boronic acids	176
5-Bromo-8-((tert-butyldimethylsilyl)oxy)quinoline (78)	176
8-((Tert-butyldimethylsilyl)oxy)-5-(4,4,5,5-tetramethyl-1,3,2-dioxaborolan-2-yl)quinoline (79)	177
(8-Hydroxyquinolin-5-yl)boronic acid (80)	178
6.2.9 Triazoles	179
2-(2-Hydroxyphenyl)-4 <i>H</i> -benzo[e][1,3]oxazin-4-one (88a)	179
6-Chloro-2-(5-chloro-2-hydroxyphenyl)-4 <i>H</i> -benzo[e][1,3]oxazin-4-one (88b)	180
2-(2-Hydroxy-5-methoxyphenyl)-6-methoxy-4 <i>H</i> -benzo[e][1,3]oxazin-4-one (88c)	181
6-Bromo-2-(5-bromo-2-hydroxyphenyl)-4 <i>H</i> -benzo[e][1,3]oxazin-4-one (88d)	182
5-Fluoro- <i>N</i> -(5-fluoro-2-hydroxybenzoyl)-2-hydroxybenzamide (88e)	182
4-(3,5-Bis(2-hydroxy-5-methoxyphenyl)-1 <i>H</i> -1,2,4-triazol-1-yl)benzoic acid (90c)	183
2,2'-(1-Phenyl-1 <i>H</i> -1,2,4-triazole-3,5-diyl)bis(4-methoxyphenol) (90h)	184
3,5-Bis(5-bromo-2-methoxyphenyl)-1-phenyl-1 <i>H</i> -1,2,4-triazole (91)	185
4-Benzyl-2-(3-(5-benzyl-2-methoxyphenyl)-1-phenyl-1 <i>H</i> -1,2,4-triazol-5-yl)phenol (93)	186
4-(3,5-Bis(2-hydroxyphenyl)-1 <i>H</i> -1,2,4-triazol-1-yl)- <i>N</i> -(prop-2-yn-1-yl)benzamide (94a)	187
4-(3,5-Bis(2-hydroxy-5-methoxyphenyl)-1 <i>H</i> -1,2,4-triazol-1-yl)- <i>N</i> -(prop-2-yn-1-yl)benzamide (94b)	188
4-(3,5-Bis(2-hydroxyphenyl)-1 <i>H</i> -1,2,4-triazol-1-yl)benzoic acid (Deferasirox 54)	190
4-(3,5-Bis(5-fluoro-2-hydroxyphenyl)-1 <i>H</i> -1,2,4-triazol-1-yl)benzoic acid (90e)	191

4-(3,5-Bis(5-bromo-2-hydroxyphenyl)-1 <i>H</i> -1,2,4-triazol-1-yl)benzoic acid (90d).....	192
2,2'-(1-Phenyl-1 <i>H</i> -1,2,4-triazole-3,5-diyl)bis(4-chlorophenol) (90b)....	193
2,2'-(1-Phenyl-1 <i>H</i> -1,2,4-triazole-3,5-diyl)bis(4-bromophenol) (90f)	193
2,2'-(1-Phenyl-1 <i>H</i> -1,2,4-triazole-3,5-diyl)bis(4-benzylphenol) (90n) ...	194
2,2'-(1-Phenyl-1 <i>H</i> -1,2,4-triazole-3,5-diyl)bis(benzene-1,4-diol) (90m)	195
4-(3,5-Bis(2-hydroxyphenyl)-1 <i>H</i> -1,2,4-triazol-1-yl)benzonitrile (90g)	196
2,2'-(1-(2-Methoxyphenyl)-1 <i>H</i> -1,2,4-triazole-3,5-diyl)diphenol (90i)..	197
2,2',2''-(1 <i>H</i> -1,2,4-Triazole-1,3,5-triyl)triphenol (90l).....	198
2,2'-(1-(Pyridin-2-yl)-1 <i>H</i> -1,2,4-triazole-3,5-diyl)diphenol (90j).....	199
2,2'-(1-(Quinolin-8-yl)-1 <i>H</i> -1,2,4-triazole-3,5-diyl)diphenol (90k)	200
<i>N</i> -(3-(4-((4-(3,5-Bis(2-hydroxyphenyl)-1 <i>H</i> -1,2,4-triazol-1-yl)benzamido)methyl)-1 <i>H</i> -1,2,3-triazol-1-yl)propyl)-3',6'- dihydroxy-3-oxo-3 <i>H</i> -spiro[isobenzofuran-1,9'-xanthene]-5- carboxamide (96a)	201
<i>N</i> -(6-(4-((4-(3,5-Bis(2-hydroxyphenyl)-1 <i>H</i> -1,2,4-triazol-1-yl)benzamido)methyl)-1 <i>H</i> -1,2,3-triazol-1-yl)hexyl)-3',6'- bis(dimethylamino)-3-oxo-3 <i>H</i> -spiro[isobenzofuran-1,9'-xanthene]- 5-carboxamide (96b)	202
4-(3,5-Bis(2-hydroxyphenyl)-1 <i>H</i> -1,2,4-triazol-1-yl)- <i>N</i> -((1-(37-oxo-41-(2- oxohexahydro-1 <i>H</i> -thieno[3,4- <i>d</i>]imidazol-4-yl)- 3,6,9,12,15,18,21,24,27,30,33-undecaoxa-36-azahentetracontyl)-1 <i>H</i> - 1,2,3-triazol-4-yl)methyl)benzamide (96c).....	204
6.2.10 Thiazoles.....	205
Thiophene-2-carbothioamide (98a)	205
<i>N</i> ,2-Dimethoxy- <i>N</i> -methylbenzamide (104a)	206
<i>N</i> -Methoxy- <i>N</i> ,2-dimethylbenzamide (106b)	207
<i>p</i> -Tolyl 2-phenylacetate (102).....	208
1-(2-Hydroxy-5-methylphenyl)-2-phenylethan-1-one (101a).....	209
1-(2-((<i>Tert</i> -butyldimethylsilyl)oxy)-5-methylphenyl)-2-phenylethan-1-one (101b).....	210
1-(2-Methoxyphenyl)-2-phenylethan-1-one (101c)	211
2-Phenyl-1-(<i>o</i> -tolyl)ethan-1-one (101d).....	211
2-Bromo-1-(5-bromo-2-hydroxyphenyl)-2-phenylethan-1-one (97d) .	212
2-Bromo-1-(2-((<i>tert</i> -butyldimethylsilyl)oxy)-5-methylphenyl)-2- phenylethan-1-one (97a).....	213
2-Bromo-1-(2-methoxyphenyl)-2-phenylethan-1-one (97b)	214
2-Bromo-2-phenyl-1-(<i>o</i> -tolyl)ethan-1-one (97c).....	215

2-Bromo-2-phenyl-1-(thiophen-2-yl)ethan-1-one (97e)	216
6.3 Protected thiazoles	217
2,4-Bis(2-methoxyphenyl)thiazole (107a)	217
2,4-Bis(2-methoxyphenyl)-5-phenylthiazole (107e)	218
4-Bromo-2-(2-(2-methoxyphenyl)-5-phenylthiazol-4-yl)phenol (107c)	219
4-(2-((<i>Tert</i> -butyldimethylsilyl)oxy)-5-methylphenyl)-2-(1 <i>H</i> -imidazol-4-yl)- 5-phenylthiazole (107b)	220
6.3.1 2-(2-methoxyphenyl)-5-phenyl-4-(thiophen-2-yl)thiazole (107d)	221
2,2'-(Thiazole-2,4-diyl)diphenol (99c)	221
2,2'-(5-Phenylthiazole-2,4-diyl)diphenol (99b)	222
4-Bromo-2-(2-(2-hydroxyphenyl)-5-phenylthiazol-4-yl)phenol (99a)	223
2-(2-(2-Hydroxyphenyl)-5-phenylthiazol-4-yl)-4-methylphenol (99g)	224
4-Methyl-2-(5-phenyl-2-(pyridin-2-yl)thiazol-4-yl)phenol (99d)	225
4-Methyl-2-(5-phenyl-2-(thiophen-2-yl)thiazol-4-yl)phenol (99f)	226
4-Methyl-2-(5-phenyl-2-(pyrazin-2-yl)thiazol-4-yl)phenol (99k)	227
2-(2-(1 <i>H</i> -Imidazol-4-yl)-5-phenylthiazol-4-yl)-4-methylphenol (99e)	227
4-Methyl-2-(5-phenyl-[2,2'-bithiazol]-4-yl)phenol (99l)	228
2-(5-Phenyl-4-(thiophen-2-yl)thiazol-2-yl)phenol (99h)	229
4-Methyl-2-(5-phenyl-2-(<i>o</i> -tolyl)thiazol-4-yl)phenol (99j)	230
2-(5-Phenyl-4-(<i>o</i> -tolyl)thiazol-2-yl)phenol (99i)	231
6.3.2 Oxazoles	232
2-(4-(2-Methoxyphenyl)oxazol-2-yl)phenol (108c)	232
4-(2-Methoxyphenyl)-2-(thiophen-2-yl)oxazole (108a)	233
2-(4-(2-Methoxyphenyl)-5-phenyloxazol-2-yl)phenol (108b)	234
2,2'-(Oxazole-2,4-diyl)diphenol (109c)	234
2-(2-(Thiophen-2-yl)oxazol-4-yl)phenol (109a)	235
2,2'-(5-Phenyloxazole-2,4-diyl)diphenol (109b)	236
2-(5-Phenyl-4-(thiophen-2-yl)oxazol-2-yl)phenol (109d)	237
References	239
Appendix	261
A. Abbreviations	261
B. List of Compound Synonyms	265
C. List of Publications	268

List of Figures

<i>Figure 1</i>	Cytosine modifications present in DNA.....	2
<i>Figure 2</i>	Schematic representation of the higher order of DNA.....	4
<i>Figure 3</i>	Approved drugs targeting epigenetic enzymes.	6
<i>Figure 4</i>	A) Crystal structure of the histone demethylase LSD1. B) Demethylation reaction catalysed by LSD1 using the cofactor FAD.	8
<i>Figure 5</i>	Left: Crystal structure of the catalytic JmjC domain of KDM4A. Right: Zoom-in on the metal binding-site.	10
<i>Figure 6</i>	Domain architecture of selected histone demethylases.....	12
<i>Figure 7</i>	Catalytic mechanism of the demethylation of methylated lysine residues by Jmj-KDMs.....	14
<i>Figure 8</i>	Schematic principle of the formaldehyde dehydrogenase-based assay (FDH assay).	23
<i>Figure 9</i>	Detection reactions of chemical formaldehyde-based assays.....	24
<i>Figure 10</i>	Schematic representation of the AlphaLISA™ principle.	26
<i>Figure 11</i>	Schematic representation of the LANCEUltra® assay.	27
<i>Figure 12</i>	Schematic representation of the assay principle of competitive fluorescence polarization assays.	31
<i>Figure 13</i>	Chemical structures of the KDM inhibitor prodrug methylstat and the derived fluorescent probe.....	32
<i>Figure 14</i>	Chemical structure of the co-substrate 2-OG (8) and its analogs....	38
<i>Figure 15</i>	Chemical structures of 2,4-PDCA (22) and its analogs.....	40
<i>Figure 16</i>	Chemical structures of 2,2'-biheterocyclic inhibitors.....	42
<i>Figure 17</i>	Chemical structures of catechol-based inhibitors.....	46
<i>Figure 18</i>	Chemical structures of 8-hydroxyquinoline-based inhibitors.....	47
<i>Figure 19</i>	Chemical structures of hydroxamate-based inhibitors.	49

Contents

Figure 20	Chemical structures of Jmj-KDM inhibitors displaying diverse modes of action.	52
Figure 21	Chemical structures of covalent KDM5 inhibitors.....	55
Figure 22	Chemical structures of peptide-based Jmj-KDM inhibitors.	56
Figure 23	Chemical structures of zinc-ejecting KDM4 inhibitors.	58
Figure 24	Overview over the main projects of this thesis.	60
Figure 25	Lysine derivatives as potential KDM4A inhibitors.	68
Figure 26	Docking of the sulfonamide-containing 2,4-PDCA derivative 83b into KDM4A.....	81
Figure 27	a) IC ₅₀ values of published hydrazide-based KDM inhibitors. b) Proposed binding mode of tetrazolyhydrazide 21	84
Figure 28	¹ H-NMR spectrum of compound 90d	98
Figure 29	Section of the HMBC spectrum of 90d	99
Figure 30	Section of the HMBC spectrum of 90j	100
Figure 31	a) Docking of deferasirox (54) (beige sticks) to KDM4A. b) Docking poses of the triazoles 90d (green sticks) and 90e (cyan sticks).	103
Figure 32	Inhibition values of labelled deferasirox derivatives.	105
Figure 33	Calibration curve for the fluorescence intensity of 96a	107
Figure 34	Influence of the central metal on the fluorescence polarization signal.	107
Figure 35	Competitive displacement of the fluorescent probe 96a	108
Figure 36	Upon binding to the enzyme, fluorescence quenching is observed for the probe 96a	109
Figure 37	Top: Section of the HMBC spectrum of 99b showing the correlations of the phenolic hydroxy groups. Bottom: Section of the HMBC spectrum of 99b showing the correlations for aromatic protons..	121
Figure 38	Left: Docking of deferasirox (light blue sticks) and 99g (magenta sticks) into KDM4A. Right: Normal (green sticks) and flipped (blue	

	sticks) orientation of the brominated derivative 99a . Bottom: Tautomers of imidazole derivative 99e	124
Figure 39	Docking of oxazole 109b (blue sticks) into the catalytic pocket of KDM4A.....	127
Figure 40	Left: Overlay of 54b (light blue sticks), thiazole 99g (magenta sticks) and pyrazole 110a (green sticks) shows a perfect overlap of the structures. Right: Overlay of thiazole 99g (magenta sticks) and imidazole 111e (cyan sticks) reveals a flipped orientation of the imidazole.	130
Figure 41	Top: Tautomers of 1,2,3-triazole 111u . Bottom: The triazolopyridine 111y (dark red sticks) is able to chelate the central metal ion while the pyrrolopyridine 111w (dark grey sticks) does not chelate the metal ion but undergoes hydrogen bonding to Asp191.	133
Figure 42	Cellular potency of deferasirox derivatives on the oesophageal cancer cell line KYSE150.....	138
Figure 43	Immunofluorescence staining of KYSE-150 cells.	141
Figure 44	Comparison of the known KDM inhibitors IOX1 and JIB-04 with the newly discovered thiazole derivative 112f	143
Figure 45	Left: The Lineweaver-Burk plot of 112f shows not solely competitive behaviour towards 2-OG. Right: Fitting to a mixed mode inhibition model shows a good curve fit.....	146

List of Schemes

Scheme 1	Synthetic route for the preparation of sulfone and sulfoxide derivatives of 2,4-PDCA.....	71
Scheme 2	Proposed reaction mechanism for the oxidation of sulphides to sulfones.	71

Contents

<i>Scheme 3</i>	Synthetic route for the preparation of benzyl-substituted sulfoxide and sulfone derivatives of 2,4-PDCA.....	72
<i>Scheme 4</i>	Protodeboronation of 2-pyridine boronic acid.	75
<i>Scheme 5</i>	Synthetic route for the generation of the boronic acid derivative of IOX1 (42).	76
<i>Scheme 6</i>	Synthetic route towards deferasirox (54) and related triazoles.	89
<i>Scheme 7</i>	Synthetic procedures for the generation of the palladium catalyst for the Kumada coupling and the synthesis of 93	95
<i>Scheme 8</i>	Synthetic procedures for the synthesis of labelled deferasirox derivatives.	96
<i>Scheme 9</i>	Generic naming of rings and atom numbering for triazole (X = N), thiazole (X = C, S, N) and oxazole (X = C, O, N) compounds.	98
<i>Scheme 10</i>	Postulated mechanism for the Hantzsch thiazole synthesis.	111
<i>Scheme 11</i>	Synthetic procedure for the synthesis of thioamide 98a	112
<i>Scheme 12</i>	Synthetic procedures for the synthesis of ketone precursors.	113
<i>Scheme 13</i>	Bromination reactions for the synthesis of precursors for the Hantzsch thiazole/oxazole synthesis.	114
<i>Scheme 14</i>	The main side reactions occurring during thiazole formation.	116
<i>Scheme 15</i>	Synthetic procedures for the synthesis of thiazoles and oxazoles.	117

List of Tables

<i>Table 1</i>	Overview over localization and biologic significance of major histone methylation marks.	5
<i>Table 2</i>	Overview of KDMs, their substrate specificity and role in disease.	18
<i>Table 3</i>	Inhibitory activity of sulfone and sulfoxide derivatives.	73
<i>Table 4</i>	Inhibitory activity of tetrazolyl-2-aminopyridine derivatives.	78
<i>Table 5</i>	IC ₅₀ values of 2,4-PDCA analogs.	80

Table 6	Inhibitory activity of 2-ethylaminopyridine derivatives.....	83
Table 7	IC ₅₀ values of tetrazolyldrazide derivatives.....	85
Table 8	Reaction conditions for coupling trials with 90f	94
Table 9	IC ₅₀ values of close deferasirox derivatives.....	102
Table 10	IC ₅₀ values of 1N- and 3C-substituted deferasirox derivatives.....	104
Table 11	Optimisation of reaction conditions for the microwave-assisted formation of oxazoles.	119
Table 12	Inhibitory activity of thiazole derivatives.	123
Table 13	Inhibitory activity of oxazole derivatives.	126
Table 14	Inhibitory activity of pyrazole derivatives.	128
Table 15	Inhibitory activity of imidazole derivatives.	131
Table 16	Inhibitory activity of N-ethylpyridin-3-amine-substituted imidazole derivatives.	134
Table 17	Selectivity data of selected compounds.	136
Table 18	Inhibitory activity of 2-hydrazonylthiazoles and -selenazoles.....	144

1 Introduction

In the last decades huge progress has been made in the elucidation of mechanisms underlying human diseases, that have led to the development of new treatment options. Still, there is an unmet need for therapeutic approaches for numerous diseases, such as cancer, infectious, metabolic as well as neurodegenerative diseases. A research field relevant for all the above-mentioned areas is the study of epigenetics, which influences a variety of physiologic and pathophysiologic mechanisms and for which the development of small-molecule modulators is of great interest.

1.1 Epigenetics

A fundamental cornerstone for the development of complex multicellular organisms is the ability of cells to differentiate towards their respective functions and to maintain that specialization over time. This competence depends on differential expression of genes encoded by the underlying uniform DNA sequence and requires mechanisms regulating and maintaining distinct expression profiles. According to the definition of Cavalli and Heard, research concerning these processes, specifically “the study of molecules and mechanisms that can perpetuate alternative gene activity states in the context of the same DNA sequence”, are termed epigenetics.¹ This definition includes all persistent changes in gene activity and chromatin function, irrespective of whether these changes are inheritable – either mitotically or transgenerational, which was a prerequisite in the widely accepted definition of epigenetics by Riggs *et al.*² – or merely apparent in non-dividing cells. The broadening of the applicability of the term epigenetics to non-dividing cell states obviates the ambiguous differentiation between heritable and non-heritable changes, as the underlying molecular mechanisms are the same. The

main epigenetic mechanisms are histone modifications, regulatory non-coding RNAs and DNA modifications not impairing Watson-Crick base pairing but influencing binding affinities to effector proteins.³ Epigenetic mechanisms are vital for the stability of certain cell states, but meanwhile maintain the ability to adapt to genetic, metabolic or environmental stimuli. Thereby, they provide the basis for cellular plasticity in dependence on developmental stage and external conditions.

1.1.1 DNA Modifications

The most abundant epigenetic DNA modification is cytosine methylation at C5, which amounts to approximately 4% of the total genomic cytosines and occurs mainly at cytosine nucleotides precedent to guanine (CpG sites).⁴ DNA methylation of promoter regions is closely linked to transcriptional repression thereby playing a major role in fundamental mechanisms, such as X-chromosome inactivation, genomic imprinting, as well as silencing of developmental genes.⁵ By contrast, methylation of gene bodies is positively linked to transcription, suggesting context-specific effects of methylation marks.⁶

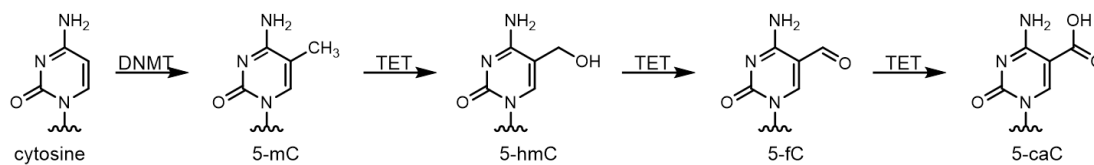


Figure 1 Cytosine modifications present in DNA. Methylation is performed by DNA-methyltransferases (DNMTs) and successive oxidation by TET dioxygenases. 5-mC – 5-methylcytosine, 5-hmC – 5-hydroxymethylcytosine, 5-fC – 5-formylcytosine, 5-caC – 5-carboxylcytosine.

Methyl groups are installed by DNA methyltransferases (DNMTs), which are responsible for the propagation of methylation patterns during cell division (DNMT1) and *de novo* methylation (DNMT3a and b). Although the methyl mark is considered a stable modification mainly involved in long-term regulation, plasticity is maintained via several demethylation mechanisms. These include passive demethylation via dilution over several rounds of cell division as well as active removal via oxidation of methyl-cytosine to hydroxy-, formyl-, and carboxymethyl-

cytosine by TET-dioxygenases (cf. Figure 1) triggering replacement by unmethylated cytosine via base excision repair or direct deformylation or decarboxylation.⁷ Additionally, these oxidized cytosine nucleotides can elicit regulatory functions of their own, such as context-dependant transcriptional activation or repression and regulation of alternative splicing.⁸⁻¹⁰

Further putative epigenetic DNA modifications include 6-methyladenine, 1-methyladenine, 7-methylguanine and 4-methylcytosine. However, their extremely low abundance in human genomic DNA – for 6-methyladenosine an occurrence of 0.05% of the total adenines is reported, while the other three are estimated to be even rarer – requires highly sensitive detection techniques, and renders sequencing results prone to errors caused by contamination or artefacts, which has impeded analysis of their biological roles.^{11, 12} Therefore, their implication in epigenetic regulation is not entirely clear to date.¹³

1.1.2 Histone Modifications

The genomic DNA is wrapped around histone octamers consisting of the core histones H2A, H2B, H3 and H4 (cf. Figure 2). Along with the linker histone H1, these nucleosomes form the chromatin fibre allowing the dense packing of DNA in the nucleus while maintaining accessibility. The highly condensed form, termed heterochromatin, is characterized by low transcriptional activity, whereas the more loosely packed euchromatin is more accessible for transcription factors, other regulatory proteins and the transcription machinery. Packing density and protein affinity is mainly regulated by chromatin-remodelling complexes and is highly dependent on histone variants and post-translational modifications of the N-terminal histone tails protruding from the nucleosomes. A high level of complexity is attained by multiple available modification sites, the variety of functional modification marks – including acetyl-, methyl-, phosphoryl-, ADP-ribosyl-, SUMOyl- and ubiquitinyl-groups – and the possible cross-talk between these

1 Introduction

modifications.¹⁴ Acetylation of the ϵ -amino group of lysine is mainly associated with an open chromatin structure and active transcription, because neutralisation of the otherwise positively charged amine moiety decreases the interaction of histones with the negatively charged DNA backbone.¹⁵ Methylation of lysine or arginine is either linked to transcriptional activation or to repression depending on the position, the degree – ranging from mono- to trimethylation for lysine and mono- and symmetric or asymmetric dimethylation for arginine – and the context to other epigenetic marks.¹⁶ The most important lysine methylation marks and their biologic functions are summarized in Table 1 and a more detailed description of methylation marks is included in the description of biological roles of histone demethylases in section 1.2.

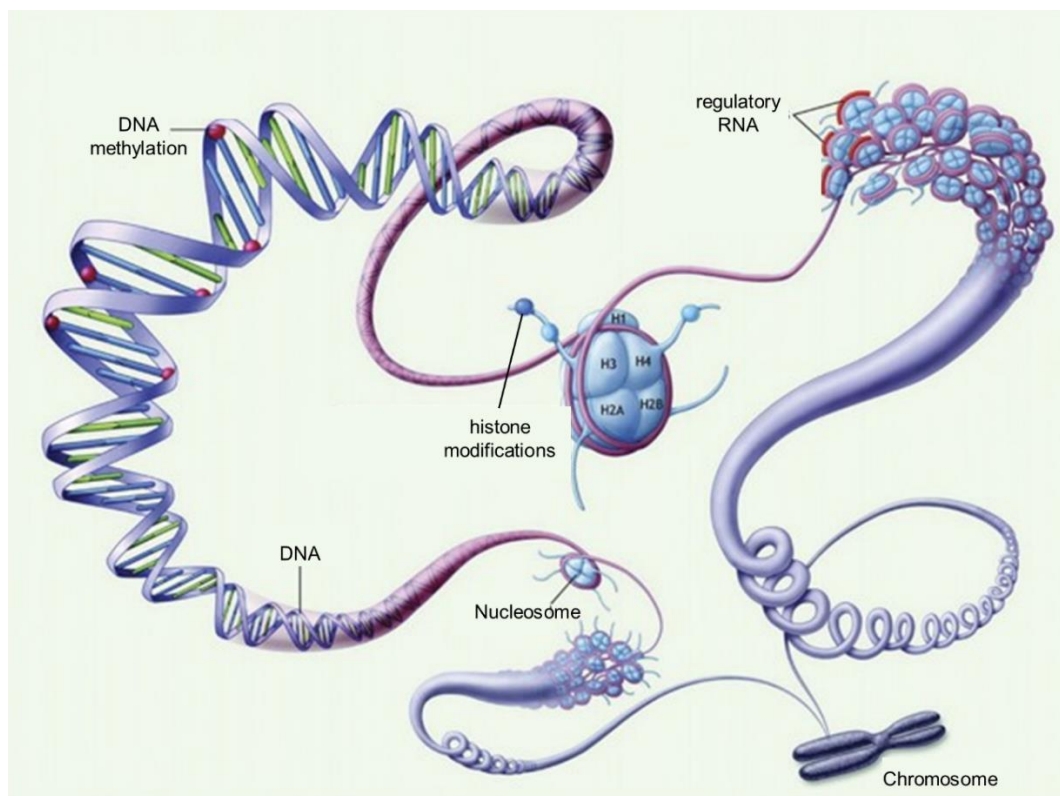


Figure 2 Schematic representation of the higher order of DNA. DNA is wrapped around histone proteins forming nucleosomes. The resulting “bead string” is further compacted to form the chromatin fibre, which can be spiralized to give the chromosome. The three main epigenetic regulation mechanisms are DNA-methylation, post-translational histone modifications and RNA based mechanisms (adapted from Lee *et al.*¹⁷).

Epigenetic modifications are installed by writer proteins, such as lysine acetyltransferases (KATs), lysine and arginine methyltransferases (KMTs and

PRMTs) and removed by eraser proteins, like lysine deacetylases (HDACs, also termed KDACs), lysine and arginine demethylases (KDMs and RDMs). Reader proteins recognising specific modifications elicit regulatory functions. Reader domains may recruit protein complexes involved in transcriptional regulation, chromatin remodelling, DNA replication and damage repair, as well as writer or eraser proteins.

Table 1 Overview over localization and biologic significance of major histone methylation marks. As most marks employ various, sometimes contrasting functions in different contexts, only major known roles are given.¹⁹⁻²²

methylation site	degree of methylation	main localization	main physiologic role or associated processes
H3K4	H3K4me ₁	enhancers	transcriptional activation poising of promoters
	H3K4me ₂	5' end of transcribed genes	
	H3K4me ₃	promoter regions	
H3K9	H3K9me ₁	gene bodies	transcriptional silencing heterochromatin formation related to DNA methylation H3K9me _{2/3} : alternative splicing
	H3K9me ₂	centromeric and telomeric regions	
	H3K9me ₃	transposable elements	
H3K27	H3K27me ₁	gene bodies	transcriptional activation
	H3K27me ₂	intra- and intergenic regions enhancers	transcriptional repression prevention of H3K27 acetylation
	H3K27me ₃	promoter regions	transcriptional repression
H3K79	H3K79me _{2/3}	gene bodies chromosome boundaries	transcriptional activation elongation telomeric silencing
H4K20	H4K20me _{1/2}	promoter regions gene bodies	transcriptional activation cell cycle control
	H4K20me ₃	promoter regions transposons	heterochromatin formation genome stability DNA damage repair

The epigenetic reader domains include bromodomains, recognising acetylated lysine residues, and the methyl-recognising chromo-like reader domains, including chromo-, chromo-barrel, double chromo- (DC), tudor, tandem tudor (TT), and

1 Introduction

malignant brain tumour (MBT) domains, as well as plant homeodomains (PHD). Furthermore, distinct methylation marks can be recognised by ADD, Ankyrin, BAH, HEAT, PWWD, WD40 and zinc finger-CW (zfCW) domains.¹⁸

1.1.3 Epigenetics in Disease and Therapy

Given their essential role in development, cell differentiation, cellular memory, aging and numerous other basic biologic functions, the importance of understanding and potentially influencing epigenetic mechanisms in regard to human health stands without question. Their implication in various diseases, for example in cancer, autoimmune diseases, inflammation, neurodegenerative and neuropsychiatric disorders, has triggered the development of diverse pharmacologically active substances targeting epigenetic regulators, leading to the approval of several epigenetic drugs while many more are currently undergoing clinical trials.²³

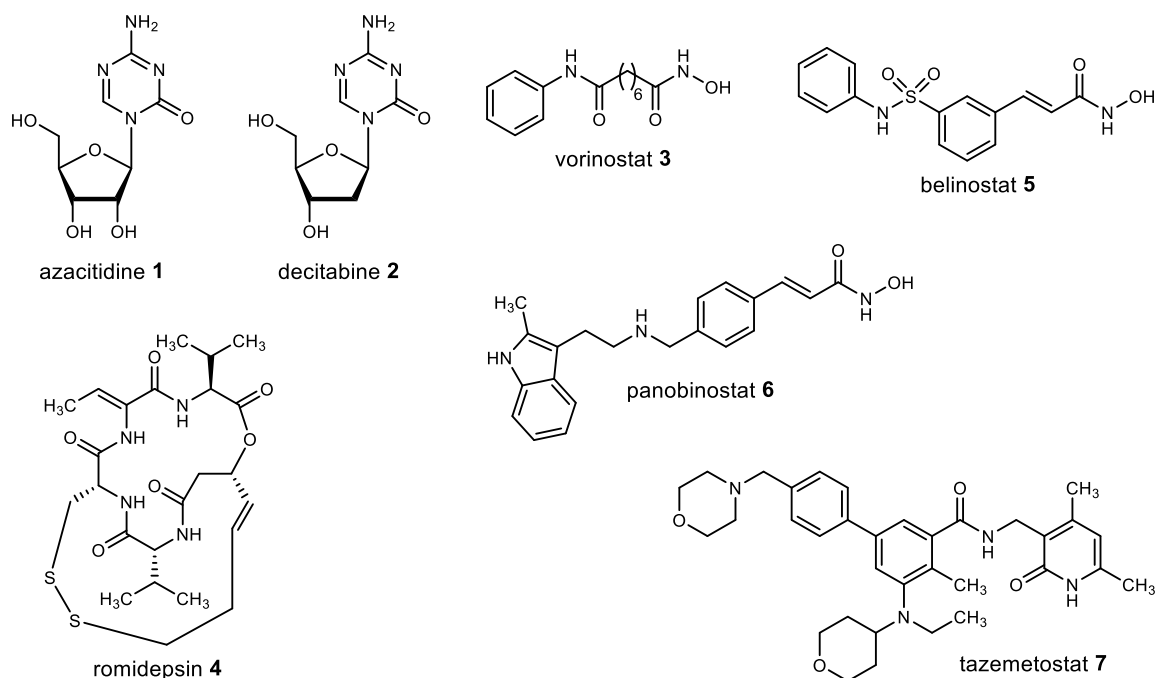


Figure 3 Approved drugs targeting epigenetic enzymes.

The most clinical advances have been made in the field of cancer, leading to the approval of the first epigenetic drugs, namely azacitidine **1** (Vidaza®, 2004; cf. Figure 3) and decitabine **2** (Dacogen®, 2006) inhibiting DNMTs, as well as the

HDAC inhibitors vorinostat **3** (Zolinza®, 2006), romidepsin **4** (Istodax®, 2009), belinostat **5** (Beleodaq®, 2014), and panobinostat **6** (Farydak®, 2015). All these drugs are used for the treatment of haematological malignancies, such as myelodysplastic syndrome (MDS), T-cell lymphoma (TCL) and multiple myeloma (MM).²⁴ More recently, tazemetostat **7** (Tazverik®, 2020), an inhibitor targeting the histone methyltransferase EZH2, was approved as the first epigenetic treatment for a solid tumour, namely epithelioid sarcoma.²⁵

1.2 Histone Demethylases

The enzymes capable of removing methyl marks from histone tails – and in some cases also non-histone substrates – are essential players in the epigenetic regulation. Lysine-specific demethylases (LSDs), discovered in 2004, are FAD-dependent, while the larger group of jumonjiC domain-containing histone demethylases (JmjC-KDMs), first described in 2006, depend on iron and 2-oxoglutarate **8** (2-OG, also called α -ketoglutarate).^{26,27} A systematic nomenclature covering all family members discovered so far terms the histone demethylases more generally as lysine demethylases (KDMs) as some members also have non-histone substrates, such as the transcription factors p65 and NF- κ B for KDM2A.²⁸ However, other names are also common in literature. An overview of the demethylases, their alternative names, substrate specificity and examples for their putative roles in disease are given in Table 2.

1.2.1 FAD-dependent Lysine-specific Demethylases

The FAD-dependent demethylases LSD1 and 2 (also called KDM1A and B or AOF2 and 1) catalyse the demethylation of mono- or dimethyl-lysine 4 of histone H3 (H3K4me_{1/2}). LSD1 also demethylates H3K9me_{1/2}. Both enzymes cannot convert trimethylated lysines, because the reaction proceeds via an iminium intermediate,

which requires at least one hydrogen atom bound to the amino group (cf. Figure 4B). The protein structure contains the catalytic AOL (amine oxidase-like) domain, a SWIRM domain enabling substrate recognition and protein-protein interactions as well as further protein-binding domains, namely the tower domain in LSD1 and two zinc finger domains in LSD2 (cf. Figure 4A).^{29, 30}

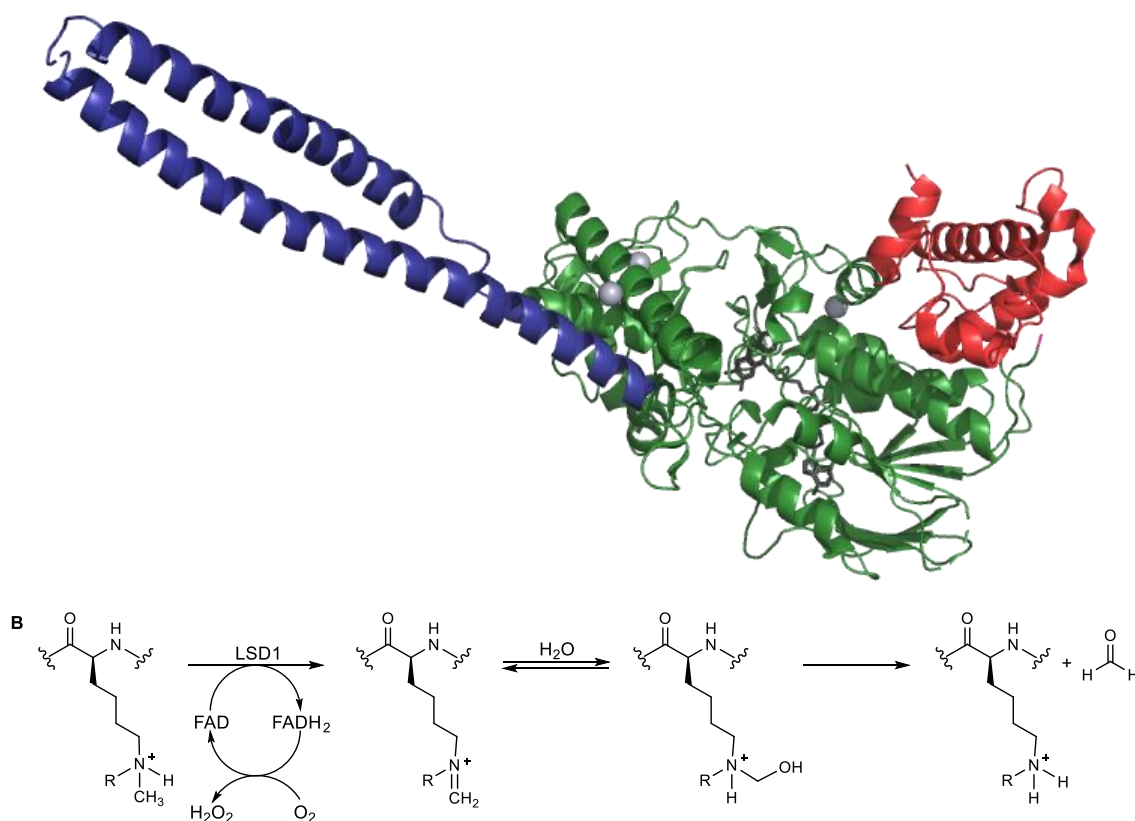


Figure 4 A) Crystal structure of the histone demethylase LSD1. The tower domain is displayed in blue, the AOL domain in green, the SWIRM domain in red, zinc ions as light grey spheres and the cofactor FAD as dark grey sticks. (PDB: 2HKO, first published in Ref. 45).

B) Demethylation reaction catalysed by LSD1 using the cofactor FAD. Demethylation of mono- and dimethylated residues can be catalysed (R = H or CH₃).

LSD1 can either act as a transcriptional activator or repressor dependent on the location and degree of methylation, other epigenetic marks and interactions with regulatory proteins. In association with CoREST (corepressor of RE1-silencing transcription factor), NuRD (nucleosome remodelling and deacetylase) or CtBP (C-terminal-binding protein 1) complexes, demethylation of H3K4me_{1/2} contributes to transcriptional repression.^{31, 32} Contrastingly, transcriptional activation via demethylation of H3K9me₂ is induced by binding to androgen or estrogen nuclear

receptors.^{33, 34} Additionally, LSD1 elicits important biological functions independent of its demethylase activity, mainly via stabilisation or destabilisation of interaction partners, such as the transcriptional regulator estrogen-related receptor α (ERR α) or the tumour suppressor F-box/WD repeat-containing protein 7 (FBXW7), respectively. It may also activate downstream-processes, like a lethal prostate cancer gene network, which is involved in prostate cancer cell survival.³⁵⁻³⁷ Although LSD2 is also an H3K4me_{1/2} demethylase, its biological roles differ considerably from LSD1, as it binds to different interaction partners. Unlike LSD1, which is primarily associated to promoter regions, LSD2 is mainly found at sites within gene bodies of actively transcribed genes, suggesting a regulatory role in transcription.³⁸

Both LSD1 and LSD2 are promising targets in cancer therapy, as their overexpression has been shown in various diseases, such as breast, prostate, lung or brain tumours and hematologic malignancies for LSD1 as well as breast cancer, colorectal adenocarcinoma and Ewing sarcoma for LSD2.³⁹⁻⁴¹ Additionally, LSD1 is implicated in inflammation, neurodegenerative diseases and viral infections where it might prove to be a valid therapeutic target in the future.⁴²⁻⁴⁴

1.2.2 JmjC Domain-containing Histone Demethylases

The second class of lysine demethylases are iron-dependent JmjC-KDMs, belonging to the cupin superfamily of metalloenzymes. This class consists of approximately 30 members identified in the human genome, which can be divided into seven families according to their structure and phylogenetic relationships.⁴⁶ In contrast to the LSDs, JmjC-KDMs can not only demethylate mono- and dimethylated lysine substrates but also trimethylated ones. Furthermore, some subtypes also recognise and convert methylated arginine substrates, although the biological significance of this process is still not clear.⁴⁷

1.2.2.1 Structure of Jmj-KDMs

All JmjC-KDMs share the conserved catalytic JumonjiC domain, formed by a double-stranded β -helix (DSBH, also called jelly-roll fold) which is comprised of eight antiparallel β -strands.²⁷ The catalytic ferrous iron is bound via complexation of the side chains of two histidine and an aspartate or glutamate residue of the conserved HxD/E...H motif. For KDM4A, the responsible amino acids are His188, Glu190 and His276.⁴⁸ In the resting state, the remaining three coordination sites of the octahedral iron complex are occupied by three water molecules, which are replaced by the co-substrate 2-OG – via bidentate chelation of the C1 carboxylate and the C2 keto-group – and molecular oxygen upon activation. The C5 carboxylate of 2-OG points towards the catalytic pocket and is stabilized via electrostatic and hydrogen interactions with basic, alcoholic, phenolic and/or amide residues of the DSBH.^{48, 49} In the case of KDM4A, 2-OG is stabilized via three hydrogen bonds formed between the side chains of Tyr132, Asn198, and Lys206 (cf. Figure 5).⁴⁸

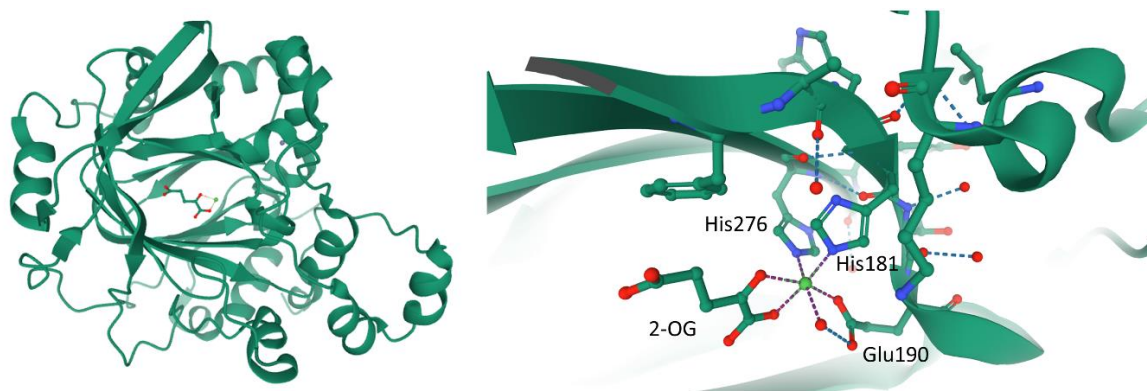


Figure 5 Left: Crystal structure of the catalytic JmjC domain of KDM4A with bound co-substrate 2-oxoglutarate. The central ferrous iron is replaced by nickel (green sphere) for stability reasons. Right: Zoom-in on the metal binding-site with the so-called facial triad formed by His181, Glu190 and His276. (PDB: TVR5, first published in Ref. 51).

Furthermore, the DSBH is involved in substrate recognition and thereby contributes to the subtype selectivity towards distinct histone substrates. The main substrate-binding cleft is localized adjacent to the catalytic site and places the methylated lysine chain into close proximity of the central ferrous iron. The binding site contains a methylammonium binding pocket, whose architecture determines

selectivity for distinct methylation states ($\text{me}_{1/2/3}$) mainly via size and hydrophobic interactions. Specific interactions with the peptide chain are formed by characteristic inserts between the β -strands of the DSBH, which vary between subtypes.⁵⁰ Apart from the inserts, the JmjC domain is highly conserved across the KDM family. The x-ray structure of the catalytic domain of KDM4A in complex with Ni^{2+} as a stable replacement for Fe^{2+} and the co-substrate 2-OG is shown in Figure 5. Additionally, KDMs 4 and 5 contain the JmjN domain adjacent to the JmjC domain. Its main functions are the stabilisation and activation of the catalytic domain via interactions with various methyl lysine reader domains such as TUDOR, ARID or PHD domains.⁵² The JmjN domain may also be involved in the formation of homo- and heterodimers of KDM4A and KDM4C, which possess increased catalytic activities.⁵³ Similar domains are also found in all other Jmj-KDMs and it has therefore been proposed that these domains should also be called JmjN domains and should be regarded as an integral part of the catalytic domain of all Jmj-KDMs.⁵⁰ However, this nomenclature has not gained acceptance in literature up to now. Furthermore, KDMs contain additional domains, which are mainly reader domains to recognise certain histone modifications or interact with DNA as well as domains interacting with other regulatory proteins such as transcription factors. KDM4, KDM5 and KDM7 family members contain up to three PHD domains, which belong to the zinc finger binding domains. They bind to methylated lysine or arginine residues, while some also recognise unmodified or acetylated lysine. PHDs are therefore involved in substrate recognition and specificity and may serve as allosteric modulators of the catalytic function.⁵⁴ Another methyl lysine binding domain is the tandem Tudor domain, which is part of the KDM4 isoforms A-D and is also implicated in substrate recognition.⁵⁵ KDM5 proteins additionally contain the AT-rich interacting domain (ARID), which recognises distinct DNA sequences consequently supporting targeting of histones bound to these specific strands.⁵⁶ Additional protein-protein interaction domains are the F-Box domain present in KDM4A and KDM4B, the leucine-rich repeat (LRR) domain in KDM2 and the

tetratricopeptide (TPR) domain in KDM6A and KDM6C. Moreover, some KDMs contain further zinc finger domains involved in DNA interactions such as the C5HC2 domain in KDM5 and the CXXC domain in KDM4A-C.⁵⁰ An overview of the domain architecture of selected KDMs is given in Figure 6.

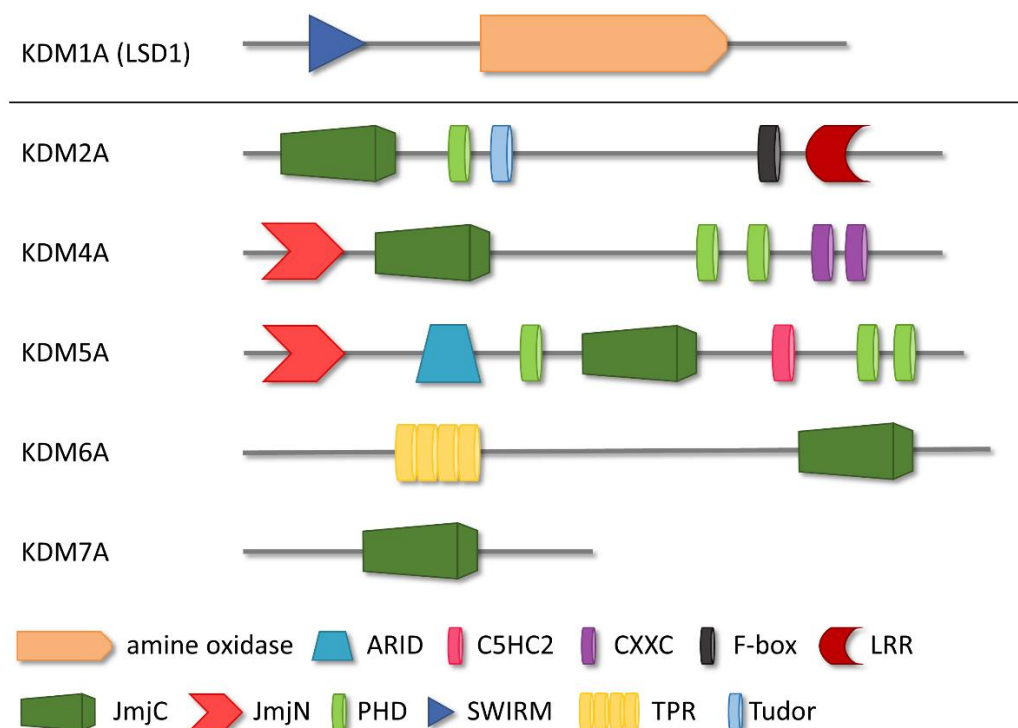


Figure 6 Domain architecture of selected histone demethylases. (Modified after Ref. 52).

The catalytic activity of KDMs is highly dependent on protein interactions of their reader domains with histones, especially for the substrate recognition domains, as becomes evident when comparing demethylase activities on differently modified histone substrates. For example, H3K4me₃K9me₃ is demethylated significantly faster at K9 by KDM4A than H3K9me₃ even though K4me₃ is not a substrate of KDM4A. This effect is more pronounced for full-length protein than for the catalytic core domain alone, which underlines the allosteric modulation by the reader domains.⁵⁷ This effect should be kept in mind when analysing data from *in vitro* enzyme assays which are often performed with shortened substrates and enzyme constructs devoid of reader domains.

The domain architecture of KDMs is conserved across species. For example, the KDM4A-C orthologs exist in all vertebrates and additionally share the same

substrate specificity for H3K9me_{3/2} and H3K36me_{3/2}. The KDM4 protein has even been shown to be present in at least one isoform in all analysed eukaryotes ranging from yeast and flagellates to complex multicellular organisms.⁵⁸

1.2.2.2 Catalytic mechanism

The demethylation reaction catalysed by JMJ-KDMs proceeds via an oxidation mechanism characteristic for Fe²⁺/2-OG-dependent dioxygenases, which is followed by spontaneous decomposition to release the demethylated substrate. Iron is bound to the enzyme via the facial triad consisting of two histidine residues and glutamate or aspartate residue. The other three coordination sites are occupied by three water molecules when the enzyme is in the resting state completing the octahedral complex. In the first catalytic step, the co-substrate 2-OG coordinates to the central Fe²⁺ ion – displacing two water molecules – which facilitates binding of molecular oxygen by weakening the coordinative bond to the third water molecule. Upon oxygen binding, one electron is transferred from Fe²⁺ to O₂ yielding a highly reactive Fe(III)–OO• superoxide radical intermediate **IM1** (cf. Figure 7). From this transition state – probably a quintet state, as shown by energy calculations and spectroscopic measurements⁵⁹ – the distal oxygen is transferred to the keto group of the co-substrate via classical nucleophilic attack resulting in a peroxo-linked intermediate **IM2**. For mono- or dimethylated lysine substrates the NH-group of the lysine residue forms a bond with C1 of 2-OG, stabilizing the transition state. Next, decarboxylation of the co-substrate takes place while the peroxo-bond is cleaved heterolytically yielding the reactive Fe(IV)=O oxo intermediate **IM3** with coordinatively bound succinate. Formation of this intermediate and release of CO₂ make enough room for the methyl group of the substrate to be placed close to the iron centre. Consequently, the Fe(IV)=oxo group abstracts one hydrogen radical from the substrate resulting in the hydroxylated intermediate **IM4**. The intermediate transfers the hydroxyl radical onto the substrate, yielding the

1 Introduction

hydroxymethyl lysine intermediate **IM5**. This hemiaminal spontaneously decomposes to release formaldehyde and the mono-demethylated substrate. The catalytic cycle is completed upon succinate release making room for a new 2-OG co-substrate to bind to the enzyme.^{59, 60}

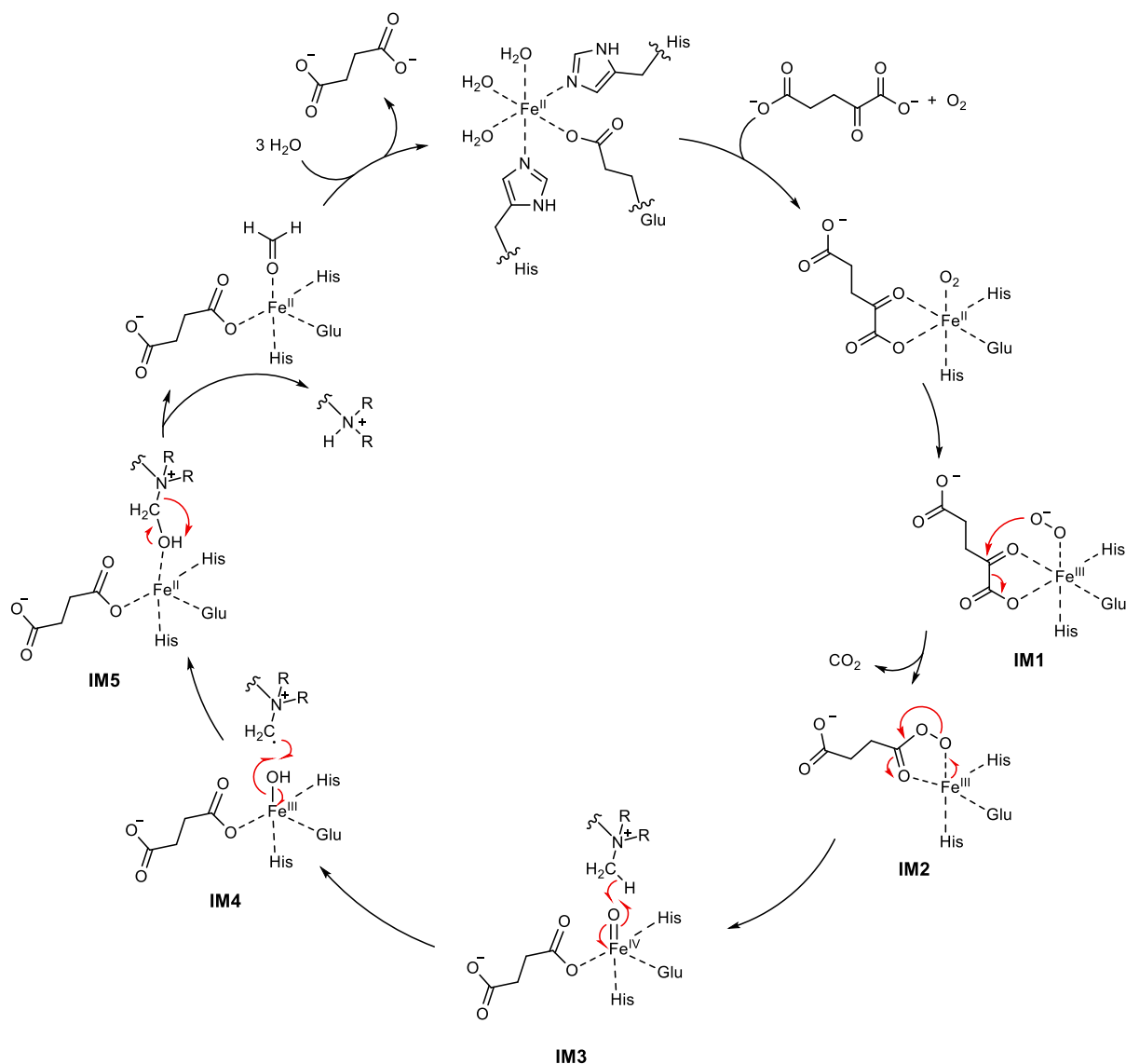


Figure 7 Catalytic mechanism of the demethylation of methylated lysine residues by Jmj-KDMs.^{59, 60}

In summary, the catalytic reaction comprises of the transfer of one oxygen to the substrate, which results in the release of formaldehyde and the mono-demethylated substrate and the transfer of the other oxygen atom onto the co-substrate 2-OG yielding carbon dioxide and succinate. As the underlying mechanism is a radical oxidation, it is not limited to mono- and dimethylated substrates but also works on

trimethylated ones, because – contrasting to the FAD-dependent mechanism performed by KDM1A and KDM1B (LSD1 and 2) – the ϵ -lysine nitrogen lone pair is not involved in the reaction and no imine intermediate is formed.

1.2.2.3 Physiologic Roles

Like the FAD-dependent KDMs, Jmj-KDMs are also involved in transcriptional regulation, dependent on their respective target substrate as well as interactions with transcription factors and other regulatory proteins. Furthermore, they influence other genome-related processes such as cell cycle control and DNA damage repair. Consequently, they are implicated in various cellular processes ranging from egg cell implantation to neuronal plasticity. Their roles have extensively been reviewed.^{19, 61-65} The following section highlights some important biologic functions with special focus on KDM4A, as this isoform is the main subject of this thesis.

KDMs play a major role in embryonic development starting with epigenetic reprogramming of the germline and followed by the lineage commitment of developing cells. Reprogramming is an event occurring shortly after fertilization, where most parental epigenetic marks are removed in a “resetting” protocol. Here, demethylases such as KDM3A and KDM3C play an important role via removal of histone methylation marks and also via regulating the replacement of modified histones.^{66, 67} KDM4A is also involved in early development, as it is relevant for epigenomic integrity and zygotic gene activation in oocytes. It demethylates H3K9me₃ at promoters marked by broad domains of H3K4me₃, which is a typical marker of oocyte-specific genes and is necessary for proper gene activation.⁶⁸

During lineage commitment, a vast set of genes, which are transcriptionally repressed in embryonic stem cells, has to be activated for transcription to allow for lineage-specific genes to be expressed. KDMs like KDM2 and KDM6 confer this activation via removal of repressive H3K27me₃ and H3K36me_{1/2} marks and a

decrease in the activity of repressive complexes such as Polycomb. KDM recruitment to these sites is mainly directed by recognition of CpG islands and the interaction with transcription factors.^{69, 70}

A further important role of KDMs is the regulation of neurologic functions. Several KDMs are implicated in synaptic plasticity, memory formation and cognitive behavioural patterns as well as embryonic neural development.^{52, 71, 72} For example, KDM4A is crucial for the formation of the neural crest, a tissue giving rise to peripheral and enteric neurons and other tissues, via demethylation of repressive H3K9me₃ at the promoters of the transcription factor genes *Sox10* and *Snail2*, thereby poising those genes for transcription.⁷³ Additionally KDM4A and KDM4C control neural stem cell differentiation by activating the brain-derived neurotrophic factor *BDNF* gene via H3K9me₃ demethylation and RNA polymerase II recruitment while simultaneously repressing the astrocyte-characteristic gene *GFAP* (glial fibrillary acidic protein) via H3K36me₃ demethylation.⁷⁴

The influence of KDM4 activity on higher neurologic functions such as behaviour and mood has been shown in the nucleus accumbens, a brain region controlling reward circuits. Here, H3K9me_{2/3} demethylation by KDM4A seems to be crucial for the proper function of this pathway, as increased H3K9me_{2/3} levels upon KDM inhibition lead to depression-like symptoms in mice.⁷⁵

KDMs are also involved in metabolic processes and the development of adipose tissue. KDM4A and KDM4B are major regulators of differentiation of stromal cells into adipocytes by activating adipocyte-specific genes. They are therefore involved in the regulation of body weight and fat metabolism. KDM4B inactivation in adipocytes via knock-out in mouse models showed acceleration of obesity and increased glucose intolerance and hepatic steatosis.^{76, 77}

Furthermore, Jmj-KDMs are involved in the regulation of DNA replication and cell cycle control. For example, KDM5C has been shown to be highly expressed in early S-phase and to demethylate H3K4me₃ at origins of replication of early replicating genes and to be thereby involved in the initiation of replication.⁷⁸

Since the discovery of KDMs as histone demethylases, it has become more and more evident that they also possess physiological roles besides direct epigenetic regulation by recognising non-histone substrates. This has been shown for example for KDM2A and KDM4A. Possible target proteins are DNA methyltransferases (DNMTs), the transcription factors p53 and NF- κ B, retinoblastoma protein 1 (RB1), oestrogen receptors (ERs) and many others. KDM4A additionally is present in the cytosol in high concentrations making targeting of non-nuclear proteins highly likely. The roles of demethylation of non-histone substrates in physiologic processes are not completely elucidated to date, although some studies have shown links between protein methylation and protein stability via regulation of ubiquitinylation as well as modulation of affinity towards reader domains of interaction partners.⁷⁹

1.2.2.4 Roles in Disease

Given their essential role in transcriptional regulation and diverse other physiologic mechanisms, it is not surprising that dysregulation of these processes, be it via overexpression, downregulation or mutation of the involved demethylases is related to a variety of diseases. The most abundant and also best-studied disease type is cancer, and dysregulation for almost every Jmj-KDM could be linked to certain cancer types.⁵² Other disease areas, where the involvement of KDMs is highly probable, are neurologic diseases, such as Alzheimer's disease, schizophrenia and autism spectrum disorders, metabolic diseases like diabetes and obesity, inflammatory and autoimmune diseases.⁵² The link of KDMs to the primary metabolism via its co-substrate 2-OG as well as the role of the side product succinate and other intermediates of the tricarboxylic cycle as physiologic KDM inhibitors (cf. section 1.4.2) establishes their role in metabolic diseases and also links them to aging processes.⁸⁰ A comprehensive review of the implications of Jmj-KDMs in diseases is beyond the scope of this thesis, yet examples for KDM involvement in several diseases is given in Table 2 and a more elaborate description for the roles of KDM4A

1 Introduction

is given in the sections below. More extensive reviews can be found in literature, a recent example being Ref. 52 by Arifuzzaman *et al.*^{52, 55, 81-86}

Table 2 Overview of KDMs, their substrate specificity and role in disease.⁵²

Systematic Name	Synonyms	Preferred Substrates	Examples for Disease Implication
KDM1A	LSD1, AOF2	H3K4me _{2/1} H3K9me _{2/1}	↑ neuroblastoma, prostate and breast cancer X increased risk of type 2 diabetes mellitus
KDM1B	LSD2, AOF1	H3K4me _{2/1}	↑ urothelial carcinoma
KDM2A	FBXL11, JHDM1A1	H3K36me _{2/1}	↑ leukaemia
KDM2B	FBXL10, JHDM1B	H3K4me ₃ , H3K36me _{2/1}	X impaired spermatogenesis
KDM3A	JMJD1A, JHDM2A	H3K9me _{2/1}	X impaired fertility, prostate, renocellular and hepatocellular carcinoma ↓ increased risk of obesity
KDM3B	JMJD1B, JHDM2B	H3K9me _{2/1}	X decreased spermatogenesis
KDM4A	JMJD2A, JHDM3A	H3K9me _{3/2} H3K36me _{3/2}	↑ prostate and breast cancer ↓ bladder cancer
KDM4B	JMJD2B, JHDM3B	H3K9me _{3/2} H3K36me _{3/2}	↑ malignant peripheral nerve sheath tumour ↓ increased risk of obesity
KDM4C	JMJD2C, JHDM3C, GASC1	H3K9me _{3/2} H3K36me _{3/2}	↑ medulloblastoma, oesophageal and breast cancer X related to autism
KDM4D	JMJD2D, JHDM3D	H3K9me _{3/2} H3K36me _{3/2}	↑ gastrointestinal stromal tumour ⁸⁷
KDM4E	JMJD2E	H3K9me _{3/2}	X squamous cell lung cancer ⁸⁸
KDM5A	JARID1A, RBP2	H3K4me _{3/2}	X lung, gastric, breast and liver cancer
KDM5B	JARID1B, PLU1	H3K4me _{3/2}	X impaired spermatogenesis, hepatocellular carcinoma, malignant melanoma, prostate and colorectal cancer
KDM5C	JARID1C, SMCX	H3K4me _{3/2}	↑ prostate cancer X related to autism and cognitive dysfunction
KDM5D	JARID1D, SMCY	H3K4me _{3/2}	X prostate cancer
KDM6A	UTX, MGC141941	H3K27me _{3/2}	↑ Hodgkin's lymphoma, lung and liver carcinoma X Kabuki syndrome ↓ increased risk of diabetes mellitus
KDM6B	JMJD3, KIAA0346	H3K27me _{3/2}	↑ breast cancer ⁸⁹ ↓ advanced arteriosclerosis ⁹⁰
KDM7A	KIAA1718	H3K9me _{2/1} H3K27me _{2/1}	↑ prostate cancer
KDM7B	KIAA1111, PHF8, ZNF422	H3K9me _{2/1} H4K20me ₁	↑ breast cancer X cleft lip/palate
KDM8	JMJD5	H3K36me ₂	↑ prostate cancer ⁹¹
↑ overexpression and/or amplification ↓ downregulation and/or deficiency X deletion or missense mutation			

As shown in Table 2 KDM4A is overexpressed in prostate⁹² and breast⁹³ cancer. These two diseases both belong to the hormone-dependent malignancies, where disease progression is linked to androgens and oestrogens, respectively. Another hormone-receptor dependent tumour influenced by KDM4 overexpression is endometrial carcinoma.⁹⁴ KDM4A acts as a co-activator of the androgen and oestrogen receptors (AR and ER) by forming a complex with the respective receptor and activating demethylations at promoters of hormone-dependent genes, thereby driving cancer development and progression.^{92, 93} Consecutively, KDM4 inhibition suppresses tumour growth via downregulation of AR- or ER-controlled genes.^{95, 96} KDM4A inhibition was even able to subdue proliferation of triple-negative breast cancer stem-cells, which are resistant to treatment with hormone receptor antagonists, underlining the crucial role of KDM4A in cancer development via several mechanisms and its great potential for clinical treatments.⁹⁶ Besides the binding of hormone receptors, another mechanism of KDM4A is binding to the transcription factor ETV1, whose downstream targets may act as oncogenic proteins.⁹⁷

KDM4A overexpression has also been shown in various other solid tumours, namely bladder,⁹⁸ cervical,⁹⁹ colorectal,¹⁰⁰ gastric,¹⁰¹ liver,¹⁰² lung,¹⁰³ and nasopharyngeal¹⁰⁴ carcinoma as well as glioblastoma.¹⁰⁵ In these cancers, increased demethylation correlates with tumour progression, migration, invasion, and poor prognosis, while inhibition or knockdown causes growth inhibition.^{103, 106} In pancreatic cancer low levels of KDM4A have been found in senescent tumour cells thereby correlating decreased KDM4A activity with tumour suppression.¹⁰⁷ Involved mechanisms comprise downregulation of tumour suppressors,⁹⁹ upregulation of oncogenic proteins such as c-Myc,¹⁰² and cancer-specific metabolic changes such as the Warburg effect.¹⁰⁴ Additionally, KDM4A is also overexpressed in hematologic malignancies such as acute myeloid leukaemia (AML)¹⁰⁸ and chronic lymphocytic leukaemia (CLL), though CLL cells show decreased levels of KDM4B, showing that these similar demethylases are not completely redundant.¹⁰⁹

However, there are also tumour types, where a decreased expression of KDM4A has been discovered, for example in urothelial carcinoma, underlining the complex epigenetic regulation in different tumours and proving the need for careful research in this disease area.¹¹⁰ Recent findings in the field of cancer research around KDM4 are reviewed in Ref. 111 by Lee *et. al.* Another disease area where KDM4A overexpression plays a role is hypertrophic cardiomyopathy. Here, H3K9me₃ demethylation leads to the overexpression of FHL1, a protein involved in the mechanotransducer machinery of the heart and thereby increases hypertrophy of the heart muscle in response to pressure overload.¹¹² Therefore, KDM4A inhibition seems to be an interesting option to treat cardiomyopathy or even prevent it.

KDM4A overexpression has also been shown in a model for cerebral ischemic stroke, and KDM inhibition was associated with ameliorated neurological deficits and a normalization of aberrant H3K9 methylation in striatal neurons.¹¹³

Moreover, KDM4A is implicated in the development of another cardiovascular disease, namely atherosclerosis. Increased KDM4A expression is triggered by oxidized LDL (low-density lipoprotein), a main factor in the development of atherosclerotic plaques, and induces macrophage polarization towards a pro-inflammatory phenotype. Inflammation is a hallmark of atherosclerosis and thereby contributes to disease progression.¹¹⁴

On the other hand, reduced KDM4 expression has been shown in the development of liver fibrosis, another disease involving inflammatory processes. Here KDM4 downregulation is accompanied by the transition of quiescent hepatic cells into activated myofibroblasts producing pro-fibrogenic proteins, thereby driving the disease forward.¹¹⁵

In summary, KDM4A overexpression is relevant in numerous diseases, particularly cancer, which yields the therapeutic opportunity for treatment with KDM4A inhibitors to reverse these negative effects. However, in some cases, such as urothelial carcinoma and liver fibrosis, low KDM4A activity seems to favour disease progression. This underlines the importance of the development of potent and

selective inhibitors in order to characterise the effects of KDMs in disease in more detail as well as to elucidate potential therapeutic areas and to uncover mechanism-based undesired side-effects.

1.3 Assays for JmjC Domain-containing Histone Demethylases

As outlined in the previous section, inhibition of histone demethylases constitutes a valuable means to target various diseases. Hence, the development of potent inhibitors is of utmost importance. A vital prerequisite for developing enzyme inhibitors is the availability of suitable assay formats to evaluate compound activity. Assays can either be based on measurement of enzyme activity or binding to the isolated enzyme in an *in vitro* setting, assessment of cellular effects in target-relevant cell lines or evaluation of *in vivo* effects in more complex systems or whole organisms. For screening of larger compound libraries and early inhibitor development the first two methods are often preferable due to comparably low cost and complexity as well as to avoid animal studies for ethical reasons. Thus, a number of different biochemical *in vitro* assays for JmjC domain-containing histone demethylases have been established to date. Assays are either based on the measurement of enzyme activity or on determination of compound binding affinity. The main principles used for detection in activity assays are:

- quantification of the formation of reaction by-products such as succinate or formaldehyde via absorption or fluorescence intensity measurement of coupled reaction products or substrates
- Antibody-based recognition of demethylated peptides and subsequent detection using fluorescence, time-resolved fluorescence energy transfer or amplified luminescent proximity via antibody-labelled chromophores
- MS-assisted detection of demethylated peptides or reaction by-products

- Measurement of radioactivity using radiolabelled substrates or co-substrates

For all biochemical assays, the choice of suitable reagents is crucial and some important factors have to be taken into consideration for the development and use of Jmj-KDM assays. As the enzymes are iron/2-oxoglutarate-dependent, a sufficient amount of these factors must be present in solution. However, since most of the inhibitors are at least partially competitive towards 2-OG, concentrations should be kept low and should not be varied between assay runs in order to obtain comparable results. To account for the susceptibility of the catalytic ferrous iron towards oxidation, an antioxidant compatible to the enzyme and not interfering with the assay readout should be added to all samples. Ascorbic acid, which is also believed to support KDM activity *in vivo*,¹¹⁶ was proven to be suitable for this purpose.¹¹⁷ Furthermore, peptide substrates must be chosen according to the respective enzyme's selectivity, as the demethylase activity is not only dependent on the substrate sequence, the methylation degree and site of the targeted methyl lysine, but also on the modifications of adjacent amino acids, especially if enzymes containing reader domains are used in the assay.¹¹⁸

1.3.1 Formaldehyde Dehydrogenase Assay

One of the first protocols developed for the quantification of the demethylation reaction is the formaldehyde dehydrogenase assay. It makes use of the detection of the by-product formaldehyde, which is generated in the demethylation reaction in stoichiometric amounts (as outlined in section 1.2.2.1). For quantification of the formaldehyde formation, a second enzyme – a formaldehyde dehydrogenase (FDH) isolated from *Pseudomonas sp.* – is added to the assay mixture. This enzyme catalyses the oxidation of formaldehyde to formic acid using nicotinamide adenine dinucleotide (NAD⁺) as oxidizing agent. Thereby, a stoichiometric amount of NADH is released, which can be detected via measurement of fluorescence intensity due to

1.3 Assays for JmjC Domain-containing Histone Demethylases

its intrinsic fluorescence properties ($\lambda_{\text{ex}} = 330 \text{ nm}$ and $\lambda_{\text{em}} = 460 \text{ nm}$), which differ from the non-fluorescent NAD^+ as shown in Figure 8. The assay has first been described by Shi *et al.* to study the FAD-dependent histone demethylase LSD1²⁶ and has been adapted to Jmj-KDMs by Couture *et al.*^{26, 117} Further optimizations of the assay protocol by various groups, notably by Sakurai *et al.*,¹¹⁹ facilitated the simplification, miniaturization and applicability to high-throughput screening. The FDH assay has also been established for KDM4A in our group¹²⁰ and was used for the characterisation of some compounds described in this work. The detailed assay setup and experimental conditions can be found in section 3.1.1 and the experimental section.

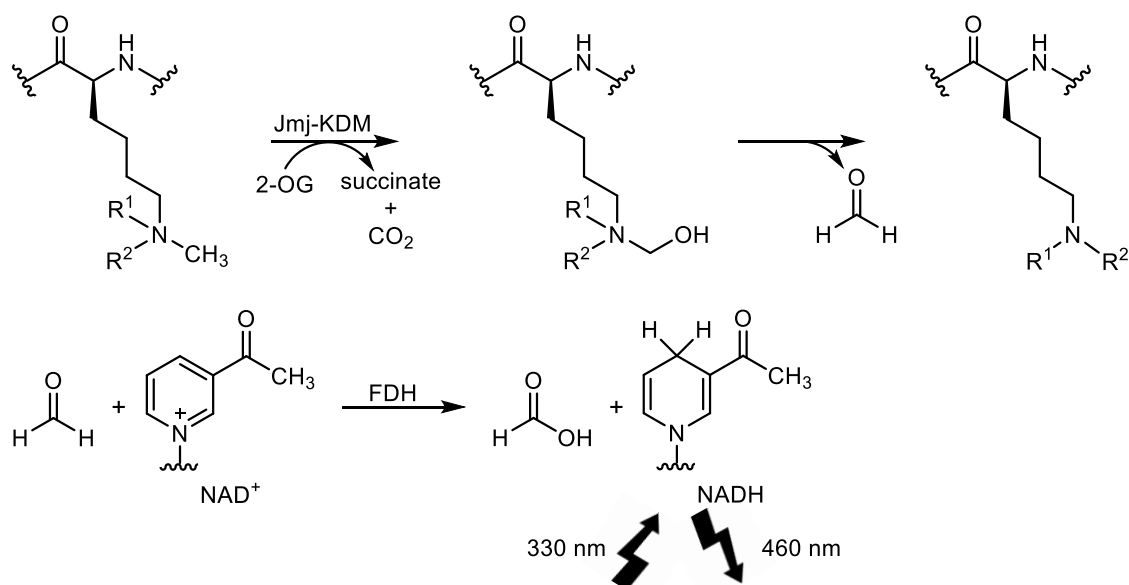


Figure 8 Schematic principle of the formaldehyde dehydrogenase-based assay (FDH assay). Demethylation of the methylated peptide releases a stoichiometric amount of formaldehyde, which is converted to formic acid by FDH concomitantly generating NADH. NADH is detected via its fluorescence properties.

The assay can be used for real-time kinetic measurements, because the FDH reaction does not interfere with the demethylase and FDH can therefore be added to the assay mixture at the start. Furthermore, the formaldehyde oxidation is quite fast making the demethylase reaction the rate-determining step.¹²⁰ The fluorescence signal recorded immediately after addition of the reagents can be used to identify auto-fluorescent compounds that interfere with the assay readout.¹¹⁹ Additionally,

a counter-screen assay using only FDH and formaldehyde or an orthogonal KDM assay should be performed in order to eliminate false positive results that stem from FDH inhibition instead of KDM inhibition.

1.3.2 Other Assays based on Formaldehyde Quantification

An alternative to enzymatic conversion by FDH is the addition of reagents that spontaneously react with formaldehyde and yield a coloured and/or fluorescent product. One versatile reaction is the Hantzsch dihydropyridine cyclisation of formaldehyde, acetoacetanilide, and ammonia. The product can be detected via fluorescence measurement ($\lambda_{\text{ex}} = 370 \text{ nm}$ and $\lambda_{\text{em}} = 470 \text{ nm}$; cf. Figure 9a).¹²¹ This assay was published for a screen of organic iridium(III)-complexes as putative inhibitors of KDM4D.¹²²

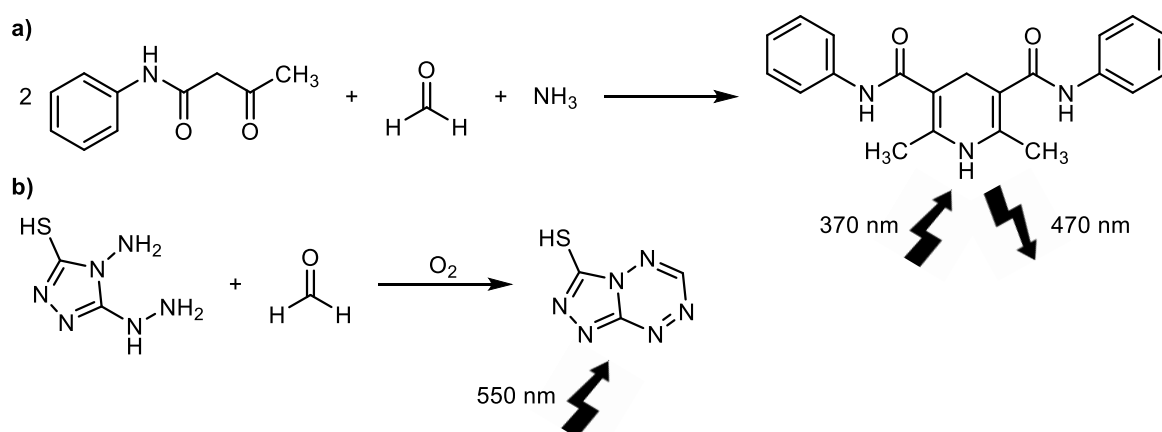


Figure 9 Detection reactions of chemical formaldehyde-based assays.

- Hantzsch dihydropyridine cyclisation of formaldehyde, acetoacetanilide, and ammonia generates a fluorescent product.
- Cyclisation and ambient air oxidation of formaldehyde with the commercial Purpald® reagent yields a strongly absorbing product.

The commercial reagent Purpald® (4-amino-3-hydrazino-5-mercapto-1,2,4-triazole, cf. Figure 9b) can also be used as formaldehyde sensor. The product of the reaction with formaldehyde is oxidized by ambient oxygen yielding a chromogenic product ($\lambda_{\text{abs}} = 550 \text{ nm}$).¹²³ However, as is the case for most homogenous colorimetric assays, assay reagents absorbing light in the same range as the product cause high background noise and quantification may additionally be impeded by the presence

of coloured test compounds. To circumvent these shortcomings, Wang *et al.* developed a demethylase assay based on surface enhanced Raman scattering spectroscopy (SERS). In this assay, the chromogenic oxidation product of the Purpald® reaction is covalently bound to the surface of peptide-coated gold nanoparticles thereby modifying their Raman emission profile, which is used as assay readout. This homogenous assay yields low background signals and prevents interference with coloured test compounds. However, quantification may still be hampered by thiol-reactive compounds that react with the Purpald® reagent or the chromogenic product or by compounds that bind to the gold nanoparticles.¹²⁴

1.3.3 Antibody-based Assays

Instead of detecting the formaldehyde generated by the demethylase reaction, it is also possible to quantitate the peptide substrate, either the methylated substrate or the demethylated product. Peptides can be recognised by specific antibodies. Obviously, binding affinity of the antibodies must allow the discrimination between the methylated and demethylated peptide. Therefore, careful antibody selection must be performed, as the methyl group is a rather small moiety not altering the positive charge of the lysine residue. For detection, common assay formats using labelled antibodies such as enzyme-linked immunosorbent assays (ELISAs), amplified luminescent proximity homogeneous assays (e.g. AlphaScreen™ and AlphaLISA™; PerkinElmer) or Förster resonance energy transfer assays (FRET assays) can be applied.

1.3.3.1 ELISA and AlphaScreen™

In classical ELISA measurements the target of interest is immobilized on a surface using a specific antibody. Readout depends on the use of a detection antibody, which either binds to the target directly or to a primary antibody bound to the target. The detection antibody is tagged with an enzyme capable of transforming a

reagent into a coloured or fluorescent reaction product, which can be quantified after a washing step to remove unbound antibodies. For KDM assays, instead of a primary antibody, usually a biotinylated peptidic substrate, which can be immobilized on streptavidin-coated surfaces, and a labelled antibody recognising the distinct methylation site and degree are used. An example for an ELISA-based KDM assay was used for a screen of natural products by Nielsen *et al.*¹²⁵ In order to simplify the procedure and omit washing steps, homogenous assay formats such as the commercial AlphaScreen™ and AlphaLISA™ (PerkinElmer) can be employed.¹²⁶ Here, the biotinylated peptide is immobilized on donor beads, which are additionally coated with a photosensitizer that releases singlet oxygen upon excitation with light ($\lambda_{\text{ex}} = 680 \text{ nm}$). The antibody is bound to acceptor beads coated with a chemiluminescent cascade, which emits light upon reaction with singlet oxygen ($\lambda_{\text{em}} = 520\text{--}620 \text{ nm}$ for AlphaScreen™, $\lambda_{\text{em}} = 615 \text{ nm}$ for AlphaLISA™).¹²⁷ Due to the short lifetime of singlet oxygen, emission only occurs when donor and acceptor beads are in close proximity, which is the case when the antibody is bound to the respective peptidic substrate (cf. Figure 10).

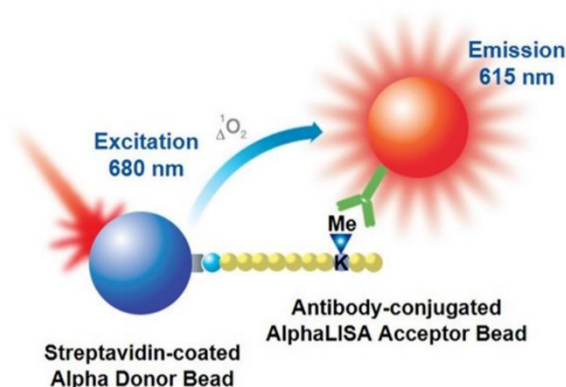


Figure 10 Schematic representation of the AlphaLISA™ principle. The biotinylated peptide is bound to a donor bead coated with detection reagent generating singlet oxygen upon excitation. A distinct methylation state is recognised by the antibodies on the acceptor bead, which emits light upon reaction with singlet oxygen. (Modified from Ref. 130).

This assay format has been adapted to various KDM subtypes and has been used extensively for the identification and characterisation of KDM inhibitors for example for the crop protectant daminozide **9** and macrocyclic peptides.^{128, 129} A main disadvantage of the assay setup is the possible interference with compounds

acting as singlet oxygen quenchers and thereby disrupting the signal transfer from the donor to the acceptor beads.

1.3.3.2 FRET-assays

Another possibility to use the proximity of adequately coated donor and acceptor beads as assay readout is the use of the FRET-Effect. To this end, the beads are coated with a pair of fluorophores with overlapping excitation and emission wavelengths. Upon excitation, the donor fluorophore emits energy, which is absorbed by the acceptor fluorophore, if the distance between them is less than 10 nm, resulting in the emission of light.¹³¹ In order to minimize compound interference, a donor with a stable excitation state and long emission lifetime, for example a europium(III) chelate ($\lambda_{\text{ex}} = 320\text{-}340\text{ nm}$, cf. Figure 11), can be used.

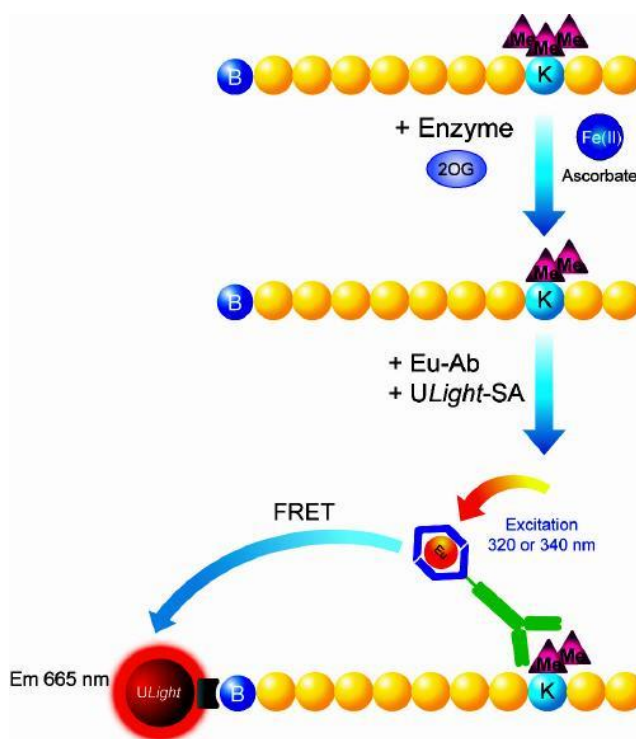


Figure 11 Schematic representation of the LANCEUltra® assay. After demethylation by a KDM the demethylated peptide is recognised by a specific europium-labelled antibody. The biotinylated peptide is bound to an acceptor bead coated with a FRET acceptor. Upon excitation of the europium chelate emission of the acceptor bead can be recorded. (Modified from Ref. 135).

Advantageously, the TR-FRET effect with europium and a suitable acceptor (e.g. allophycocyanin; $\lambda_{em} = 650\text{ nm}$) reduces interference by auto-fluorescent compounds because of the high difference between donor and acceptor excitation and emission wavelengths, which is unlikely to occur as Stokes shift in a single compound. Secondly, the long lifetime of the europium excited state allows for a time-delayed measurement after 100-200 μs after excitation, by which compound fluorescence has usually already decayed.¹³² Due to the very low background signal and high sensitivity of the method the assay requires very low enzyme and substrate concentrations (cf. section 3.2.1). However, compounds showing strong absorption at 320-340 nm may reduce europium excitation and thereby diminish the fluorescence signal. This effect can be corrected by additionally measuring europium emission ($\lambda_{em} = 615\text{ nm}$) and forming the ratio between acceptor fluorophore and europium emission. The TR-FRET technology has been commercially realized in the LANCE® and LANCEUltra® assay systems by PerkinElmer.¹³³ The assay was published by PerkinElmer for the screening of LSD1 inhibitors and later also adapted to other KDMs.^{133, 134} In our group, the LANCEUltra® assay has been established for KDM4A, KDM5A and KDM6B¹²⁰ and the KDM4A assay was used for the screening and characterisation of the compounds described in this work. The detailed assay setup and experimental conditions can be found in section 3.2.1 and the experimental section.

Another application of the TR-FRET effect using europium chelates is the dissociation-enhanced lanthanide fluorescence immunoassay (DELFIA®; PerkinElmer).¹³⁶ Similar to the ELISA format described in Section 1.3.3.1, the biotinylated peptide is immobilized on the well surface and the europium-tagged methyl-specific antibody is added after the enzymatic reaction. After washing off the unbound antibodies, the europium complex is dissociated from the antibody chelate via addition of a suitable detection reagent and incorporated into a micellar system to enhance its fluorescence intensity. As the assay is performed in a heterogenous fashion containing several washing steps, compound or matrix

interference is minimized making the assay especially useful for the analysis of complex samples such as cell lysates or tissue homogenates.¹³⁶ The DELFIA® assay has been described for the development of the KDM4 inhibitor prodrug methylstat **10b**.¹³⁷

1.3.4 Mass spectrometry-based Assays

To avoid the drawbacks of the previously described assays based on UV/Vis-measurements a different approach can be taken via mass-spectrometry based assays. MS-assays are suitable to detect the change in molar mass which is caused by the demethylation of the peptide substrate and corresponds to the loss of 14 units per methyl group. Therefore, MS assays can be used to easily distinguish between different methylation states and are useful for the screening of different peptides to determine the selectivity of certain demethylases towards their respective substrates. For example, the conversion of H3K27me₃ and H3K27me₂ substrates in addition to the known H3K9me_{3/2} substrates by KDM4C and KDM4E was first shown in an MS-based assay.¹³⁸ Originally, matrix assisted laser desorption/ionisation (MALDI) assays with a rather limited throughput were used¹³⁸ until a much faster assay technique, namely the RapidFire® system, was developed for the use with histone demethylases in 2012. The RapidFire® assay uses an automated electrospray ionisation (ESI) approach which allowed a sampling time of 7 s per well.¹³⁹ A multiplexing approach using pooled mass-tagged substrates was employed to further shorten the analysis time, therefore making the MS-based assay amenable to high-throughput screening.¹⁴⁰

Another high-throughput assay published by Wigle *et al.* in 2015¹⁴¹ uses self-assembled monolayer desorption/ionization (SAMDI) mass spectrometry, a technique where peptides are immobilized on the assay plate in a monolayer via biotin-neutravidin interactions after the demethylase reaction. Samples are rapidly purified by a simple washing step, omitting time consuming chromatographic

purification which is necessary in ESI-based approaches, before they are transferred to the mass spectrometer and analysed via MALDI-TOF-TOF. This assay could be miniaturized to a 384-well format and allowed short analysis times of 20 min per plate making it even faster than the non-tagged RapidFire® assay.¹⁴¹

1.3.5 Assays based on Radiometric Detection

One of the first assays to evaluate the demethylation catalysed by JmjC-KDMs was introduced by Tsukada *et al.* in 2006. They used tritium-labelled nucleosomal histone substrates and cellular extracts containing Jmj-KDMs. The histone demethylation generated tritiated formaldehyde, which could be detected after conversion to radioactive 3,5-diacetyl-1,4-dihydrolutidine, which was extracted and counted.²⁷

A second assay based on radioactivity is the scintillation proximity assay developed by Yu *et al.* Here, peptide substrates were demethylated by KDMs and remethylated in a second step by a protein methyltransferase, which used a tritium-labelled S-adenosyl methionine (SAM) co-substrate. The generated radiolabelled peptides were bound to a special assay plate and the scintillation was measured after a washing step. Based on the amount of remethylation, demethylase activity could be assessed.¹⁴²

1.3.6 Affinity-based Assays

All assays described above rely on the measurement of enzymatic activity of the respective KDM. As a prerequisite for activity assays, optimal enzyme activity should be ensured by choice of suitable assay conditions. However, this also leads to a main drawback of activity assays: their susceptibility towards small changes in the assay setup. This is especially problematic for the comparison of assay results originating from different assays. Even if the same detection technique and assay components are chosen, results obtained from different measurements may vary

1.3 Assays for JmjC Domain-containing Histone Demethylases

dependent on factors that are difficult to control. Besides the inter-assay comparability for one target, a second issue is the comparison of results for different enzyme subtypes or isoforms, which are necessary for the assessment of inhibitor selectivity. As the different enzymes usually require different conditions to gain maximal enzyme stability and activity it is nearly impossible to create identical assays for different enzymes. One strategy to tackle this problem is the use of well-characterised reference inhibitors to which the results of new inhibitors can be normalized. A conceptionally different approach is the determination of the binding affinity of the target molecule towards the protein of interest instead of the activity. As high enzyme activity is not essential for this kind of assay, it may be simpler to find assay conditions that are suitable for different enzyme subtypes and thereby increase comparability of assay results. Furthermore, affinity assays allow for the calculation of binding constants that are largely independent from assay parameters such as enzyme, substrate or co-substrate concentration.¹⁴³ Nevertheless, binding constants still rely on the assay conditions such as buffer composition, etc. and should therefore be given as apparent values.

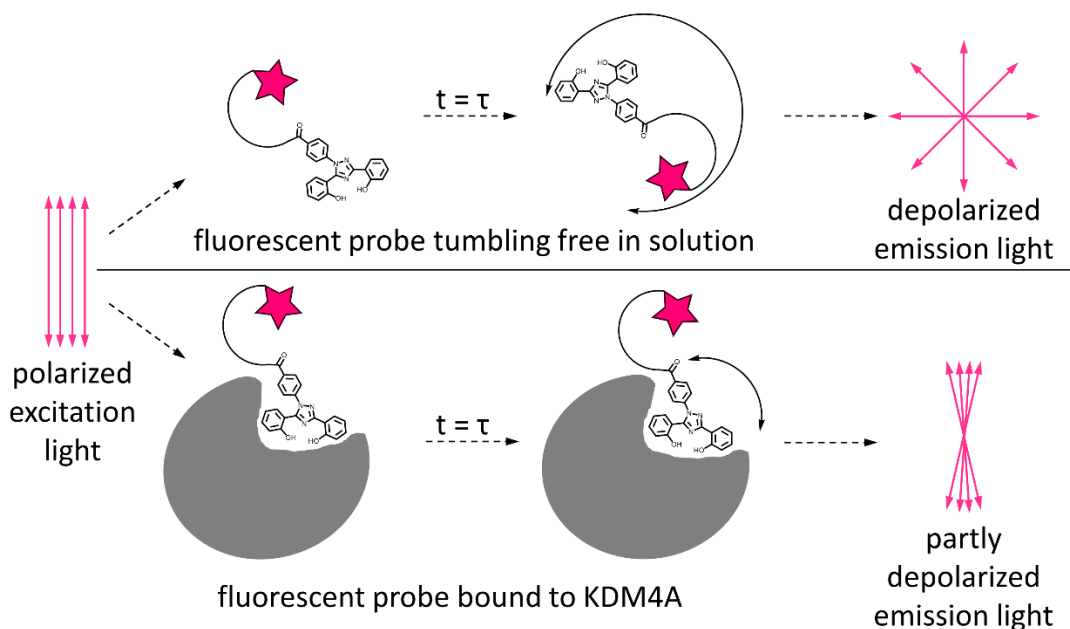


Figure 12 Schematic representation of the assay principle of competitive fluorescence polarization assays.

1 Introduction

One versatile method of determining binding of a small ligand to a protein is the measurement of fluorescence polarization (FP). FP assays are based on the observation that a fluorophore which is excited with linearly polarized light will also emit linearly polarized light. However, in solution, fluorophores are able to rotate freely and therefore move while in the excited state. Consequently, the fluorophore emits the light from a different orientation than when it absorbed it and polarization is lost. Yet, the degree of depolarization depends on the rotation velocity, which is mainly dependent on molecular size. For large molecules such as proteins rotation is rather slow, thus the polarization remains rather strong. On the other hand, small molecules such as low molecular ligands will cause large depolarization. This phenomenon can be used for binding assays when the ligand is tagged with a fluorophore. As long as the ligand is in solution it will tumble freely and therefore measured light will be depolarized, but as soon as the ligand can bind to the protein its rotation will be hindered resulting in a larger portion of emitted polarized light. Binding of unlabelled ligands can be determined via competition with a labelled ligand (cf. Figure 12) resulting in an increase of depolarization upon binding of the unlabelled ligand.

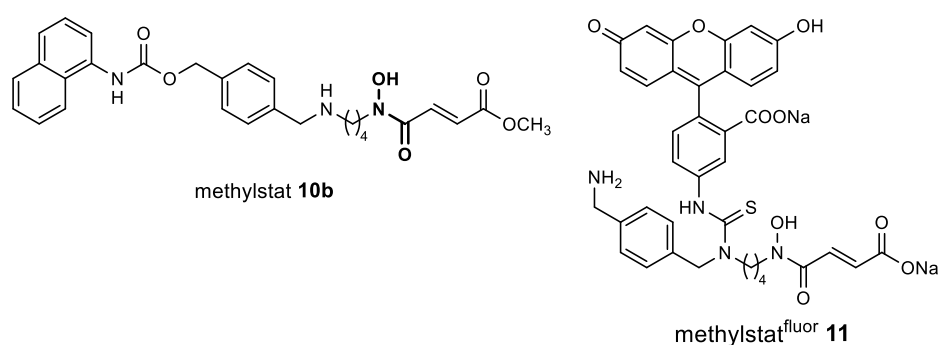


Figure 13 Chemical structures of the KDM inhibitor prodrug methylstat and the derived fluorescent probe.¹⁴⁴

This strategy has been employed in a binding assay for Jmj-KDMs. A derivative of the known KDM inhibitor prodrug methylstat (cf. section 1.4.2.6) was coupled to a fluorescein moiety (cf. Figure 13) to obtain the ligand **11** with micromolar inhibitory potency in an activity-based assay ($IC_{50} = 0.9 \mu M$ against KDM2A, determined in a DELFIA[®]-based assay) and high binding affinity ($K_d = 9.3 nM$ on KDM2A). A

1.3 Assays for JmjC Domain-containing Histone Demethylases

competitive binding assay was developed, where the enzyme of interest (e.g. KDM2A) was preincubated with Ni^{2+} , which is inert towards oxidation, as a stable replacement for Fe^{2+} , as well as with the inhibitor intended for evaluation. Then, the fluorescent methylstat probe **11** was added and fluorescence polarization was recorded after a sufficient incubation time.¹⁴⁴

Although based on fluorescence measurement, the assay is not prone to assay interference by auto-fluorescent inhibitors, because depolarization can still be observed when the fluorescent probe is displaced from the enzyme. Corrective calculations have to be performed for exact quantification in those cases, though. However, interference is possible with compounds that are able to extract the central nickel ion from the enzyme. This would lead to dissociation of the probe and therefore mimic competitive displacement. Furthermore, enzyme inhibitors that employ a different mode of action than co-substrate competition, such as substrate replacement, are possibly not able to displace the fluorescent probe from the active site and would therefore appear as false negatives. Nonetheless, the binding assay yields a good orthogonal assay principle for the high-throughput screening of potential inhibitors as well as for further characterization of hits found in other assay formats. The FP-assay has been used for screening of the HitFinder collection containing 14,400 compounds and identified two unselective novel KDM inhibitor scaffolds.¹⁴⁵

A different binding assay was realized via nondenaturing electrospray ionization mass spectrometry (ESI-MS) of the KDM4E protein to assess stoichiometry and binding strength of compounds towards KDM4E. As binding of inhibitors to metalloenzymes is usually rather strong the complex is stable during the solution-to-gas phase transition occurring in ESI-MS. Consequently, the binding event can be detected via a mass shift corresponding to the mass of the bound inhibitor. This allows assessment of the binding stoichiometry, however, further assays to confirm active-site binding versus binding on the surface or to other irrelevant pockets of

the enzyme or orthogonal assays to show enzyme activity inhibition should be performed.¹⁴⁶

In conclusion, numerous assays for the screening and characterization of KDM inhibitors based on different mechanisms ranging from fluorescence-based activity assays over MS-based assays to affinity assays are available to date. They all have certain advantages and disadvantages and can also result in different false positive and negative results. A combination of techniques is therefore recommended in order to identify as many inhibitors as possible minimizing false negative results while confirming positive hits with orthogonal assays to rule out compound interference.

1.4 Inhibitors

Owing to their universal role in diverse biological functions and their implication in numerous diseases a great effort to develop potent inhibitors of certain Jmj-KDMs has been undertaken and a variety of inhibitors, ranging from micromolar to low nanomolar potency of unselective to subtype-selective compounds, have been published to date. The great majority of Jmj-KDM inhibitors present in literature are active-site binding inhibitors that are mainly competitive towards the co-substrate 2-OG **8**. Some are additionally or exclusively competitive towards the peptide substrate. Other postulated mechanisms include zinc ejection of a structural zinc ion and oxygen displacement from the catalytic centre. The following sections give an overview of the inhibitors known to literature, which have also been extensively reviewed in recent publications, the most recent comprehensive review also covering potential therapeutic applications being Ref. 52 by Arifuzzaman *et al.*^{52, 132,}

147-156

1.4.1 Concept of Prodrugs and Bioisosteres

Owing to the fact that many of the inhibitors described in the following sections contain one or more carboxylic acid moieties some general characteristics, definitions and their use in drug molecules will be discussed first. Carboxylic acids are trigonal planar structures due to the sp^2 hybridization of the central carbon atom. They contain a hydrogen bond acceptor, namely the carbonyl oxygen as well as the hydroxy group, which acts as a hydrogen bond donor at low pH-values and as acceptor when deprotonated at high pH-values. These moieties allow strong interactions with a variety of functional groups such as basic amino acid residues like lysine. The pK_a values of carboxylic acids typically cover a range of 3-6, therefore they are mostly deprotonated at physiologic pH, the negative charge being equally distributed over the two oxygen atoms. Due to the high polarity and negative charge cellular permeability of carboxylic acid-containing compounds may be – depending on the overall structure – rather low.¹⁵⁷ One strategy to overcome this shortcoming is the introduction of protective groups masking the charge of the carboxylic acid and its hydrogen bonding ability and thereby increase cellular permeability. The active compound may then be released intracellularly e.g. via enzymatic cleavage or spontaneous decomposition. This approach is called prodrug concept, where prodrugs are defined as pharmacologically inactive compounds that release the active parent drug upon chemical or enzymatic activation.¹⁵⁸ If the main purpose of the prodrug is to increase cellular permeability, however, it is insignificant if the prodrug itself also displays pharmacologic activity. The most commonly employed prodrug moiety for carboxylic acids is the respective methyl ester due to its simplicity, both in terms of synthesis as well as in molecular structure, and its high cleavability by endogenous esterases. For polar drugs, more lipophilic moieties such as ethyl, *tert*-butyl or octyl esters can be employed. If enzymatic cleavage and drug release is unsatisfactory a two-step deprotection including enzymatic cleavage followed by spontaneous decomposition using

moieties such as pivaloyl esters may be amenable.¹⁵⁹ The prodrug approach has been applied for several KDM inhibitors using methyl, ethyl and octyl esters (cf. section 1.4.2.).^{137, 160-165}

The second strategy is to exchange the carboxylic acid with a functional group sharing some similar features but displaying more favourable properties for the intended use. Such moieties, exhibiting similar volume, shape, physiochemical properties and, most importantly, similar biological effects are called bioisosteres.¹⁶⁶ Due to the frequent occurrence of carboxylic acids in bioactive molecules bioisosteres have been widely studied and have recently been reviewed in Ref. 157 by Ballatore *et al.* One prominent example is the tetrazole moiety, which shares the planar structure as well as the electronic structure, the pK_a range, and the single negative charge at physiologic pH with carboxylic acids. However, tetrazoles are more lipophilic and may therefore improve cellular permeability. Additionally, the distinct properties, such as the slightly larger size compared to carboxylic acids and the ability to form *1H*- and *2H*-tautomers may improve enzyme binding or target selectivity in some cases. The use of tetrazoles as bioisosteres in KDM inhibitors is described in sections 1.4.2 and 4.2.3.¹⁶⁷

1.4.2 Co-Substrate Analogs/Iron-binding Inhibitors

As described in section 1.2.2.1 the co-substrate 2-OG is bound to the enzyme via electrostatic interactions of the terminal carboxylic acid with a basic amino acid, and hydrogen bonds to alcoholic, phenolic and/or amide residues. The main interaction proceeds via chelation of the active-site iron by the 1-carboxy and 2-oxo groups. Therefore, most co-substrate analogs contain an iron-binding moiety to mimic this interaction. In order to put emphasis on the iron-binding motif it is depicted in bold in all figures of this section. However, care must be taken when evaluating those iron-binding compounds in *in vitro* enzyme activity assays, because it may be difficult to distinguish between active-site binding and iron-chelation in solution.

Binding of iron in solution limits the amount of iron available for enzyme binding and may thereby lead to iron removal from the active site. Even using an excess of iron in the buffer does not compensate the iron-chelation of compounds completely. As the ferrous iron is essential for catalytic activity, iron sequestration leads to enzyme inactivation. However, this indirect inactivation may not be of great biological significance as intracellular iron concentrations vary due to a dependency on diverse factors such as the presence of iron-regulating enzymes and may not be well represented in *in vitro* assays. Consequently, assay techniques able to differentiate between iron sequestration and active-site based inhibition should be applied for the validation of primary assay hits to verify active-site based inhibition. Examples are kinetic measurements showing competitiveness towards the co-substrate, biophysical binding measurements such as surface plasmon resonance (SPR), as well as NMR and MS analysis of the binding event. A variety of applicable methods can be found in a publication by Roatsch *et al.* describing the elucidation of the inhibitory mode of action for the clinically used iron chelator deferasirox against KDM4A.¹⁶⁸

1.4.2.1 Close 2-oxoglutarate Analogs

The first described inhibitor of Jmj-KDMs is the 2-OG mimic *N*-oxalylglycine (**12**) (NOG; cf. Figure 14), a metabolite also naturally occurring in rhubarb and spinach leaves,¹⁶⁹ where carbon 3 of 2-OG is substituted with an NH group. This modification inhibits enzymatic cleavage into carbon dioxide and succinate therefore providing a stable co-substrate mimic. This compound, a known inhibitor for 2-OG-dependent hydroxylases such as the prolyl hydroxylases PHD1-3, was first shown to inhibit KDM4E in an FDH-based assay with an IC₅₀ of 24 μ M by Rose *et al.*¹⁷⁰ It is not subtype selective also inhibiting other Jmj-KDMs although with a varying potency range. Crystal structures have shown a binding mode similar to 2-OG suggesting competitive inhibition, where the non-cleavable NOG (**12**) blocks

1 Introduction

the catalytic pocket.¹⁷¹ However, the low selectivity against other 2-OG-dependent dioxygenases and its low cellular permeability limit the applicability of NOG (**12**) for cellular studies and (pre-)clinical applications. Cellular permeability may be enhanced by masking the two carboxylic acids as methyl esters to decrease the molecular charge (cf. section 1.4.1 for prodrug approaches). Indeed, the resulting dimethyl N-oxalylglycine (**12b**) was shown to exert cellular effects concomitant with 2-OG-dioxygenase inhibition.¹⁷² Approaches to optimize the NOG-scaffold towards higher potency and selectivity used derivatives of oxalylglycine with bulky substituents and non-natural amino acids. However, the dimethylaminophenyl analogue **13**, supposed to employ additional hydrogen bonds to the active site proved to be only slightly active and unselective.¹⁷³ Contrastingly, the D-tyrosine derivative **14** displayed increased potency against KDM4E and some selectivity over PHD2 via addressing an additional hydrophobic subpocket in the vicinity of the active site.¹⁷⁰

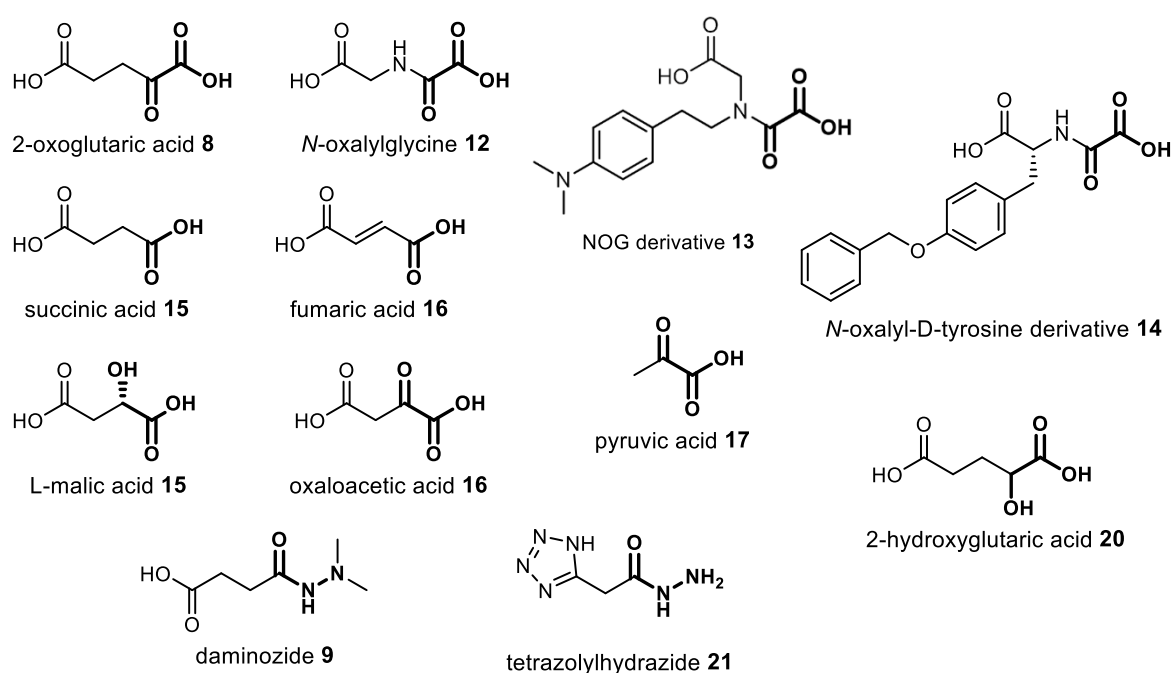


Figure 14 Chemical structure of the co-substrate 2-OG (**8**) and its analogs as Jmj-KDM inhibitors.

A set of metabolites from the primary ch as succinic acid (**15**), fumaric acid (**16**), L-malic acid (**17**), pyruvic acid (**19**) and 2-hydroxyglutaric acid (**20**) were also inst Jmj-KDMs and are

thought to be physiologic regulators of KDM activity. Of these, 2-hydroxyglutaric acid (**20**) is particularly relevant due to its comparably high inhibitory potential and its role as an oncometabolite in gliomas and leukaemias. In the respective cancer cells, it accumulates due to mutations of the isocitrate dehydrogenase IDH2 resulting in pronounced KDM inhibition and hypermethylation. This effect was shown by dysregulation of KDM-controlled genes in respective cancer cells.^{174, 175}

A 2-OG analogue bearing a different iron-binding motif is the plant growth regulator daminozide (**9**). The hydrazide compound displays some selectivity towards KDM2 and KDM7 and may – due to its fragment-like character and its unusual chelating group – be a useful starting point for new inhibitor developments.¹²⁸

Another hydrazide-based fragment-like inhibitor is 2-(1*H*-tetrazol-5-yl)aceto-hydrazide (**21**), which was shown to be a micromolar inhibitor of KDM4A (IC_{50} = 2.4 μ M, determined in a LANCEUltra[®] assay) and even displayed some selectivity over KDM5A (4-fold) and KDM6B (41-fold).¹⁶⁷ Elaboration on this scaffold is described in this work (cf. section 4.2.4).

1.4.2.2 Pyridine-based inhibitors

Another low molecular co-substrate competitor is pyridine-2,4-dicarboxylic acid (2,4-PDCA; **22**; cf. Figure 15), which inhibits Jmj-KDMs with surprisingly high potency (IC_{50} in the single-digit micromolar to nanomolar range). Effective iron chelation is achieved by the pyridine nitrogen and the 2-carboxylic acid, while the 4-carboxylic acid undergoes electrostatic interactions with basic amino acid residues of the enzyme. The molecule inhibits a range of KDMs, with a slight preference for KDMs 4 and 5 (70 fold higher activity on KDM4C compared to KDM6A), and has, also due to its simplicity and high stability, become a standard reference inhibitor for *in vitro* and cellular settings (also as methyl ester prodrug).¹⁶⁰ The slight selectivity for KDMs 4 and 5 motivated the development of 2,4-PDCA

1 Introduction

derivatives employing a higher selectivity for those enzymes. Substitution at carbon 3 proved to be suitable for this purpose. Screening of a series of amino derivatives yielded the fluorophenyl derivative **23**, which displayed comparable potency to 2,4-PDCA on KDMs but yielding higher selectivity over other 2-OG dioxygenases.¹⁷⁶

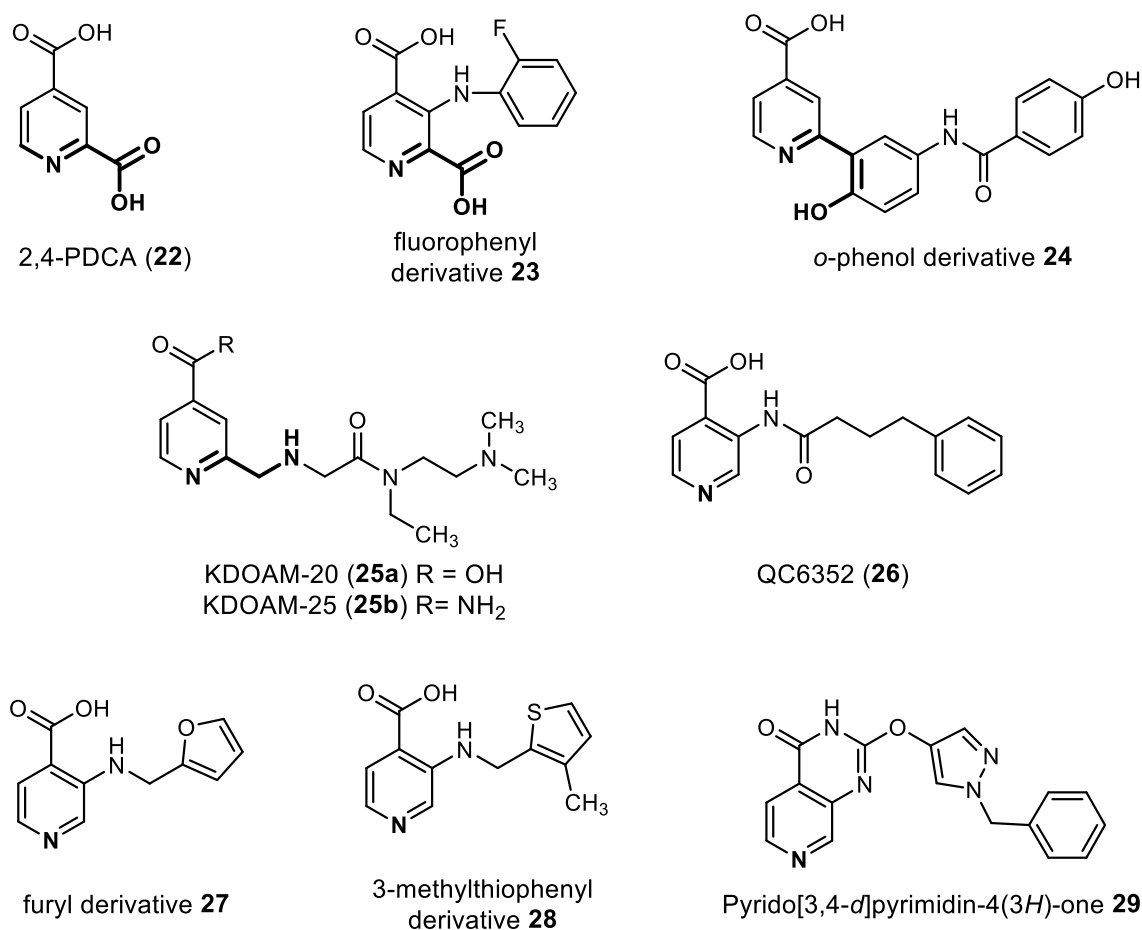


Figure 15 Chemical structures of 2,4-PDCA (**22**) and its analogs as inhibitors of Jmj-KDMs.

The high polarity of 2,4-PDCA derivatives due to the double negative charge at physiologic pH and their concomitant low cellular polarity sparked efforts to develop derivatives with alternative substituents for the 2-carboxylic acid moiety. Efforts went into the direction of replacing the 2-carboxylic acid moiety by other, less polar groups. Replacement with a *p*-substituted *o*-phenol moiety yielded compound **24**, which was found by a fragment docking and linking approach, where 600,000 fragments were docked into KDM4A. Promising fragments were covalently linked and further optimized. The resulting inhibitor showed low micromolar activity against KDM4C ($IC_{50} = 2.6 \mu M$, $K_i = 43 \text{ nM}$, determined in a TR-

FRET assay) and slight selectivity against other KDMs (2-fold against KDM6B, 7-fold against KDM2A).¹⁷⁷ The binding mode determined by crystallography was similar to 2,4-PDCA, although the intramolecular distance of the iron-chelating moieties (pyridine-*N* and phenol or carboxylic acid, respectively) is five atoms instead of four.¹⁷⁷

Synthesis and screening of a library of 2-methylamino derivatives yielded the KDM5-selective inhibitor KDOAM-20 (also termed KDM5-C49; **25a**; IC₅₀ = 7 nM, 25-fold selectivity over KDM4C, determined in an AlphaScreen™ assay). Its amide derivative KDOAM-25 (also termed KDM5-C70, LQT or GTPL-8576; **25b**) was slightly less active but showed increased selectivity (IC₅₀ = 19 nM, > 250-fold selectivity over KDM4C) and high cellular permeability which could be shown by an increase of H3K4me₃ in HeLa cells.¹⁷⁸

In another approach compounds lacking a substituent in position 2 were identified. A high-throughput screening against KDM6B revealed the 4-phenylbutyrate derivative QC6352 (**26**) as a low micromolar inhibitor of KDM4, 5 and 6. The compound shows the same orientation as 2,4-PDCA (**22**) although being only a monodentate iron chelator. Optimization studies uncovered the furyl and 3-methylthiophenyl derivatives **27** and **28**, which displayed even lower IC₅₀ values (IC₅₀ against KDM4 and KDM5 ≤ 0.1 μM, determined in an MS-based assay) and higher selectivity towards other Jmj-KDMs (≥ 50-fold against KDM6B). As intended, these compounds possess high cellular permeability and their on-target effects could be shown in a cellular assay assessing KDM4C inhibition.¹⁷⁹

In an effort to further improve cellular permeability, bicyclic motifs replacing the 4-carboxylic acid yet able to maintain the interaction with basic active-site amino acid residues were screened. Pyrido[3,4-*d*]pyrimidin-4(3*H*)-one derivatives proved to be suitable, as the carbonyl group and the neighbouring NH group can form hydrogen bonds to the relevant lysine and tyrosine residues in KDMs 4 and 5. As intended, the non-charged cyclic structure resulted in higher cellular permeability. Furthermore, the rigidification of the structure and the additional anchor point for

1 Introduction

substitution led to an increased potency of the inhibitor **29**, which displayed excellent inhibitory activity against KDM4 isoforms and KDM5C ($IC_{50} < 1$ nM, determined in a RapidFire® MS assay) and practically no inhibition of related KDMs such as KDM6. Cellular activity in the low micromolar range was shown in cells overexpressing KDM4C or KDM5C. Inhibition was visualized via measurement of hypermethylation using immunofluorescence targeting H3K4me₃ or H3K4me₃, respectively.¹⁸⁰

1.4.2.3 *N,N'*-Biheterocyclic Inhibitors

A further extension of the 2,4-PDCA structure was the combination of the core pyridine with another nitrogen-containing heterocycle in position 2 of the pyridine ring to obtain bidentate iron chelators (cf. Figure 16).

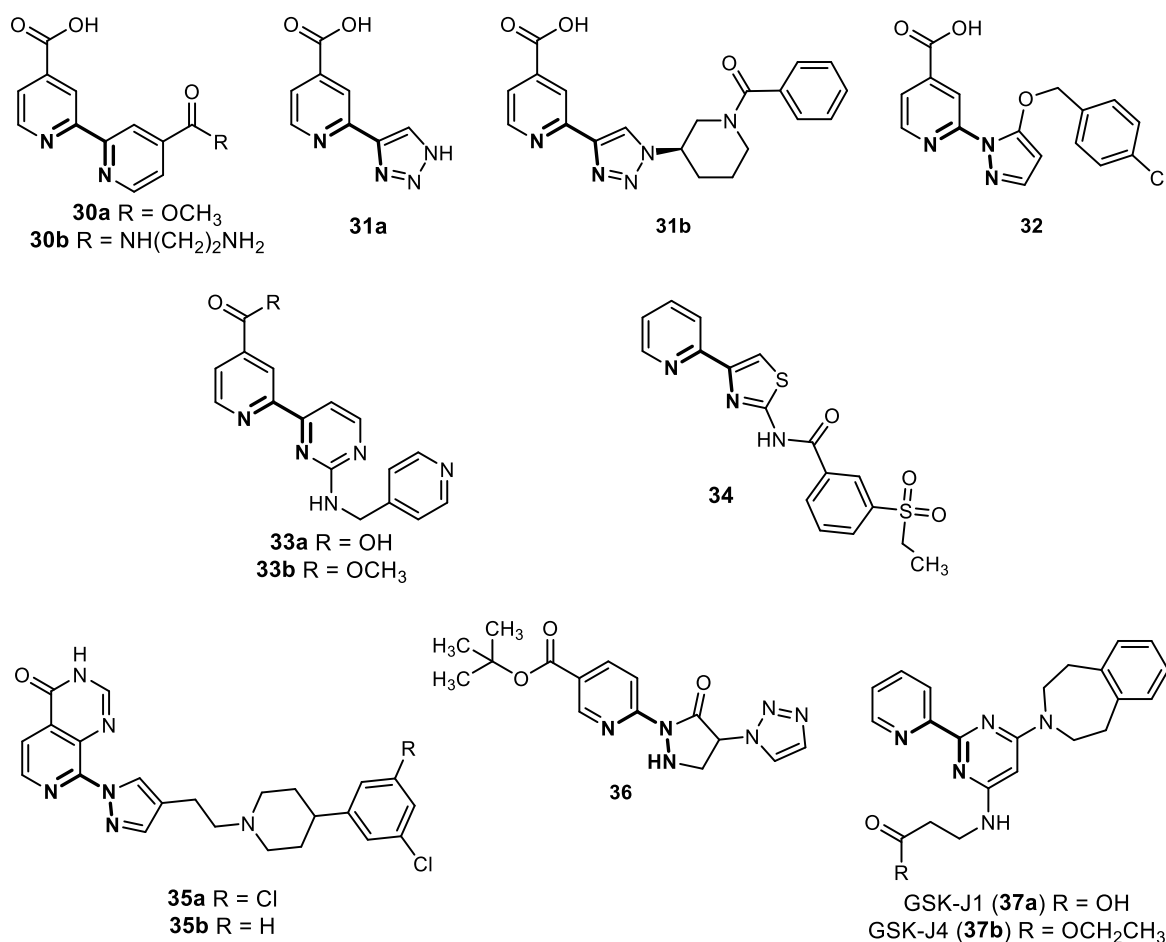


Figure 16 Chemical structures of 2,2'-biheterocyclic inhibitors of Jmj-KDMs.

The close 2,4-PDCA derivative methyl 2,2'-bipyridine-4,4'-dicarboxylate (**30a**) was among the inhibitors discovered in the first KDM4E inhibitor collection of Rose *et al.* and showed moderate activity against KDM4E ($IC_{50} = 24 \mu M$, approx. 5-fold less than 2,4-PDCA, determined in an FDH-based assay).¹⁷⁰ Elaboration of the structure yielded the diaminoethylene derivative **30b** with improved activity ($IC_{50} = 180 nM$), which could be attributed to an additional interaction of the primary amine with an aspartate residue in the active site.¹⁸¹

A set of compounds containing a 1,2,3-triazole moiety were developed in order to improve potency and selectivity for certain KDM subtypes. The simple triazole derivative **31a** showed nanomolar activity on a panel of KDMs and mild selectivity for KDM2/4 ($IC_{50} = 5 nM$ on KDM2A, 4-fold selectivity over KDM3A, determined in an AlphaScreenTM assay). Alteration of the triazole substitution pattern proved to be suitable for fine-tuning of inhibitor selectivity for distinct subtypes. Selectivity for KDM2 could be greatly improved by the addition of a piperidinyl moiety, yielding compound **31b**, which displayed 30-fold selectivity over KDM5C, >100-fold selectivity over KDM4 and was inactive on KDM3A.¹⁸²

Furthermore, a number of diverse compounds possessing the pyridine-2-carboxylic acid or its bioisosteres linked to nitrogen-containing heterocycles have been patented as KDM inhibitors.¹⁸³ A review of these structures is given by McAllister *et al.* and Chin *et al.* in Refs 153 and 183. One example is the use of a substituted pyrazole moiety, disclosed in a patent by Quantice Pharmaceuticals, which yielded the nanomolar inhibitor **32** on KDM4C, KDM5A and KDM5B, whose methyl ester prodrug was active on breast cancer cells via histone H3K4 hypermethylation.¹⁶¹

Another compound series derived from 2,4-PDCA was created based on virtual screening of the ZINC clean drug-like database against KDM4A. It yielded 2-aminopyrimidine compounds bearing different substituents at the amino group. The pyridine derivative **33a** inhibited KDM4A and KDM5B in the submicromolar range ($IC_{50} = 941 nM$ and $442 nM$, respectively, determined in a LANCEUltra[®] assay) with 40-fold selectivity over KDM6B. Its methyl ester prodrug **33b** showed

hypermethylation in an KDM4-overexpressing HeLa cell line and moderate toxicity on the oesophageal cancer cell line KYSE150.¹⁶²

In a high-throughput screen with 150,000 compounds against KDM4C to identify novel structures with high cellular permeability, pyridylaminothiazole **34** was discovered as a micromolar hit. Extensive optimization studies yielded compound **35**, where the thiazole moiety was exchanged by a substituted pyrazole. Additionally, the bicyclic pyrido[3,4-*d*]pyrimidin-4(3*H*)-one **35a** (cf. compound **29** above) was incorporated into the structure as a carboxylic acid bioisostere. Crystallographic studies confirmed the predicted binding mode with bidentate iron chelation of the pyridine-pyrazole motif and hydrogen bonding of the pyridopyrimidin-4-one to lysine 206 and tyrosine 123 in KDM4A. The lipophilic phenylpiperidine substituent addresses the histone peptide binding site thereby adding to the compound affinity to the enzyme. *In vitro* assays revealed high compound potency and selectivity (IC_{50} = 17 nM on KDM4B and 14 nM on KDM5B, > 50-fold selectivity over KDM2A, > 100-fold over KDM3A, determined in an AlphaScreen™ assay) and cellular assays with the related 3-monochlorinated derivative **35b** showed marked H3K9 and H3K4 hypermethylation.¹⁸⁴

An inhibitor bearing a pyrazolone substructure was discovered in a screen for the iron/2-OG-dependent hypoxia-inducible factor prolyl hydroxylases PHD1-3. Compound **36** proved to be not only active on PHD2 in the low nanomolar range but also on KDM6B in the low micromolar range. Interestingly, the structure bears a carboxylate derivative in position 3 of the pyridine as opposed to position 4 usually observed in pyridine-based inhibitors. Additionally, the free carboxylic acid was inactive on KDM6B at 20 μ M while still displaying nanomolecular inhibition of PHD2.

One of the best studied biheterocyclic inhibitors is the pyrimidino-pyridine GSK-J1 (**37a**) published by GlaxoSmithKline in 2013.¹⁶³ It was published as a selective KDM6 inhibitor with an IC_{50} value of 60 nM (determined in an AlphaScreen™ assay) against KDM6B and was later found to also inhibit KDM5 with slightly less potency

(28 nM on KDM6B vs. 170 nM on KDM5B, determined in an AlphaLISA™ assay).¹⁸⁵

Cellular activity was evaluated using the ethyl ester prodrug GSK-J4 (**37b**) and revealed H3K27 hypermethylation consistent with KDM6 inhibition as well as inhibition of KDM4C, KDM5B and KDM6B in the micromolar range.^{163, 185} Taken together, these data suggest that the primarily reported high selectivity for KDM6 cannot be fully reproduced in different *in vitro* and *in vivo* studies, therefore caution should be taken when evaluating cellular effects in disease models and associating effects with single targets. Crystallographic data on GSK-J1 (**37a**) shows bidentate chelation of iron by the pyrimidino-pyridine moiety inducing a unique metal-shift as well as binding of the tetrahydrobenzazepine group to the histone peptide binding site by mimicking a proline residue.¹⁶³ Attempts to improve potency and selectivity of GSK-J1 (**37a**) by replacing the pyridine ring with thiazole, pyrazole, or triazole groups and the tetrahydrobenzazepine unit with diverse hydrophobic residues did not yield promising compounds but may give further insights for other structure-based KDM inhibitor developments.¹⁸⁶

1.4.2.4 Catechol-based inhibitors

One of the first systematic screens for Jmj-KDM inhibitors was performed by Sakurai *et al.*, who had managed to miniaturize the FDH-coupled KDM assay (cf. section 1.3.1).¹¹⁹ They screened a library of natural products which yielded various catechol derivatives able to bind to iron via the 1,2-diphenol group. Exemplary structures are (*S*)-carbidopa (**38**), dopamine (**39**), and β -lapachone (**40**). Representative compounds of the set are depicted in Figure 17.

The compounds inhibited KDM4 in the low micromolar range and their inhibitory activity was confirmed in an MS-based assay.¹¹⁹ Similar compounds, including caffeic acid (**41**), were found in an antibody-based assay for KDM4C and KDM6B.¹²⁵

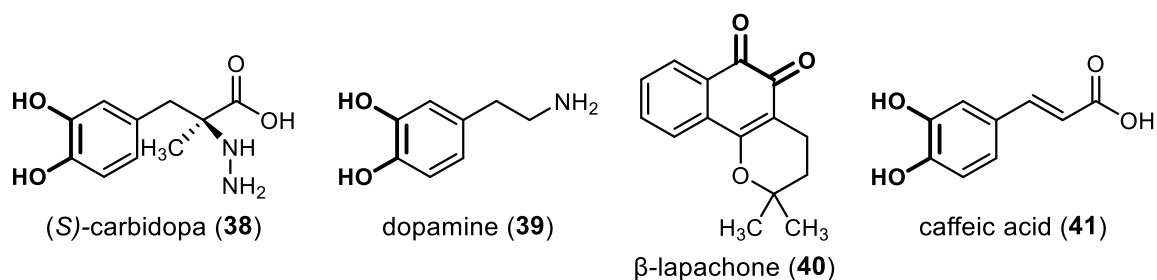


Figure 17 Chemical structures of catechol-based inhibitors of Jmj-KDMs.

However, all these compounds are known to elicit pleiotropic biologic functions and for many of them much higher activity on other targets has been shown in various *in vitro* and *in vivo* assays. Therefore, no efforts to develop these molecules into more potent and selective KDM inhibitors have been reported. Nonetheless, their inhibitory potential for Jmj-KDMs should be kept in mind when evaluating their activity in cellular or more complex biologic systems depending on the analysed effects.

1.4.2.5 Hydroxyquinoline-based inhibitors

The same assay used for the natural product library described above was also used to screen a diverse library consisting of 236,000 compounds.¹⁶⁴ This campaign yielded 8-hydroxyquinolines such as 5-carboxy-8-hydroxyquinoline (**42**; also called IOX1; cf. Figure 18) as new iron-chelating inhibitors of KDMs (IC_{50} (IOX1) = 0.2 μ M against KDM4E). Similar to 2,4-PDCA, the ring nitrogen and the adjacent hydroxy group bind to iron while the carboxylic acid undergoes ionic interactions with a basic amino acid residue in the active site (lysine 206 in the case of KDM4A).

Moderate cellular activity could be shown for IOX1 (**42**), which was greatly improved by using an octylester prodrug with enhanced cellular permeability. While IOX1 (**42**) is relatively unselective, KDM4 selectivity could be achieved via substitution in position 7 of the quinoline ring. The derivative **43** bearing a methylthiophene and a benzamide moiety showed 5 μ M-inhibition against KDM4C and KDM4E with greater than 20-fold selectivity over KDM6B. Increased H3K9me₃ levels were shown in HeLa cells overexpressing KDM4A.¹⁶⁴ Substitution in position

6 also gave KDM4-selective inhibitors, such as compound **44**, which inhibited KDM4 in the nanomolar range ($IC_{50} = 10$ nM against KDM4B, determined in an antibody-based fluorometric assay) while displaying negligible activity against KDM5A. This inhibitor was not only tested in cellular models, where its on-target effects and effectiveness against prostate cancer cell lines could be proven, but even went into animal studies in a prostate cancer model. There, it inhibited tumour growth via suppression of AR-regulated genes again underpinning the importance of the involvement of KDM4 in prostate cancer via the AR-pathway. As proof of concept siRNA knockdown of KDM4B was performed, which lead to results similar to enzyme inhibition with **44**.⁹⁵

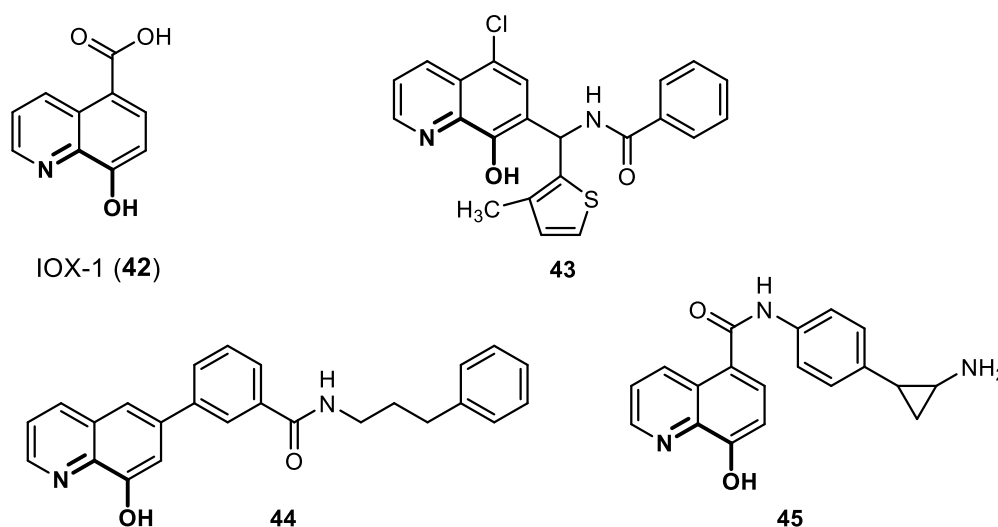


Figure 18 Chemical structures of 8-hydroxyquinoline-based inhibitors of Jmj-KDMs.

Another use of the IOX1 moiety was the incorporation into a biotin-tagged photoreactive probe (structure not shown) which allows linking of the probe to 2-OG-dependent dioxygenases e.g. in cellular extracts and their isolation via affinity purification using a streptavidin matrix. Thereby, it may be used for protein profiling and substrate identification.¹⁸⁷

IOX1 (**42**) and the bicyclic 2,4-PDCA analogue **30a** have also been used in the design of dual Jmj-KDM/LSD1 inhibitors, where each of the moieties have been coupled to the LSD inhibitor tranilcypromine. The resulting pan-KDM inhibitors (e.g.

compound **45**) showed increased hypermethylation in HeLa cells and induced cytotoxicity in the prostate cancer cell line LNCaP.¹⁸⁸

1.4.2.6 Hydroxamate-based inhibitors

A different well-known metal-binding group and therefore a promising motif for Jmj-KDM inhibitors is the hydroxamic acid motif. Indeed, the first inhibitor screen by Rose *et al.* also contained some hydroxamates, such as the HDAC inhibitors trichostatin A (TSA; **46**) and suberoylanilide hydroxamic acid (SAHA, vorinostat; **3**; cf. Figure 19). Both displayed micromolar inhibition ($IC_{50} = 28 \mu M$ and $14 \mu M$ against KDM4E, respectively, determined in an FDH-based assay). Despite their known activity on different targets, these structures provide a valuable starting point for more selective inhibitors, if selectivity-inducing substituents that impair binding to other targets can be identified.

The co-substrate-competitive hydroxamate **47** bearing a propanoate side-chain to mimic the 5-carboxylate residue of 2-OG and a hydrophobically linked dimethylamino group to emulate the lysine substrate was found to be a potent inhibitor of KDM4A and KDM4C with >100-fold selectivity over the iron/2-OG dioxygenase PHD2. Its methyl ester prodrug was shown to inhibit the growth of cancer cell lines in combination with LSD1 inhibitors and was therefore the first hydroxamate-based Jmj-KDM inhibitor displaying cellular activity.¹⁶⁵

Based on a crystal structure of KDM7B, the same group attempted to shift selectivity towards this enzyme by optimizing the hydrophobic side chain. By exchanging the dimethylamino moiety with a cyclopropyl residue they succeeded in generating the inhibitor **48** displaying potent inhibition of KDM7A, KDM7B and KDM2A ($IC_{50} = 0.20 \mu M$, $1.2 \mu M$ and $6.8 \mu M$, respectively, determined in a MALDI-based assay) but only weak inhibition of KDM4 members. Cellular assays showed increased H3K27me₂ levels, a hallmark for KDM7 inhibition, as well as cytotoxic activity on HeLa and KYSE150 cancer cells.¹⁸⁹

Similarly, they were able to devise a KDM5-selective compound **49** by targeting a tyrosine residue in the active site (Tyr472 in KDM5A), that is oriented differently in other subtypes. The interaction was achieved via a methylpentylamino substituent linked to the hydroxamate via a 4-carbon linker. The compound displayed an IC_{50} value of 3.3 μ M against KDM5A, 13-fold selectivity over KDM4A as well as H3K4 hypermethylation and cytotoxicity in a lung cancer cell line.¹⁹⁰

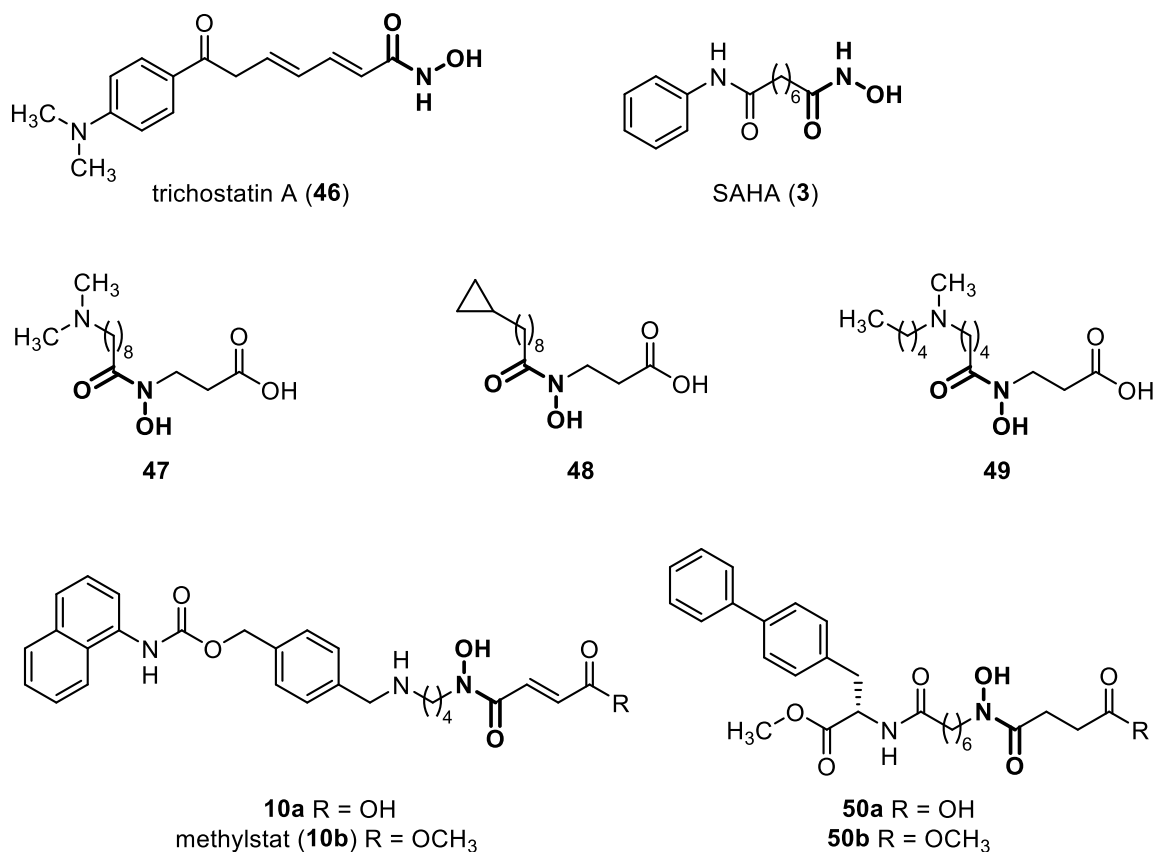


Figure 19 Chemical structures of hydroxamate-based inhibitors of Jmj-KDMs.

Methylstat (**10b**), which has become a well-known reference inhibitor for cellular KDM inhibition is another hydroxamate-based methyl ester prodrug. It consists of the iron chelating hydroxamate, a fumarate moiety mimicking the co-substrate, and a long hydrophobic part addressing the histone peptide binding pocket and inducing selectivity towards histone demethylases. The fumarate moiety is methylated in the prodrug form. However, the compound displays no distinct selectivity towards Jmj-KDM subtypes and also inhibits other iron/2-OG-dependent dioxygenases. Furthermore, the fumarate moiety is a Michael acceptor, which may

lead to undesired off-target effects in a cellular setting. Nonetheless, methylstat (**10b**) was shown to induce H3K4, H3K9, H3K27, H3K36, H3K79 and H4K20 hypermethylation in a cellular assay.¹³⁷

Despite the known activity of hydroxamates against zinc-dependent HDACs no selectivity data towards this enzyme class has been reported on the above-mentioned compounds, which should be carefully assessed when using the compounds in cellular settings. However, internal hydroxamates have been shown to display no or low inhibitory activity on HDACs, therefore it can be assumed that this is also true for the abovementioned inhibitors **10a**, **47**, **48**, and **49**.

A hydroxamate-based inhibitor with proven selectivity over HDACs (approx. 10% inhibition at 10 μ M against HDACs 1 and 6) is compound **50a** displaying low micromolar inhibition of KDM4 and KDM5 (IC_{50} = 8.8 μ M and 1.7 μ M, respectively, determined in a LANCEUltra[®] assay) and competitive behaviour towards the co-substrate 2-OG. The compound is *N*-substituted with a propanoate moiety at the hydroxamic acid, which seems to be selectivity-inducing, as similar inhibitors bearing the free hydroxamic acids were strong HDAC inhibitors. Selectivity is most probably induced by steric clashes in the rather narrow active site of HDACs. Additionally, compound **50a** was cytotoxic against the oesophageal cancer cell line KYSE150 and the leukaemia cell line HL-60, while its methyl ester showed even improved activity (14% vs 82% inhibition of KYSE150 at 100 μ M and GI_{50} 116 μ M vs 18 μ M on HL-60).¹⁹¹

1.4.3 Diverse Small Molecule Inhibitors

In addition to the described established KDM inhibitor scaffolds, there are some compounds containing various functional groups which may not act as co-substrate analogs or display an unknown mechanism of action.

The fragment-like 4-hydroxypyrazole **51** (cf. Figure 20) is a weak KDM4C inhibitor (K_i = 51 μ M, determined in an FDH-based assay; no selectivity data available) and

was proposed as a starting point for the development of new KDM inhibitors due to its novel iron-binding 4-hydroxyl-3-carbonyl motif.¹⁹² However, no further inhibitors based on this structure have been published.

The natural product tripartin (**52**), which was isolated from a *Streptomyces* strain associated with dung beetle larvae, was shown to increase H3K9me₃ in HeLa cells, which is consistent with KDM4 inhibition.¹⁹³ However, the molecular mechanism of action could not be elucidated and a later report showed that tripartin (**52**) and some 1-dichloromethylinden-1-ol analogs did not inhibit KDM4 isoforms in an *in vitro* assay.¹⁹⁴

Deferiprone (**53a**), a clinically approved iron-chelator for the treatment of iron overload diseases, was found to inhibit a range of Jmj-KDMs in the micromolar range. It displayed selectivity for KDM2, -5C, -6A and -7 (lowest IC₅₀ = 4.2 μM on KDM6A) over KDM3A, -3B, -4A-E, -5A, -5B and -6B for which no inhibition was observed at 25 μM in an AlphaScreen™ assay.¹⁹⁵ Molecular docking to KDM6A suggests active-site iron-chelation and hydrogen bonding between the oxygen moieties of deferiprone (**53a**) and the hydroxy groups of Tyr1135 and Ser1134. Similar docking poses could be obtained for KDM2A, 7A and 7B but not for KDM5A, which is in accordance with the observed *in vitro* activity in this study.¹⁹⁵ However, another publication found low micromolar inhibition of KDM4A in a LANCEUltra® assay. These contrasting results may be explained by the different assay setups used for evaluation and the high sensitivity of inhibition to variations in iron and 2-OG concentrations. Furthermore, deferiprone (**53a**) was found to act not competitive towards the co-substrate 2-OG in this assay, therefore it is possible that apparent KDM4A inhibition stemmed rather from iron sequestration than from active-site binding for this isoform (cf. section 1.4.2 for general information about sequestration vs. active-site site binding). Unfortunately, no competition experiments were published for the more potently inhibited KDMs in the first study, so no mechanism of action could be deduced for these enzymes.¹⁶⁸ Anyhow, proof of *in vivo* modulation of histone methylation by deferiprone (**53a**) was given

1 Introduction

by increased H3K4me₃ and H3K27me₃ in MCF-7 and MDA-MB-231 cells. Subsequent optimisation of the deferiprone scaffold yielded the triazole-containing compound **53b**, which displayed increased cytotoxicity on a range of cancer cell lines and showed anti-cancer activity in a murine breast tumour xenograft model.¹⁹⁵

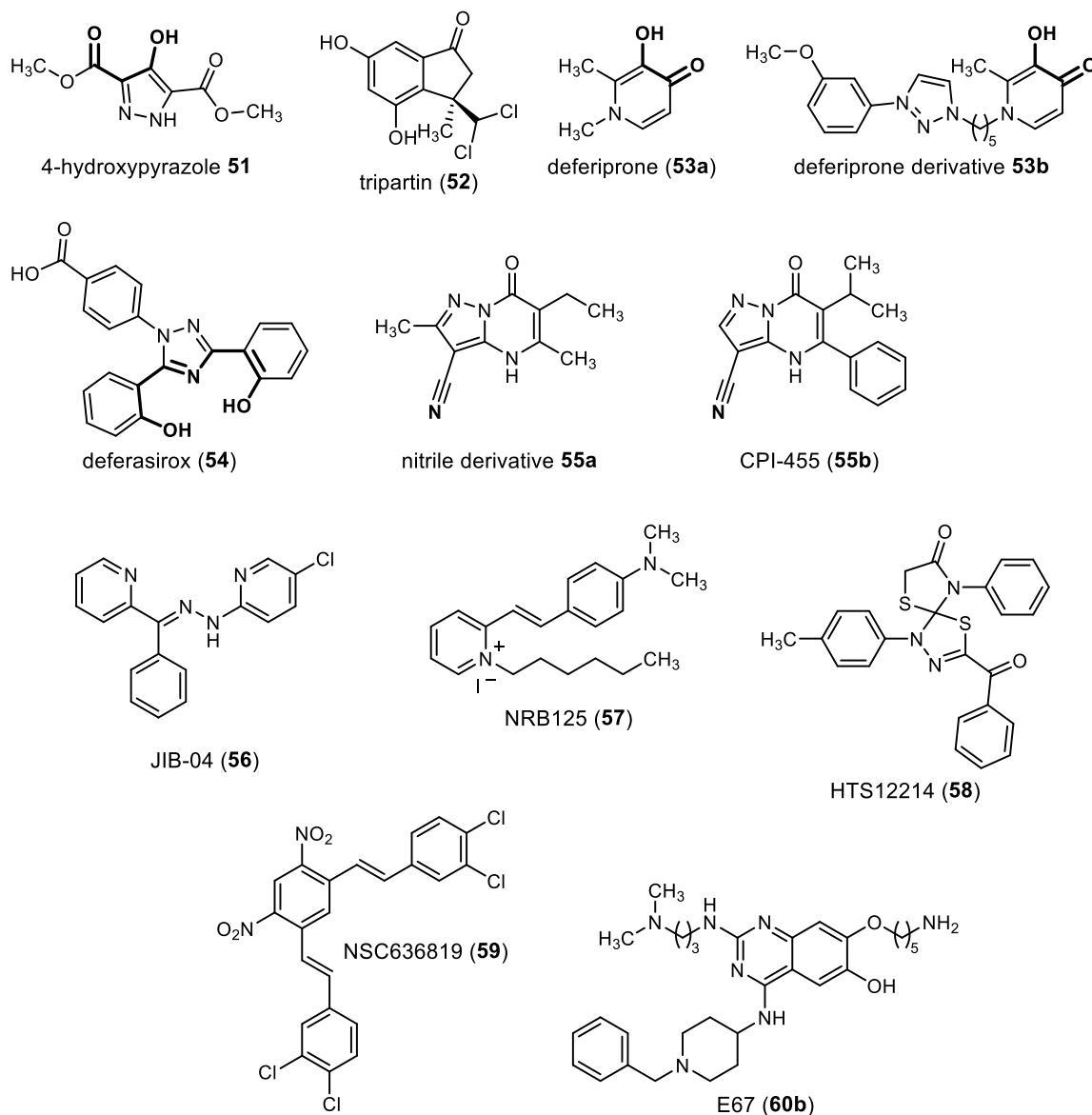


Figure 20 Chemical structures of Jmj-KDM inhibitors displaying diverse modes of action.

Deferasirox (**54**) is another clinically approved iron chelator with KDM-inhibiting properties. It is a non-selective micromolar KDM inhibitor acting via active-site chelation of iron and displaying mixed-mode inhibition towards the co-substrate 2-OG.¹⁶⁸ As the development of derivatives of this scaffold is part of this work, this compound is discussed in more detail in section 4.3.

Another unique scaffold was found in an MS-based high-throughput screen of a 102,400-compound library against KDM4C. The initial pyrazolo[1,5-a]pyrimidin-7(4*H*)-one **55a** which bears a nitrile as iron-binding moiety was a submicromolar inhibitor of KDM5A with moderate selectivity over KDM4C. Optimisation yielded compound CPI-455 (**55b**), a 10 nM KDM5 inhibitor with improved selectivity (200-fold) over KDM4C.

Crystallographic data showed – besides iron-chelation via the nitrile moiety – subtype-specific hydrogen bonding, hydrophobic interactions of the isopropyl side chain as well as π : π stacking and edge-to-face aromatic interactions of the aromatic core with characteristic amino acids of KDM5A (and supposedly other KDM5 isoforms).

The compound is competitive towards the co-substrate as shown by overlap of the structures in the respective co-crystal structures and by biochemical competition assays.¹⁹⁶ In cellular assays with several cancer cell lines, specific increase of H3K4me₃ and H3K4me₂, concomitant with selective KDM5 inhibition, was observed. Additionally, since KDM5 overexpression is known to be associated with the development of drug tolerance in cancer treatments, the effect of KDM5 on this phenomenon was observed. As expected, CPI-455 (**55b**) treatment of a lung cancer cell line treated with the kinase inhibitors erlotinib or lapatinib resulted in a significant reduction of the number of drug-tolerant cells, which was also observed in other models of drug tolerance and in mouse xenografts of an adenocarcinoma cell line.¹⁹⁷

A phenotypic reporter-gene assay was employed to discover the hydrazone JIB-04 (**56**) as a non-selective Jmj-KDM inhibitor in the high nanomolar range. Despite its structural similarity to some pyridine-based inhibitors it does not act solely as a co-substrate competitive inhibitor, but shows mixed-mode inhibition towards 2-OG and the peptide substrate.¹⁹⁸ Furthermore, although the hydrazone and the two adjacent pyridine nitrogen atoms might serve as tridentate iron chelator, docking into KDM4A and crystallographic data suggest a different binding mode not

including iron chelation but hydrogen bonding with a lysine and a tyrosine residue (Lys241 and Tyr177). As Tyr177 is normally involved in binding of the peptide substrate this interaction might explain the partial competitiveness towards the peptide. Lys241 usually stabilizes the oxygen molecule needed for catalytic activity, so it was postulated that JIB-04 (**56**) disrupts oxygen binding. Indeed, an oxygen-sensitive assay revealed competitiveness towards O₂, which is a quite unique mechanism of action for Jmj-KDM inhibitors. The authors of this study suggest that oxygen competitiveness might cause some selectivity *in vivo* as KDM4 exhibits low binding affinity towards O₂ and might therefore be especially vulnerable towards oxygen disruption. Furthermore, as the effect of the inhibitor is greater in a low oxygen environment, they suggest selectivity towards hypoxic tissues such as tumours. This would be an exceptional case of tumour targeting with a KDM inhibitor. However, experimental proof of this hypothesis is lacking so far.

A binding assay based on competitive replacement of a fluorescent probe (cf. section 1.3.6) yielded two unrelated scaffolds NRB125 (**57**) and HTS12214 (**58**), which were micromolar unselective inhibitors of KDM2A and KDM4A. Based on the assay principle used for their discovery it is obvious that they are able to replace an active-site binder from the enzyme. However, no further elucidation of the respective mechanisms of inhibition was undertaken for these compounds. They both showed hypermethylation of H3K9 and H3K36 in a cellular assay using a pancreatic adenocarcinoma cell line.¹⁴⁵

The peptide substrate-competitive inhibitor NSC636819 (**59**) was found in a virtual screening of the National Cancer Institute compound database against structures of KDM4A and KDM4B. It is moderately potent (IC₅₀ = 6.4 µM against KDM4A, determined in an FDH-based assay). *In vitro* selectivity against other KDMs was not assessed. However, cellular studies with the prostate cancer cell line LNCaP showed selective H3K9me₃ increase while other methylation marks remained unchanged, which can be interpreted as indirect proof for compound selectivity for the KDM4 family. Furthermore, cellular experiments with NSC636819 (**59**)

underlined the importance of the androgen-receptor (AR)-related signalling of KDM4 and its role in prostate cancer development.¹⁹⁹

An evaluation of the G9a-inhibitor BIX-01294 (**60a**) and its analogue E67 (**60b**) revealed that they additionally inhibit KDM7A in the low micromolar range (determined in an MS-based assay). G9a is a histone methyltransferase and therefore, like histone demethylases, recognises specific methylated histone lysine residues. Hence, it is not surprising that an inhibitor of G9a targeting the histone peptide binding site – in this case via an aminoalkyl chain – may also bind to a histone demethylase recognising the same substrate. E67 (**60b**) was shown to be cytotoxic against various cancer cell lines, however, an attribution of the cellular effects towards one of the putative target enzymes could not be achieved.²⁰⁰

1.4.4 Covalent Inhibitors

Based on the position of characteristic cysteine residues (Cys480 and -497) in the active site of KDM5 not present in other subtypes, Vazquez-Rodriguez *et al.* developed covalent selective KDM5 inhibitors.²⁰¹ They coupled cross-linking moieties to the structures of known inhibitors, such as the pyrido[3,4-*d*]pyrimidin-4(3*H*)-one **29** and the nitrile CPI-455 (**55b**), yielding for example the acrylamide **61** and the chloroacetamide **62** (cf. Figure 21). Crystal structures of acrylamide **61** confirmed the covalent link to Cys480 and placement of the chloroacetamide moiety of **62** in close proximity to Cys497 although no covalent bond was seen in the latter case.

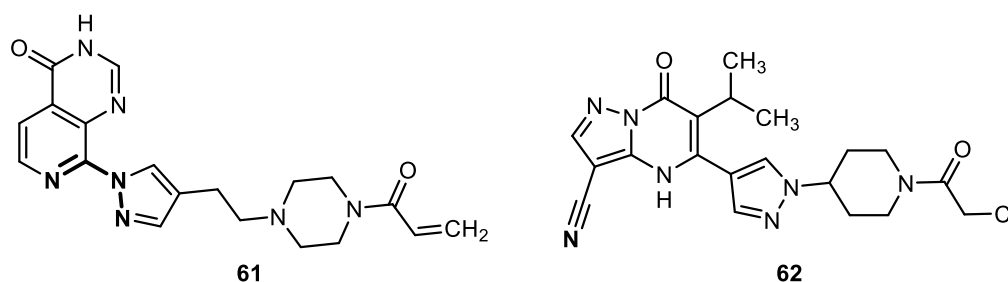


Figure 21 Chemical structures of covalent KDM5 inhibitors.

Kinetic measurements of the binding characteristics supported effective covalent binding of both inhibitors (k_{inact}/K_i $1.4 \cdot 10^3 \text{ M}^{-1} \text{ s}^{-1}$ and $19 \cdot 10^3 \text{ M}^{-1} \text{ s}^{-1}$, determined in an AlphaScreen™ assay; note: the determination of simple IC_{50} values is not significant for covalent inhibitors; higher k_{inact}/K_i corresponds to higher inhibitory activity). Cellular target engagement and ChIP-seq analysis showed KDM5 inhibition at nano- to micromolar levels and an increase of H3K4me₃ for both compounds.²⁰¹

1.4.5 Peptidic Inhibitors

As described in section 1.4.3 inhibition via competition with the histone peptide substrate is an eligible mode of action. This may be efficiently achieved by compounds containing peptidic structures.

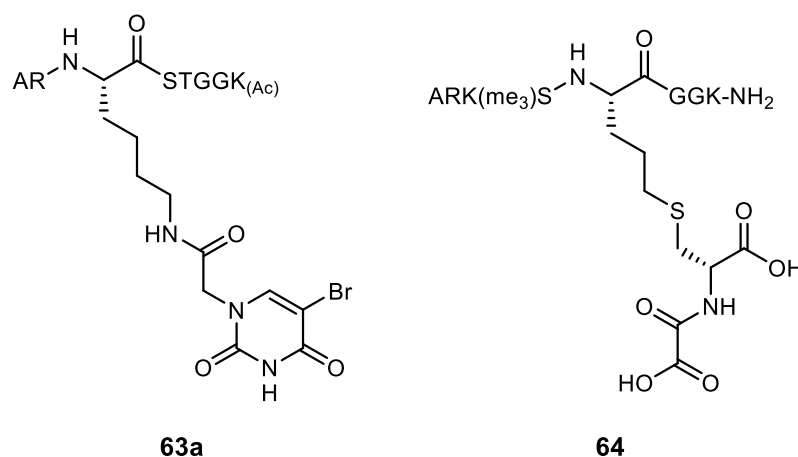


Figure 22 Chemical structures of peptide-based Jmj-KDM inhibitors.

A truncated version of the histone tail 3 (H3₍₇₋₁₄₎K9_(i); **63a**) bearing a modified lysine residue as trimethyllysine mimic (cf. Figure 22) was shown to be a micromolar inhibitor of KDM4. The lysine mimic was coupled to a bromouracil moiety in order to incorporate an iron-binding group, thereby increasing the inhibitory activity and selectivity ($K_i = 52 \text{ } \mu\text{M}$ on KDM4C, $98 \text{ } \mu\text{M}$ on KDM4A, no inhibition of KDM7, determined in an FDH-coupled assay). By choosing a shorter peptide (H3₍₇₋₁₁₎K9_(i); **63b**), selectivity for KDM4C towards KDM4A could be increased to a 4-fold difference, which is remarkable given the high sequence similarity of those two subtypes.²⁰²

Based on a co-crystal structure of KDMA in complex with its peptidic substrate, another peptidic inhibitor bearing a metal-binding group could be devised. *N*-oxalyl cysteine was chosen as co-substrate mimic and the optimal position for the linkage with the peptide via a disulphide bridge was deduced from the co-crystal structure. Co-crystallization of KDM4A with the resulting inhibitor **64** confirmed the intended binding mode covering both the substrate and the co-substrate binding pocket. Inhibitory activity against KDM4A was 0.27 μM (determined in a luminescence based assay) and no significant inhibition of KDM6 and KDM7 family members was observed.²⁰³

A different approach used cyclic peptides that do not address the peptide substrate binding site but a remote binding pocket on the surface of KDM4. Targeting this binding site caused allosteric inhibition of the enzyme. Screening of a library of randomized peptides against KDM1 and KDM4 by phage display followed by optimization via truncation, amino acid replacement and chemical modification yielded two KDM4-selective inhibitors (IC_{50} = 0.6 μM and 8.5 μM on KDM4C, determined in a LANCEUltra[®] assay; structures not depicted here). Due to the fact that the inhibitor binding site lies in a region less conserved than the catalytic site, these inhibitors may serve as interesting starting point for the development of isoform-selective inhibitors.¹¹⁸

Despite their high selectivity and unique binding modes peptidic inhibitors have not been advanced any further as they suffer from the typical drawbacks of peptide-based compounds such as low cellular permeability and low metabolic stability.

1.4.6 Zinc ejecting Inhibitors

A unique feature of KDM4 is a zinc-binding motif close to the methyllysine binding site, which seems to be necessary for catalytic activity. Therefore, attempts to selectively inhibit KDM4 via targeting this zinc ion have been undertaken.^{204, 205}

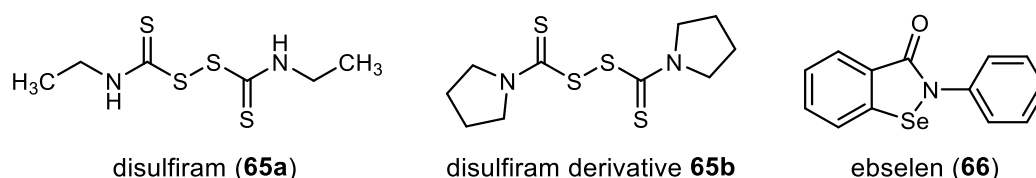


Figure 23 Chemical structures of zinc-ejecting KDM4 inhibitors.

To this end, known zinc-binding compounds were screened for their ability to eject the respective zinc ion from the enzyme and inhibit the catalytic activity. The dehydrogenase inhibitor disulfiram (**65a**) and a pyrrolidine-containing derivative thereof (**65b**), as well as the selenazolone-containing anti-inflammatory and cytoprotective drug candidate ebselen (**66**; cf. Figure 23) were shown to inhibit KDM4A in the micromolar range via a mechanism independent of substrate or co-substrate competitiveness.

The three compounds did not inhibit the iron/2-OG-dependent prolyl hydroxylase PHD2 further underlining the 2-OG independency. The suggested mode of action is covalent binding of the inhibitor to one of the cysteine residues of the zinc binding site with concomitant ejection of the bound zinc ion. A corresponding adduct between disulfiram **65a** (after cleavage of the disulphide bond) and KDM4A could be detected via MS supporting this mode of action.²⁰⁴ However, effects on other KDMs, which contain structural zinc ions in additional domains, such as zinc finger domains, or other zinc-containing enzymes were not evaluated therefore limiting the significance of the postulated selectivity.

1.4.7 Discussion

Due to their important role in physiology and disease, numerous inhibitors for Jmj-KDMs have been published since their discovery in 2006. The majority of them bear an iron-chelating moiety to bind to the central ferrous iron and are therefore at least partly competitive towards the co-substrate 2-OG. The inherent metal-binding capacity might be a drawback in terms of selectivity, as metalloenzymes are quite abundant in cells and therefore pose possible off-targets for metal binding

inhibitors. Furthermore, those inhibitors may reduce the availability of the cytosolic iron – or more generally di- and trivalent metal ion – pool and thereby elicit other, potentially undesired, biologic effects. Therefore, it is important that inhibitors display a high potency on their respective target in order to minimize the required concentration and the possible off-target effects. Concerning target selectivity for metal-binding drug molecules, Day, Chen and Cohen screened a broad variety of experimental as well as clinically approved drugs against various metalloenzymes and found that, contrary to common belief, metal-binding drugs are usually rather selective for their target of interest and not especially prone to off-target effects.^{206,}

²⁰⁷ Besides the selectivity over non-related metalloenzymes, there remains the question of subtype or even isoform selectivity for certain KDMs. Some of the published inhibitors display remarkable selectivity while others are non-selective or selectivity has not been fully evaluated. However, given the physiological redundancy of some KDMs it is currently not known which degree of selectivity is desirable for good clinical outcomes because too selective inhibitors might not be reaching all necessary targets due to compensation of the inhibitory effects by other demethylases while too broad inhibition is possibly related to an increased risk of undesired side effects. As no Jmj-KDM inhibitor has entered clinical trials to date, there is still a dire need for new inhibitory molecules spanning a wider range of selectivity and potency with optimized properties favouring good *in vivo* efficacy both for the development of molecular probes for scientific studies as well as for potential therapeutic drugs.

2 Aim of the Project

Given their crucial role in various diseases, first and foremost in cancer and neurological diseases,^{52, 55, 81-86} inhibitors of Jmj-KDMs are valuable tools for the study of the role of these enzymes in pathophysiological pathways. Additionally, Jmj-KDMs can be envisioned as potential therapeutic targets in the above-mentioned disease areas. Although numerous inhibitors of various subtypes of Jmj-KDMs have been developed,^{52, 132, 147-156} no clinical candidate is available to date and there is still a high demand for potent inhibitors displaying a favourable selectivity profile and high cellular permeability.

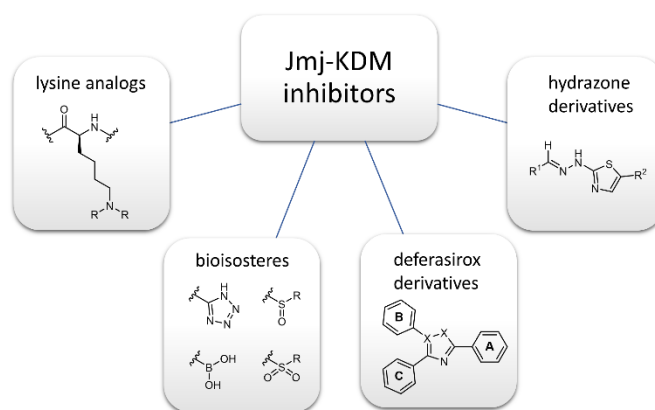


Figure 24 Overview over the main projects of this thesis.

The main aim of this work was the synthesis and *in vitro* evaluation of new Jmj-KDM inhibitors, mainly focused on KDM4A, which are based on lead structures of known inhibitors. To this end, the synthesis of bioisosteres of the non-selective inhibitors 2,4-PDCA (**22**) and IOX1 (**42**) was established. Furthermore, a broad variety of derivatives of the clinically approved iron-chelator deferasirox (**54**) was generated. The synthesis of α -brominated ketones and the successive Hantzsch-thiazole or oxazole cyclization were developed and optimized for different starting materials. Additionally, coupling reactions for the generation of labelled derivatives were performed. Smaller projects comprised the characterization of a compound series focussed on the lysine substrate as well as a novel inhibitor class based on the

hydrazone motif. The different inhibitor classes covered in this work are summarized in Figure 24.

Biochemical evaluation of compound potency was performed in two *in vitro* enzyme activity assays previously established in the lab. Furthermore, fluorescently labelled compounds were evaluated in a newly developed fluorescence polarization assay in order to gain insights into binding characteristics of the compounds.

For potent inhibitors, the results of docking studies, selectivity evaluation as well as cellular activity will also be discussed herein.

3 Assays

In order to evaluate new KDM inhibitors, a set of robust assays for their identification and characterisation is needed. To this end, two enzyme activity assays for KDM4A, namely the FDH assay and the antibody-dependent LANCE assay, have been previously established in our lab by Dr. Martin Roatsch, as described in his PhD thesis.¹²⁰ They were used in this work following the pre-established protocols. The general assay setup and important characteristics of the two assays are described in the following sections.

3.1 Activity Assays used in this Work

As described in section 1.3.1, the FDH assay is based on the detection of NADH, which is generated by the auxiliary enzyme formaldehyde dehydrogenase upon release of formaldehyde produced in the demethylation reaction (cf. Figure 8). In contrast to that, the LANCE assay detects the demethylated peptide via recognition by a di-methyl specific antibody for H3K9me₂, which is labelled with a europium chelate amenable for time-resolved FRET measurements. Optimisation of both assay formats was already performed by Dr. Martin Roatsch, and is extensively described in his PhD thesis.¹²⁰ Therefore, and in order to increase comparability with previously obtained inhibition constants, no major modifications to that setup were performed in this work. Consequently, only a short overview over the assay conditions and the parameters used to ensure constant assay performance are given here. Both assays were used for compound screening and for determination of IC₅₀ values using the equations given in the experimental section.

3.1.1 FDH-coupled Assay

Main parameters critical for assay performance are the choice of a suitable peptide substrate and the concentrations of enzyme, substrate and the co-substrate 2-OG.

As KDM4A demethylates H3K9me_{3/2} and H3K36me_{3/2}, histones bearing these modifications might be used for activity measurements. However, using short peptide substrates bearing one of these modifications is much easier, more cost-effective and yields a higher reproducibility of results, because the peptides can be generated synthetically instead of being isolated from cells, where uniform modifications are difficult to obtain. Therefore, a peptide substrate consisting of the amino acids 7-14 of histone 3 trimethylated at lysine 9 (peptide sequence ARK(me₃)STGGK-NH₂) was chosen. Demethylation activity on this substrate is higher than towards a peptide bearing the H3K36me_{3/2} modification. Additionally, further demethylation of the H3K9me₂ peptide to H3K9me_{1/0} is negligible when using sufficiently high concentrations of H3K9me₃ as well as short reaction times.⁵⁸ To save costly materials, concentrations should be chosen as low as possible while maintaining a stable read-out signal. Based on literature reports of similar assays^{119, 170, 208} and kinetic measurements¹²⁰ a peptide concentration of 35 μ M was chosen to obtain a quick enzymatic transformation while requiring rather low substrate consumption. A suitable KDM4A concentration was chosen that allowed about 60% substrate turnover in 60 min resulting in a reasonable assay window. As enzyme concentration and activity varied between batches activity was measured for each new batch to determine the concentration needed to obtain the same activity as the previous batches. This resulted in an enzyme concentration of approximately 1.75 μ M for the FDH assay. The third important assay component is the co-substrate 2-OG. As most Jmj-KDM inhibitors are at least partially competitive towards 2-OG, its concentration in the assay is crucial, because variations lead to different inhibition constants for the inhibitors. High 2-OG concentrations would lead to higher IC₅₀ values for the inhibitors, because a higher amount of compound would be needed to displace 2-OG from the catalytic pocket. However, too low concentrations should also be avoided, not only because they lead to low IC₅₀ values and lower reproducibility, but also to prevent a lack of 2-OG which would slow down the demethylation reaction in the non-inhibited enzyme. Therefore, a

concentration of 50 μM , which is about two times the K_M value ($29 \pm 11 \mu\text{M}$; determined via Michaelis-Menten curve) and allows fast enzymatic turnover, was chosen.¹²⁰

Further components needed for the assay are ferrous iron (supplied as FeSO_4), which is needed for the catalytic activity of the enzyme as well as ascorbic acid, which suppresses oxidation of Fe^{2+} to Fe^{3+} and thereby increases the stability of the assay mixture. Both reagents were supplied in large excess to the chosen enzyme concentration (10 μM FeSO_4 , 100 μM ascorbic acid) to avoid variations in the measurements caused by oxidation by ambient oxygen. Additionally, these component solutions were prepared freshly each week and added to the enzyme solution immediately prior to the assay to avoid degradation. For the formaldehyde detection, formaldehyde dehydrogenase and its cofactor NAD^+ are needed. High concentrations, namely 0.001 Units/ μL FDH and 500 μM NAD^+ , which ensured that the demethylation and not the detection reaction was the rate determining step, were chosen. 50 μM HEPES buffer at pH 7.50 containing 0.01% TWEEN 20 proved to be suitable for both the demethylation reaction and the formaldehyde oxidation and was therefore chosen as assay buffer.

As described in section 1.3.1, the FDH assay is prone to interference with autofluorescent compounds whose absorption and emission spectra overlap with those of NADH. Therefore, a counterscreen for fluorescence was performed at $\lambda_{\text{em}} = 460 \text{ nm}$. Furthermore, all potential hits were confirmed in the LANCEUltra[®] assay.

3.1.2 LANCEUltra[®] assay

Basically, all the above-mentioned considerations concerning the enzyme, peptide substrate and co-substrate are also true for the LANCE assay. However, a slight variation of the peptide substrate was necessary because the assay principle depends on binding of the substrate to the acceptor beads in order to allow the FRET

effect to take place (cf. Figure 11). For that purpose, a biotin tag on the peptide, which is able to bind to the streptavidin-coated acceptor bead, is suitable. As suggested by the assay reagent supplier (PerkinElmer),¹³³ a biotin-H3K9me₃ 1-21 peptide (peptide sequence ARTKQTARK(me₃)STGGKAPRKQLA-GGK(biotin)) was used. Due to the much lower quantification limit and higher sensitivity of the LANCE assay compared to the FDH assay, much lower concentrations of the peptide substrate (0.4 μM), KDM4A (60 nM) and 2-OG (1 μM) could be employed. As for the FDH assay, enzyme activity of each batch was confirmed via activity measurements. The other assay parameters were similar to the FDH assay and can be found in the experimental section. As explained in section 1.3.3 the LANCE assay is much less prone towards compound interference than the FDH assay and was therefore used as the standard assay for the determination of IC₅₀ values. Unless stated otherwise, all IC₅₀ values given in the following sections were determined in this assay.

In addition to the determination of IC₅₀ values, the LANCE assay was also used to evaluate competitiveness of inhibitors against the co-substrate 2-OG using the Michaelis-Menten equation. To this end, varying concentrations of inhibitor (in the range of the IC₅₀ value) were titrated against different concentrations of 2-OG (0–5 μM). To calculate the amount of converted substrate the calibration function (3.1), obtained by plotting the LANCE fluorescence signal against defined concentrations of demethylated peptide, was used (cf. Ref.120 for details).

$$[\text{H3K9me}_2] = \frac{\text{LANCE}-200}{275} \cdot 1 \text{ nM} \quad (3.1)$$

The concentration can be used to calculate the reaction velocity v over the incubation time using equation 3.2.

$$v = \frac{\Delta[\text{H3K9me}_2]}{\Delta t} = \frac{[\text{H3K9me}_2]}{45 \text{ min}} \quad (3.2)$$

Fitting the thus obtained velocities against the Michaelis-Menten equation

$$v = \frac{v_{\text{max}} \cdot [2\text{-OG}]}{K_{\text{M}}^{\text{app}} + [2\text{-OG}]} \quad (3.3)$$

gives the apparent K_M values for the respective inhibitor concentrations under the specified assay conditions. For competitive inhibitors, apparent K_M values can be used to calculate the inhibition constant K_i via linear regression to the following equation.

$$K_M^{\text{app}} = K_M^0 \cdot \left(1 + \frac{[\text{inhibitor}]}{K_i} \right) \quad (3.4)$$

4 Development of novel Inhibitors for JmJC-containing histone demethylases

Based on the mechanism of action of Jmj-KDMs and the structures of previously published inhibitors, the development of new inhibitors was envisaged and is described in the following sections. Compounds were synthesized or obtained from collaboration partners and their activity was tested on KDM4A.

4.1 Lysine Mimics

As histone demethylases recognise peptidic substrates containing methylated lysine residues, compounds acting as lysine mimics might serve as substrate-competitive inhibitors. The aim of this project was to identify modifications of the ϵ -amino group of lysine capable of binding to the enzyme and inhibiting its activity. To this end, a library of 22 lysine derivatives synthesized by Dr. Nicolas Barthes as well as Marleen Bokern and Raphaela Kümmerle, two bachelor students under his supervision, was tested. The library consists of *N*-benzyloxy- and *O*-benzyl-protected lysine derivatives, whose ϵ -amino groups were modified with different substituents or incorporated into heterocycles (cf. Figure 25). Unfortunately, seven compounds could not be evaluated in the KDM4 assay due to precipitation upon addition to the assay medium. Furthermore, neither **67a**, the free ϵ -amine, nor the derivatives bearing aliphatic or aromatic substituents showed an inhibitory activity on KDM4A at 250 μ M. A weak activity was only observed for some of the derivatives containing rings that incorporated the ϵ -amino group. 22% inhibition at 250 μ M was observed for **67b** bearing a 4-(2-pyridinyl)-1,2,3-triazole moiety. However, the other four 1,2,3-triazole-containing derivatives of the library were either inactive or precipitated during the assay, therefore no structure-activity relationship could be deduced from these results. The imidazo[1,5-*a*]pyridine- (**67c**) and succinimide- (**67d**) containing derivatives also displayed weak inhibitory

potential (27% and 50%, respectively). The derivative showing the highest activity with an IC₅₀ value of 28 μM was the pyridinium compound **67e**.

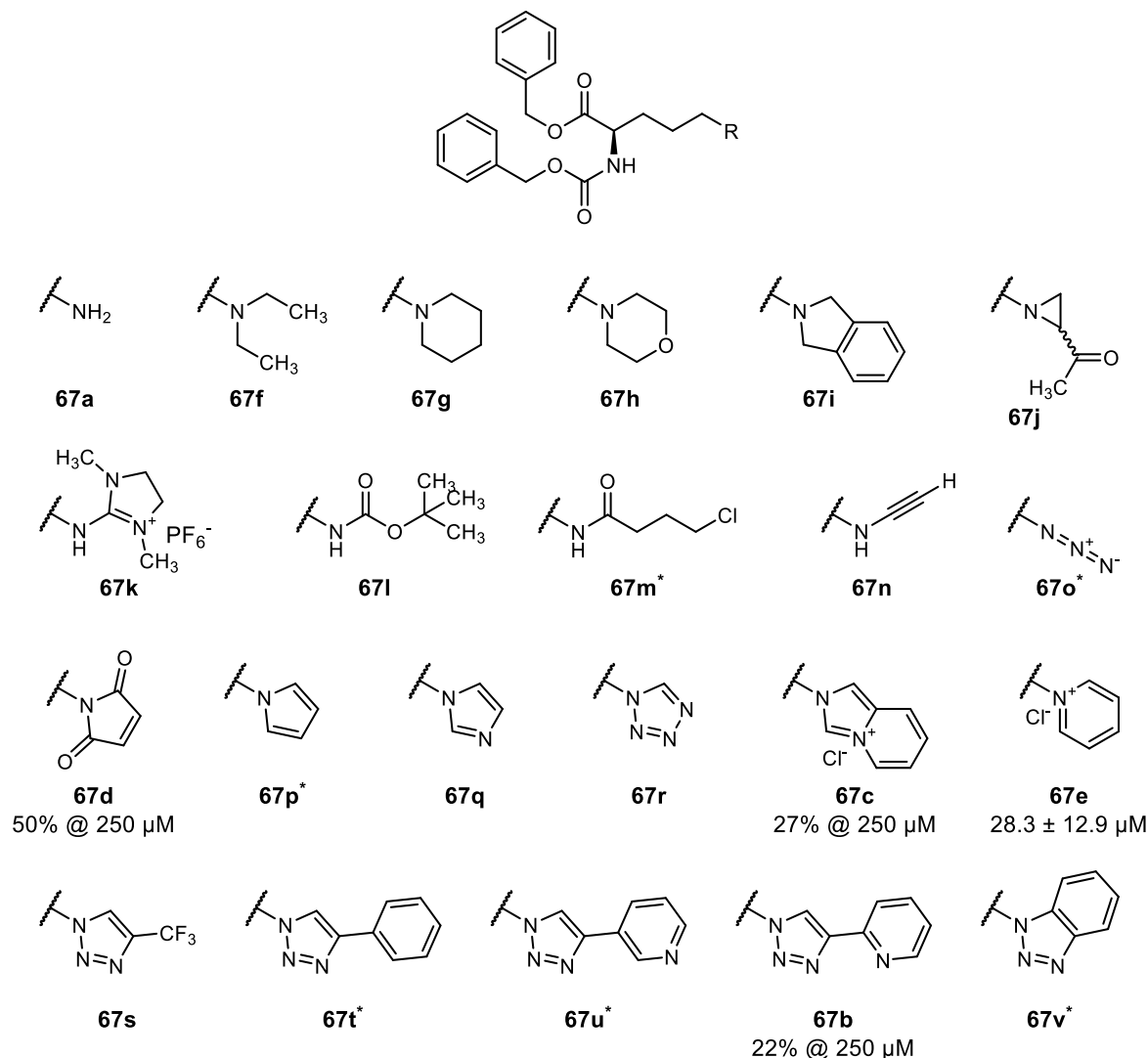


Figure 25 Lysine derivatives as potential KDM4A inhibitors. Inhibitors marked with an asterisk * were insoluble in the assay buffer and could therefore not be tested. Inhibition values are given for active compounds, the other compounds displayed no inhibition (inhibition < 10%) at 250 μM.

In summary, screening of the small library of lysine derivatives yielded one micromolar KDM4A-inhibitor, whereas the other tested compounds were inactive, poorly active (≤50% inhibition at 250 μM) or precipitated under the assay conditions. A potential application of the discovered lysine derivative is the incorporation into a peptidic substrate or a cos-substrate competitive inhibitor which might improve potency and, more importantly, selectivity towards certain subtypes depending on the nature of the chosen substrate.

4.2 Carboxylic Acid Bioisosteres based on known Inhibitors

As outlined in section 1.4.2 some inhibitors contain one or more carboxylate groups to chelate the active-site iron and to undergo ionic interactions with basic amino acid residues (e.g. Lys206 in KDM4A, c.f. section 1.4.2). However, due to their negative charge at physiologic pH values, carboxylic acids often poorly penetrate cell membranes limiting the cellular uptake of the compounds. The first main strategy to overcome this obstacle is the generation of prodrugs by the introduction of a functional group masking the negative charge, which can subsequently be cleaved intracellularly thereby releasing the active compound. Successful examples of prodrugs of KDM inhibitors are summarized in section 1.4.2. The second approach is to exchange the carboxylic acid by a group retaining the biological activity but meanwhile increasing membrane permeation. This bioisostere strategy has also been effectively used for the generation of KDM inhibitors (cf. section 1.4.1). However, as many inhibitors published to date were either not sufficiently active, cell permeable or subtype-selective, improvement of inhibitors using the bioisostere strategy was attempted. Sulfoxides, sulfones, boronic acids and tetrazoles were chosen, because they all have been successfully employed as bioisosteres in numerous medicinal chemistry projects.^{209, 210}

4.2.1 Sulfoxides, Sulfones

Sulfoxides and sulfones are functional groups that can be found in some pharmaceuticals, such as the antibiotic agent dapsone and the proton-pump inhibitor omeprazole. They are not considered classical carboxylic acid bioisosteres because of their high lipophilicity, high pK_a values and their non-planar structure. Nonetheless, sulfones have been employed as carboxylic acid isosteres in some studies.^{209, 211} Additionally, sulfoxides have been reported as highly potent metal chelators which can bind metals either via the oxygen or the sulphur electron lone

pair depending on oxidation state of the metal and binding geometry.²¹² Sulfones are able to chelate metals via one of the oxygen atoms.

The non-selective KDM inhibitor 2,4-pyridine carboxylic acid was chosen as basic scaffold because of its remarkably high potency ($IC_{50} = 34$ nM, determined in a LANCEUltra® assay) despite the rather simple low-molecular structure. The simple scaffold allowed a straightforward synthetic modification of the C2 substituent.

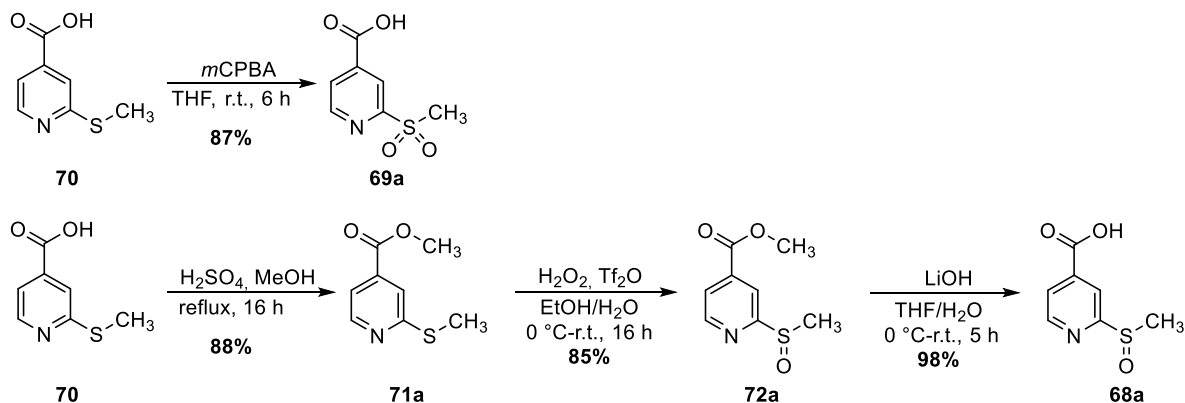
4.2.1.1 Synthesis

Two sulphur analogs which resemble 2,4-pyridine carboxylic acid are the methyl sulfoxide **68a** and the methyl sulfone **69a**. They can be synthesized via oxidation of the corresponding sulphide **70** using a suitable oxidant. The sulfone could easily be obtained in 87% yield using *meta*-chloroperoxybenzoic acid (*m*CPBA) in THF followed by purification via preparative TLC (cf. *Scheme 1*). However, synthesis of the sulfoxide proved to be more difficult due to insufficient separation of product and starting material during purification. Attempts to reach full conversion in order to avoid the separation were unsuccessful, since increasing the amount of the oxidant or the reaction time as well as the use of a more drastic oxidant led to overoxidation to the sulfone, which could also not be separated from the sulfoxide. The applied reagents tested under several conditions were *m*CPBA, hydrogen peroxide — alone or in combination with trifluoromethanesulfonic anhydride (triflic anhydride) — and sodium periodate, all of which have been published for the preparation of sulfoxides from sulphides on similar structures.²¹³⁻²¹⁵

Intending to facilitate purification and improve the selectivity of oxidation, the methyl ester **71a** was used instead of the carboxylic acid **70**, as outlined in *Scheme 1*. This strategy permitted the oxidation to the sulfoxide **72a** following a procedure published by Khodaei *et al.* by using a mixture of hydrogen peroxide and triflic anhydride in ethanol. The reaction reached nearly full conversion to the sulfoxide while no overoxidation was observed under these conditions. The methyl ester

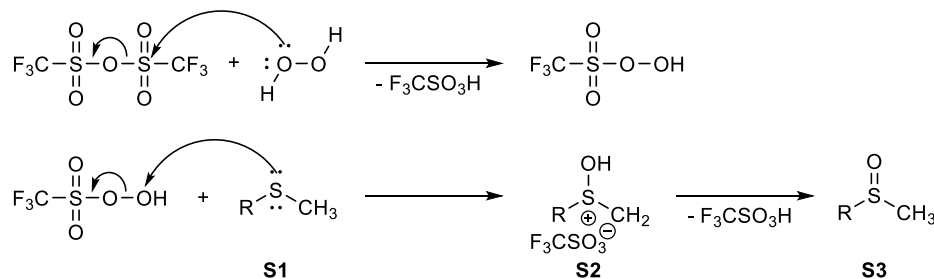
4.2 Carboxylic Acid Bioisosteres based on known Inhibitors

seemed to reduce the susceptibility of the sulfoxide towards oxidation compared to the carboxylic acid, where overoxidation to the sulfone had occurred under the same conditions.



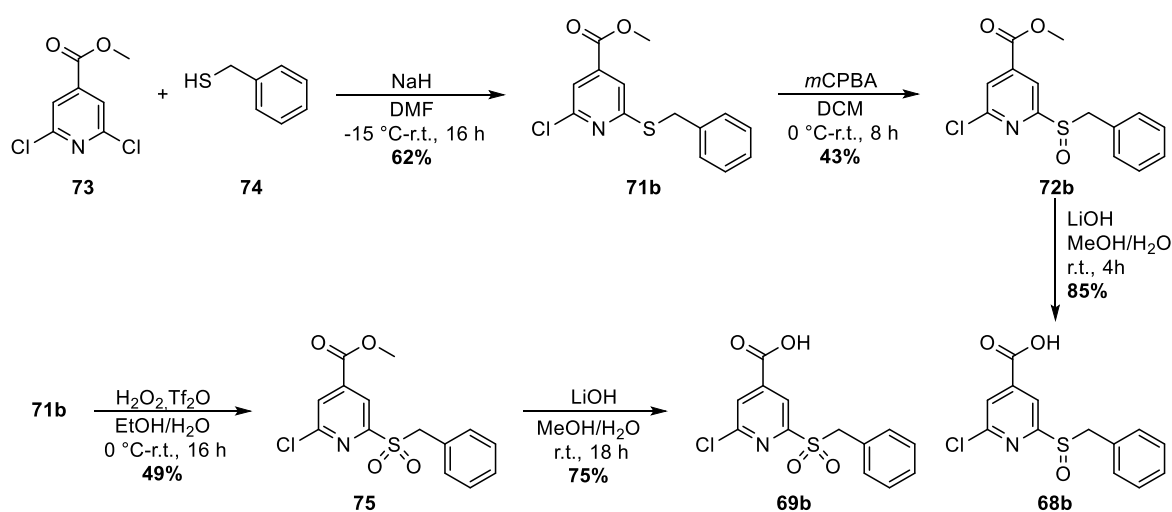
Scheme 1 Synthetic route for the preparation of sulfone and sulfoxide derivatives of 2,4-PDCA.

The reaction mechanism comprises the activation of triflic anhydride by hydrogen peroxide to trifluoromethanesulfonoperoxoic acid (cf. Scheme 2). The terminal oxygen of the peroxoic acid is more electrophilic than H_2O_2 , which facilitates the nucleophilic attack of the sulphide **S1**. Upon release of triflate, the hydroxy-sulfenium cation **S2** is formed, which yields the corresponding sulfone **S3** via hydrogen abstraction. The high selectivity of mono- versus dioxidation might be explained by the lower reactivity of the hydroxy-sulfenium cation towards oxidation compared to the sulphide. Owing to the clean reaction without formation of by-products, purification could be performed via simple extraction with dichloromethane yielding the product in 85% yield. Hydrolysis of the methyl ester yielded the sulfoxide **68a**. Both sulfoxides were synthesized as racemates.



Scheme 2 Proposed reaction mechanism for the oxidation of sulphides to sulfones by hydrogen peroxide and trifluoromethanesulfonic anhydride.²¹⁴

In an effort to attain compounds which might be able to form stronger interactions with the catalytic pocket of the enzyme, the benzyl-substituted compounds **68b** and **69b** were synthesized next (cf. Scheme 3). The sulphide precursor **71b** was obtained from methyl 2,6-dichloroisonicotinate **72** via nucleophilic aromatic substitution with phenylmethanethiol **73** and sodium hydride in DMF as published by Dally *et al.*²¹⁶ In contrast to the methyl derivative described above, oxidation with hydrogen peroxide/triflic anhydride in ethanol yielded only a small amount of the sulfoxide **68b** while the main product was the sulfone **69b**.



Scheme 3 Synthetic route for the preparation of benzyl-substituted sulfoxide and sulfone derivatives of 2,4-PDCA.

An oxidation reaction using one equivalent of *m*CPBA also gave a mixture of sulfoxide and sulfone, but in this case the sulfoxide **68b** was predominant. Luckily, removal of the minor product could be realized via chromatographic purification in both cases, giving the sufficiently pure sulfone and sulfoxide in moderate yields of 49 and 85%, respectively. The somewhat contradictory observations concerning the selectivity of different oxidation reagents for the S-methyl and -benzyl compounds suggest a high sensitivity of the oxidation reaction towards change of substituents. However, no further optimization of reaction conditions was performed as soon as the desired product was obtained in sufficient purity and amount for analytical purposes and biological testing. Additionally, the reproducibility of the observed product ratios was not tested. Therefore, the observed differences between the two

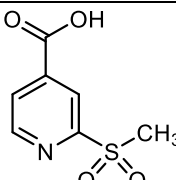
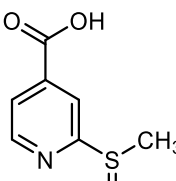
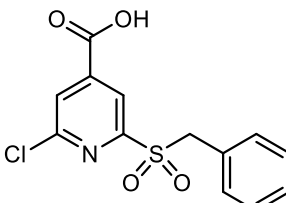
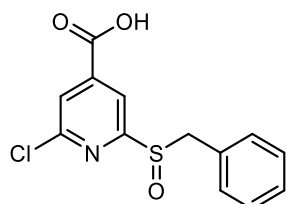
4.2 Carboxylic Acid Bioisosteres based on known Inhibitors

compounds might be coincidental and could stem from small variations of reaction conditions such as the exact amount of oxidant used or the precise control of reaction temperature.

4.2.1.2 Evaluation of enzyme activity

Exchange of the 2-carboxylic acid of 2,4-PDCA by a methylsulfonyl moiety in compound **69b** lead to a marked decrease in potency to only 60% inhibition at 500 μ M. The methylsulfoxide **68a** also displayed very weak inhibition of 293 μ M. Furthermore, the hill slope in the inhibition curve was > 5 , which is suggestive for a mechanism of action not reliant on a 1:1 compound enzyme complex.

Table 3 Inhibitory activity of sulfone and sulfoxide derivatives against KDM4A. Data are mean \pm s. d. of at least two independent experiments.

Compound	Structure	% inhibition or IC ₅₀
69a		60 \pm 8 % @ 500 μ M
68a		292.8 \pm 6.0 μ M*
69b		57 \pm 8 % @ 500 μ M
68b		248.9 \pm 32.6 μ M

* Hill slope of the inhibition curve is > 5 , suggesting compound/enzyme precipitation or other unspecific effects.

High hillslopes can either result from cooperative binding of several compound molecules or – more likely in this case – from unspecific effects like compound/enzyme precipitation or unspecific binding.

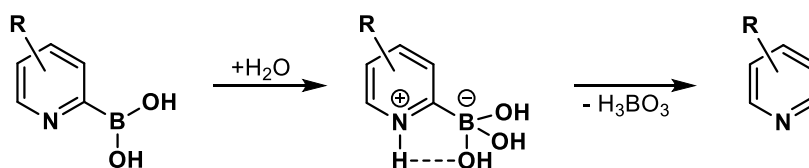
Similarly, the benzyl-substituted derivatives also displayed very weak inhibition of 57% at 500 μ M for the sulfone **69b** and an IC_{50} value of 249 μ M for the sulfoxide **68b**. Consequently, the sulfoxide and sulfone moieties are unsuitable for the bioisosteric replacement of the 2-carboxylic acid in 2,4-PDCA probably due to unfavourable binding geometries.

4.2.2 Boronic acids

Boronic acids and their derivatives have gained more and more importance in medicinal chemistry development programmes in the past few years.²¹⁷ The FDA-approval of the proteasome inhibitor bortezomib as the first boron-containing drug in 2003 proved that it is essentially possible to incorporate this moiety into active pharmaceuticals thereby eliciting growing interest in boronic acid research. To date, two more boron derivatives, namely the antifungal drug tavaborole and crisaborole for the treatment of atopic dermatitis have been approved while numerous others are evaluated in preclinical and clinical trials for a variety of diseases like cancer, psoriasis, and bacterial, parasitic as well as viral infectious diseases.²¹⁷ Boronates have also been used as bioisosteres for carboxylic acids, as exemplified in the case of an oseltamivir derivative where increased antiviral activity was observed for the modified compound.²⁰⁹ Despite the rapid evolution in various disease areas, no boron-containing inhibitor targeting a demethylase has been published yet, therefore it was envisioned to probe into that direction and evaluate the effect of the incorporation of a boronic acid into a KDM inhibitor.

4.2.2.1 Scaffold choice

The primary goal was to synthesize a simple boronic acid derivative of a known inhibitor to assess the suitability of this moiety as a carboxylic acid isostere. As for the sulfoxides and sulfones, the exchange of the 2-carboxylic acid of 2,4-PDCA **22** by a boronic acid could have served this purpose. However, 2,4-PDCA seemed to be rather unfeasible as a starting point for two main reasons. Firstly, 2-borylated and, to a lesser extent, 4-borylated pyridines are known to be highly prone to protodeboronation via the formation of a reactive zwitterion in aqueous media (cf. Scheme 4).²¹⁸ Therefore, these compounds would probably not be stable in cells. Secondly, a pyridine compound containing a carboxylic acid as well as a boronic acid moiety would be highly polar (clogP of 0.409, calculated with OSIRIS Data Warrior) and bear multiple charges at physiologic pH values, which might lead to low cellular permeability.



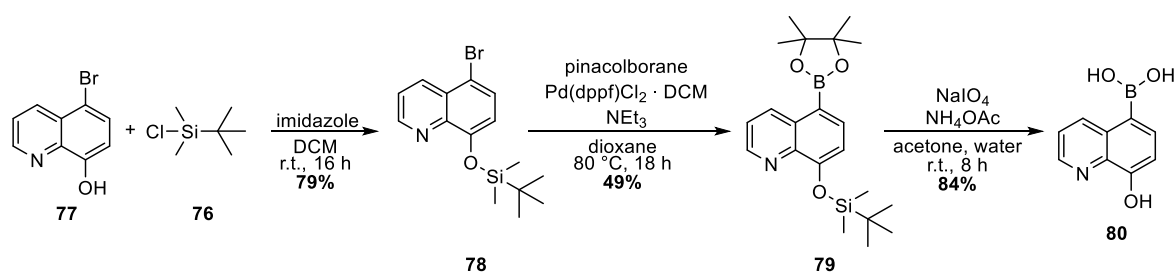
Scheme 4 Protodeboronation of 2-pyridine boronic acid. Upon addition of water a reactive zwitterionic species is formed, which spontaneously decomposes releasing boric acid and the deboronated pyridine.

Therefore, the less polar compound 8-hydroxy-5-quinolinecarboxylic acid **42** (IOX1) was selected. The predicted logP of 1.3533 of the resulting boronic acid derivative promises higher cellular permeability.

4.2.2.2 Synthesis and testing

The synthesis, as outlined in Scheme 5, comprises the protection of the phenolic hydroxy group with *tert*-butyldimethyl chlorosilane **76** (TBS-Cl), the installation of the boronate as pinacol ester, and finally the cleavage of both the *tert*-butyldimethylsilyl (TBS) and the pinacol moieties. TBS protection was performed

according to the procedure described in a patent by Anderson *et al.* using 5-bromquinolin-8-ol **77** and TBS-Cl. Imidazole was added to activate TBS-Cl catalytically and as stoichiometric base.²¹⁹ The reaction was run in dichloromethane allowing a simple work-up of the protected compound **78** by washing with diluted HCl and water followed by purification via flash chromatography (79% yield). The next step was realized using a published protocol by Babudri *et al.* via palladium-catalysed borylation of **78** with pinacolborane and triethylamine in 1,4-dioxane. Work-up by extraction with cyclohexane and chromatographic purification yielded **79** in 49% yield. Deprotection of the boronic acid and the phenol moiety was accomplished via oxidative ester cleavage with sodium periodate yielding compound **80**.²²⁰



Scheme 5 Synthetic route for the generation of the boronic acid derivative **80** of IOX1 (**42**).

However, purification proved to be rather difficult. This was not unexpected, as isolation of pure boronic acids is known to be challenging due to their high polarity and their propensity to form oligomeric anhydrides.²²¹ Furthermore, **80** is amphoteric due to the basic quinoline moiety. That property impeded purification via normal-phase flash column chromatography because the compound could not be eluted from the column even with polar solvents. Ion-exchange chromatography using a sephadex column was also unsuccessful, as no separation of the desired compound from the impurities was observed. Finally, purification was realized via semi-preparative HPLC on a C18 column with polar endcapping (Phenomenex Synergi® 10u Hydro-RP 80) and a water/acetonitrile/trifluoroacetic acid mixture as eluent. However, final purity was only 92.8% as determined via HPLC and the

remaining impurities could not be identified in the NMR spectra due to the small sample amount.

In vitro testing of **80** in the FDH assay revealed a fairly low compound activity of 47% inhibition at 100 μ M which is much lower than the inhibitory activity of IOX1 (**42**; IC_{50} = 0.7 μ M in the LANCE assay). Thus, no further attempts to synthesize the compound in higher purity were undertaken. As the compound potency dropped massively compared to IOX1, the exchange of the carboxylic acid by a boronic acid is detrimental for the inhibitory activity. Therefore, no other boronic acids were synthesized and tested.

4.2.3 Tetrazoles

Since both the sulfoxides/sulfones and the boronic acid had proven to be ineffective as replacement for carboxylic acids in the KDM inhibitors 2,4-PDCA and IOX1, respectively, tetrazoles were considered as alternative bioisosteres. The tetrazole moiety is one of the most commonly used bioisosteres for carboxylic acids, and has been successfully employed in the development of numerous pharmaceuticals. Prominent examples are the angiotensin II receptor antagonist Losartan and its analogs. Like carboxylic acids, 5-substituted tetrazoles usually display pK_a values in the range of 4.5-4.9 and are hence deprotonated at physiologic pH. Furthermore, they have a planar structure and an electronic structure similar to carboxylic acids.²¹⁰

4.2.3.1 Inhibitory activity of tetrazole derivatives

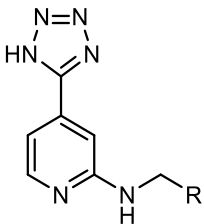
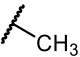
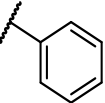
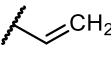
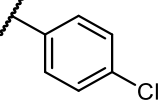
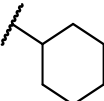
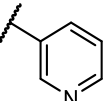
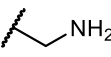
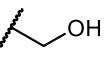
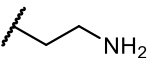
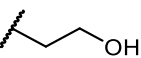
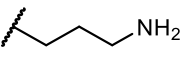
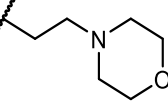
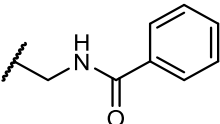
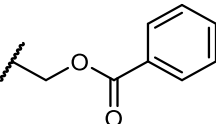
As for the sulfoxides and sulfones, 2,4-pyridine carboxylic acid was chosen as the lead structure due to its high inhibitory activity and simple molecular structure. The 4-carboxylic acid was replaced by the tetrazole moiety in order to keep the interaction with Lys 206 in KDM4. Additionally, the 2-carboxylic acid, which is part of the iron-chelating motif, was exchanged by an amine function (cf. Table 4), which can also chelate iron via the nitrogen lone pair. Furthermore, the secondary amine

4 Development of novel Inhibitors for JmjC-containing histone demethylases

allows the introduction of variable side chains, which might increase interactions with the enzyme. Compound synthesis was performed by Dr. Georg Fassauer (Link group, EMAU Greifswald) and results are also discussed in his thesis.²²²

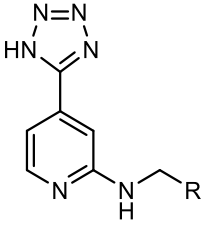
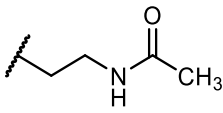
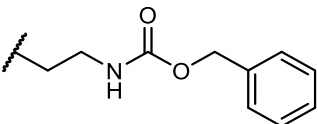
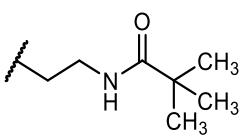
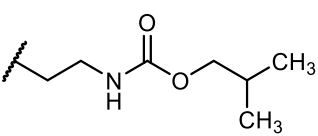
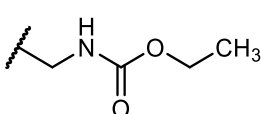
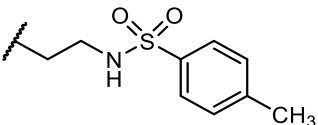
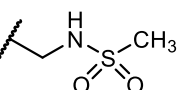
Unfortunately, a massive decrease of the inhibitory activity was observed for the thus modified compounds. Neither simple aliphatic nor aromatic substituents present in **81a**, **81b** and **81c** or in **81d**, **81e** and **81f**, respectively, yielded potent compounds showing considerable inhibition at 250 μ M.

Table 4 Inhibitory activity of tetrazolyl-2-aminopyridine derivatives against KDM4A. Compounds were kindly provided by Dr. Georg Fassauer. Data are mean \pm s. d. of at least two independent experiments.

					
No	R	% inhibition @ 250 μ M	No	R	% inhibition @ 250 μ M
81a		22%	81d		n. i.
81b		n. i.	81e		n. i.
81c		n. i.	81f		n. i.
81j		n. i. @ 125 μ M*	81g		n. i.
81l		n. t.**	81i		58%
81k		51%	81m		n. i.
81n		n. i.	81h		n. i.

4.2 Carboxylic Acid Bioisosteres based on known Inhibitors

Table 4 continued

					
No	R	% inhibition @ 250 μ M	No	R	% inhibition @ 250 μ M
81o		25%	81r		n. i. @ 125 μ M*
81p		n. i.	81s		n. i.
81q		n. i.	81u		n. i.
81t		46%			

* highest tested concentration due to low compound solubility in DMSO

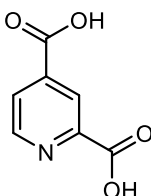
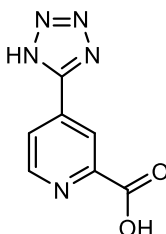
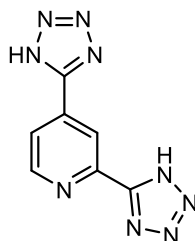
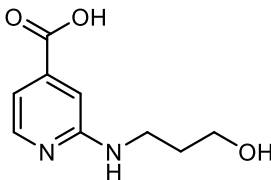
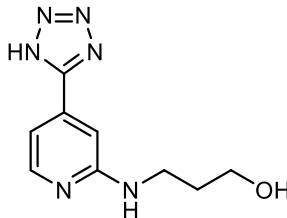
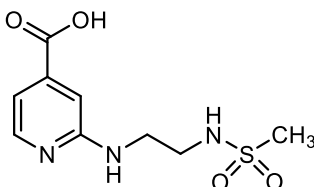
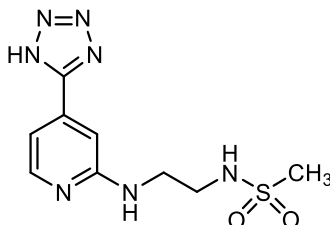
** n. t. = not tested due to very low compound solubility in DMSO

The substitution with an ethanol moiety in **81g** or its benzoate ester **81h** also gave inactive compounds, whereas a slight increase of potency to 58% inhibition at 250 μ M could be achieved by elongating the hydroxy-alkyl chain by one carbon in **81i**. Similarly, the ethylamine compound **81j** was also inactive, while chain elongation by two carbons led to an increased potency of 51% at 250 μ M for **81k**. However, the introduction of the second amine group lowered compound solubility in DMSO drastically, rendering the activity evaluation of the propylamine compound **81l** impossible. Due to the poor solubility this substitution pattern was not pursued any further. The exchange of the primary amine with a morpholine moiety in order to increase solubility resulted in an inactive compound (**81m**), as did the derivatisation to amides or carbamates bearing different aliphatic or

aromatic substituents (**81n**, **81o**, **81p** and **81q**, **81r**, **81s**). Only the methyl sulfonamide **81t** derived from the ethylamine **81j** showed some activity, though also rather weak (46% at 250 μ M), while the tolyl sulfonamide **81u** derived from the propylamine derivative **81l** was devoid of any activity.

In summary, none of the tested 2-aminopyridine compounds showed satisfactory inhibitory potential on KDM4A, as the most potent compound of this series **81i** only showed 58% inhibition, which is a > 5,000-fold drop compared to 2,4-PDCA.

Table 5 IC₅₀ values of 2,4-PDCA analogs against KDM4A. Compounds were kindly provided by Dr. Georg Fassauer. Data are mean \pm s. d. of at least two independent experiments.

 <p>2,4-PDCA IC₅₀ = 0.027 ± 0.012 μM</p>	 <p>82 IC₅₀ = 6.4 ± 2.9 μM</p>	 <p>84a IC₅₀ = 13.6 ± 0.6 μM</p>
 <p>83a IC₅₀ = 58 ± 20 μM</p>	 <p>81i IC₅₀ = 314 ± 124 μM*</p>	
 <p>83b IC₅₀ = 91 ± 27 μM</p>	 <p>81t IC₅₀ = 206 ± 5 μM*</p>	

* no full inhibition reached due to limited compound solubility, therefore IC₅₀ values must be considered as rough approximation

As 2,4-PDCA itself is a highly active compound, the next step was to elucidate which moiety caused the immense drop in potency. To determine if the tetrazole

4.2 Carboxylic Acid Bioisosteres based on known Inhibitors

moiety was detrimental to compound activity, two tetrazole analogs of 2,4-pyridine carboxylic acid, as well as two carboxylic acid analogs of the slightly active tetrazole compounds **81i** and **81t**, were synthesized in the Link group. The latter two compounds also allowed the evaluation of the amine part. Assay results are summarized in Table 5. The comparison between 2,4-PDCA and its 4-tetrazolyl analogue **82** revealed a more than 200-fold decrease in potency, suggesting that the tetrazole substituent was not able to bind to the enzyme as effectively as the carboxylic acid. However, only a 2–5-fold potency reduction was observed between the carboxylic acid-containing amino-compounds **83a** and **83b** and their tetrazole analogs **81i** and **81t**, proving that the contribution of the tetrazole moiety to compound potency cannot be assessed isolatedly in this case, but is highly dependent on the overall molecular structure.

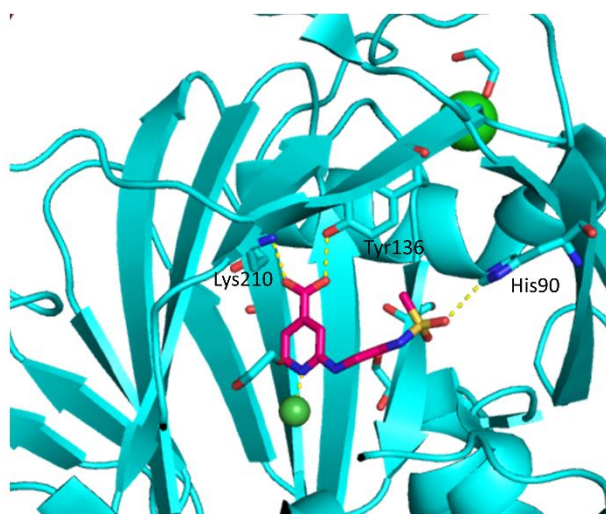


Figure 26 Docking of the sulfonamide-containing 2,4-PDCA derivative **83b** into KDM4A. No interaction between the central nickel ion and the secondary amine can be observed, explaining the low inhibitory activity of the compound. **83b** is depicted as pink sticks, Ni^{2+} as pale green sphere and Cl^- as light green sphere. Interactions are marked with yellow dashed lines. (PDB:6F5Q).

Comparing the amino-compounds **83a** and **83b** to 2,4-PDCA a 2150–3370-fold decrease was observed. Thus, the amino group seems to be unfavourable as an iron-chelating moiety. This observation was also supported by crystallographic data of **83b** bound to KDM4D (AA 1-342, cf. Figure 26), which was obtained by the Weiss

group (Macromolecular Crystallography, Helmholtz-Zentrum Berlin für Materialien und Energie; detailed procedures and results can be found in the PhD thesis of Dr. Georg Fassauer).²²² The crystal structures of both compounds show that the amino group does not participate in the metal binding, probably due to an unfavourable orientation, which explains the dramatic loss in potency. Therefore, a more suitable moiety was envisaged.

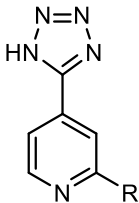
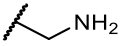
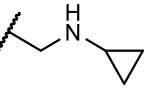
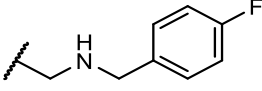
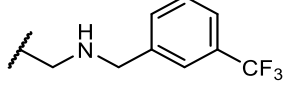
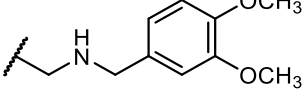
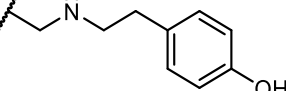
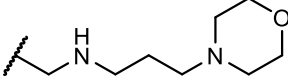
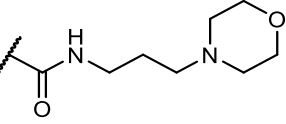
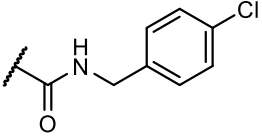
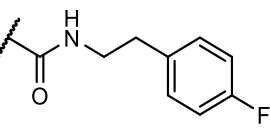
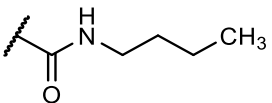
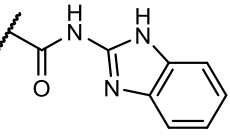
In the 2,4-PDCA analogue **84a**, not only the 4-carboxylic acid, but also the 2-carboxylic acid, which is part of the iron-binding motif, was exchanged by a tetrazole moiety, which led to a twofold potency reduction compared to **82**. As this is only a small decrease in relation to the pronounced potency loss observed for the amino compounds **81a–81u**, it was concluded that this moiety might be more suitable than the 2-amino group. However, tetrazoles only allow limited substitution and may be synthetically challenging, therefore secondary amines were chosen as a similar but more convenient alternative. Like the tetrazole, they have a distance of two carbon atoms between the iron-binding nitrogen atoms, which might be more favourable for iron-chelation than one carbon atom.

Indeed, several KDM inhibitors containing a pyridine moiety and another nitrogen in a two-carbon-distance have been published to date (cf. section 1.4.2.2 and Ref. 178).¹⁷⁸ Therefore, a compound series containing 2-ethylamino derivatives was synthesized and tested (cf. Table 6). While the unsubstituted amino derivative **84b** showed at least moderate inhibitory activity with an IC_{50} value of 20.9 μ M, monosubstitution with a cyclopropyl moiety eliminated the inhibitory capacity of the molecule **84c**. Substitution with fluorinated benzyl derivatives in **84d** and **84e** also caused a drop in potency to about 50% inhibition at 250 μ M, and to 19% for the dimethoxybenzyl derivative **84f**. The ethylphenyl derivative **84g** was also only very weakly active (41% inhibition at 250 μ M). The morpholine-containing compound **84h** showed assay interference probably due to low solubility. Next, derivatives bearing an amide function instead of the amino group were tested. However, these

4.2 Carboxylic Acid Bioisosteres based on known Inhibitors

also displayed rather weak inhibitory potential, the most active compound being **84i** bearing a propylmorpholino moiety and displaying an IC_{50} value of 100 μ M, while the other compounds **84j-m** showed no or weak inhibition.

Table 6 Inhibitory activity of 2-ethylaminopyridine derivatives against KDM4A. Compounds were kindly provided by Dr. Georg Fassauer. Data are mean \pm s. d. of at least two independent experiments.

					
No	R	IC_{50} or % inhibition @ 250 μ M	No	R	IC_{50} or % inhibition @ 250 μ M
84b		20.9 \pm 3.6 μ M	84c		n. i.
84d		51%	84e		49%
84f		19%	84g		41%
84h		assay interference	84i		100 \pm 29 μ M
84j		161 \pm 9 μ M	84k		26%
84l		n. i.	84m		57%

Summarized, a bulky cyclic substituent at the ethylamino moiety seems to be detrimental to inhibitory activity, which is in contrast to the linearly or branched substituents in published inhibitors such as KDOAM-20 (**25a**) that display nanomolar potency against KDM4 and KDM5 (170 nM on KDM4C, 7 nM on

KDM5B, determined in an AlphaScreen™ assay).¹⁷⁸ The second reason for the lower potency compared to the published inhibitors is the replacement of the 4-carboxylic acid with the tetrazole moiety, which is also detrimental to inhibition, as discussed above.

In summary, exchange of either carboxylic acid in 2,4-PDCA with tetrazole lead to a drop in potency against KDM4A. Exchange of the 2-carboxylic acid with amino moieties also decreased potency considerably, while substitution with an methylamino substituent regained some activity. The highest activity for the amino-containing derivatives with an IC_{50} of 21 μ M was observed for the 2-methylamino derivative **84b** bearing no further substituents, while large substituents again decreased inhibitory potential.

4.2.4 Tetrazolyhydrazides

Another tetrazole-containing compound series using a different molecular approach was evaluated next. Based on the finding that the plant growth regulator daminozide **9** (cf. Section 1.4.2.1) is a selective KDM2/7 inhibitor,¹²⁸ inhibitors bearing a similar hydrazide moiety were developed by Rüger *et al.* (cf. Figure 27a).¹⁶⁷

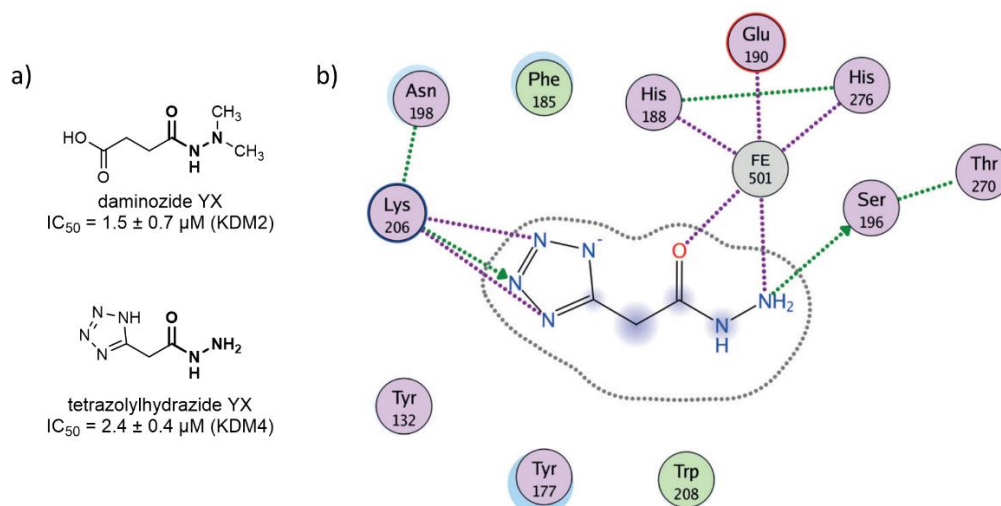


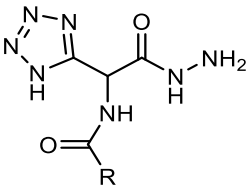
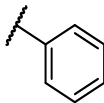
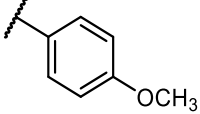
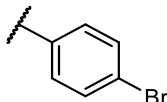
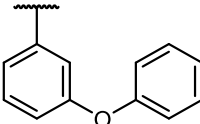
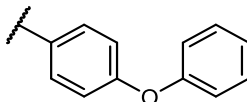
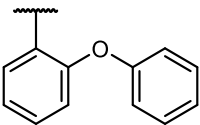
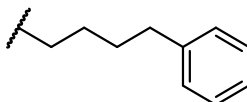
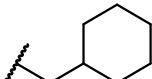
Figure 27 a) IC_{50} values of published hydrazide-based KDM inhibitors.^{128, 167}

b) Proposed binding mode of tetrazolyhydrazide **21** based on published co-crystal structures of KDM4 with known inhibitors. (Modified from Ref. 167).

4.2 Carboxylic Acid Bioisosteres based on known Inhibitors

Daminozide, which contains a hydrazide moiety as iron-chelating motif, acts as a co-substrate competitor where the hydrazide moiety replaces the 2-oxo-carboxylic acid of 2-OG. The terminal carboxylic acid undergoes polar interactions with a lysine and tyrosine residue in the active site of the enzyme. Rüger *et al.* used a tetrazole moiety as bioisosteric replacement of the carboxylic acid which is also able to form the critical interactions with the enzyme as suggested by docking (cf. Figure 27b). Their most potent compound 2-(1H-tetrazol-5-yl)acetohydrazide **21** displayed an activity of 2.4 μM against KDM4A and ~4- and 41-fold selectivity relative to KDM5A and KDM6B.¹⁶⁷ This fragment-like structure served as starting point for the development of 2-amido-substituted derivatives targeting further amino acid residues in KDM4.

Table 7 IC₅₀ values of tetrazolylhydrazide derivatives against KDM4A. All compounds were tested as racemates. Compounds were kindly provided by the research group of Andreas Link (EMAU Greifswald). Data are mean \pm s. d. of at least two independent experiments.

					
No	R	IC ₅₀ or % inhibition @ 125 μM	No	R	IC ₅₀ or % inhibition @ 125 μM
85a		4.38 \pm 2.95 μM	85b		81%
85c		47%	85d		7.09 \pm 0.16 μM
85e		52.4 \pm 0.4 μM	85f		56%
85g		83%	85h		40%

Tetrazolylhydrazides (cf. Table 7) were synthesized and provided by the research group of Prof. Andreas Link (EMAU Greifswald). Compounds were used as racemates. The phenyl-substituted derivative **85a** retained similar activity to the fragment **21** ($IC_{50} = 4.4 \mu M$). A *para*-methoxy substituent lead to a decrease of inhibition to 81% at 125 μM for compound **85b**, while *para*-bromo substitution gave 47% inhibition (**85c**). Elaboration of the phenyl substituent with an oxophenyl residue in position 3 **85d** lead to a slight decrease in potency ($IC_{50} = 7.1 \mu M$) while the same substituent in position 4 or 2 (**85e** and **85f**) decreased potency > 10-fold (52 μM and 56% inhibition at 125 μM , respectively), which is probably caused by steric clashes with the catalytic pocket of the enzyme. Other large substituents also decreased activity substantially (**85g**, **85h**).

In summary, larger substituents proved detrimental for inhibitory activity and none of the substituted compounds displayed a higher activity than the fragment **21**, which had served as starting point.

4.2.5 Summary and Discussion

To sum up the results from the bioisosteric replacement attempts, it can be concluded that the use of a boronic acid in IOX1 (**42**) was unsuitable for KDM4 inhibition. Furthermore, sulfoxides and sulfones as replacement for the 2-carboxylic acid in 2,4-PDCA decreased inhibitor potency substantially, as did the simple exchange with tetrazole. Replacement of the 4-carboxylic acid with tetrazole and the 2-carboxylic acid with amino substituents also lead to a drop in potency. A moderately active compound with an IC_{50} value in the two-digit micromolar range was obtained for the 2-ethylamino-4-tetrazolyl derivative **84a**, while other ethylamino derivatives bearing an additional substituent at the amine function were less active. Finally, substitution of a tetrazole-bearing analogue of daminozide **9** yielded two compounds displaying low micromolar activity, namely the phenyl- and 3-phenoxyphenyl derivatives **85a** and **85d**. Therefore, the use of a tetrazole

moiety as a bioisosteric replacement for the carboxylic acid undergoing ionic interactions with basic amino acid residues in the catalytic pocket of Jmj-KDMs, seems to be a viable strategy for the synthesis of new KDM inhibitors. This could be observed for two different inhibitor families, namely the 2,4-PDCA-derived and the daminozide-derived compounds. However, a significant decrease was observed in the former case, while the latter compounds showed similar activity to the parent compound.

4.3 Deferasirox Derivatives

Next, a different strategy starting from the known KDM inhibitor deferasirox (**54**) will be discussed. Deferasirox (Exjade®) is a clinically approved iron chelator used for the treatment of chronic iron overload disease caused by frequent blood transfusions or hereditary hemochromatosis. Deferasirox is capable of lowering iron levels by binding iron ions in the bloodstream and promoting their renal excretion. Furthermore, deferasirox has been shown to have anti-neoplastic effects in several cancer models, including hepatocellular²²³ and renal cell²²⁴ carcinoma, oesophageal²²⁵ and gastric²²⁶ cancer as well as multiple myeloma (MM)²²⁷ and myelodysplastic syndrome (MDS).²²⁸ Proposed mechanisms of action, besides the direct effects of a decreased intracellular iron concentration, include downregulation of the mTOR pathway (mammalian target of rapamycin)²²⁹ and inhibition of the NFκB pathway (nuclear factor kappa-light-chain-enhancer of activated B cells),²²⁸ which are implicated in cell growth, proliferation, differentiation, and tumour migration. However, further research is needed to delineate the molecular mechanisms contributing to the activity of deferasirox in cancer cells. Despite its promising potential in cancer models, significant beneficial effects of deferasirox in clinical trials have only been observed in patients suffering from MDS to date.²³⁰ Yet, the use of deferasirox, particularly in combination with

cytostatic drugs, may still be a promising strategy in various cancer treatments.^{231,}

232

Considering its anti-neoplastic activity, its status as an approved drug and, most importantly, its iron-chelation capacity, deferasirox posed an interesting starting point for the development of KDM4 inhibitors based on the 1,2,4-triazole structure. Roatsch *et al.* could show that deferasirox is a potent KDM4A inhibitor acting via complexation of iron in the active site and competitive displacement of the co-substrate 2-OG. Several close deferasirox derivatives also displaying inhibitory activity in the micromolar range were included in that publication.¹⁶⁸ Based on these results, a broader variety of deferasirox analogs, ranging from closely related 1,2,4-triazoles to thiazoles and oxazoles bearing various substituents, was synthesized and tested in this work. Furthermore, pyrazoles and imidazoles were also evaluated.

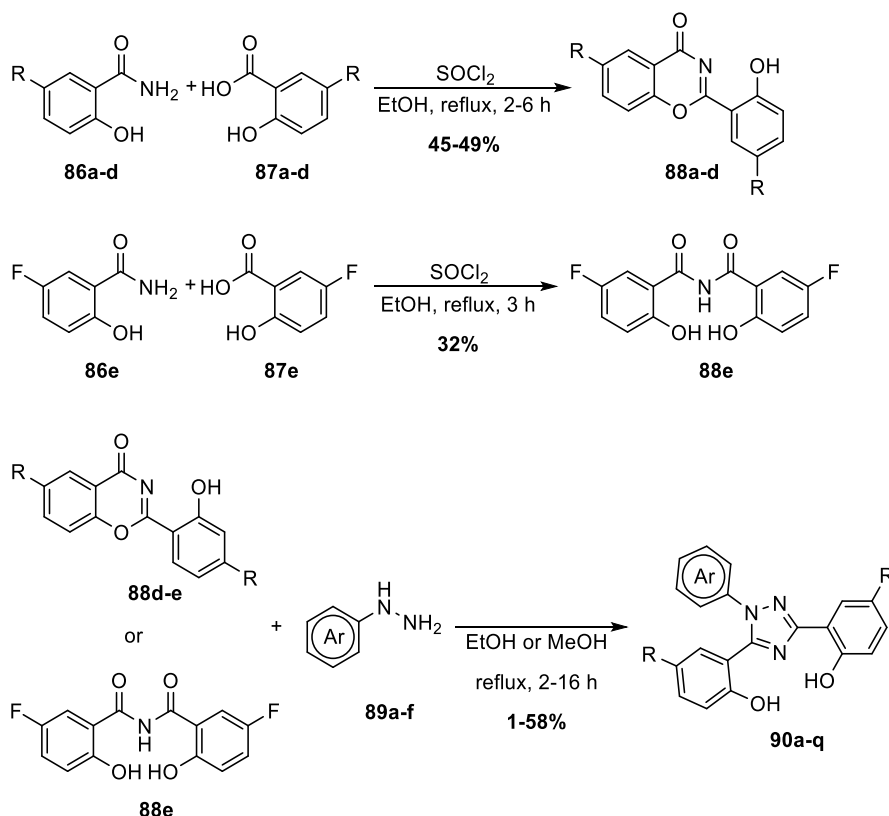
4.3.1 1,2,4-Triazoles

The 1,2,4-triazole scaffold was chosen based on the parent drug deferasirox (**54**), which consists of a triazole core motif bearing three aromatic substituents. Furthermore, triazoles are a versatile starting point for inhibitor development due to the availability of various synthetic routes.²³³ Additionally, the structure is viewed as a privileged scaffold in medicinal chemistry and is already a well-established moiety, not only in deferasirox, but also in other approved drugs, such as the antifungals fluconazole, itraconazole and voriconazole, antivirals like ribavirin, or the antimigraine drug rizatriptan.^{234, 235}

4.3.1.1 Synthesis of Triazoles

The synthetic route for deferasirox derivatives was based on the synthetic pathway developed by Dr. Martin Roatsch, which was oriented towards the methods applied for the commercial production of deferasirox (**54**) and literature reports.^{168, 236, 237} The

synthesis route, depicted in Scheme 6, is a two-step procedure starting from easily accessible monoaromatics. First, derivatives of salicylic acid and salicylamide are condensed to form 4*H*-benzo[*e*][1,3]oxazin-4-ones. These can be transformed to triazoles via cyclisation with hydrazine derivatives.



Scheme 6 Synthetic route towards deferasirox (**54**) and related triazoles. R = H, Cl, Br or OCH₃. See Table 9 for assignment of structures to abbreviations **a-q**.

4.3.1.1.1 Oxazinones

The condensation reaction of salicylic acid derivatives with amides is initiated by activation of the carboxylic acid with thionyl chloride in refluxing xylenes (mixture of isomers). The thus generated acid chloride reacts with the amide to form an imide intermediate, which undergoes an intramolecular cyclisation reaction, where one of the phenol moieties reacts in a nucleophilic addition-elimination reaction with one of the imide carbon atoms. An excess of thionyl chloride is used to trap the water generated by this reaction. Product precipitation was observed after addition of thionyl chloride upon cooling. The precipitate could be purified by recrystallisation

from a mixture of ethanol and acetic acid. As the reaction is not regioselective,²³⁸ a mixture of products is obtained when differently substituted salicylic acid and amide derivatives are used. To avoid the necessity of an additional step to separate different products, only identically substituted salicylic acid and amide derivatives were employed in this work. While the synthesis of the deferasirox precursor **88a**, the *para*-chlorinated **88b** and the *para*-methoxy-substituted **88c** have already been published before,¹⁶⁸ the *para*-brominated derivative **88d** is novel to the literature. Reaction yields ranged from 45 to 59%. The main by-product of the reaction is the imide, which can either originate from an incomplete reaction or from hydrolysis of the benzoxazinone. To avoid hydrolysis, the benzoxazinones have to be used in the next step immediately or be stored under exclusion of humidity. Using the same procedure, the synthesis of the fluorinated derivative was also attempted. However, only the imide intermediate **88e** could be isolated in 32% yield due to the susceptibility of the benzoxazinone to hydrolysis, although the successful synthesis of the fluorobenzoxazinone is described in two patents.^{239, 240} Nevertheless, no further attempts to achieve the synthesis of the fluorobenzoxazinone were undertaken, because the imide intermediate also proved to be sufficiently reactive for the next reaction step.

4.3.1.1.2 Triazole formation

The triazole heterocycle was generated from benzoxazinones—or the imide in the case of the fluorinated **90e**—via cyclization with suitably substituted hydrazine derivatives. The reaction proceeds via nucleophilic addition of the two hydrazine nitrogen atoms to the carbonyl and imine carbon atoms, ring opening of the benzoxazinone (**88a-d**) and elimination of water. For the fluorinated imide **88e** the reaction course is similar, starting with the nucleophilic addition of the hydrazine derivative to the imide carbonyls and subsequent elimination of two water molecules. As only symmetrically substituted benzoxazinones and imides were used, the low regioselectivity of the reaction was irrelevant, because the same

product is obtained irrespective of the position of the first nucleophilic attack. Reaction conditions were chosen based on the procedures for the synthesis of deferasirox (**54**) and close derivatives published by Patil *et al.*²³⁶ and Steinhäuser *et al.*,²³⁷ using either methanol or ethanol as solvent depending on the solubility of the hydrazine derivative used for the reaction. Reactions were performed at reflux temperature. For compounds crystallising from the reaction mixture upon cooling, purification was performed via recrystallisation from methanol, if necessary. This procedure was feasible for deferasirox (**54**), the brominated derivative **90d**, the methoxylated **90c** and the fluorinated **90e**. For some of the other compounds precipitation from the reaction mixture could be achieved via addition of hydrochloric acid. The obtained precipitates could then also be recrystallised from methanol. This procedure was used for the N-phenyl substituted derivatives bearing chlorine (**90b**) or bromine (**90f**) substituents on the phenol moieties as well as for the N-*p*-benzonitrile substituted **90g**. The methoxy substituted phenyl derivative **90h**, as well as the N-*o*-methoxy substituted derivative **90i** were highly soluble in methanol, preventing recrystallisation from this solvent, therefore 2-propanol was used instead. The lowest reaction yield of 9% (**90c**; published yield 18%)¹⁶⁸ and 10% (**90h**) was obtained for the two derivatives bearing methoxy substituents. This can be explained by the electron donating +M-effect of the methoxy groups, which increases the electron density of the aromatic rings and thereby decreases the electrophilicity of the adjacent carbonyl or imine groups.²³⁸ This effect lowers reactivity towards the nucleophilic attack of the hydrazine derivatives. The fluorinated derivative **90e** was obtained in 13% yield due to the lower reactivity of the imide precursor compared to benzoxazinone derivatives. For the other compounds, yields ranged from 16% to 47% mainly depending on the purification process, whereby the highest yield was obtained for deferasirox (**54**; published yield 41–99%).^{241, 242} The N-pyrid-2-yl and N-quinolin-8-yl compounds **90j** and **90k** did not precipitate from the reaction mixture even after the addition of hydrochloric acid, which is probably due to their higher basicity compared to the

other compounds. They were recovered from the reaction mixture via evaporation and purification via flash column chromatography. Unfortunately, this procedure did not yield the compounds in sufficient purity, therefore a second purification step via semi-preparative HPLC for the *N*-pyrid-2-yl compound **90j** respectively recrystallisation from 2-propanol for the *N*-quinolin-8-yl compound **90k** was necessary, which lowered the isolated yield to 1% and 11%.

Demethylation of the *N*-2-methoxyphenyl compound **90i** and the *p*-methoxyphenol compound **90h** via cleavage with boron tribromide yielded the phenolic compounds **90l** in 39% yield and **90m** in 43% yield after chromatographic purification.

As pointed out in Section 1.4.2 the *in vitro* assay results for KDM4 inhibition can be affected by iron chelators, which bind Fe²⁺-ions in solution and sequester iron from the enzyme thereby reducing enzyme activity and leading to false positive results. To compare the effects of an active-site binding inhibitor to a mere iron-chelator displaying no or weak binding to the enzyme, the synthesis of a derivative containing the same iron-binding motif as the active compounds but bearing bulky substituents inducing steric clashes with the active site was envisioned. The first approach using the same synthetic procedure as for the other derivatives with phenyl-substituted salicylic acid derivatives proved to be ineligible because only trace amounts of benzoxazinone were observed in the first reaction step. Instead, a mixture of several degradation products was obtained. In order to minimize the formation of side products, milder reaction conditions were tried by replacing the one-pot procedure with thionyl chloride in refluxing xylenes by a three-step procedure consisting of activation of the acid, coupling to the amide and cyclisation. In the first step, the salicylic acid derivative was activated to the acid chloride with thionyl chloride in dichloromethane at r.t. After removal of the excess of chlorinating agent, the acid chloride and the amide were condensed to form the imide intermediate in acetonitrile at room temperature using diazabicyclo[5.4.0]undec-7-ene (DBU) as catalytic base. However, the cyclisation of the

imide to the benzoxazinone was neither successful under acid catalysis with sulfuric or *para*-toluenesulfonic acid in different solvents (acetonitrile, methanol, toluene) nor under μ W-irradiation in DMSO. The use of dehydrating agents like phosphorus pentoxide or orthoformic acid was ineffective as well. Additionally, direct triazole formation from the imide intermediate, as performed for the fluorinated derivative **90e**, was also unsuccessful.

Next, a synthetic strategy introducing the bulky substituents in the last reaction step was envisioned to circumvent the benzoxazinone synthesis. As the brominated derivative **90f** was already available, it was chosen as the starting point for a cross-coupling reaction. Cross-coupling reactions are convenient for the generation of carbon-carbon or carbon-heteroatom bonds due to the availability of numerous different starting materials, catalysts and experimental procedures. However, this diversity complicates the selection of the most suitable approach, especially because the reaction performance is often highly sensitive to confounding factors like catalyst inactivation, incompatible functional groups or inappropriate solvents. Therefore, a screening of various conditions is often necessary. Most cross-coupling reaction procedures make use of catalysts consisting of a transition metal like copper, nickel or palladium and ligands stabilizing the favoured oxidation state and modifying the reactivity. As the deferasirox derivatives are strong metal chelators, they most likely interfere with the catalyst via displacement of the ligands and consecutive inaccessibility of the metal ion for the reaction. Indeed, no coupling could be observed between **90f** and phenylboronic acid under several standard conditions used for Suzuki couplings as summarized in Table 8 (top). Experiments with Buchwald-Hartwig cross coupling of **90f** and morpholine were also unsuccessful (cf. Table 8 bottom).

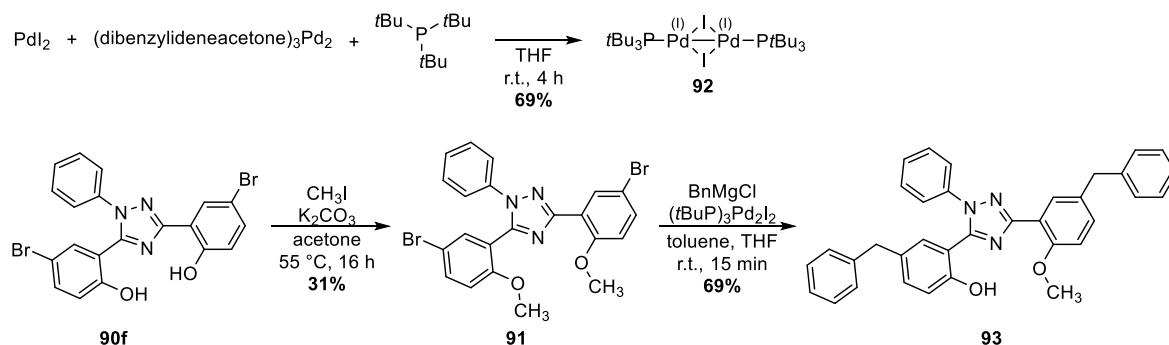
In order to resolve this problem by decreasing the affinity of **90f** to the palladium catalyst, the two phenol groups were masked with methyl groups yielding compound **91**. The high sensitivity of some palladium catalysts towards oxygen and moisture from ambient air proved to be another obstacle that hampered the

reaction. This drawback could be solved by the use of an air-stable $[\text{Pd}(\mu\text{-I})(\text{P}t\text{Bu}_3)]_2$ -catalyst **92** published by Aufiero *et al.*²⁴³ (cf. Scheme 7) in a Kumada coupling of **91** and benzylmagnesium chloride. Following the procedure of Kavlet *et al.*²⁴⁴ the reaction was performed at room temperature in toluene and the Grignard reagent was added as THF solution.

Table 8 Reaction conditions for coupling trials with **90f**. However, none of the conditions yielded the desired product.

catalyst and ligand	base	solvent	temperature
Suzuki coupling of 90f with phenylboronic acid YX			
$\text{Pd}(\text{PPh}_3)_4$	Na_2CO_3	THF	90 °C
$\text{Pd}(\text{PPh}_3)_4$	Na_2CO_3	toluene	90 °C
$\text{Pd}(\text{OAc})_2$	Na_2CO_3	water	r.t.
$\text{PdCl}_2(\text{PPh}_3)_2$	Cs_2CO_3	water/dioxane	100 °C, μW
Buchwald-Hartwig coupling of 90f with morpholine YX			
$\text{Pd}_2(\text{dba})_3 \cdot \text{HCCl}_3$ <i>t</i> Bu-XPhos	Na t BuO	toluene	90 °C
$\text{Pd}(\text{OAc})_2$ CyJohnPhos	Na t BuO	toluene	150 °C, μW
$\text{Pd}(\text{OAc})_2$ DCPB	Na t BuO	toluene	150 °C, μW
$\text{Pd}(\text{OAc})_2$ Cy ₂ -2,4,6-trimethoxybiphenylP	Na t BuO	toluene	150 °C, μW
$\text{Pd}(\text{OAc})_2$ <i>t</i> Bu-XPhos	LHMDS	THF	80 °C, μW
μW microwave irradiation PPh_3 triphenylphosphine dba dibenzylideneacetone <i>t</i> Bu-XPhos 2-di- <i>tert</i> -butylphosphino-2',4',6'-triisopropylbiphenyl CyJohnPhos (2-biphenyl)dicyclohexylphosphine DCPB 1,4-dicyclopropylbuta-1,3-diyne Cy ₂ -2,4,6-trimethoxybiphenylP dicyclohexyl(2',4',6'-trimethoxy[1,1'-biphenyl]-2-yl)-phosphine LHMDS Lithium bis(trimethylsilyl)amide			

After aqueous work-up, extraction and chromatographic purification the dibenzylated product **93** could be obtained in 40% yield (cf. Scheme 7). Interestingly, demethylation of one of the methoxy groups was observed despite the short reaction time of 15 min.



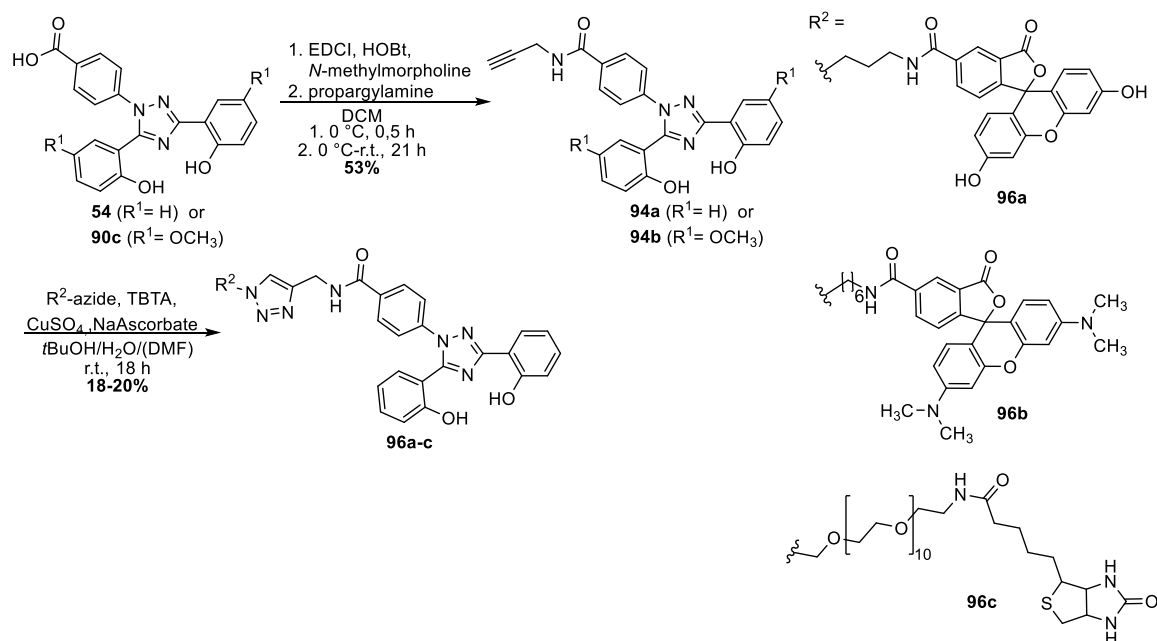
Scheme 7 Synthetic procedures for the generation of the palladium catalyst for the Kumada coupling and the synthesis of **93**, which was demethylated with boron tribromide to yield **90n**.

However, no attempts to avoid this deprotection were undertaken, as it did not seem to prevent product formation. Demethylation of the second methoxy group was accomplished by the standard procedure using boron tribromide yielding compound **90n**.

4.3.1.1.3 Labelling reactions

In order to develop a fluorescence polarization assay (cf. Section 4.3.1.3), two chemical probes consisting of deferasirox (**54**) coupled to a fluorescent moiety via a linker were synthesized. The synthesis was set up as a two-step procedure firstly installing a reactive moiety on deferasirox and secondly tagging the molecule with the fluorophore via click reaction (cf. Scheme 8). Click reactions are defined as modular reactions which are wide in scope, easy to perform and purify and result in high product yields.²⁴⁵ One of the most prominent click reactions is the copper(I)-catalysed alkyne-azide cycloaddition (CuAAC) of a terminal alkyne and an organic azide giving a 1,2,3-triazole.²⁴⁶ An advantage of such an approach is that once a precursor with a suitable “click”-moiety is available it can be easily modified with

various compounds bearing the corresponding “click”- motif. As the CuAAC is used for many applications a variety of suitably tagged fluorophores is commercially available, therefore this approach was chosen for the synthesis of fluorescently labelled deferasirox derivatives. The carboxylic acid of deferasirox (**54**) was chosen as an anchor point for the terminal alkyne because it can conveniently be transformed to an amide bearing the desired alkyne moiety. More importantly, docking of deferasirox to KDM4A revealed that the carboxylic acid is pointing out of the catalytic pocket, therefore a modification at this position would probably not interfere with compound binding to the catalytic iron (cf. section 4.3.1.2). Deferasirox was amidated with propargylamine following a standard procedure using 1-ethyl-3-(3-dimethylaminopropyl)carbodiimide hydrochloride (EDCI) and 1-hydroxybenzotriazole hydrate (HOBt) as activating agents and *N*-methylmorpholine as a base in DMF.²⁴⁷ Purification via extraction and flash column chromatography gave the desired product **94a** in sufficient yield (53%) for the next step. The same procedure was also successfully employed to the deferasirox derivative **90c** yielding **94b**.



Scheme 8 Synthetic procedures for the synthesis of labelled deferasirox derivatives.

The reaction conditions for the CuAAC were chosen in accordance with a literature procedure and no optimisation attempts were undertaken.²⁴⁸ CuSO₄ was used as

copper source while sodium ascorbate and tris(benzyltriazolylmethyl)amine (TBTA) were added to stabilize the Cu⁺-Ions needed for catalysis. 6-Carboxyfluorescein azide (6-FAM azide) **95a** for the synthesis of compound **96a** and 5-carboxamido-(6-azidohexanyl)tetramethylrhodamine (5-TAMRA azide) **95b** for compound **96b** were used as fluorophores. The definition of click reactions by Kolb *et al.*²⁴⁵ states that the desired product should be obtained in sufficient purity without a chromatographic purification step. They recommend purification via crystallization or distillation. However, these methods could be applied neither to **96a** nor to **96b**, because the reactions did not give full conversion and too low product amounts for recrystallization. Therefore, separation of the starting materials from the final products via chromatographic purification was mandatory. This was effectively realised via reversed-phase flash column chromatography or semi-preparative HPLC. However, some amount of product was lost to unsuccessful purification trials lowering the final yield to 18–20%. The biotinylated deferasirox probe **96c** intended for the use in *in vitro* or cellular binding assays was synthesized following the same procedure in 15% yield.

4.3.1.1.4 NMR assignments

To confirm the molecular structure of the synthesised compounds, NMR studies were performed. As all synthesised compounds contain four aromatic rings the ¹H- and ¹³C-signals cover a rather narrow range. To allow unambiguous signal attribution, COSY-, HSQC- and HMBC-experiments were performed for most of the final compounds. The following section exemplary discusses the signal assignment for triazole compounds.

The brominated deferasirox derivative **90d** was chosen as first example, because the assignment is quite straightforward and there are no signal overlaps complicating analysis. Numbering for all compounds follows the generic structure shown in Scheme 9.



Scheme 9 Generic naming of rings and atom numbering for triazole (X = N), thiazole (X = C, S, N) and oxazole (X = C, O, N) compounds.

The aromatic proton displaying the highest chemical shift is the proton *ortho* to the triazole and the bromine substituent, as they both lead to deshielding (cf. Figure 28).

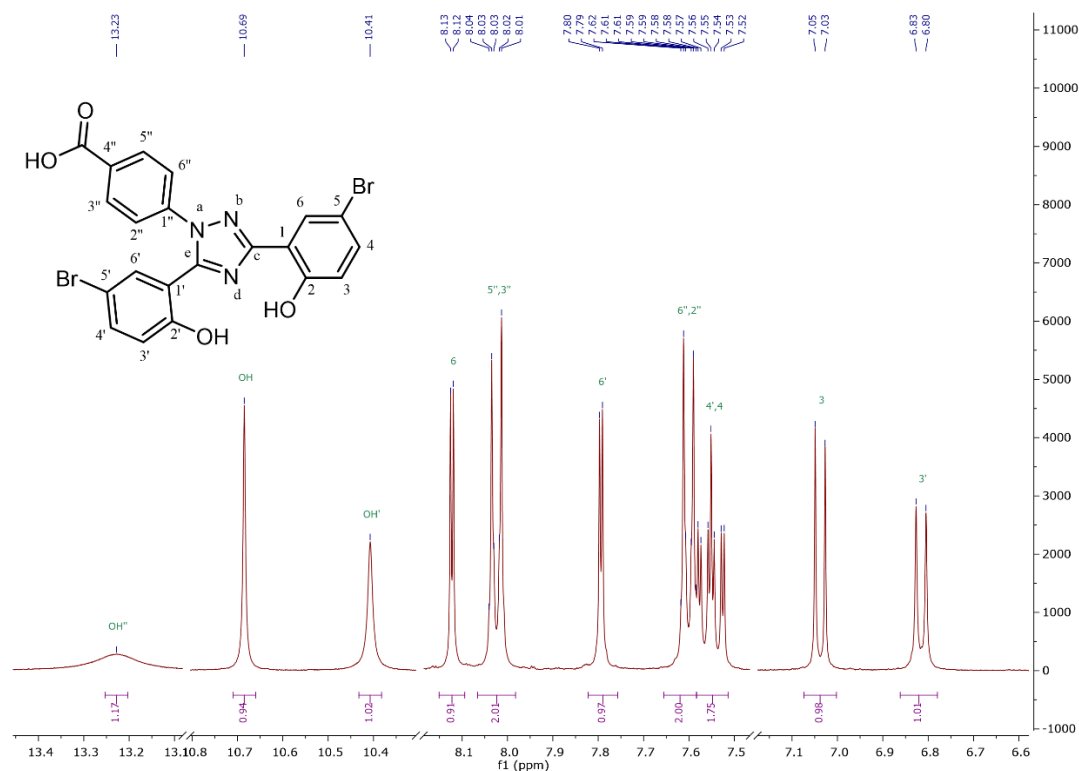


Figure 28 ^1H -NMR spectrum of compound **90d**. The hydroxy groups give (broad) singlets which are shifted furthest downfield. The aromatic protons of the phenol rings give doublets (*ortho*-coupling for H3 and 3', *meta*-coupling for H6 and 6') or doublets of doublets for H4 and 4' (*ortho*- and *meta*-coupling). *Para*-coupling is not resolved in the spectrum. The ring bearing the carboxy group yields two multiplets typical for an AA'BB' spin system.

The two phenol moieties differ in their chemical shifts due to the influence of the substituted triazole ring. Assignments to each of the phenol rings can be deduced from the HMBC correlation between the respective proton *ortho* to the triazole and the carbon atoms of the triazole ring (C_c and C_e). As C_c is shifted downfield compared to C_e due to the stronger deshielding by the adjacent unsubstituted

triazole nitrogen these two can easily be distinguished.²⁴⁹ As shown in Figure 29 C_e correlates with H6 corresponding to the doublet at 8.12 ppm while C_e correlates with H6' (d, 7.79 ppm). The shift difference probably results from the stronger deshielding effect of the unsubstituted triazole nitrogen in the vicinity of H6. H4 and H4' couple with H3 and H6 or H3' and H6', respectively, giving rise to overlapping doublets of doublets between 7.58 – 7.51 ppm, the H4' signal being shifted slightly more downfield. The protons H3 and H3' *ortho* to the phenolic hydroxy groups are shifted upfield due to the electron donating effect of the hydroxy group and appear as doublets owing to the *meta*-coupling with H4 and H4', respectively. *Para*-couplings are not resolved in the spectrum. Of the two, H3' is shifted further upfield. The third aromatic ring bearing the carboxy group gives two multiplet signals corresponding to an AA'BB' spin system, where the signal further downfield belongs to the protons *ortho* to the carboxylic acid due to strong deshielding.

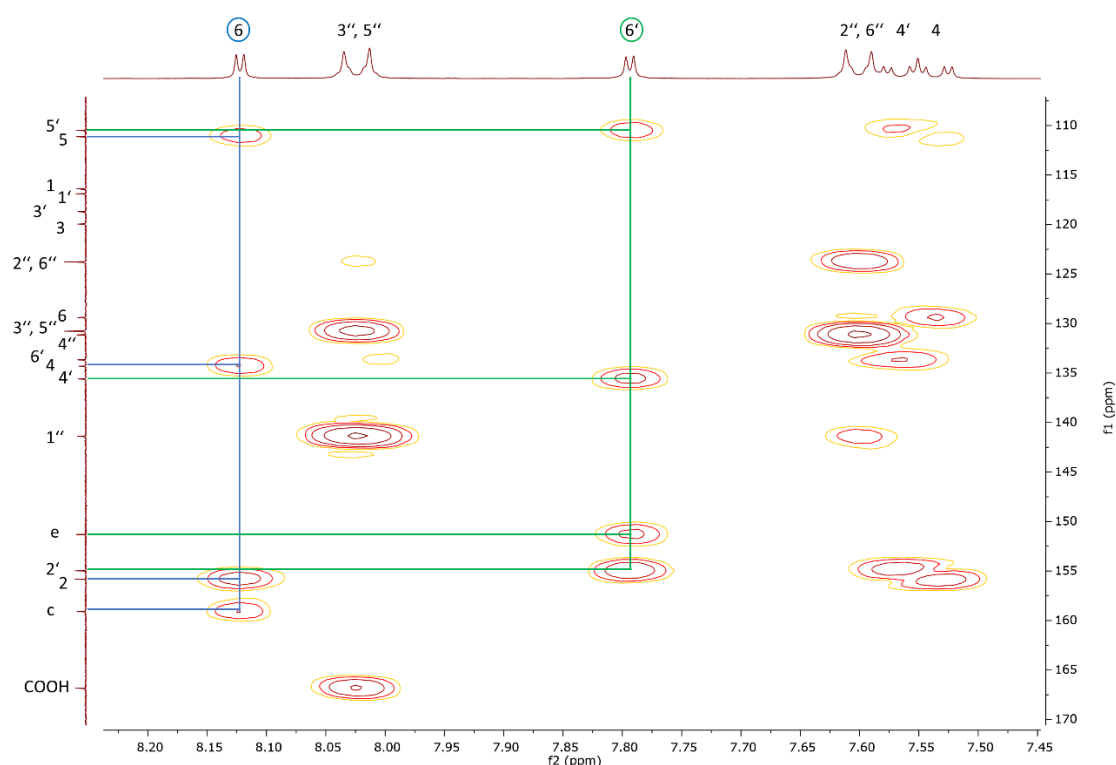


Figure 29 Section of the HMBC spectrum of **90d**. The 3J correlations for H6 are shown in blue and in green for H6'.

The hydroxy groups give signals between 10 and 13.5 ppm, the carboxy OH being the most downfield, followed by the phenolic OH and OH'. The assignments of the carbon atoms can be deduced from correlations in the HSQC and HMBC spectra as exemplified in Figure 29.

As a second example the pyridine-containing **90j** will be discussed. The protons of the pyridine ring are shifted downfield due to the deshielding effect of the nitrogen atom, the effect being strongest for the protons in *ortho* (H6'', 8.36 ppm) and *para* (H4'', 8.10–8.04 ppm) position. H4'' overlaps with proton H6 from the phenol rings. As for **90d**, assignment to one of the phenol rings can be deduced from the HMBC correlation between the respective proton *ortho* to the triazole and the carbon atoms of the triazole ring (C_c and C_e; cf. Figure 29). Again, this reveals H6 being the one further downfield, which in this case overlaps with H4''.

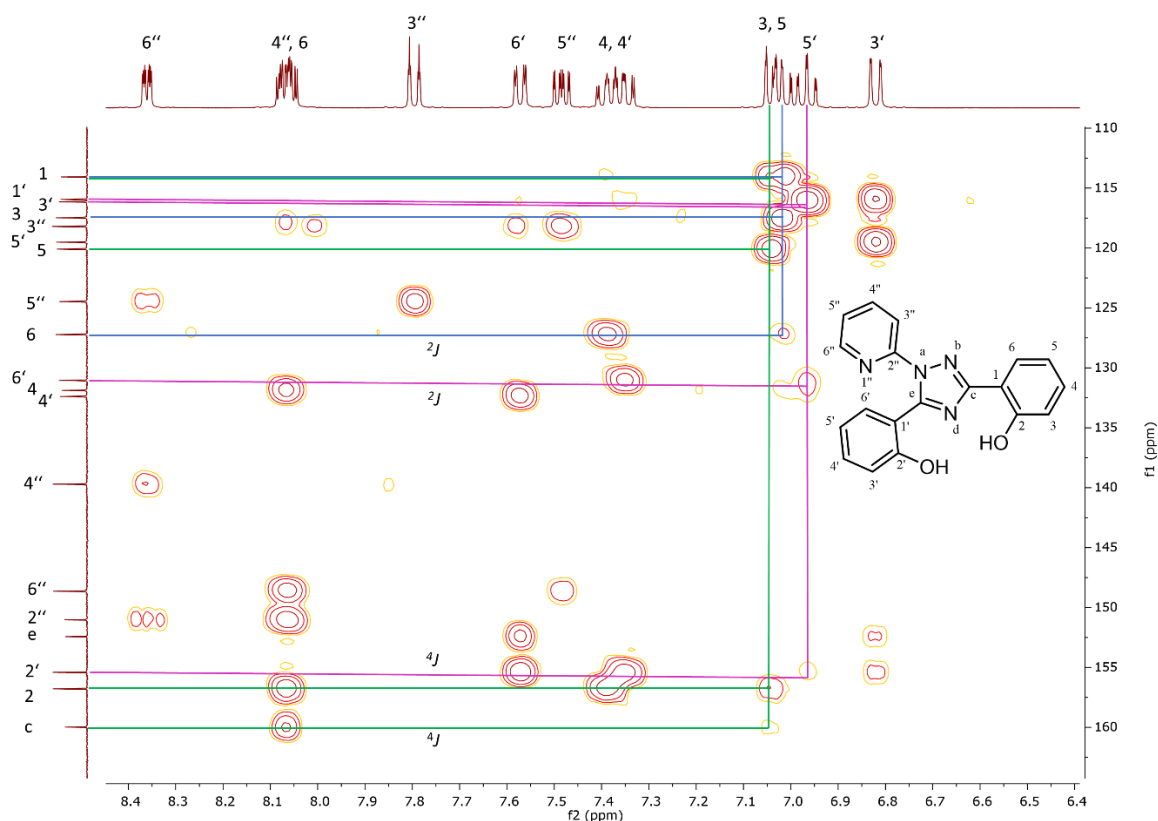


Figure 30 Section of the HMBC spectrum of **90j**. Correlations for H3 are marked with green lines, blue lines for H5, and purple lines for H5'. Unless noted otherwise lines represent couplings over three bonds.

The multiplicity of the pyridine signals is in accordance with the substitution pattern. H3'' appears as doublet of triplets due to the *ortho*-coupling and *meta*- and

para-couplings with the same coupling constant ($^3J = 8.1$ Hz, $^4J = 1.0$ Hz and $^5J = 1.0$ Hz). H5'' appears as doublet of doublet of doublets due to the two *ortho*-couplings and one *meta*-coupling ($^3J = 7.5$ Hz, $^3J = 4.9$ Hz and $^5J = 1.0$ Hz) with the typically lower coupling constant for the proton adjacent to the pyridine nitrogen. H6'' also appears as doublet of doublet of doublets with one *ortho*-, *meta*-, and *para*-coupling, respectively ($^3J = 4.9$ Hz, $^4J = 1.9$ Hz and $^5J = 1.0$ Hz). Multiplicity of H4'' cannot be read out due to the overlap with H6. For the phenol ring protons and the carbon atoms, assignment can again be performed via HSQC and HMBC spectra. Exemplary assignments are shown in the HMBC spectrum depicted in Figure 30.

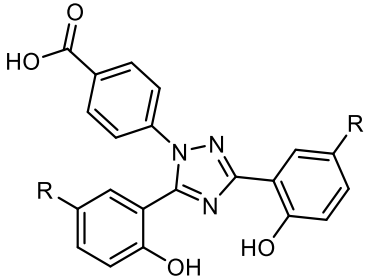
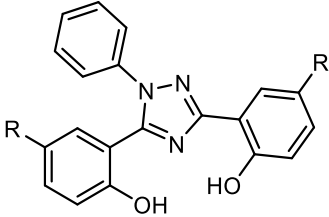
4.3.1.2 Biochemical Activity of Triazoles

Inhibitory activity of the deferasirox derivatives was evaluated in the KDM4A-LANCE assay (cf. section 3.1.2 for the assay description and Table 9 for results).

As previously reported by our group,¹⁶⁸ deferasirox (**54**) acts as a KDM4A inhibitor displaying an IC_{50} value of 5 μ M with no selectivity over other KDMs. However, as discussed in section 1.4.2, determination of IC_{50} values via this assay is insufficient to prove an active-site based mechanism of action, because sequestration of iron from the enzyme also causes apparent enzyme inactivity. Therefore, confirmation of active-site binding should be performed for every new compound family via alternative methods. An extensive discussion of applicable procedures and the results obtained for deferasirox (**54**) can be found in the publication of Roatsch *et al.*¹⁶⁸ of 2019. In short, mixed-type competition towards the co-substrate 2-OG was observed in kinetic measurements, molecular docking suggested a plausible binding mode and NMR- and EPR-data indicated interactions of the inhibitor with the active site of the enzyme. However, in absence of a solved crystal structure of the inhibitor in the catalytic pocket, no definitive proof was available. Therefore, another indirect verification for structure-based enzyme inhibition was attempted.

4 Development of novel Inhibitors for JmjC-containing histone demethylases

Table 9 IC₅₀ values of close deferasirox derivatives against KDM4A. Data are mean ± s. d. of at least two independent experiments.

					
No	R	IC ₅₀ / μM	No	R	% inhibition or IC ₅₀ / μM
54	H	4.8 ± 0.2 ¹⁶⁸	90o	H	5.3 ± 1.0 ¹⁶⁸
90c	OCH ₃	3.7 ± 0.1 ¹⁶⁸	90m	OH	4.1 ± 0.1
90e	F	4.2 ± 0.2 ¹⁶⁸	90n	benzyl	50% @ 50 μM
90p	Cl	5.1 ± 0.1 ¹⁶⁸	90b	Cl	3.4 ± 0.7
90d	Br	21.6 ± 2.3	90f	Br	assay interference

As it is apparent from the docking pose for deferasirox (**54**) displayed in Figure 31 small substituents in *para*-position to the phenolic moieties can be accommodated in the catalytic pocket whereas larger substituents would cause steric clashes, particularly in a subpocket lined by Tyr132, Asn198 and Lys206. In conclusion, given an active-site-based mode of action, moderate effects on inhibitory activity should be observed for small substituents, while bulkier ones should induce a significantly decreased potency. Contrastingly, if inhibition were only caused by iron chelation in solution, substituent effects should be negligible independent of their size, as their impact on the chelating motive is rather small.

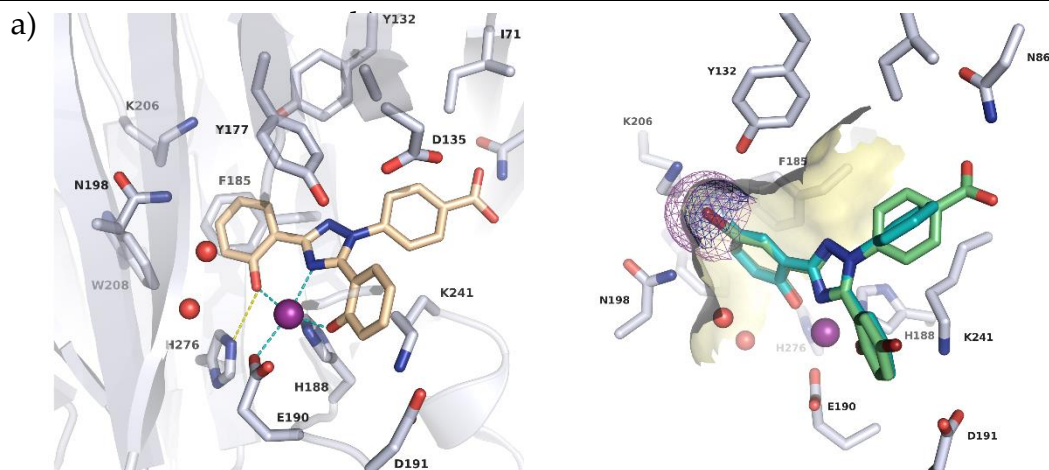


Figure 31 a) Docking of deferasirox (**54**) (beige sticks) to KDM4A. The central Ni^{2+} ion is depicted as purple sphere and water molecules as red spheres. Metal coordination is shown as teal dashed lines, H-bonds as yellow dashed lines.

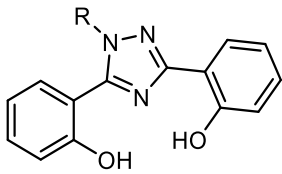
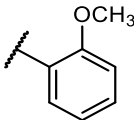
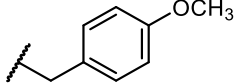
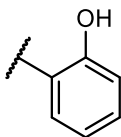
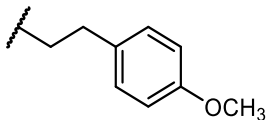
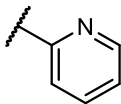
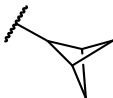
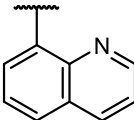
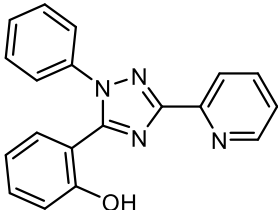
b) Docking poses of the triazoles **90d** (green sticks) and **90e** (cyan sticks). The van-der-Waals surface around the bromo-substituent is shown as purple mesh while the surface of the fluoro substituent is shown as blue mesh. The surface of the subpocket lined by Tyr132, Asn198 and Lys206 is depicted in yellow. Steric clashes between the subpocket and the bromine substituent lead to a decrease of inhibitory activity for **90d**. (Figures and docking provided by Dr. Dina Robaa, MLU Halle-Wittenberg, KDM4A template is PDB: 3RVH)

Indeed, the assay revealed that small substituents, specifically fluoro, chloro or methoxy substituents (**90e**, **90p** and **90c**; as previously published¹⁶⁸), as well as hydroxy groups in *para*-position to the phenol moieties (**90m**) had little effect on potency ($\text{IC}_{50} = 3.4\text{--}5.1\text{ }\mu\text{M}$, cf. Table 9). Contrastingly, incorporation of bromo (**90d**) or benzyl moieties (**90n**) led to a decreased activity of $22\text{ }\mu\text{M}$ and 50% inhibition at $50\text{ }\mu\text{M}$, respectively, thereby substantiating the hypothesis of active-site inhibition. However, it should be noted that, although specific interactions with the enzyme seem to be crucial for compound activity, potent iron chelation to the enzyme-bound iron is still the main precondition for compound activity. Hence, some iron chelation in solution may also contribute to inhibition. The influence of the potency of iron chelation could be shown via replacement of the phenol moiety in ring A with 2-pyridine (**90t**, synthesis performed by Dr. Nicolas Barthes), which resulted in a less favourable geometry for iron chelation and significantly decreased compound activity (67% inhibition at $100\text{ }\mu\text{M}$).

4 Development of novel Inhibitors for JmjC-containing histone demethylases

As a next step, the influence of the aromatic ring not directly involved in iron chelation was assessed. Previous results had shown that removal of the carboxylic acid did not decrease compound activity (see deferasirox (**54**) vs **90o**).¹⁶⁸ This observation was confirmed with the chlorinated analogs **90p** vs **90b**. Furthermore, exchange of the phenyl group with a 2-methoxyphenyl- (**90i**), 2-hydroxyphenyl- (**90l**) or 8-chinoliny-moiety (**90k**) also influenced compound potency merely insignificantly ($IC_{50} = 4,2\text{--}5.5\ \mu\text{M}$).

Table 10 IC_{50} values of 1*N*- and 3*C*-substituted deferasirox derivatives against KDM4A. Data are mean \pm s. d. of at least two independent experiments.

					
No	R	$IC_{50} / \mu\text{M}$	No	R	$IC_{50} / \mu\text{M}$
90i		4.5 ± 1.1	90q*		7.3 ± 1.5
90l		5.5 ± 0.4	90r*		6.1 ± 0.4
90j		23.8 ± 1.5	90s*		2.7 ± 0.2
90k		4.2 ± 0.1	90t*		67% @ $100\ \mu\text{M}$

* Compounds were kindly provided by Dr. Nicolas Barthes.

A five-fold reduction was observed for the 2-pyridyl compound **90j** which could not be explained by docking, though. Replacement of the aromatic ring by a *p*-methoxybenzyl (**90q**) or *p*-methoxyphenethyl moiety (**90r**) or the phenyl bioisostere

bicyclo[1,1,1]pentane (**90s**) did not change the inhibitory activity significantly (IC_{50} values 7.3 μ M, 6.1 μ M and 2.7 μ M). These three compounds were synthesized by Dr. Nicolas Barthes and their IC_{50} values were determined by Karin Schmidt-kunz (Jung group).

To sum up the results for the triazole derivatives, the marked drop in potency observed for the two derivatives **90d** (bromo) and **91** (phenyl) bearing bulky substituents provided a further piece of evidence for an active-site based mode of action. Furthermore, changes on the aromatic ring in position 1 had no distinct impact on enzyme inhibition, the 2-pyridyl derivative **90j** being the only exception where a decrease of inhibitory activity was observed. Conclusively, position 1 was considered as a potential attachment point for functional modifications like fluorescent labels or affinity tags.

The first fluorescently labelled compound **96a** bears a fluorescein moiety which is linked to deferasirox (**54**) via a 1,2,3-triazole-containing linker (cf. Figure 32).

The second structure **96b** is labelled with TAMRA connected via a linker which is three CH_2 groups longer than in **96a**.

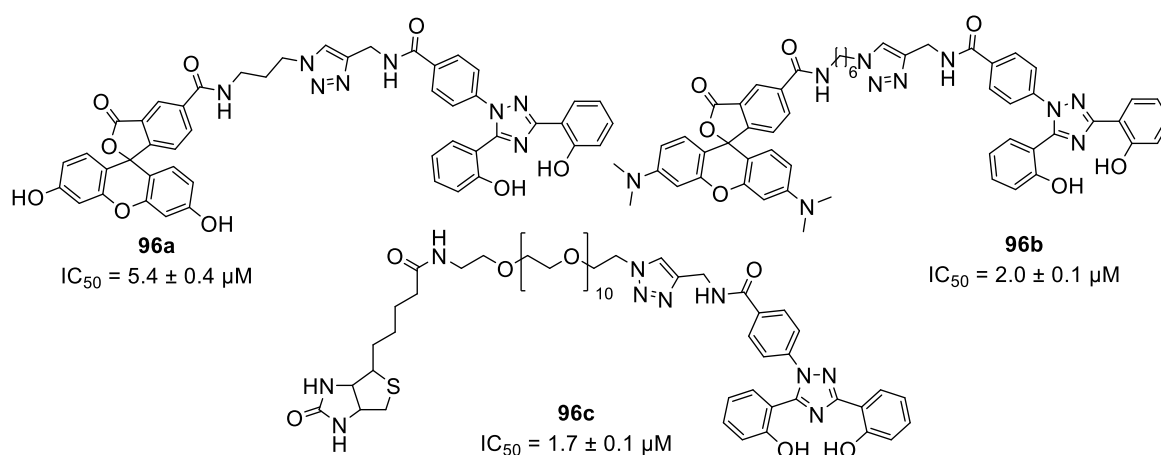


Figure 32 Inhibition values of labelled deferasirox derivatives. Data are mean \pm s. d. of at least two independent experiments.

In both cases the attachment of the fluorescent moiety did not impede KDM4A inhibition and IC_{50} values of 5.4 μ M and 2.0 μ M were obtained. Additionally, a

biotin-labelled compound, which is amenable for binding experiments using streptavidin, was tested. This compound yielded an even lower IC₅₀ value of 1.7 μ M.

4.3.1.3 Evaluation of Labelled Derivatives

With two fluorescently labelled deferasirox derivatives at hand, binding characteristics of these derivatives were assessed using a fluorescence polarization assay.

4.3.1.3.1 Fluorescence Polarisation Assay

The fluorescein- and TAMRA-labelled deferasirox derivatives **96a** and **96b** were evaluated in a fluorescence polarization (FP) assay. As explained in section 1.3.6 the assay principle relies on the different rotational velocity of small and large molecules in solution. This movement can indirectly be registered via measurement of the degree of polarization of light emitted by fluorescent probes. For small molecules fast rotation correlates with high depolarization of emitted light due to the movement of the molecule in the excited state. For larger molecules rotation is slow, therefore polarization is mainly kept and a high FP signal can be measured. When a small fluorescently labelled probe is used, binding to a protein target leads to an increase of polarization due to the high molecular weight of the overall complex, therefore the assay can be used for the detection of binding events.

To ensure that no quenching of the fluorescent probe occurred in the applied concentration range a calibration curve was recorded. Indeed, it showed linear correlation between fluorescence intensity and probe concentration (cf. Figure 33). Next, the fluorescent probe **96a** was incubated with KDM4A and the FP signal was registered. As binding of deferasirox derivatives to the enzyme is dependent on iron-chelation, iron was added to the mixture in order to ensure saturation of the enzyme with iron. However, only a weak FP signal was registered even at high enzyme concentrations (cf. red squares in Figure 34). A possible explanation is the

susceptibility of Fe^{2+} to oxidation. In the activity assays this problem is circumvented by the use of ascorbic acid as antioxidant, yet the addition of ascorbic acid in the FP assay did not lead to satisfactory results. Therefore, the more stable Ni^{2+} was used as a replacement, which led to a stable FP signal (cf. blue squares in Figure 34). Ni^{2+} is a well-known replacement for Fe^{2+} in experiments where high stability is advantageous and no catalytic activity is necessary. For example, Ni^{2+} was used in crystallisation of Jmj-KDMs and also in a fluorescence polarization assay using the fluorescently labelled methylstat probe **11** (cf. Section 1.3.6).^{51, 144}

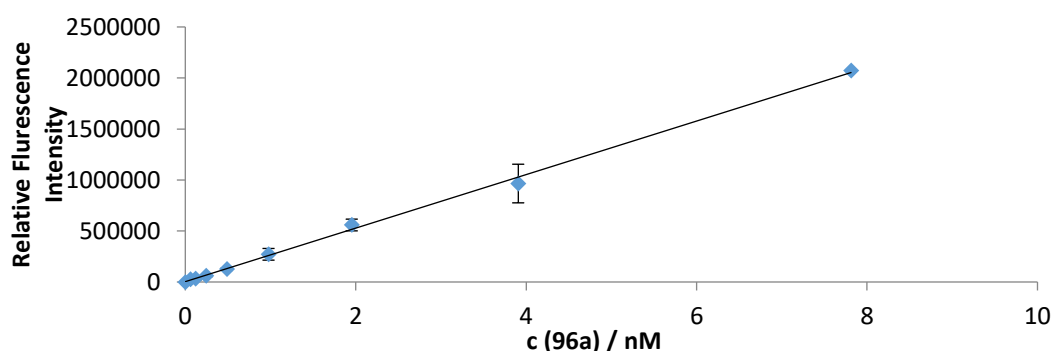


Figure 33 Calibration curve for the fluorescence intensity of **96a** to show concentration independent fluorescence output per fluorophore (brightness).

Next, a buffer screen was performed. As for the activity assays, a HEPES buffer at pH 7.50 turned out to be suitable giving a stable high FP signal. 0.01% TWEEN 20 was added to the buffer to minimize unspecific binding and aggregation.

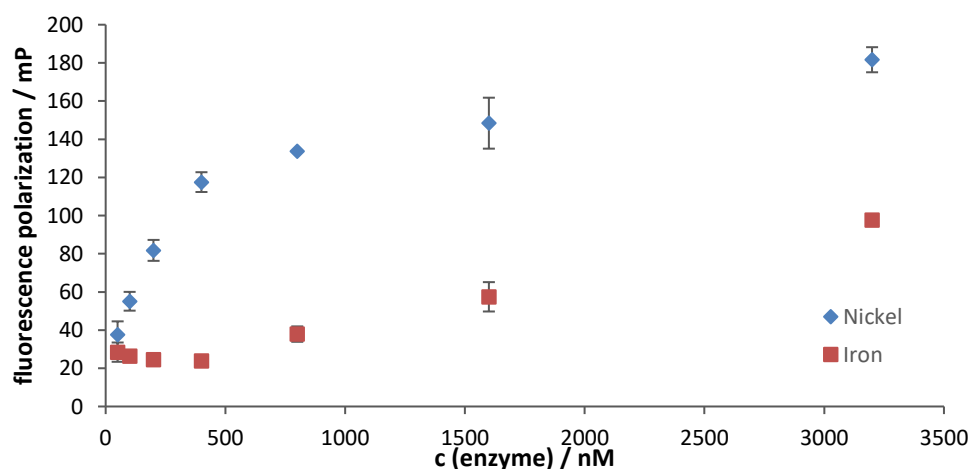


Figure 34 Influence of the central metal on the fluorescence polarization signal. For Fe^{2+} only a weak increase of the FP signal is observed for higher enzyme concentrations, while Ni^{2+} yields a significant concentration-dependent increase.

With these conditions determined, an enzyme titration was performed to get a binding curve with each of the two fluorescent probes. As expected, both gave increasing FP signals with increasing enzyme concentrations which proves binding of the respective probe to the enzyme. To show competitive binding with the unlabelled probe, deferasirox (**54**) was titrated to the complex of the enzyme with the fluorescent probe **96a**. Displacement proves specific binding of the active molecule as opposed to unspecific binding of the fluorophore moiety. Indeed, a decrease of the FP signal was observed for increasing deferasirox concentrations concomitant with displacement of the fluorescent probe from the enzyme as shown in Figure 35. For a clean 1:1 binding stoichiometry, a sigmoidal curve would be expected for the displacement. However, the resulting curve did not fit to a sigmoidal model. There are several factors influencing the resulting signal which can cause deviations from the optimal curve fit.

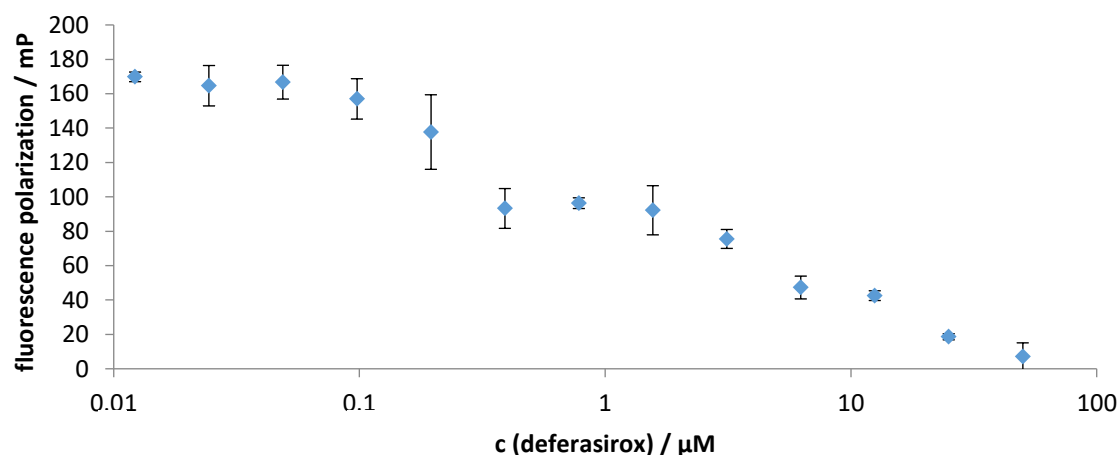


Figure 35 Competitive displacement of the fluorescent probe **96a** with deferasirox. Increasing concentrations of deferasirox lead to a decreased amount of **96a** bound to the enzyme thereby leading to a decrease in the recorded FP-signal. Displacement with the active molecule serves as proof for active-site binding of the probe **96a**.

First, although a proportional increase of fluorescence intensity was observed for the unbound probe, a decrease of intensity was registered upon enzyme binding (cf. Figure 36). Probably there are interactions between the fluorescent moiety and the enzyme that decrease the fluorescence quantum yield of the probe. This leads to a lower fluorescence intensity per molecule. Theoretically, the FP signal is

independent of the absolute fluorescence intensity, because it is calculated using the ratio of parallel and perpendicular polarized light as shown in the following equation, where P is the polarization, I_{\parallel} and I_{\perp} are the parallel and perpendicular relative fluorescence intensities and G is the grating factor, which is an instrumentation-dependent constant.

$$P = \frac{I_{\parallel} - G \cdot I_{\perp}}{I_{\parallel} + G \cdot I_{\perp}} \quad (4.1)$$

However, a variation of fluorescence intensity causes varying deviations in the measured signal. This phenomenon complicates analysis of the measured signal and may lead to deviations from the ideal behaviour of a direct competitor.

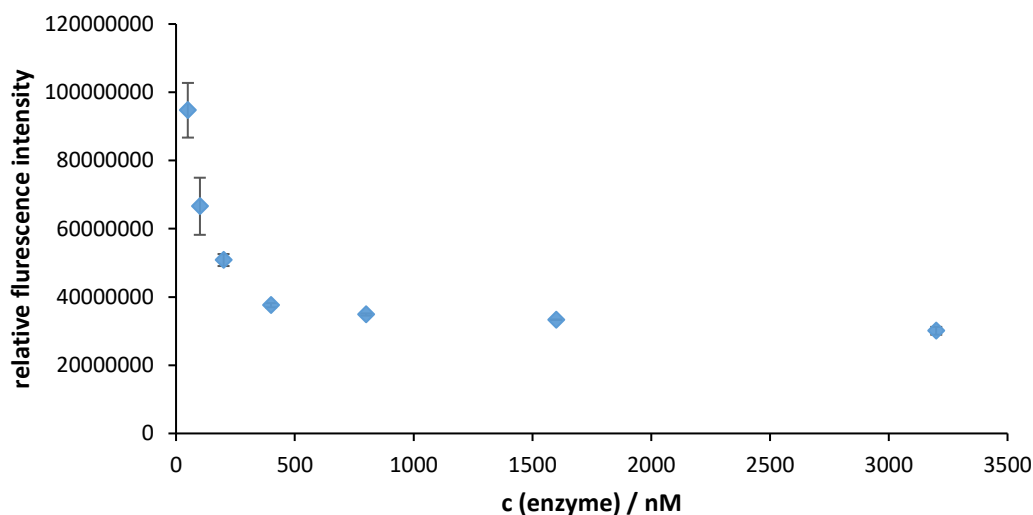


Figure 36 Upon binding to the enzyme, fluorescence quenching is observed for the probe **96a** leading to a decreased fluorescence intensity with increasing amounts of enzyme until all the probe molecules are bound to the enzyme.

The second reason for a non-sigmoidal curve may be the influence of nickel chelation of deferasirox (**54**) in solution. As the complexation of the active site metal is mandatory for probe binding to the enzyme, sequestration of nickel in the solution may lead to a shift of the binding equilibrium between nickel, the enzyme and the probe or deferasirox, respectively, thereby further complicating analysis. Nevertheless, the main purpose of the FP-assay, namely showing binding of labelled deferasirox to the enzyme and displacement with unlabelled deferasirox could be achieved. This serves as further confirmation of specific binding of the

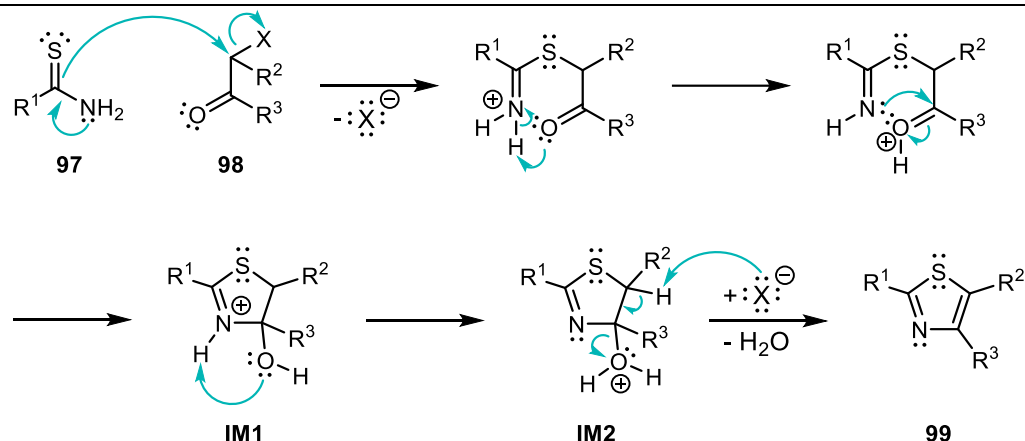
inhibitor to the enzyme in contrast to a mechanism solely based on iron sequestration. Yet, the iron-sequestration may add to the inhibitory activity. However, the extent of this phenomenon can be quantified neither with the FP-assay nor the activity assays.

4.3.2 Thiazoles and Oxazoles

As none of the tested triazole-based deferasirox analogs showed a significantly increased potency against KDM4A, an exchange of the core moiety with other 5-membered heterocycles was envisioned in order to extend the chemical space covered by the compounds. As the nitrogen atom in position 4 is essential for iron chelation, azoles were considered as potential replacement for the 1,2,4-triazole. Thiazoles and oxazoles were chosen as a first approach, because they are well established core elements in various pharmaceuticals, including anti-infective, anti-cancer, anti-inflammatory and anti-diuretic substances.²⁵⁰ Moreover, numerous synthetic routes for various thiazoles and oxazoles are available. The diversity of synthetic methods allows the attainment of unsymmetrically substituted derivatives and a broad scope of substituents.

4.3.2.1 Synthesis

One of the most frequently applied methods for the synthesis of thiazoles is the Hantzsch thiazole synthesis first described in 1887 by Hantzsch and Weber.²⁵¹ The strategy involves the reaction of an α -haloketone **97** with a thioamide **98** or thiourea (for 2-aminothiazoles) in a multistep reaction. Mechanistically, the reaction consists of the nucleophilic substitution of the halogen by sulphur followed by intramolecular attack of nitrogen at the carbonyl carbon resulting in the formation of the 2-thiazolinium intermediate **IM1**. Tautomerization to **IM2** and elimination of water yields the thiazole product **99**. (cf. Scheme 10).²⁵²



Scheme 10 Postulated mechanism for the Hantzsch thiazole synthesis.²⁵²

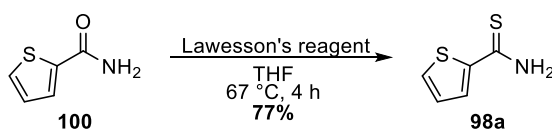
Dehalogenation of the α -haloketone is the most prominent side reaction lowering product yields. Side reactions are more likely when applying deactivated thioamides bearing electron-deficient substituents because they require longer reaction times and/or harsher reaction conditions.²⁵³ Furthermore, haloketones bearing aromatic substituents neighbouring the halogen are particularly prone to dehalogenation due to mesomeric stabilization of intermediates.²⁵⁴ Another side reaction occurring for the *ortho*-phenol-containing halogenated ketones is the intramolecular cyclisation via nucleophilic substitution, which yields a stable five-membered ether (cf. Scheme 14).

4.3.2.1.1 Precursors

The approach via Hantzsch cyclisation requires adequately substituted α -halogenated ketones and thioamides. To obtain thiazoles containing a tridentate chelating group potentially able to bind iron, both precursor molecules need to comprise a suitable substituent or a heteroatom *ortho* to the ketone or thioamide group. Proposed moieties were phenol, in referral to the parent structure deferasirox (**54**), and nitrogen- or sulphur-containing heterocycles.

4.3.2.1.1.1 Thioamide synthesis

Thiophene-2-carbothioamide **98a** was synthesized in accordance to a published procedure²⁵⁵ from thiophene-2-carboxamide **100** using Lawesson's reagent (cf. Scheme 11). Lawesson's reagent (2,4-bis(*p*-methoxyphenyl)-1,3-dithiadiphosphetane-2,4-disulphide) was chosen because it can be used for the transformation of amides to thioamides under mild reaction conditions and usually gives faster reactions and higher product yields compared to classical thionation agents like phosphorus pentasulphide.²⁵⁶ **98a** could be obtained in 77% yield after 4 h of reaction in refluxing tetrahydrofuran followed by extraction and purification via flash column chromatography.

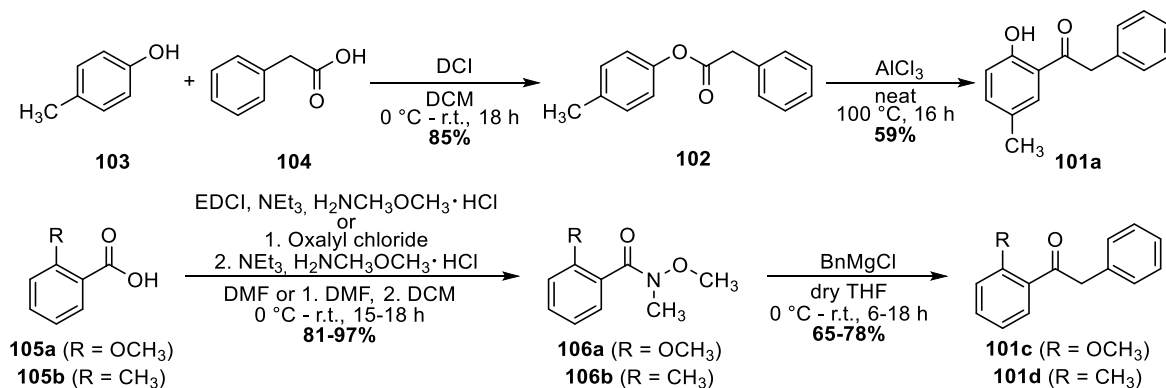


Scheme 11 Synthetic procedure for the synthesis of thioamide **98a**.

4.3.2.1.1.2 Ketone synthesis and bromination

The ketone precursors were prepared following literature procedures as depicted in Scheme 12. As precursors for analogs bearing the same iron-chelating motif as deferasirox (**54**), the phenolic compounds **101a**, bearing a *p*-methoxy group, and **101c** were synthesized. *p*-Tolyl 2-phenylacetate **102** was synthesized via 1,1'-carbonyldiimidazole-catalyzed (CDI) esterification of 4-methylphenol **103** and phenylacetic acid **104**. Ketone **101a** was obtained via Fries rearrangement of *p*-tolyl 2-phenylacetate **102** catalysed by aluminium chloride.²⁵⁷ Due to the methyl substituent in *para*-position acylation occurred solely in *ortho*-position to the phenol, which increased the ease of purification via flash column chromatography and crystallization. The unsubstituted and methoxy-protected derivative **101c** could be synthesized via Weinreb–Nahm ketone synthesis from 2-methoxybenzoic acid **105a**, which was activated with EDCI and transformed to the Weinreb amide **104a** with *N,O*-dimethylhydroxylamine hydrochloride. The ketone **101c** was formed via addition of benzylmagnesium bromide.²⁵⁸ Compound **101d**, carrying a methyl

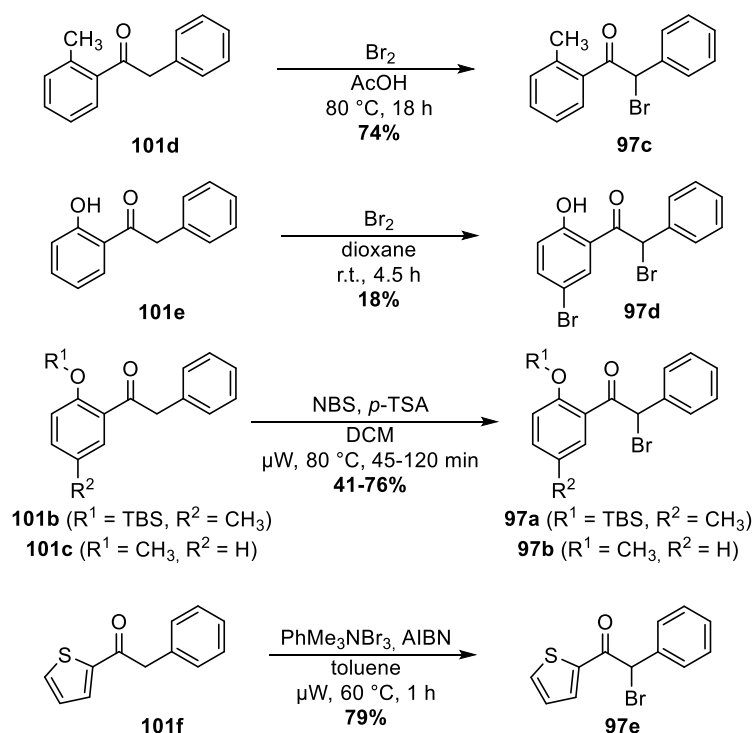
group instead of the phenol moiety, was synthesized as precursor for a negative control (cf. section 4.3.2.2) starting from 2-methylbenzoic acid **105b** in a similar manner.



Scheme 12 Synthetic procedures for the synthesis of ketone precursors.

The next step was the introduction of a bromine substituent next to the ketone moiety (cf. Scheme 13). Selective α -bromination without additional halogenation of the aromatic substituents was crucial to avoid product mixtures with variably brominated compounds, which can be difficult to separate due to similar chromatographic retention factors. Several bromination reagents and reaction conditions were screened in order to find a suitable method. The methyl-substituted compound **97c**, the precursor for the negative control, was obtained via heating with elemental bromine in acetic acid. Unfortunately, these conditions were inadequate for the bromination of 1-(2-hydroxyphenyl)-2-phenylethan-1-one **101e**, the precursor needed for the synthesis of the thiazole analogue of deferiasirox (**54**). Side-chain bromination of this compound was published by Hanaya *et al.*²⁵⁹ in 1990 with elemental bromine in a mixture of diethyl ether and 1,4-dioxane. However, following this procedure, only a mixture of variably brominated derivatives was obtained and separation of the single components could not be achieved via flash column chromatography, preparative TLC or recrystallization. The only compound isolated in sufficient purity was the additionally *para*-ring brominated compound **97d**, which was used later on for the synthesis of thiazole **99a**. The procedure tested next was adapted from a report by King *et al.*²⁶⁰ They suggest the use of CuBr₂ as

bromine source and a solvent mixture of chloroform and ethyl acetate for the selective side-chain bromination of acetophenone derivatives. CuBr₂ exhibits a low solubility in the proposed solvent mixture. Therefore, only a small amount is available for reaction at a time thereby limiting the occurrence of side reactions. Additionally, the by-products HBr and CuBr also display low solubility and are constantly removed from the reaction mixture via evaporation or precipitation, respectively. That shifts the equilibrium towards the brominated product and simplifies work-up. In their publication, King *et al.* report a high selectivity for side-chain bromination and high yields uniquely for the above-mentioned solvent combination in contrast to the use of nonpolar solvents like CS₂, which allow no reaction or give low yields, or polar solvents like methanol, which diminish the selectivity for side-chain bromination.



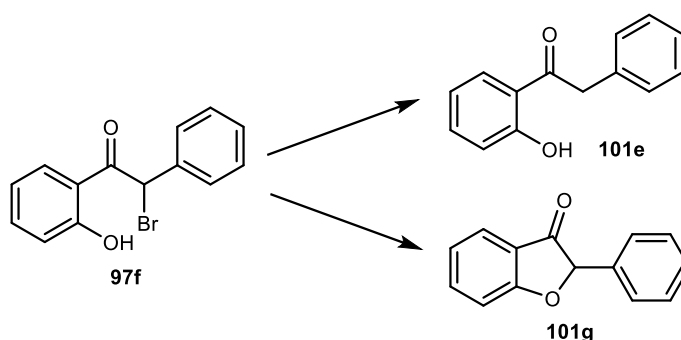
Scheme 13 Bromination reactions for the synthesis of precursors for the Hantzsch thiazole/oxazole synthesis.

In order to profit from these observations, their procedure was chosen for the bromination of 1-(2-hydroxyphenyl)-2-phenylethan-1-one **101e**. Chloroform was exchanged by dichloromethane for safety reasons. In accordance with their report, selectivity for side-chain bromination over ring-bromination was observed for **101e**,

however, an increasing proportion of ring-brominated compound was formed during the reaction course. In order to avoid the generation of polybrominated by-products, the reaction was run for a shorter time period and stopped before full conversion was reached. Although the starting material also proved to be inseparable from the product, this impurity was less problematic than the contamination with polybrominated compounds, because the non-brominated compound did not affect the next reaction step and could easily be removed during thiazole purification. However, this approach lowered the yield so drastically, that not enough compound for the next reaction step could be obtained.

Consequently, trials to optimize the bromination conditions were continued in order to find a method giving sufficient amounts of the α -brominated ketone to run several cyclization reactions with various thioamides. However, the 5-methylated derivative **101a** was used for the optimization instead of **101e**, because in the meantime assay interference had been observed with the thiazole **99b** containing the non-substituted phenol. As **101a** carries an additional methyl substituent on the phenol ring, it is even more susceptible towards ring bromination than **101d** due to the positive inductive effect of this moiety. As expected, this led to difficulties in finding suitable bromination conditions and indeed, insufficient selectivity was found using HBr, dioxane dibromide, trimethylphenylammonium tribromide or *N*-bromosuccinimide (NBS) as brominating agents. The main reason for the high amount of side reactions occurring during the bromination of **101a**, despite the use of conditions that have been published for the successful side-chain bromination of acetophenone derivatives, is the hydroxy substituent *ortho* to the ketone. It not only serves as an activator of ring bromination due to its positive mesomeric effect, but also diminishes side-chain reactivity via formation of a strong hydrogen bond to the carbonyl oxygen. This hydrogen bond decreases enolization of the ketone and thereby deactivates the α -carbon for nucleophilic attack.²⁶¹ Furthermore, the phenolic hydroxy group decreases the stability of the side-chain brominated product, because it enables an intramolecular nucleophilic substitution leading to a

stable five-membered ring (cf. Scheme 14). This side-product could be observed via GC-MS in all the above-mentioned reactions. Intending to suppress these side reactions, the phenol was masked using TBS-Cl. The thus protected compound **101b** proved to be less prone to side-reactions so that the side-chain brominated compound **97a** could be obtained via acid-catalysed bromination with NBS and *para*-toluenesulfonic acid (PTSA) in dichloromethane. Reaction yields could be increased to 76% using microwave irradiation as proposed by Guan *et al.*²⁶² The TBS protecting group was convenient for the synthesis of thiazoles, as it did not interfere with the cyclization and was cleaved off during reaction or upon work-up, hence obviating an additional deprotection step (cf. section 4.3.2.1.2). Contrastingly, the oxazole formation seemed to be hindered by the bulky protecting group, therefore, the methyl protected compound **97b** was also synthesized. Side-chain bromination was achieved using the same conditions as for **97a**, albeit in lower yield (46%) and contaminated with traces of the starting material even after purification via flash chromatography followed by recrystallization from 2-propanol.

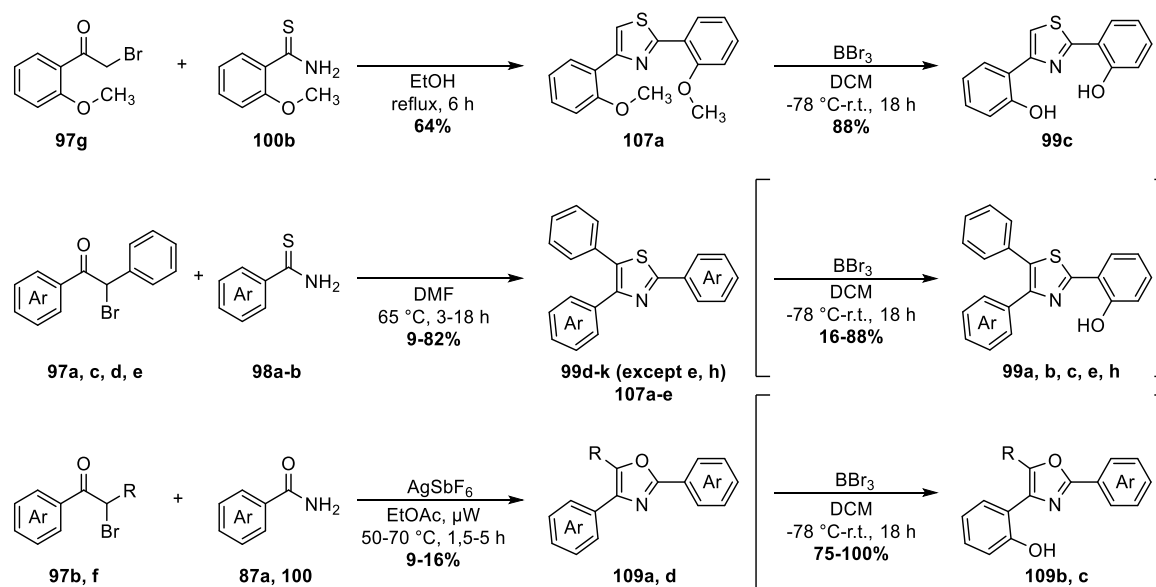


Scheme 14 The main side reactions occurring during thiazole formation are dehalogenation and intramolecular cyclisation of the brominated ketone.

The best result for the bromination of the thiophenyl-substituted compound **101f** was obtained with trimethylphenylammonium tribromide in toluene and azabisisobutyronitrile (AIBN) as radical starter using microwave irradiation. As for **97b**, the reaction was stopped before full conversion was reached in order to minimize ring bromination. Hence, the compound contained nearly 10% of starting material even after purification.

4.3.2.1.2 Hantzsch-thiazole synthesis

Classical Hantzsch conditions, namely refluxing the α -brominated ketone and the thioamide in ethanol, were applied for the synthesis of the 1,4-dimethoxy-substituted thiazole precursor **107a** giving the compound in 64% yield which yielded **99c** after deprotection (88%; cf. Scheme 15). For all the other compounds cyclisation was performed in DMF, as suggested by Moreno *et al.*,²⁶³ due to better solubility of the starting materials. For most compounds a reaction temperature of 65 °C was sufficient to induce cyclization without permitting too many side reactions. The only exception was the 2-pyrimidine-substituted thiazole **99d**, where rapid degradation of the thioamide was observed at 65 °C. Therefore, the reaction was performed at room temperature over-night instead. Usually, cleavage of the TBS protecting group, that had been installed for the bromination step, spontaneously occurred during thiazole formation, except for the imidazole-substituted compound **107b**. Thus, an additional deprotection step using tetrabutylammonium fluoride (TBAF) was required yielding compound **99e**.



Scheme 15 Synthetic procedures for the synthesis of thiazoles and oxazoles. Deprotection with BBr_3 was only performed for compounds bearing methoxy groups.

For compounds bearing one or two protective methoxy-groups demethylation was performed via a standard procedure using boron tribromide as demethylating

agent. Cyclization yields varied between 9 and 82% dependent on the stability and reactivity of the starting materials and the degree of difficulty of purification. Generally, work-up by addition of water and extraction with ethyl acetate followed by normal phase flash column chromatography yielded the final compounds in sufficient purity. Only for the 2-pyridine- and 2-thiazole-compounds **99d** and **99f** a second step using reversed-phase chromatography was necessary.

4.3.2.1.3 μ W-supported oxazole formation

In analogy to the Hantzsch thiazole synthesis, oxazoles can be built up from α -halogenated ketones and amides via the Blümlein-Lewy synthesis.^{264, 265} Analogous to thiazole formation (cf. section 4.3.2.1 and Scheme 10), the reaction is initiated by nucleophilic substitution of the halogen by the amide oxygen. Subsequent ring closure via nucleophilic attack of the nitrogen gives the 5-hydroxy-oxazolidine intermediate, which is transformed to the corresponding oxazole upon elimination of water. However, as the amide oxygen is less nucleophilic than the thioamide sulphur, reaction rates are much slower for amides and often require higher reaction temperatures than thioamides, which might not be compatible with the stability of starting materials. Thus, activation of the α -haloketone may be necessary to increase reactivity. According to reports of Ritson *et al.*²⁶⁶ and Spiteri *et al.*²⁶⁷ in 2011, α -bromoketones can be activated by addition of silver salts to the reaction mixture. Due to their halophilicity, silver ions facilitate elimination of bromide upon nucleophilic attack. Precipitation of the thus formed AgBr drives the reaction forward. Furthermore, the counterion of the silver salt, or, more precisely, its conjugate acid, may facilitate elimination of water in the last step of the reaction. Indeed, a screen of different silver salts performed by Ritson *et al.*²⁶⁶ revealed that better results were obtained for salts displaying high Lewis acidities, such as AgClO₄ and AgSbF₆. Due to its inertness towards various functional groups, hexafluoroantimonate was chosen for the oxazole formations described herein. Thereby, side reactions should be minimized and reaction yields should be

increased. As suggested in the above-mentioned publication,²⁶⁶ the reaction was performed using microwave irradiation. However, when applying the published procedure to 2-bromo-2'-methoxyacetophenone **97g** and thiophene-2-carboxamide **100** while using 1,2-dichloroethane as solvent, a complex product mixture only containing traces of the desired oxazole **108a** was obtained. Therefore, a solvent screen was performed in order to identify more suitable conditions (cf. Table 11). Best results were achieved for ethyl acetate, which is in accordance with the results published by Bailey *et al.*²⁶⁸ in 2014, who identified ethyl acetate and toluene as preferential solvents for silver-mediated oxazole formations. Hence, ethyl acetate was used in all subsequent reactions.

An appropriate reaction temperature for each substrate was determined by increasing the temperature in 5-degree steps until product formation was observed via APCI-MS. Temperatures ranged from 50 °C for the 2-thiophenyl-4-phenol-substituted oxazole **109a** to 70 °C for its methylated analogue **108a**.

Table 11 Optimisation of reaction conditions for the microwave-assisted formation of oxazoles.

<i>solvent</i>	<i>result</i>	<i>isolated yield</i>
dichloroethane (DCE)	complex mixture	–
dichloromethane (DCM)	traces of product	–
tetrahydrofuran (THF)	traces of product	–
ethyl acetate	product mixture	10%

After work-up via partitioning between an aqueous sodium hydrogen carbonate solution and ethyl acetate purification was performed via flash column chromatography. In order to remove remaining impurities, compounds were recrystallized from an alcoholic solution (methanol or 2-propanol). Yields were generally lower than for the respective thiazoles (9–16%).

4.3.2.1.4 NMR assignments for thiazoles

To confirm the molecular structure of the synthesised compounds, NMR studies were performed. As for the triazole derivatives the synthesised compounds contain four aromatic rings so that the ^1H - and ^{13}C -signals cover a rather narrow range and COSY-, HSQC- and HMBC-experiments were performed for most of the final compounds to allow unambiguous signal attribution. The following section exemplary describes the NMR spectrum of **99b** which bears one phenyl and two phenol substituents.

The ^1H -signal shifted furthest downfield (11.5 ppm) corresponds to one of the phenolic hydroxy groups. As the sulphur atom of the adjacent thiazole ring leads to deshielding due to its free lone pairs, the signal most likely corresponds to the phenol in closer vicinity to that sulphur atom (ring A). The second signal (9.8 ppm) therefore corresponds to the other phenol group (OH', ring C). Assignment of the phenol group OH to ring A could be confirmed via coupling of OH with C1, C2 and C3 (cf. Figure 37). The attribution of these carbon atoms to ring A could be deduced from coupling of C1 with H3 and H5. H5 couples to H6 in the COSY spectrum. As H6 couples to C_c (carbon 2 of the thiazole ring), it can unambiguously be attributed to ring A and not to ring C.

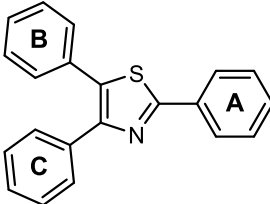
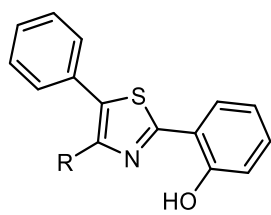
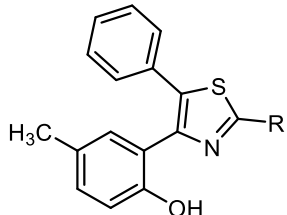
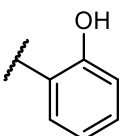
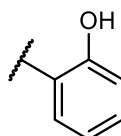
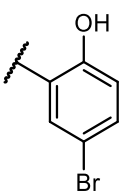
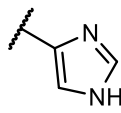
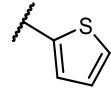
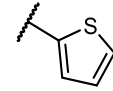
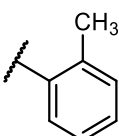
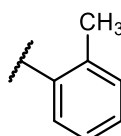
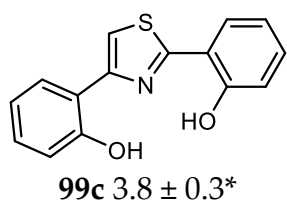
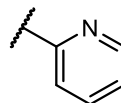
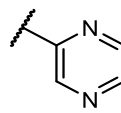
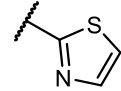
H6' couples with C_e (carbon 4 of the thiazole ring) confirming this attribution. C_c and C_e can be distinguished by the huge difference in chemical shift, C_c being further downfield due to the two adjacent heteroatoms. H6 is the aromatic proton highest downfield and appears as doublet of doublets due to its *ortho*- and *meta*-coupling to H5 and H4 ($^3J = 7.9$ Hz and $^4J = 1.7$ Hz), respectively. The *para*-coupling is not resolved. H6' would also appear with the same multiplicity, but overlaps with the signal for H4', therefore coupling constants cannot be unambiguously attributed. H4 overlaps with the multiplet of the 5 protons of the phenyl ring. H3 and H3' give doublets of doublets similar to H6, only the *ortho*-coupling constant to H4 or H4' is slightly bigger and the *meta*-coupling constant to H5 or H5' is smaller ($^3J = 8.3$ Hz and $^4J = 1.1$ Hz) than the corresponding ones for H6.

H5 and H5' give doublets of doublets of doublets owing to their two *ortho*-couplings and the *meta*-coupling. As for the triazoles, signal assignments of the carbon atoms could be deduced from the HSQC- and HMBC-spectra.

4.3.2.2 Biochemical Activity of Thiazoles and Oxazoles

Evaluation of the inhibitory activity against KDM4A was performed with the LANCE assay (cf. Section 3.1.2 for assay description and Table 12 for results). Unfortunately, compound **99b**, which is the closest deferasirox analogue bearing two phenol moieties for iron chelation and a phenyl substituent, interfered with the assay readout by increasing the fluorescence signal. This effect was rather unexpected, because the LANCE assay is quite robust towards compound interference due to the time-resolved measurement of a fluorescence signal generated by the Förster resonance energy transfer (FRET) from an excited europium chelate to an acceptor fluorophore in close proximity. The delayed fluorescence measurement after 100 μ s usually ensures that all compound fluorescence has already decayed and only the fluorescence of the acceptor fluorophore is registered. Therefore, increase of the measured signal should only occur for compounds that are amenable acceptors for the FRET from the europium chelate, meaning excitability at 615 nm and emittance at 665 nm. However, this effect could be ruled out as neither **99b** nor its iron complex are fluorescent at this wavelength. A more likely explication might be that **99b** caused precipitation of the europium-labelled antibody and the fluorescent dye, thereby bringing them into close proximity and enabling the FRET effect to occur independently of antibody binding to the demethylated peptide. Another possible mechanism might be chelation of europium thereby dissociating it from the antibody complex. This could also cause an unspecific FRET effect irrespective of antibody binding. However, as the assay interference occurred solely with compound **99b** and not with similar derivatives no effort was put into the elucidation of the mechanism of interference. In order to circumvent this unspecific effect another derivative, namely the thiazole derivative **99g** with a slightly modified structure with a *p*-methyl group on ring C was synthesized.

Table 12 Inhibitory activity of thiazole derivatives against KDM4A. Data are mean \pm s. d. of at least two independent experiments.

					
					
No	R	% inhibition or IC ₅₀ / μ M	No	R	% inhibition or IC ₅₀ / μ M
99b		assay interference	99g		7.5 \pm 1.3
99a		9.4 \pm 4.0	99e		116 \pm 13
99h		n. i. @ 125 μ M	99f		20.3 \pm 4.4
99i		n. i. @ 125 μ M	99j		41% @ 125 μ M
 99c 3.8 \pm 0.3*			99d		125 \pm 35
			99k		170 \pm 20
			99l		n.i. @ 100 μ M

* hillslope > 2, probably due to unspecific effects and/or compound precipitation

Luckily, no assay interference was observed for this compound and an IC_{50} value of $7.5\text{ }\mu\text{M}$ could be determined. This is quite similar to deferasirox (**54**) ($IC_{50} = 4.8\text{ }\mu\text{M}$) and docking shows a perfect overlap of the two structures with the phenol groups of ring A and C chelating the ferrous iron and ring B pointing outwards (cf. Figure 38 left). The *p*-brominated derivative **99a** was also active in the same range ($IC_{50} = 9.4\text{ }\mu\text{M}$). This is consistent with the predicted binding mode for the thiazole derivatives, where the bromine residue points towards an open pocket with enough space to accommodate the rather large substituent. It rules out an alternative binding mode – or at least renders it improbable – where the molecule is flipped so that ring A and C occupy the opposite binding pockets compared the other binding mode.

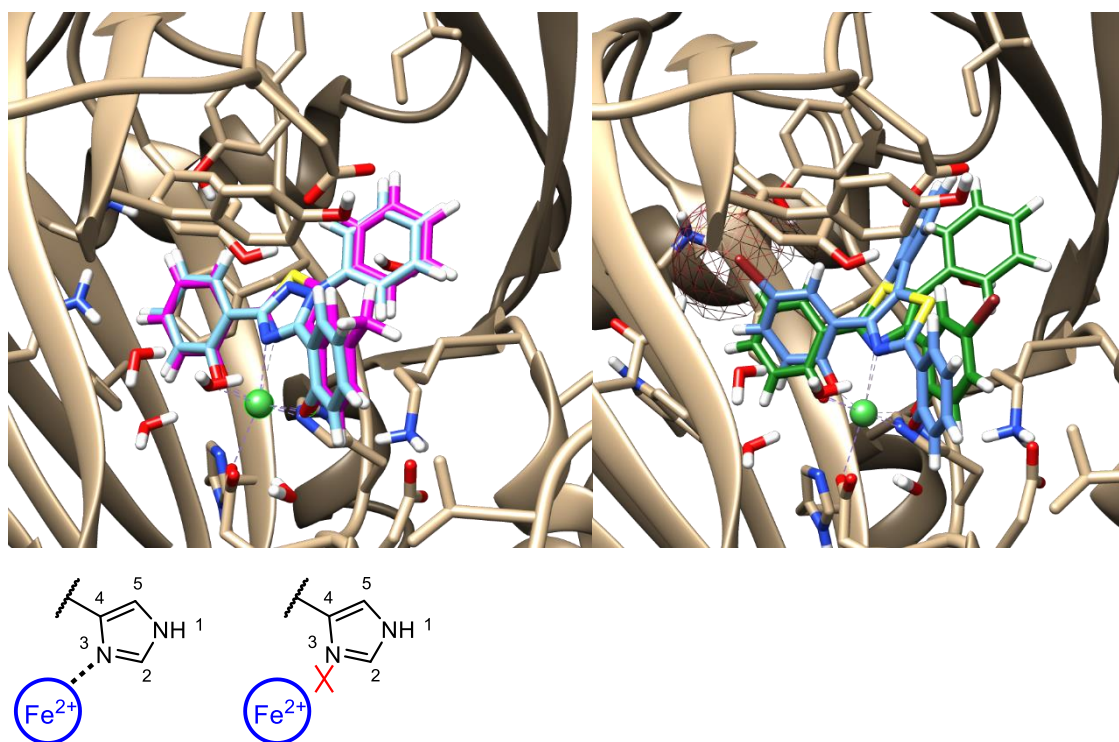


Figure 38 Left: Docking of deferasirox (light blue sticks) and **99g** (magenta sticks) into KDM4A. Both compounds adopt the same orientation. Right: Normal (green sticks) and flipped (blue sticks) orientation of the brominated derivative **99a**. The flipped orientation causes steric clashes of the bromine substituent with the catalytic pocket. The van-der-Waals surface around the bromo-substituent is shown as maroon mesh. The central Ni^{2+} ion is depicted as green sphere. Metal coordination is shown as teal dashed lines. (Docking provided by Dr. Dina Robaa, MLU Halle-Wittenberg, KDM4A template is PDB: 3RVH) Bottom: Tautomers of imidazole derivative **99e**. Only the 1*H*-tautomer is able to chelate iron.

In the flipped orientation, there would be a steric clash of the bromine substituent with Asn198, Lys206 and Tyr132 of the binding pocket (cf. Figure 38 right). A similar effect had also been observed for the dibrominated triazole derivative **90d** (cf. Section 4.3.1.2), which is *p*-brominated at both phenol rings. In that case, the steric clash led to a significantly decreased binding affinity towards the enzyme.

Replacement of the phenol ring C with a 2-thiophene moiety in **99h** led to a loss of potency. This could be rationalized by the change of the geometry of the iron-binding motif, which is less favourable for iron chelation than two phenol rings. To further demonstrate the importance of the phenol group for inhibitory activity, the tolyl derivative **99i** was synthesized, which was indeed inactive. This compound can for example be used as a negative control in cellular assays.

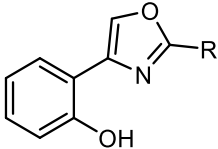
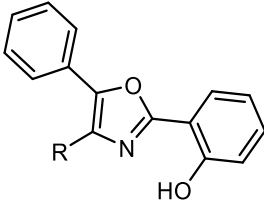
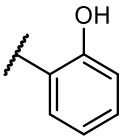
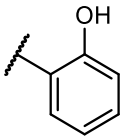
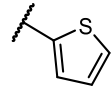
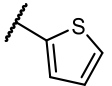
In contrast to that, compound **99j** containing a tolyl group as ring A retained some activity (41% inhibition at 125 μ M). Furthermore, the thiophene derivative **99f** showed an IC_{50} value of 20 μ M. These two observations underline that not only the nature of the iron-chelating motif itself is crucial for compound activity but also the orientation, as substituents other than phenol are tolerated in ring A but lead to a loss of activity when present in ring C. The difference may stem from the differing hydrophilicity of the two binding pockets. As the pocket accommodating ring C is more hydrophilic than the one for ring A, it most likely employs weaker binding to the hydrophobic thienyl or tolyl moieties. This effect may explain the loss in potency compared to the more hydrophilic phenol. On the other hand, the hydrophobicity of binding pocket A and the concomitant binding of hydrophobic moieties may partly compensate the decreased iron chelation of the thienyl or tolyl ring so that these compounds (**99f** and **99j**) retain some activity, although the activity is weaker than for the phenolic compound **99g** with stronger iron chelation.

Exchanging ring A by nitrogen-containing heterocycles, namely imidazole (**99e**), pyridine (**99d**), pyrazine (**99k**) and thiazole (**99l**) yielded compounds displaying weak activity (IC_{50} = 116–170 μ M, n.i. at 100 μ M for **99l**). The 6-fold loss of activity for the imidazole compared to the thiophene may partly be explained by the

tautomeric forms of imidazole (cf. Figure 38 bottom). Only the 3*H*-tautomer is able to chelate iron, while the 1*H*-tautomer cannot bind iron efficiently due to the hydrogen atom. Lower activity was also observed for the six-membered nitrogen-containing rings such as pyridine **99d** and pyrazine **99k**, which is probably due to a less favourable binding geometry of the iron-chelating motif.

The thiazole derivative **99c** bearing two phenol rings in positions A and C and a hydrogen atom in position B resulted in an IC₅₀ value of 3.8 μM. However, the inhibition curve showed a steep hill slope indicative for unspecific effects or non-stoichiometric binding, therefore this compound scaffold not bearing a substituent in position B was not pursued any further.

Table 13 Inhibitory activity of oxazole derivatives against KDM4A. Data are mean ± s. d. of at least two independent experiments.

					
No	R	% inhibition or IC ₅₀ / μM	No	R	% inhibition or IC ₅₀ / μM
109c		7.6 ± 0.8	109b		8.5 ± 0.9
109a		14% @ 100 μM	109d		n. i. @ 100 μM

Oxazoles (cf. Table 13) showed a quite similar behaviour to the thiazoles, therefore only a limited number of compounds was synthesised and tested. The derivative **109b** bearing a phenyl ring in position B and two phenol rings in positions A and C resulted in an IC₅₀ value of 8.5 μM, which is quite similar to thiazole **99g** (IC₅₀ = 7.5 μM). The derivative **109c** bearing a hydrogen atom instead of ring B also gave similar activity of 7.6 μM. Like for the thiazoles, substitution of ring A with a thienyl moiety gave the inactive compound **109d**, while the same moiety in position

C yielded the slightly active compound **109a** (14% inhibition @ 100 μ M). These results, together with docking studies, suggest similar binding modes for oxazoles and thiazoles (cf. Figure 39).

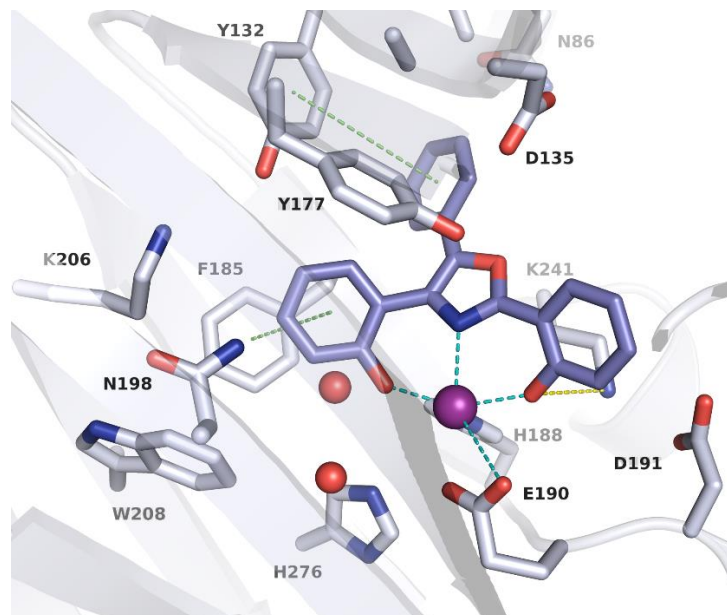


Figure 39 Docking of oxazole **109b** (blue sticks) into the catalytic pocket of KDM4A. The central Ni^{2+} ion is depicted as purple sphere and water molecules as red spheres. Metal coordinative bonds are shown as cyan dashed lines, hydrogen bonds as yellow dashed lines and $\pi:\pi$ -interactions as light green dashed lines. (Figure and docking provided by Dr. Dina Robaa, MLU Halle-Wittenberg, KDM4A template is PDB: 3RVH)

4.3.3 Pyrazoles and Imidazoles

As a next step the core heterocycle was replaced by pyrazole and imidazole rings. Synthesis for these compounds was performed by Dr. Nicolas Barthes and the students Moritz Spiske and Matthias Henn under his supervision.

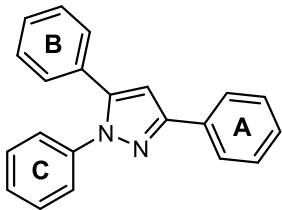
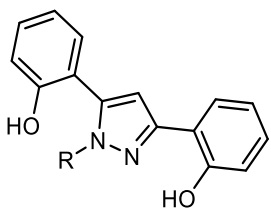
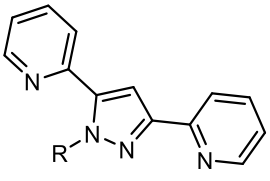
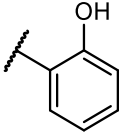
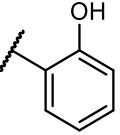
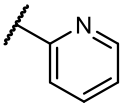
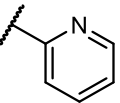
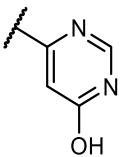
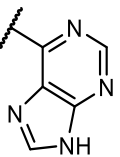
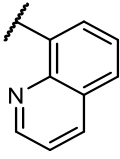
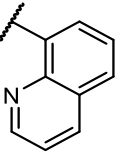
4.3.3.1 Biochemical Activity and structure-activity relationships

As the synthesis of pyrazoles was realized via symmetrically substituted 1,3-ketones only derivatives bearing the same substituent in positions A and B were generated. The derivative **110a** bearing three phenol moieties showed an IC_{50} value

4 Development of novel Inhibitors for JmjC-containing histone demethylases

of 3.5 μM . Docking studies suggest the same positioning of the compound as for the triazole, thiazole and oxazole compounds (cf. Figure 40 left).

Table 14 Inhibitory activity of pyrazole derivatives against KDM4A. Compounds were kindly provided by Dr. Nicolas Barthes. Data are mean \pm s. d. of at least two independent experiments.

					
					
No	R	% inhibition or IC_{50} / μM	No	R	% inhibition or IC_{50} / μM
110a		3.5 ± 0.8	110e		34% @ 20 μM
110b		4.4 ± 0.8	110f		30% @ 100 μM
110c		$4.1 \pm 0.4 \mu\text{M}$	110g		20% @ 20 μM
110d		55% @ 100 μM	110h		35% @ 100 μM

However, in contrast to the thiazoles, different substituents were tolerated as ring C. Both pyridine (**110b**) and 4-hydroxypyrimidine (**110c**) yielded equipotent inhibitors displaying an IC_{50} of 4 μM . Only the quinoline **110d** showed a drop in potency (55% inhibition at 100 μM), which may be explained by a geometry that is less favourable for iron-chelation. The high activity of the pyridine **110b** and the

4-hydroxypyrimidine **110c** despite their lower chelation efficiency compared to the phenol could stem from the positioning of the hydroxy group of ring B in a hydrophilic pocket increasing binding affinity. This additional interaction might compensate the decreased iron-chelating capacity.

Contrastingly, the use of pyridine in position A and B only gave weakly active compounds (**110d-h**). This supports the observation that pyridine substituents are less favourable motifs for iron chelation. Furthermore, it underlines the importance of the hydrophilic interaction of ring B with the enzyme, which is much weaker for pyridine. The loss of this interaction also adds to the drop in potency. For example, compound **110e**, bearing an inverted warhead compared to compound **110b** and pyridine instead of phenol in position B, is pronouncedly less active than **110b** (34% inhibition @ 20 μ M vs IC_{50} 4.4 μ M, respectively). The other compounds containing two pyridine moieties and bearing different heterocyclic substituents in position C like pyridine **110f**, purine **110g**, and quinoline **110h** were also low-potent inhibitors due to the low chelation efficiency and the lower binding affinity of ring B.

Next, imidazole derivatives were evaluated. Unlike for the thiazoles and oxazoles, substitution in position 1 is feasible, which allows the synthesis of a broader variety of structures. First, inhibitors bearing an imidazole moiety in position A and phenyl substituents in position B and C were evaluated and the influence of different substituents in position 1 was assessed. A methyl substituent (**111a**, cf. Table 15) gave a slightly active compound (54% inhibition at 100 μ M) as did a 1-methyl-4-propylpiperazine (**111b**; 31% at 100 μ M), an *N*-benzylethylamine (**111c**; 41% at 100 μ M), and an *O*-ethylpyridin-3-ol (**111d**; 54% at 125 μ M) substituent. A slightly higher activity was obtained for the *N*-ethylpyridin-3-amine (**111e**; IC_{50} = 63 μ M) and the one carbon longer *N*-propylpyridin-3-amine (**111f**; IC_{50} = 62 μ M) substituent. Therefore, the *N*-ethylpyridin-3-amine was chosen as the preferred moiety for further developments. Replacement of the imidazolyl with a furyl moiety in **111g** caused a drop in potency (16% inhibition at 100 μ M), which is probably

caused by the lower chelation efficiency of the furyl compared to the imidazolyl group and its inability to form hydrogen bonds to the catalytic pocket (see below). Interestingly, the tested imidazolyl compounds all displayed some inhibitory activity despite containing a non-chelating group in ring C, which is in contrast to the thiazoles where a chelating moiety in position C was crucial for inhibition.

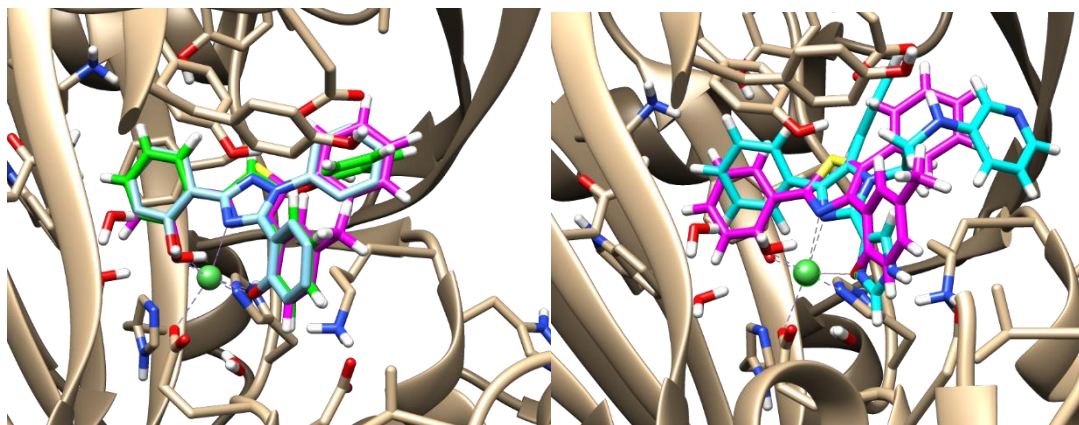


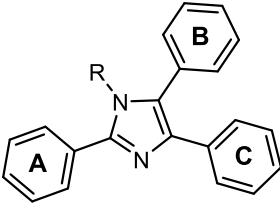
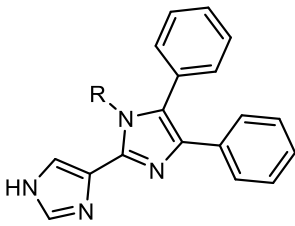
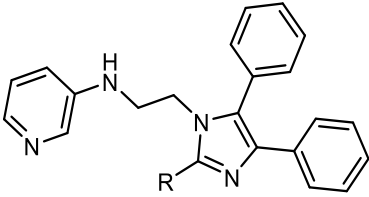
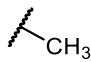
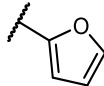
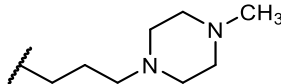
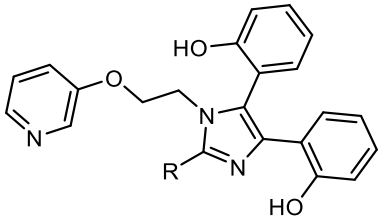
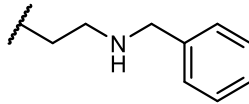
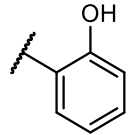
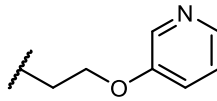
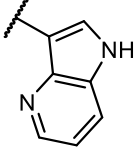
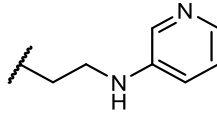
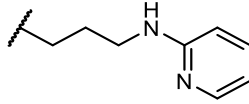
Figure 40 Left: Overlay of **54b** (light blue sticks), thiazole **99g** (magenta sticks) and pyrazole **110a** (green sticks) shows a perfect overlap of the structures.

Right: Overlay of thiazole **99g** (magenta sticks) and imidazole **111e** (cyan sticks) reveals a flipped orientation of the imidazole. The central Ni^{2+} ion is depicted as green sphere. Metal coordination is shown as teal dashed lines. (Docking provided by Dr. Dina Robaa, MLU Halle-Wittenberg, KDM4A template is PDB: 3RVH)

One reason for the observed difference between imidazoles and thiazoles is the different binding mode. According to docking into KDM4A, the additional *N*-ethylpyridin-3-amine chain in position 1 induces a flipped orientation of the imidazoles compared to the triazoles, thiazoles, oxazoles and pyrazoles (cf. Figure 40 right). The secondary amine of the side chain establishes an *H*-bond with Asp135 increasing compound affinity towards the enzyme and directing the positioning of the rest of the molecule in the flipped orientation. Consequently, ring C is placed in the hydrophobic pocket while ring A binds to the more hydrophilic one. Therefore, the phenyl substituent is tolerated in position C.

In a next step, the substituents in position 4 and 5 (ring C and B) were exchanged by phenol moieties. As expected, this increased inhibitory activity significantly. For the imidazole compound **111j** activity was increased to an IC_{50} value of 4.6 μM compared to 80% inhibition at 100 μM for **111e**.

Table 15 Inhibitory activity of imidazole derivatives against KDM4A. Compounds were kindly provided by Dr. Nicolas Barthes. Data are mean \pm s. d. of at least two independent experiments.

						
						
No	R	% inhibition or IC ₅₀ / μ M	No	X	R	% inhibition or IC ₅₀ / μ M
111a		54% @ 100 μ M	111g	N		16% @ 100 μ M
111b		31% @ 100 μ M				
111c		41% @ 100 μ M	111h			8.9 \pm 0.6
111d		54% @ 125 μ M	111i			9.6 \pm 2.4
111e		62.7 \pm 9.7				
111f		61.5 \pm 12.1				

* purity < 95%

In order to elucidate the influence of substituents in position A, different moieties were compared. As for the thiazoles and oxazoles, the use of a phenol moiety as ring A in compound **111k** led to a highly active compound ($IC_{50} = 2.9 \mu M$). The 4-(hydroxymethyl)phenol **111l**, the 3-hydroxypyridine **111m** and the pyridoxal-substituted **111n** showed an activity similar to the simple phenol with IC_{50} values between 3.0 and 4.4 μM . The hydroquinone **111o** also yielded a low IC_{50} value of 4.3 μM . However, a high hill slope > 3 was observed in the assay, which may be explained by the high redox-activity of the compound leading to unspecific effects. The pyridine **111p** was less active ($IC_{50} = 9.7 \mu M$) due to the decreased ability of pyridine to chelate the catalytic iron. However, five-membered heterocycles gave compounds displaying no or only mild inhibitory activity. The 2-thienyl **111q**, 3-furyl **111r**, and the 3-pyrrole **111s** were inactive due to their inability to effectively chelate the ferrous iron. Contrastingly, the 5-imidazole **111j** had shown a quite high activity of 4.6 μM despite employing a similar binding geometry to the thienyl **111q**. Molecular docking into KDM4A showed an *H*-bond between the external imidazolyl nitrogen and Asp191. This *H*-bond partly compensates the lower chelation efficiency compared to phenol. To substantiate the influence of the *H*-bond on compound potency two other nitrogen-containing five-membered heterocycles were synthesized and tested. The 2-imidazole **111t** with one nitrogen in the correct position for iron chelation but the other one unable to form the *H*-bond indeed showed a decreased activity of 21% inhibition at 20 μM . The 1,2,3-triazole **111u** displayed an IC_{50} value of 23 μM .

Compound **111u** exists in three tautomeric forms (cf. Figure 41 top), where the 1*H*-form can chelate iron and form the hydrogen bond, whereas the 2*H*-tautomer only undergoes the *H*-bond formation and the 3*H*-form can form neither of the interactions. The dynamic interconversion of these tautomeric forms explains the drop in potency compared to the 5-imidazole **111j**. These data confirm that five-membered heterocycles containing a nitrogen in *ortho* position to the core imidazole

are suitable iron chelators albeit with lower efficiency than phenol. A hydrogen bond to Asp191 can partly compensate the lower chelation ability.

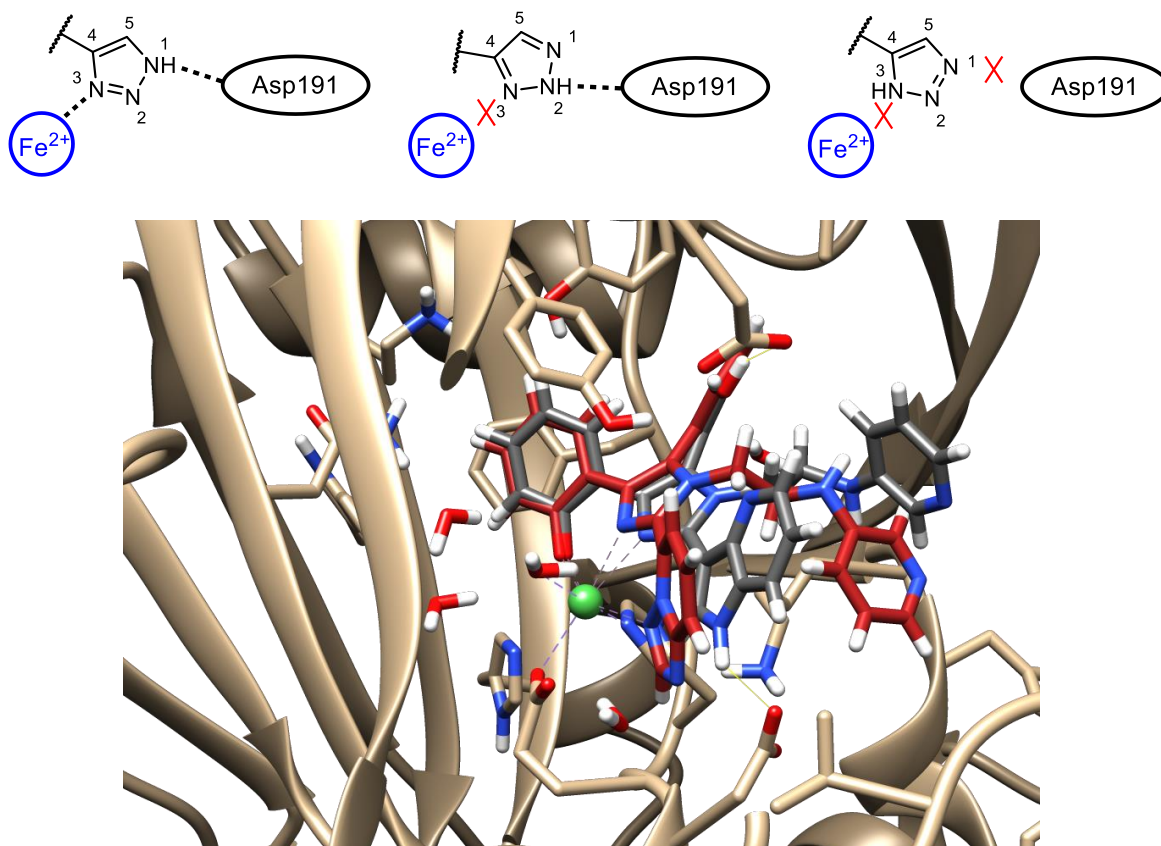


Figure 41 Top: Tautomers of 1,2,3-triazole **111u**. Only the 1*H*-tautomer can undergo interactions with the catalytic iron and Asp191 at the same time.

Bottom: The triazolopyridine **111y** (dark red sticks) is able to chelate the central metal ion (although with an unfavorable geometry) while the pyrrolopyridine **111w** (dark grey sticks) does not chelate the metal ion but undergoes hydrogen bonding to Asp191. The central Ni^{2+} ion is depicted as green sphere. Metal coordination is shown as teal dashed lines and hydrogen bonds as yellow lines. (Docking provided by Dr. Dina Robaa, MLU Halle-Wittenberg, KDM4A template is PDB: 3RVH)

Bicyclic substituents were assessed next. The 2,7-dihydroxynaphthalene **111v** showed a slight drop in potency compared to phenol **111k** ($\text{IC}_{50} = 14 \mu\text{M}$ vs $2.9 \mu\text{M}$, respectively) due to steric hindrance. The pyrrolopyridine **111w** yielded the lowest IC_{50} value of $2.3 \mu\text{M}$ of all tested imidazole derivatives. It is therefore in the same potency range as the phenol derivative **111k**. For compound **111w**, docking showed a pose where the pyrrolopyridine residue is unable to chelate iron because of a flipped-out orientation. This is probably caused by the presence of a conserved water molecule (cf. Figure 41 bottom). However, this orientation allows the

formation of a hydrogen bond with Asp191, which might explain the high inhibitory potential. Indeed, the quinoline **111x** adopting the same orientation but without a hydrogen-bond donor showed only weak activity of 35% inhibition at 100 μ M. Contrastingly, a flipped-in orientation was observed for triazolopyridine **111y**, yet the binding angle for the catalytic iron is unfavorable explaining the low inhibitory activity of 40% inhibition. However, it should be kept in mind that the presence and localization of water molecules is hard to predict via docking, therefore the flipped-out orientation for **111w** might be a docking artefact.

Table 16 Inhibitory activity of *N*-ethylpyridin-3-amine-substituted imidazole derivatives against KDM4A. Compound were kindly provided by Dr. Nicolas Barthes. Data are mean \pm s. d. of at least two independent experiments.

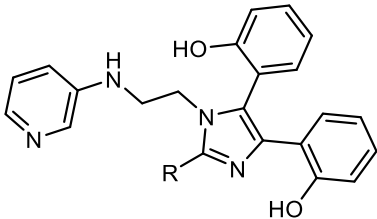
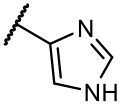
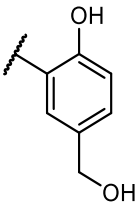
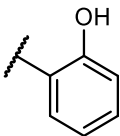
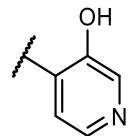
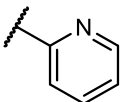
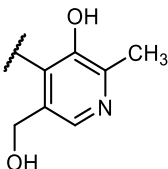
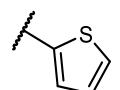
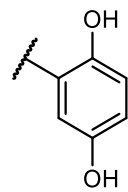
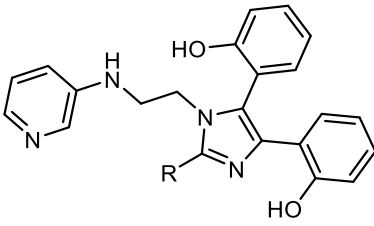
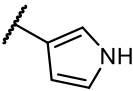
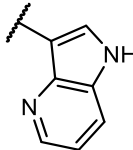
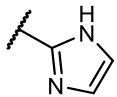
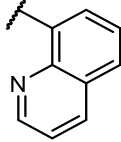
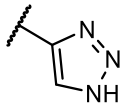
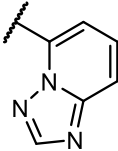
					
No	R	% inhibition or IC ₅₀ / μ M	No	R	% inhibition or IC ₅₀ / μ M
111j		4.6 \pm 0.5	111l		3.0 \pm 0.3
111k		2.9 \pm 0.2	111m		3.9 \pm 1.2
111p		9.7 \pm 0.3	111n		4.4 \pm 0.5
111q		n. i. @ 100 μ M	111o		4.3 \pm 0.4**

Table 16 continued

					
No	R	% inhibition or IC ₅₀ / μM	No	R	% inhibition or IC ₅₀ / μM
111s		n. i. @ 100 μM	111w		2.3 ± 0.1
111t		92% @ 100 μM 21% @ 20 μM	111x		35% @ 100 μM
111u		22.8 ± 1.7	111y		40% @ 100 μM

* purity < 95%

** hillslope > 3, possibly due to PAINS properties (see main text)

The superiority of the *N*-ethylpyridin-3-amine over the *O*-ethylpyridin-3-ol moiety, which had been observed for the phenyl containing **111e** and **111d**, respectively, was confirmed by comparing **111j** with **111h** as well as **111w** with **111i**. For both the phenol and the pyrrolopyridine compounds the *N*-ethylpyridin-3-amine derivatives showed about double the inhibitory potential compared to the *O*-ethylpyridin-3-ol derivatives (cf. Table 15 and Table 16).

4.3.4 Selectivity against other Jmj-KDMs

Jmj-KDMs share a high structural similarity of their catalytic domain. Therefore, the development of selective inhibitors is challenging.

4 Development of novel Inhibitors for JmjC-containing histone demethylases

Table 17 Selectivity data of selected compounds. Data are mean \pm s. d. of at least two independent experiments.

compound	structure	IC ₅₀ / μ M		
		KDM4A (LANCE® assay)	KDM5A (ELISA assay)	KDM6B (ELISA assay)
111q (negative control)		n. i. @ 100 μ M	23% @ 100 μ M	13% @ 100 μ M
deferasirox (54 ; positive control)		4.8	3.9	6.0
110a		3.5	1.9	1.6
111w		2.3	1.4	3.3
99g		7.5	\approx 50	\approx 58

In order to assess if the newly synthesized compounds displayed subtype-selectivity, a representative molecule of each class was tested against KDM5A

(JARID1A), which belongs to the subgroup sharing the highest similarity to KDM4, and KDM6B (JMJD3), which is less similar to KDM4A. Testing was performed by BPS bioscience in an ELISA-based assay.

As an inactive control displaying no inhibition against KDM4A the thienyl derivative **111q** was chosen. Expectedly, this compound also showed very weak inhibition of KDM5A (23% @ 100 μ M) and KDM6B (13% @ 100 μ M). This supports the observation that efficient iron-chelation is a prerequisite for potent inhibition of Jmj-KDMs by the structures presented here. Deferasirox (**54**) was used as a positive control as unselective inhibition of KDM4A, KDM5A and KDM6B had already been shown.¹⁶⁸ Consistently, it yielded IC₅₀ values between 4 and 6 μ M for the three demethylases (cf. Table 17). The pyrazole **110a** and the imidazole **111w** also proved to be unselective, inhibiting all three enzymes in the low micromolar range (IC₅₀ = 3.5 μ M, 1.9 μ M and 1.6 μ M for **110a** and 2.3 μ M, 1.4 μ M and 3.3 μ M for **111w** against KDMs 4A, 5A and 6B, respectively). Only the thiazole **99g** showed seven- to eightfold higher activity on KDM4A than on KDM5A and -6B (IC₅₀ = 7.5 μ M, approx. 50 μ M and approx. 58 μ M, respectively). However, this selectivity could not be explained by docking studies.

4.3.5 Cellular Activity

In order to evaluate the cellular effects of the deferasirox derivatives, cell culture studies were performed. For each compound family, the inhibitor displaying the highest *in vitro* potency was chosen for testing. Additionally, the imidazole derivative **111q**, which is devoid of activity against KDM4A but shares a high structural similarity to the active compounds, was tested to evaluate unspecific compound toxicity. Deferasirox (**54**) or its methyl ester prodrug **54b** were used as reference inhibitors.

4.3.5.1 Cell viability

As prior experiments, performed and described by Dr. Inga Hoffmann (Jung group), had shown promising effects of deferasirox (**54**) on oesophageal cancer cell lines,²⁶⁹ KYSE150²⁷⁰ cells were chosen to determine the compound effects on these cancer cells. The high sensitivity of KYSE150 cells towards KDM4 inhibition stems from their proliferation dependency on KDM4C, which is amplified in this cell line.^{137, 271} As the compounds show no selectivity towards one isoform they inhibit KDM4C in the same range as KDM4A so that this cell line can be used for compound evaluation.

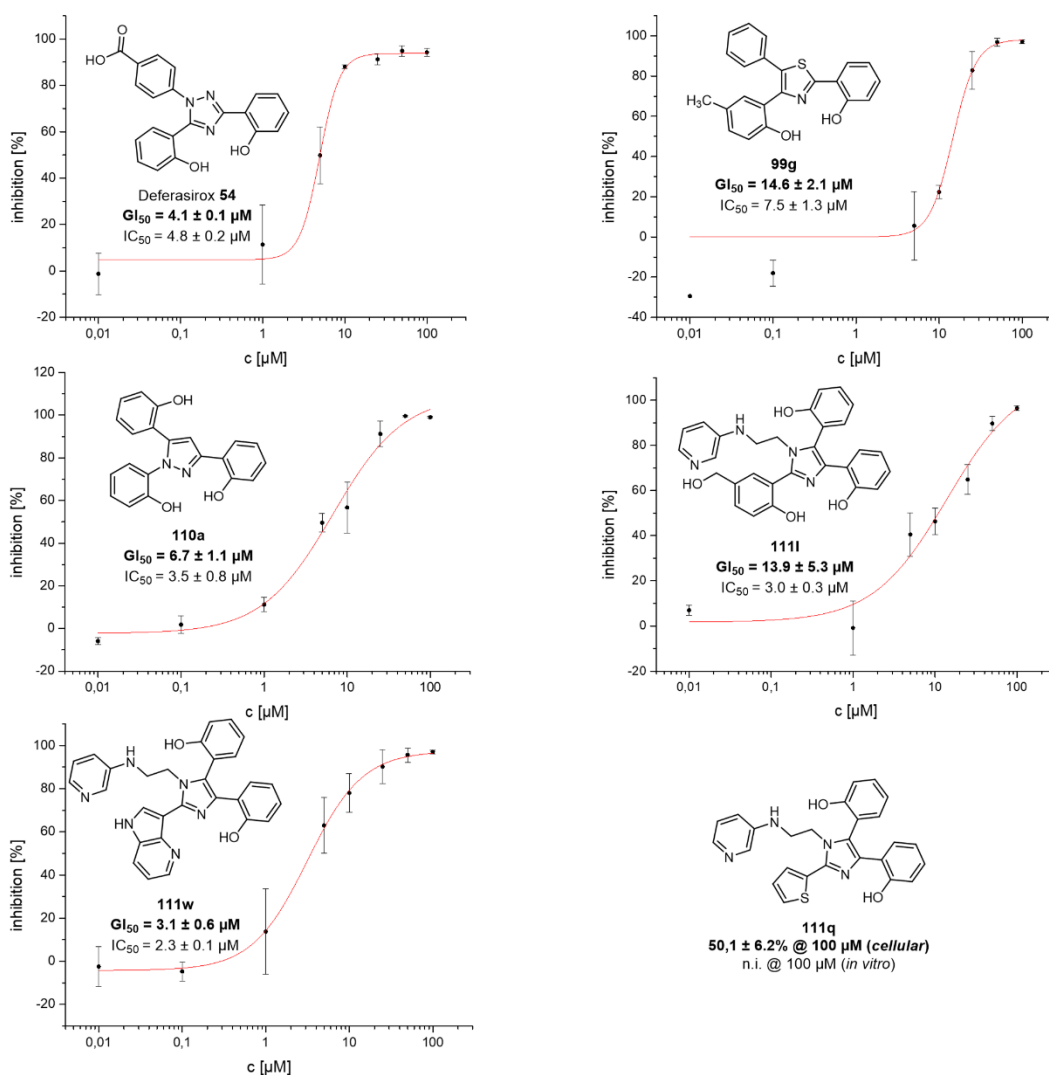


Figure 42 Cellular potency of deferasirox derivatives on the oesophageal cancer cell line KYSE150. Shown are the growth inhibition results of cell proliferation assays (MTS assay). IC_{50} -values of KDM4A-inhibition (LANCE assay) are given for comparison.

To evaluate cell viability, the MTS assay was used following standard procedures. This colorimetric assay is based on the reduction of 3-(4,5-dimethylthiazol-2-yl)-5-(3-carboxymethoxyphenyl)-2-(4-sulfophenyl)-2*H*-tetrazolium (MTS) to a coloured product (formazan) by cellular dehydrogenases in metabolically active cells. Quantification is performed via the measurement of light absorption, which correlates with the amount of viable, active cells.²⁷² Assays were performed by Karin Schmidtkunz (Jung group) following the procedure described by Dr. Inga Hoffmann in her thesis.²⁶⁹ In short, cells were incubated with the inhibitor for 72 h. Then, the MTS reagent (Promega) was added, cells were incubated for 1–4 h and absorption was measured at 492 nm. Cells treated with DMSO were used as negative control equalling 0% inhibition.

The methyl ester prodrug **54b** of deferasirox was used as a reference inhibitor displaying a GI_{50} -value of $4.1 \pm 0.1 \mu\text{M}$. Assay results are summarized in Figure 42. The imidazole **111w** (GI_{50} 3.1 μM) and the pyrazole **110a** (GI_{50} 6.7 μM) showed an inhibition similar to the deferasirox prodrug **54b**, which is in accordance with their similar *in vitro* potency (IC_{50} = 2.3 μM and 3.5 μM , respectively). The thiazole **99g** (GI_{50} 14.6 μM) displayed a three- to fourfold lower activity, which correlates to its slightly lower *in vitro* potency (IC_{50} = 7.5 μM). The imidazole **111l** (GI_{50} 13.9 μM) is also about three times less active than the deferasirox prodrug **54b**, despite its slightly lower IC_{50} -value of 3.0 μM . However, the differences in the IC_{50} - as well as the GI_{50} -values are too small to be statistically significant rendering a ranking of compound potency based on these assay results impossible. This also implies that the observed correlation between *in vitro* potency and cellular activity for **111w**, **110a** and **99g** giving the highest cellular activity for the most potent compound and the lowest activity for the least potent one might just be coincidental and cannot be regarded as proof of a target-specific mechanism of action. Another factor which might influence compound potency is cellular permeability. But as all compounds show similar *in vitro* and *in vivo* potency, cellular permeation seems to be fairly high.

The negative control **111q**, which does not inhibit KDM4A *in vitro*, caused a growth inhibition of 50% at 100 μ M and no inhibition at 10 μ M or below. This shows that the compound toxicity at high concentrations is likely to be independent of KDM4-inhibition. However, as no toxicity was observed in the concentration range where the active compounds showed an effect, their activity seems not to stem only from unspecific effects. In order to clarify the mode of action, further cellular experiments were necessary.

4.3.5.2 On-target Effects via Immunofluorescence Measurements

To characterize the cellular compound effects in more detail and to show target-specific effects, immunofluorescence assays were performed by Vivien Ngo (AG Prof. Lutz Hein, Albert-Ludwig-Universität Freiburg). As for the cell proliferation assay, KYSE150 cells were used due to their high expression of KDM4C. After compound incubation for 72 h hours, cells were stained with H3K9me₃-antibodies. As outlined in section 1.2.2, H3K9me₃ is selectively demethylated by KDM4,^{86, 273} therefore KDM4-inhibition leads to an accumulation of this methylation mark. Accordingly, an increase of H3K9me₃, visualized via staining with the specific antibody, suggests a mechanism of action consisting of or at least involving KDM4 inhibition. IOX1 was used as a reference inhibitor showing high inhibitory potential. As expected, the negative control **111q** did not lead to significant hypermethylation compared to the DMSO control, even at concentrations up to 30 μ M. In contrast to that, the tested active compounds, namely the thiazole **99g** and the imidazole **111w** resulted in a marked hypermethylation at 10 μ M (cf. Figure 43).

Unfortunately, quantification of the fluorescence intensity could not be performed successfully in a reproducible manner due to high variations in the cell numbers. Therefore, this assay could also not reveal a significant difference between the tested compounds. However, the main goal of the experiment, which was proving on-target activity on KDM4, could be achieved, as all three compounds led to a

distinctive increase of H3K9me₃, while the negative control **111q** had no significant effect on hypermethylation.

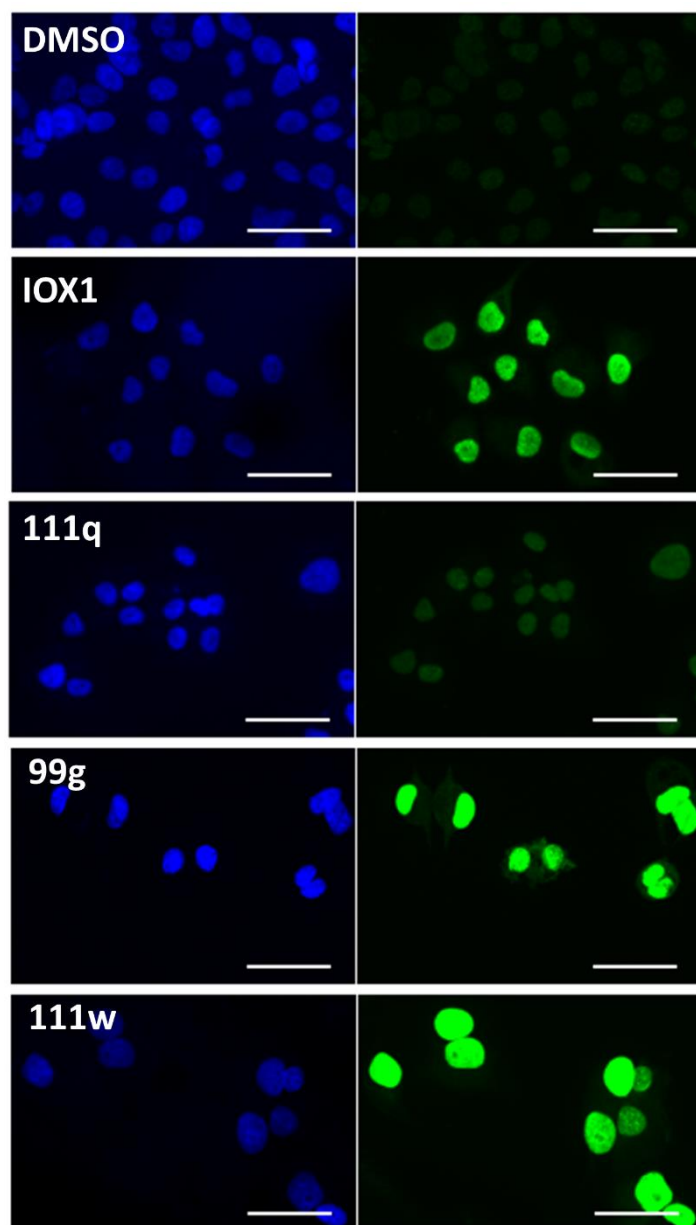


Figure 43 Immunofluorescence staining of KYSE-150 cells incubated with KDM inhibitors. IOX1 was used as reference inhibitor and 111q as negative control which is structurally related to the inhibitors but shows no *in vitro* inhibition of KDM4A. Inhibitors were used at 10 μM and the negative control at 30 μM. The white line represents 50 μm. (Experiments were performed and pictures provided by Vivien Ngo.)

4.3.6 Summary and Discussion

Five different families containing five heterocyclic core structures were evaluated for their inhibitory activity against KDM4A and for selected compounds also against KDM5A and -6B. The synthesis of substituted triazoles confirmed an active-site-based mode of action over a mechanism solely based on iron-chelation, as derivatives bearing large substituents causing steric clashes with the catalytic site displayed comparably low inhibitory activity. Furthermore, the feasibility of compound labelling with fluorophores or a biotin tag via click reaction was shown. Unsymmetrically substituted thiazoles and oxazoles were successfully synthesized and allowed a deeper understanding of the binding mode and structure-activity relationships. The highest activity was observed for the phenol-thiazole/oxazole nitrogen-phenol chelation motif, whereas less polar substituents were tolerated in ring A, albeit with substantially decreased inhibitory activity, but led to inactive compounds when present in ring C. This trend could also be observed for pyrazole derivatives.

Lastly, imidazole derivatives bearing an additional pyridine-containing chain showed an inverse binding mode compared to the other four families induced by the hydrogen bond of the side chain with Asp135 in KDM4A. Besides the phenol, imidazole and pyrrolopyridine could be identified as substituents in position A yielding the most potent compounds. Their high activity despite decreased iron-chelating capabilities could be explained by docking, which showed the formation of an H-bond between the NH-group and Asp191 in KDM4A for both compounds. Selectivity studies versus KDM5A and -6B showed no selectivity for deferasirox, the pyrazole **110a** and the imidazole **111w** whereas thiazole **99g** displayed seven- to eightfold selectivity for KDM4A.

Cellular experiments proved the cytotoxic activity of the most potent compounds against the oesophageal cancer cell line KYSE150, which is known to be sensitive against KDM4-inhibition.²⁶⁹ Furthermore, cellular on-target activity was shown by

immunofluorescence measurements of H3K9 hypermethylation, which is a hallmark of KDM4 inhibition. Overall, an extensive evaluation of the deferasirox scaffold and related structures could be performed yielding several potent inhibitors with cellular activity and a good insight into structure-activity relationships.

4.4 2-Hydrazonylthiazoles and Selenazoles

For the purpose of increasing structural diversity of 5-membered heterocycles, a small set of 2,5-disubstituted thiazole or selenazole compounds, synthesized in the group of Dr. Nenad Filipović (Department of Chemistry and Biochemistry, University of Belgrade), was tested against KDM4A (cf. Table 18). Their main structural feature is a monosubstituted hydrazone moiety in position 2 of the heterocycle. The compounds were considered as potential KDM4-inhibitors for several reasons. First, the thiazole moiety has been shown to be a suitable core structure for KDM inhibitors (cf. section 4.3.2.2), therefore an elaboration on this motif seemed to be promising. Second, the ring nitrogen atom and the doubly bound nitrogen of the hydrazone form a bidentate chelating group potentially able to bind the catalytic iron in the enzyme.

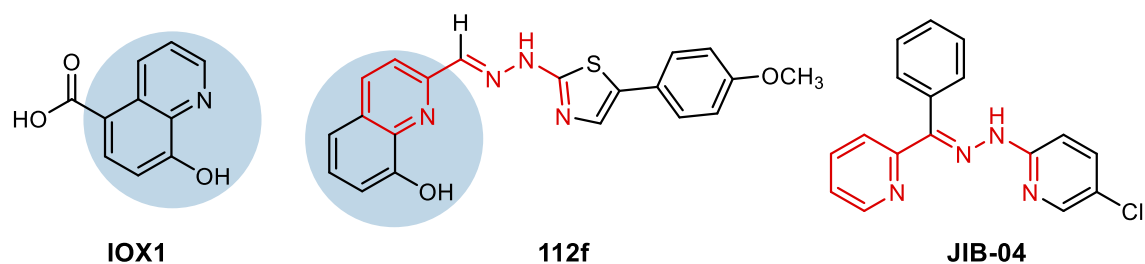


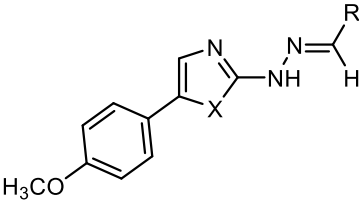
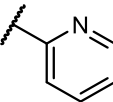
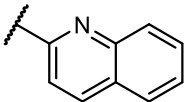
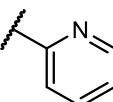
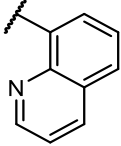
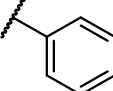
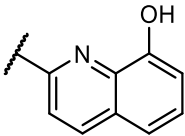
Figure 44 Comparison of the known KDM inhibitors IOX1 and JIB-04 with the newly discovered thiazole derivative **112f**.

Furthermore, the published KDM inhibitor JIB-04 **56**, displaying micromolar activity against KDM4, shares some structural features like the hydrazone moiety adjacent to a nitrogen-containing heterocycle (cf. Figure 44) suggesting that the thiazole and selenazole compounds presented here might also be active on KDM4.

4.4.1 Biochemical Activity

The set of compounds was tested for their inhibitory activity in the LANCE-assay (cf. section 3.1.2 for assay description and Table 18 for results) at a concentration of 500 μ M.

Table 18 Inhibitory activity of 2-hydrazonylthiazoles and -selenazoles against KDM4A. Compounds were kindly provided by the research group of Dr. Nenad Filipović. Data are mean \pm s. d. of at least two independent experiments.

							
No	X	R	% inhibition @ 500 μ M	No	X	R	% inhibition @ 500 μ M or IC ₅₀ / μ M
112a	S		53%	112c	S		30%
112b	Se		96%	112d	S		45%
112e	Se		68%	112f	S		4.94 \pm 0.45

The pyridine-substituted thiazole compound **112a** displayed a quite low inhibition of 53%, whereas **112b**, the selenazole analogue of **112a**, led to almost full inhibition at the same concentration. The selenazole **112e** substituted with phenyl instead of pyridine showed a decreased potency of 68%. The quinoline-substituted thiazole compounds **112c** and **112d** showed rather weak inhibition of 30-45% at 500 μ M. Therefore, it can be assumed that pyridine is superior to quinoline and phenyl. Furthermore, the selenazole motif seems to be better suited than the thiazole in this series of inhibitors. However, all of the above-mentioned compounds were rather weakly active inhibitors.

The only compound displaying an IC_{50} value of 5 μ M was the thiazole **112f**, which is substituted with an 8-hydroxyquinoline. The 8-hydroxyquinoline motif is also present in IOX1 (**42**; cf. section 1.4.2.5 and Figure 44), which is a 2-OG-competitive nonselective KDM inhibitor, binding the ferrous iron via the quinoline nitrogen and the 8-hydroxy group. Hence, compound **112f** contains two potential iron binding sites which could be responsible for its inhibitory activity on KDM4A.

In order to evaluate the mode of action of **112f**, kinetic studies were performed. In order to assess if the compound acts competitively towards the co-substrate, 2-OG was titrated against different inhibitor concentrations in the LANCE assay. Results are summarized in Figure 45. Plotting the reaction velocity v against the 2-OG concentration shows that the obtained values cannot be satisfyingly fitted to a classical Michaelis-Menten equation (cf. section 3.1.2; graph not shown). That implies an inhibitory mechanism not solely based on competition against 2-OG. The representation of the data in a linearized double reciprocal plot, also called Lineweaver-Burk plot, reveals the not solely competitive behaviour even more clearly (cf. Figure 45 left). Competitive inhibition results in linear regression curves intersecting in one point on the $1/v$ axis, which is apparently not the case for **112f**. However, fitting to a mixed-mode inhibition model gives a better curve fit (cf. Figure 45 right). Fitting was performed according to the following equation (v : reaction velocity, α : binding degree, K_i : inhibition constant, K_M^{app} : apparent Michaelis-Menten constant):

$$v = \frac{\frac{v_{max}}{1 + \frac{[112f]}{\alpha \cdot K_i}} \cdot [2-OG]}{K_M^{app} \cdot \frac{1 + \frac{[112f]}{K_i}}{1 + \frac{[112f]}{\alpha \cdot K_i}} + [2-OG]} \quad (4.1)$$

Mixed-mode inhibition implies a mode of action, where competition of the inhibitor with the co-substrate is at least not solely responsible for inhibition. Mixed-mode inhibition in respect to 2-OG was also shown for JIB-04.⁵¹ It is therefore possible that **112f** employs a similar mode of action to JIB-04. However, an oxygen-competitive

behaviour, as it was postulated for JIB-04⁵¹ could not be measured for **112f** due to the unavailability of the necessary equipment to regulate and determine oxygen concentrations.

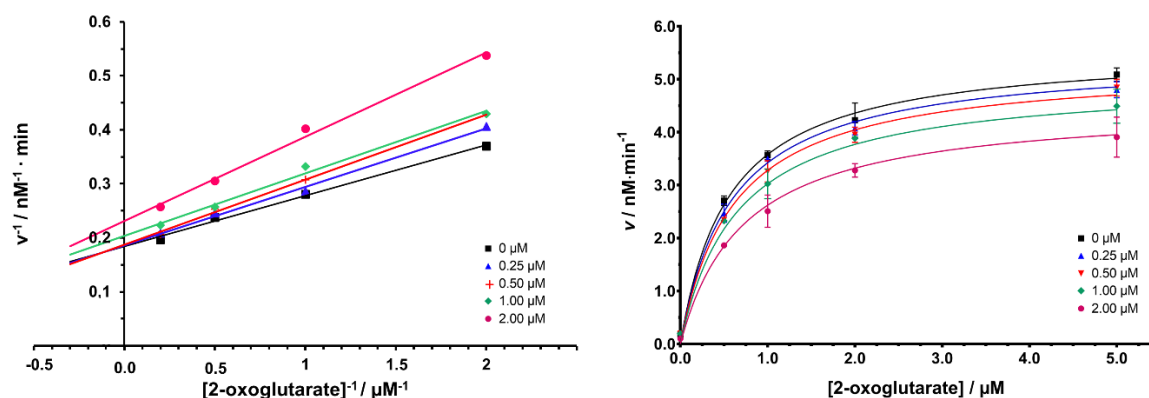


Figure 45 Left: The Lineweaver-Burk plot of **112f** shows not solely competitive behaviour towards 2-OG, as the lines do not intersect at the y-axis.
Right: Fitting to a mixed mode inhibition model shows a good curve fit. See text for explanation.

In summary, the hydrazone-containing thia- and selenazoles yielded weak KDM4A inhibitors, the hydroxyquinoline **112f** being the only exception with an IC₅₀ value in the low micromolar range. The mechanism of action is not solely based on co-substrate competition suggesting a unique mode of inhibition for this compound which might be similar to the published inhibitor JIB-04.

5 Conclusion and Outlook

Jmj-KDMs have proven to be promising drug targets in cancer and other diseases, while still many questions concerning their biological role in physiological and pathophysiological processes remain. Inhibitors of these enzymes displaying a various set of characteristics such as potency and selectivity towards certain subtypes and isoforms are valuable tools to study this enzyme class in more detail. Furthermore, those inhibitors show promising potential to be developed into therapeutic drugs.

Consequently, the main goal of this thesis was the development and characterization of new Jmj-KDM inhibitors with special focus on KDM4A. To this end, synthesis of various inhibitors was performed while other compounds were obtained from collaboration partners in order to pursue an activity-guided elaboration of promising structures. The project was divided in two main parts. First, the exploration of bioisosteric analogs of known inhibitors including sulfoxides, sulfones, boronic acid and tetrazoles was performed. While the sulphur- and boron-containing compounds showed only weak activity, two low micromolar scaffolds of tetrazoles could be identified. The first is based on 2,4-PDCA where replacement of the 2-carboxylic acid with a methylamino moiety and the 4-carboxylic acid with tetrazole was realized. The second tetrazole-containing inhibitor series was based on daminozide and yielded inhibitors in the one-digit micromolar range.

The second part of the work consisted of the synthesis and evaluation of inhibitors based on the clinically approved iron-chelator deferasirox. Here, five different core motifs, namely triazoles, thiazoles, oxazoles, pyrazoles and imidazoles were investigated. The *in vitro* evaluation resulted in elaborate structure activity relationships, which were substantiated by docking results. A fluorescence polarization assay was established to support a mechanism which is based on active-site binding. Selectivity investigations revealed one thiazole derivative to be

slightly selective for KDM4A while the other compounds were pan-selective towards the tested demethylases. The biological activity and on-target effects were confirmed for the most potent compounds via cellular studies. These revealed anti-cancer effects of all tested inhibitors on the oesophageal cancer cell line KYSE150 and H3K9 hypermethylation shown by immunofluorescence. The fact that the structures are based on an already clinically approved drug may facilitate their development into anti-cancer drugs.

Future research may elaborate the findings on active compounds by testing them in different cellular settings spanning a wider range of cancer cells thereby widening the applicability of the compounds for further anti-cancer investigations.

Two fluorescently labelled triazoles displaying low micromolar activity were synthesized. They may be used in fluorescence polarization assays to further characterize KDM inhibitors. Additionally, they can potentially also be used for cellular studies in order to study cellular permeability and subcellular localization. The biotin-labelled probe may be used for binding assays using streptavidin as an acceptor moiety.

In conclusion, the development of a highly diverse set of Jmj-KDM inhibitors spanning from pan-selective to mildly selective inhibitors with proven cellular activity and also containing molecular probes may support the elucidation of the manifold biological roles of Jmj-KDMs and may even lay the foundation for the advancement into pre-clinical studies towards anti-cancer therapeutic drugs.

6 Experimental

6.1 Biochemical Assays

6.1.1 General Remarks

Reagents, chemicals, and buffer components were purchased from commercial sources and used without further purification. Stock solutions of test compounds were in DMSO in a concentration of 20, 10, or 5 mM dependent their solubility and stored in a freezer at -20°C .

Before use, these stock solutions were thawed to room temperature and thoroughly homogenized on a vortex shaker. Water for buffers and solutions was double distilled to Milli-Q purity. Standard laboratory glassware and plastic apparatus was used, in particular micro-reaction vessels in 1.5 mL (Sarstedt) and 5 mL (VWR) size as well as pipette tips in 10 μL and 200 μL size (Sarstedt) and 1000 μL size (ULPlast Omnitipprepared).

All dilution and transfer steps were pipetted with appropriate Abimed/Kinesis HTL Discovery Comfort single-channel pipettes or Eppendorff pipetes (ranges: 0.5–10 μL , 10–100 μL , 20–200 μL , 100–1000 μL). Final dispensation steps of detection solutions were performed using an automated Brand HandyStep electronic dispenser pipette with appropriate PD tips. For fluorescence-based assays, white opaque OptiPlate-384 microtiter plates from PerkinElmer (catalogue #: 6007299) with Lid-384 clear non-sterile lids (catalogue #: 6007617) were used. Plates were sealed with airtight PerkinElmer TopSeal®-A 384 (catalogue #: 6005250) or TopSeal®-A PLUS (catalogue #: 6050185) adhesive sealing tapes during incubation.

6.1.1.1 Reagents and Chemicals

Aqueous solutions of the assay components 2-oxoglutarate disodium salt dihydrate, ferrous sulphate heptahydrate, and L(+)-ascorbic acid at a concentration of 10 mM were prepared in 10 mL conical tubes and diluted with Milli-Q water to

6 Experimental

the working concentrations. These stock solutions were stored at room temperature and replaced with freshly prepared solutions at least once a week to avoid oxidation or other degradation of the reagents. The oxidized form of nicotinamide adenine dinucleotide (NAD⁺) was obtained from different commercial sources at different times including Sigma-Aldrich, AppliChem, and Carl Roth. Stock solutions were regularly prepared at a concentration of 80 mM in Milli-Q water, aliquoted, shock-frozen in liquid nitrogen, and stored in a freezer at –20 °C.

Reagent	Supplier	purity (if applicable), remarks	Catalogue number
2-[4-(2-hydroxyethyl)piperazin-1-yl] ethanesulfonic acid (HEPES)	VWR	≥99.5% for biochemical assays	441485H
2-oxoglutarate disodium salt dihydrate	AppliChem	BioChimica purity	A6408
bovine serum albumin (BSA)	CarlRoth	Fraction V	8076
ferrous sulphate heptahydrate	VWR	Normapur purity	24244.232
L(+)-ascorbic acid	AppliChem	BioChimica purity	A1052
Detection Buffer LANCEUltra® 10X	PerkinElmer		CR97
ULight coupled to streptavidin (LANCEUltra®)	PerkinElmer		TRF0102

BSA for buffers was diluted in MilliQ water to a concentration of 5%, aliquoted, shock-frozen in liquid nitrogen, and stored in a freezer at -20°C . Ethylenediaminetetraacetic acid (EDTA) disodium salt dihydrate was from bulk chemical stock as supplied from the chemical store and used without further purification.

6.1.2 Peptides and Antibodies

Peptide/Antibody	Sequence	Supplier	Catalogue number
H3K9me ₃ 7–14	ARK(me ₃)STGGK-NH ₂	PSL (Peptide Specialty Laboratories, Heidelberg)	custom synthesis
biot-H3K9me ₂ 1–21	ARTKQTARK(me ₂)STGGK-APRKQLAGGK(biotin)	BPS BioScience (San Diego, CA)	50351
biot-H3K9me ₃ 1–21	ARTKQTARK(me ₃)STGGK-APRKQLAGGK(biotin)	BPS BioScience (San Diego, CA)	50350
Eu-labelled H3K9me ₂		PerkinElmer	TRF0403

Peptides from BPS were obtained as 40 μM aqueous solutions, aliquoted, and stored in a freezer at -80°C . The peptide from PSL was obtained as lyophilized powder and reconstituted in Milli-Q water according to the declared amount and molecular weight supplied by the manufacturer to a concentration of 10 mM, shock-frozen in liquid nitrogen, and stored in a freezer at -20°C . The antibody was stored at $5-8^{\circ}\text{C}$ and used at the declared concentration.

6.1.3 Buffers

The standard HEPES buffer was filtered through a 0.2 µm sterile cellulose acetate filter after preparation and stored at 5-8 °C. The LANCEUltra® assay buffer was freshly prepared via addition of BSA stock solution (5% in Milli-Q water) to the standard HEPES buffer prior to use and stored on ice. LANCE detection buffer was freshly prepared via 10-fold dilution of the commercial LANCE detection buffer 10X prior to use and stored on ice.

FDH-coupled assay	50 mM HEPES, pH 7.50, 0.01% (v/v) Tween-20
LANCEUltra® assay	50 mM HEPES, pH 7.50, 0.01% (v/v) Tween-20, 0.01% (m/m) BSA
LANCE detection buffer	Unknown; prepared from LANCE detection buffer 10X from PerkinElmer (catalogue number: CR97)

6.1.4 Enzymes

KDM4A was kindly provided by the research group of Prof. Dr. Roland Schüle (Central Clinical Research, University Medical Center, Freiburg i. Br.). Using standard protein expression and purification methods, the catalytic domain of this enzyme (i. e. residues 1–359) was expressed in an *E. coli* strain and purified via its His-Tag on Nickel chelate beads. The approximate protein concentration of these enzyme batches was determined by Bradford assay. The expression method followed that previously published by Ng *et al.*²⁷⁴ Shortly, the plasmid pNIC28-Bsa4 JMJD2A encoding human KDM4A residues 1–359 was transformed in BL21-CodonPlus-Ril competent cells. Six litres of TB media containing kanamycin(50 µg /mL) and chloramphenicol (34 µg/mL) were inoculated with a 15 mL/L overnight culture and grown at 37 °C. Expression was induced by addition of 0.2 mM IPTG at A260 = 0.6. Then, the culture was incubated at 18 °C for another 18 h. After harvesting and lysis of the bacteria, the protein was purified by a Talon bead column. The purity of KDM4A estimated by sodium dodecylsulfate polyacrylamide

gel electrophoresis (SDS-PAGE) was above 90%. As a control for continually equal enzyme quality, every new batch of this enzyme was tested in activity assays (FDH-coupled kinetic measurements and LANCEUltra®) to verify that the delivered fractions were active enzyme. It was verified that every batch, when diluted to the same nominal working concentration, showed comparable activity to previous batches. Furthermore, every new batch of enzyme was tested in an FDH-coupled inhibition assay against the reference inhibitor 2,4-PDCA, which should yield an IC₅₀ value of around 1 µM. KDM4A was aliquoted and stored at –80 °C. Before use, it was thawed on ice and gently homogenized on a vortex shaker. Aliquots were shock-frozen in liquid nitrogen, stored at –80 °C and reused but only subjected to maximal two freeze-thaw cycles, before loss of activity could be observed.

FDH from *Pseudomonas sp.* was obtained commercially (Sigma Aldrich, catalogue number F1879). Upon arrival, this enzyme was reconstituted in Milli-Q water to a concentration of 0.1 Unit/µL (based on the declared activity of the particular batch), aliquoted, shock-frozen in liquid nitrogen, and stored in a freezer at –20 °C.

6.1.5 Equipment and Software

Fluorescence measurements for the FDH assay were performed with the POLARstar Optima microplate reader (BMG Labtech). The reader was run in fluorescence mode with gain adjustment set to 2100 and 330 nm excitation and 460 nm emission filters using white 384 OptiPlates™ (PerkinElmer). TR-FRET measurements were performed with the EnVision 2102 multilabel plate reader (PerkinElmer) in TR-FRET LANCE mode using a 340 nm excitation and a 665 nm emission filter and white 384 OptiPlates™ (PerkinElmer). The software used for the fitting of dose-response curves was GraphPad Prism 4.00 (GraphPad Software, Inc.) using 4-parameter logistic curve fitting (cf. Section 3.1).

6.1.6 FDH-Coupled Enzyme Activity Assay

6.1.6.1 Inhibition curves for IC₅₀-value determination

The FDH enzyme-coupled demethylase activity assay was carried out following the description of Dr. Martin Roatsch in his thesis.¹²⁰ It was performed in a total volume of 20 μL on white OptiPlate-384 microtiter plates (PerkinElmer) using the standard 50 mM HEPES buffer at pH = 7.50 containing 0.01% (v/v) Tween-20. The enzyme KDM4A 1–359 was pre-diluted to the working concentration of 0.10 mg/mL (2.40 μM) resulting in a final assay concentration of 1.75 μM . A 13-point dilution series (typically 0–20 mM) of the test compound in DMSO was prepared with 2-fold dilution steps. The substrate solution was prepared in HEPES buffer according to the following table:

	assay concentration	substrate solution concentration	stock solution concentration	volume for 200 μL
ascorbic acid	100 μM	400 μM	3 mM	26.7 μL
FeSO ₄	10 μM	40 μM	1 mM	8.0 μL
FDH	0.001 U/ μL	0.004 U/ μL	0.1 U/ μL	8.0 μL
NAD ⁺	500 μM	2000 μM	80 mM	5.0 μL
2- oxoglutarate	50 μM	200 μM	10 mM	4.0 μL
peptide	35 μM	140 μM	1 mM	28.0 μL
HEPES buffer				120.33 μL

Experiments were performed as duplicates. The compound pre-dilution or DMSO were mixed with enzyme or buffer and pre-incubated at room temperature for 10 min. Then, the substrate solution was added into all the corresponding tubes and

mixed via aspiration with the pipette. 20 μL of the mixture was immediately transferred into the wells of a 384-well plate.

The assay mixtures for every well were prepared in 1.5 mL micro-reaction tubes according to the following pipetting scheme:

	blank	positive control	negative control	samples
enzyme ($C_{\text{final}} \times 1.37$)	--	17.5 μL	17.5 μL	17.5 μL
assay buffer	17.5 μL	--	6.0 μL	--
compound ($C_{\text{final}} \times 48$)	--	--	--	0.5 μL
DMSO	0.5 μL	0.5 μL	0.5 μL	--
substr. soln. ($C_{\text{final}} \times 4$)	6.0 μL	6.0 μL	--	6.0 μL
	24 μL	24 μL	24 μL	24 μL

Fluorescence intensity (FI) of NADH generated by the enzymatic reaction was measured at $\lambda_{\text{ex}} = 330 \text{ nm}$ and $\lambda_{\text{em}} = 460 \text{ nm}$ on a POLARstar Optima microplate reader (BMG Labtech) immediately after addition ($t = 0$) and after 1 h of incubation on a horizontal shaker at 37 °C. The values for all wells were blank-subtracted and the difference in intensity at $t = 1 \text{ h}$ and $t = 0$ was taken as a measurement of enzyme activity. Activity in % was then calculated in comparison to compound-free DMSO control (positive control, defined as 100% activity) and no-substrate control (negative control, defined as 0% activity) according to the following equation:

$$\text{Activity} = \frac{FI_{\text{Sample}} - FI_{\text{Negative}}}{FI_{\text{Positive}} - FI_{\text{Negative}}} * 100\% \quad (6.1)$$

The obtained activity values were plotted using GraphPad Prism 4.00 and sigmoidal curve fitting was performed according to the following 4-parameter logistic curve function:

$$y = \frac{y_{max} - y_{min}}{1 + \left(\frac{x}{EC_{50}}\right)^H} * 100\% \quad (6.2)$$

The y-values correspond to the percentage of activity, y_{min} and y_{max} correspond to minimal and maximal activity as defined by the fit curve, and x to the concentrations used. EC_{50} represents the particular concentration at which the half-maximal effect is observed, meaning the reduction in activity between y_{max} and y_{min} in this case. H is termed the Hill slope parameter or Hill coefficient and defines the curve slope between y_{max} and y_{min} at the EC_{50} concentration. Furthermore, the Hill slope may be used as a measure of the binding stoichiometry of inhibitor molecules to enzyme molecules and can, thus, be expected to be around 1 in the case of direct binding of one molecule of inhibitor per enzyme molecule in simple cases. Higher hill slopes may stem from cooperative binding of more than one inhibitor molecule or from unspecific effects such as compound and enzyme aggregation.²⁷⁵

These curve parameters were used for the calculation of IC_{50} values, which denote the concentration at which 50% inhibition compared to the maximal inhibition took place. For inhibitors reaching full inhibition at high concentrations, meaning that the minimal measured enzymatic activity is as low as for the negative control, EC_{50} and IC_{50} are basically the same. IC_{50} values were calculated from the fit parameters as follows:

$$IC_{50} = \left(\frac{y_{max} - y_{min}}{50 - y_{min}} - 1\right)^{\frac{1}{H}} * EC_{50} \quad (6.3)$$

IC_{50} values were calculated from at least two independent experiment for each compound and the values shown correspond to their mean \pm standard deviation.

6.1.6.2 Kinetic Activity Measurements

Kinetic activity measurements using the FDH-coupled assay were performed following the same protocol as for the inhibition curves (cf. Section 6.1.6.1) with slight modification, namely without addition of test compounds. For quality control of each new batch of enzyme the new and the current batch of enzyme were both diluted to the working concentration of 0.10 mg/mL (2.40 μ M) with HEPES buffer, which resulted in a final assay concentration of 1.75 μ M. To these samples 0.5 μ L DMSO was added and the mixture was pre-incubated at room temperature for 10 min. Then, 6.0 μ L of the substrate solution were added and 20 μ L of the total mixture were transferred into the wells of a 384-well plate. This was measured at the same conditions on the POLARstar Optima microplate reader as for the inhibition experiments, but in kinetic mode. This means that the plate reader chamber was pre-heated to 37 °C and kept at this temperature during measurement. The fluorescence intensity was continuously measured (e. g. every 30 seconds) over a total time of 1.5 h. The obtained values were used to generate a fluorescence-over-time curve, which should give similar results for both the old and the new batch of enzyme. Blank and negative control measurements should result in a flat line with no change of fluorescence over time. These assays were typically performed in triplicate.

6.1.7 LANCEUltra® Assay

6.1.7.1 Inhibition curves for IC₅₀-value determination

The commercial antibody-based LANCEUltra® demethylase activity assay (PerkinElmer) was carried out following the description of Dr. Martin Roatsch in his thesis.¹²⁰ It was performed in a total volume of 10 μ L on white OptiPlate-384 microtiter plates using a 50 mM HEPES buffer at pH = 7.50 containing 0.01% (v/v) Tween-20 and 0.01% (m/m) BSA (LANCE buffer).

6 Experimental

KDM4A 1–359 was pre-diluted to the working concentration of 85.7 nM in two steps, which results in a final assay concentration of 60 nM. A 13-point dilution series (typically 0–20 mM) of the test compound in DMSO was prepared with 2-fold dilution steps.

The substrate solution was prepared in LANCE buffer according to the following table:

	assay concentration	substrate solution concentration	stock solution concentration	volume for 100 μ L
ascorbic acid	100 μ M	400 μ M	3 mM	13.3 μ L
FeSO ₄	5 μ M	20 μ M	1 mM	2.0 μ L
2-oxoglutarate	1 μ M	4 μ M	0.1 mM	4.0 μ L
peptide	400 nM	1.6 μ M	40 mM	4.0 μ L
LANCE buffer				76.7 μ L

Each experiment was performed in duplicates. The assay mixtures were prepared in the wells of a 384-well plate according to the following pipetting scheme:

	blank	positive control	negative control	samples
enzyme ($C_{\text{final}} \times 1.37$)	--	7.0 μ L	--	7.0 μ L
assay buffer	9.5 μ L	--	7.0 μ L	--
compound ($C_{\text{final}} \times 48$)	--	--	--	0.5 μ L
DMSO	0.5 μ L	0.5 μ L	0.5 μ L	--
substr. soln. ($C_{\text{final}} \times 4$)	--	2.5 μ L	2.5 μ L	2.5 μ L
	10 μ L	10 μ L	10 μ L	10 μ L

The compound pre-dilution or DMSO were mixed with enzyme or buffer and pre-incubated at room temperature for 10 min. Then, the substrate solution was added

into all the corresponding wells, centrifuged for 1 min at 700 rpm to ensure that all solution was at the bottom of the wells and incubated on a horizontal shaker at 600 rpm at r.t. for 45 min. Shortly before the end of this incubation period, the detection mix was freshly prepared according to the following table:

	assay concentration	detection mix concentration	stock solution concentration	volume for 400 μ L
Eu α -H3K9me ₂ Ab	2 nM	4 nM	0.625 μ M	2.56 μ L
<i>ULight</i> Streptavidin	50 nM	100 nM	10 μ M	4.00 μ L
EDTA	1 mM	2 mM	10 mM	80.0 μ L
LANCE det. buffer				313.44 μ L

At the end of the 45 min incubation period for enzymatic transformation, 10 μ L of the detection mix were dispensed in each well. The large excess of EDTA serves as an iron chelator removing iron from solution and from the enzyme thereby stopping the enzymatic reaction. After addition of the detection mix, the plate was centrifuged for 1 min at 700 rpm and incubated on a horizontal shaker at 600 rpm for 60 min at r.t. Care must be taken that room temperature does not exceed 25 $^{\circ}$ C to ensure proper antibody binding and avoid degradation of reagents. After incubation, time-resolved FRET intensity was measured on a PerkinElmer EnVision 2102 multilabel plate reader at $\lambda_{\text{ex}} = 340$ nm and $\lambda_{\text{em}} = 665$ nm with a delay of 100 μ s. The values for all wells were blank-subtracted and activity in % is in comparison to compound-free DMSO control (positive control, defined as 100%) and no-enzyme negative control (defined as 0%) according to equation 5.1. The obtained activity values were plotted using GraphPad Prism 4.00 and sigmoidal curve fitting was performed according to the 4-parameter logistic curve function 5.2. IC₅₀ values were calculated using equation 5.3 as described above.

6.1.7.2 Competitivity Investigations against 2-Oxoglutarate

In order to assess the competitiveness of enzyme inhibition by test compounds towards the co-substrate 2-oxoglutarate (2-OG), the LANCEUltra® assay was performed as described in Section XY with varying concentrations both of 2-OG (0–5.0 μ M) and inhibitor, including at least two inhibitor concentrations below and one above the IC₅₀ value prior determined in the LANCEUltra assay. Each combination of concentrations was tested in duplicate. Calculations were performed as described in Section XY. Shortly, the blank-corrected LANCE signal was compared to the pre-established calibration curve (cf. Section XY) to determine the amount of demethylated product formed using the following equation:

$$[H3K9me_2] = \frac{LANC E - 200}{275} * 1nM \quad (3.1)$$

The reaction velocity was calculated as follows:

$$v = \frac{\Delta[H3K9me_2]}{\Delta t} = \frac{[H3K9me_2]}{45 \text{ min}} \quad (3.2)$$

Fitting the thus obtained velocities against the Michaelis-Menten equation

$$v = \frac{v_{\max} \cdot [2-OG]}{K_M^{\text{app}} + [2-OG]} \quad (3.3)$$

gives the apparent K_M values for the respective inhibitor concentrations under the specified assay conditions. For competitive inhibitors, apparent K_M values can be used to calculate the inhibition constant K_i via linear regression to the following equation:

$$K_M^{\text{app}} = K_M^0 \cdot \left(1 + \frac{[inhibitor]}{K_i} \right) \quad (3.4)$$

6.1.8 Fluorescence Polarization assay

6.1.8.1 General remarks

The FP assay was performed in a total volume of 20 μ L on black 384-well non-binding microplates (catalogue #: 11866091, Greiner Bio-One) using a 50 mM HEPES buffer at pH = 7.50 containing 0.01% (v/v) Tween-20.

After dispensing of assay components, plates were centrifuged for 1 min at 700 rpm to ensure that all solution was at the bottom of the wells, sealed with adhesive foil (PerkinElmer TopSeal®-A 384; catalogue #: 6005250) and incubated on a horizontal shaker at 600 rpm at r.t. for 2 h. Blank controls containing 20 μ L assay buffer were included in all measurements. The fluorescein-labelled **96a** and the TAMRA-labelled **96b** were utilized as fluorescent probes. The fluorescence intensity signals of polarized light in parallel (I_{\parallel} ; P-plane) and in perpendicular plane (I_{\perp} ; S-plane) with respect to the excitation light were quantified using a 2102 EnVision® Multilabel Reader (PerkinElmer, Waltham, USA) operating in FP-mode ($\lambda_{\text{ex}} = 480$ nm, λ_{em} (P-plane) = 535 nm, λ_{em} (S-plane) = 535 nm for **96a**; $\lambda_{\text{ex}} = 531$ nm, λ_{em} (P-plane) = 595 nm, λ_{em} (S-plane) = 595 nm for **96b**).

6.1.8.2 Fluorescence intensity of **96a** and **96b**

The fluorescence intensities of **96a** and **96b** were measured at different concentrations. To this end, a serial dilution of the fluorescent probes in assay buffer containing a final concentration of 2.5% DMSO and spanning a concentration range of 0–8 nM, was generated and 20 μ L of each concentration were transferred to a 384-well assay plate in triplicate. The plates were centrifuged for 1 min at 700 rpm and the fluorescence signal ($\lambda_{\text{ex}} = 480$ nm, $\lambda_{\text{em}} = 535$ nm for **96a**; $\lambda_{\text{ex}} = 531$ nm, $\lambda_{\text{em}} = 595$ nm for **96b**) was measured after 2 h. After blank correction, the mean values of fluorescence intensity were plotted against the fluorescent probe concentration and linear regression (using Excell2010 software) was used to determine the linearity of signal increase.

6.1.8.3 Enzyme titration

To determine probe binding towards the enzyme, increasing amounts of **96a** were added to a solution of the fluorescent probe in HEPES buffer. To this end, 18.5 μ L of a serial enzyme dilution (final concentration ranging from 0–3200 nM) in HEPES buffer

6 Experimental

were mixed with 0.5 μL of the fluorescent probe dilution in DMSO (final probe concentration 10 nM) in HEPES buffer. 1 μL of an aqueous solution of either NiCl_2 or FeSO_4 (final concentration 50 μM) were added. Incubation, measurement and blank correction were performed as described in the general section. The resulting FP signal was plotted against the enzyme concentration.

6.1.8.4 Competitivity towards deferasirox

Competitive displacement of the fluorescent probe with deferasirox was measured via addition of a serial dilution of deferasirox (final concentration 0–50 μM) according to the following pipetting scheme. The fluorescent probe was diluted in HEPES buffer containing 0.2% DMSO and deferasirox was diluted in DMSO containing 0.2 % HEPES buffer resulting in a final DMSO concentration of 2.5% in the assay.

	blank	positive control	negative control	samples
enzyme ($C_{\text{final}} \times 20/19$)	--	19 μL	--	19 μL
assay buffer	19.5 μL	--	19 μL	--
assay buffer + 0.2% DMSO	--	0.5 μL	--	--
assay buffer + 98.8% DMSO	--	--	0.5 μL	--
DMSO	0.5 μL		--	--
fluorescent probe	--	0.5 μL	0.5 μL	0.5 μL
compound ($C_{\text{final}} \times 40$)	--	--	--	0.5 μL
	20 μL	20 μL	20 μL	20 μL

Incubation, measurement and blank correction were performed as described in the general section. The resulting FP signal was plotted against the deferasirox concentration.

6.2 Synthesis

6.2.1 General Remarks

Reactions were carried out in standard laboratory glassware. Reagents were purchased from commercial sources and used without further purification. Solvents were purified by distillation prior to use. Dry solvents were purchased from commercial sources or obtained via drying over molecular sieves. Reaction progress was monitored via thin-layer chromatography (TLC) on pre-coated silica gel plates with fluorescence indicator (Merck silica gel 60 F254 or silica gel 60 RP-18 F_{254s}, layer thickness 0.2 mm) and analyzed under UV light (254 nm and 365 nm). Microwave-assisted syntheses were conducted on a CEM Discover microwave reactor in septum-sealed glass pressure vials at the indicated conditions.

6.2.2 Compound Purification

Flash column chromatography was performed on a Biotage® Isolera Prime/One purification system using 40–60 µm pre-packed silica gel columns (40–60 µm) from Telos, HP-spherical silica gel columns (50 µm) from Interchim or C18-modified silica gel columns (50 µm) from Telos. The crude material was either dissolved in a low amount of solvent and then transferred to the column, or it was adsorbed on Telos™ Bulk Sorbent, which was filled in an empty cartridge and attached to the column.

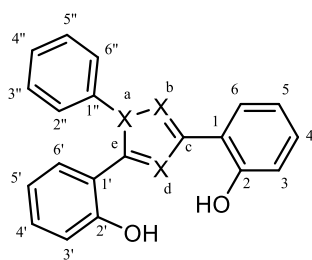
Semi-preparative high-performance liquid chromatography (HPLC) was performed on an Agilent Technologies 1260 Infinity system using UV detection at 210 nm using a Phenomenex Synergi® 10u Hydro-RP 80 Å 250 × 15.00 mm column. Eluent A was water containing 0.05% trifluoroacetic acid (TFA) and eluent B was acetonitrile containing 0.05% TFA. Linear gradient conditions were as indicated for the specific compounds and the flowrate was set to 3 ml/min.

Preparative TLC was performed on pre-coated silica gel plates (Merck silica gel 60 F₂₅₄, layer thickness 0.5 mm) using the indicated solvent mixtures.

6.2.3 Nuclear Magnetic Resonance-Spectrometry

¹H-NMR and proton-decoupled ¹³C-NMR spectra were recorded in the indicated deuterated solvents on a Bruker Advance II+ 400 MHz spectrometer. Chemical shifts (δ) are reported in parts per million (ppm), multiplicity abbreviations are as follows: s = singlet, bs = broad singlet, d = doublet, dd = doublet of doublets, dt = doublet of triplets, t = triplet, td = triplet of doublets, q = quartet, p = quintet, m = multiplet. Coupling constants (*J*) are expressed in Hz and were calculated using Mestrelab Mnova software version 11.0. Chemical shifts are normalized to the expected chemical shift of the residual solvent signal, i. e. ¹H = 2.5 ppm and ¹³C = 39.52 ppm for DMSO-*d*₆ and ¹H = 7.26 ppm and ¹³C = 77.16 ppm for CDCl₃-*d*₁. Assignments were deduced from two-dimensional NMR experiments such as ¹H, ¹H-correlation spectroscopy (COSY), ¹H, ¹³C-heteronuclear multiple bond correlation (HMBC), and ¹H, ¹³C-heteronuclear single quantum coherence (HSQC) as appropriate as well as from the expected chemical shifts based on the chemical structure. ¹³C signals marked with (*) could only be detected in HSQC and HMBC spectra. Atoms were numbered as indicated for the respective structure and abbreviated as follows: ar = aromatic, biot = biotin, flu = fluorescein, pin = pinacol, PEG = polyethylene glycol, *t*-butyl = *tert*-butyl and triazole = 1*H*-1,2,3-triazole.

Numbering for triazoles, thiazoles and oxazoles followed the scheme below.



6.2.4 Mass Spectrometry

Low-resolution mass spectra (LRMS) were recorded on an Advion expression CMS using an atmospheric solids analysis probe (ASAP®) and atmospheric pressure chemical ionization (APCI) at a temperature of 250 °C. High-resolution mass spectra (HRMS) were recorded on a Thermo Scientific Exactive mass spectrometer using APCI with ammonia gas and electrospray ionization (ESI) with nitrogen as auxiliary gas as ion sources at a capillary temperature of 250 °C. Positive or negative mode were used as indicated.

GC-MS analyses were performed on a 6890N Network GC system equipped with a 5973 Network Mass Selective Detector (both Agilent Technologies) a DB-5ms column (length = 30 m, diameter = 0.25 mm, film = 0.25 µm; Agilent Technologies) and helium with a flow rate of 1 ml/min as carrier gas. Injection was performed as split injection of 1 µL with a split ratio of 47.5:1 at an injector temperature of 250 °C. Column oven temperature was as follows: 0–3 min: 60 °C; 3–14 min: linear increase to 280 °C; 14–19 min: 280 °C and ion source temperature was 230 °C.

For all compounds containing chlorine or bromine the expected isotopic pattern was observed. For reasons of clarity, only the mass of the lowest m/z peak is given.

6.2.5 Analytical High-performance Liquid Chromatography

HPLC analysis to determine the purity of all final compounds was performed on an Agilent Technologies 1260 Infinity system using UV detection at 210 nm. All columns were protected with a suitable guard cartridge from Phenomenex. The following from Phenomenex columns were used, as indicated in brackets for the respective retention time: Kinetex® 5u XB-C18 100 Å 250 x 4.6 mm, Synergi® 4u Hydro-RP 80 Å, 250 x 4.6 mm and Synergi® 4u Polar-RP 80 Å, 250 x 4.6 mm column was used. Eluent A was water containing 0.05% TFA and eluent B was acetonitrile containing 0.05% TFA. Linear gradient conditions were as follows: 0–4 min: A/B

(90:10); 4–29 min: linear increase to 100% of B; 29–31 min: 100% B; 31–40 min: A/B (90:10) at a flow-rate of 1 ml/min.

6.2.6 General Procedures

General procedure A for the deprotection of methylated compounds: Triazoles, thiazoles and oxazoles bearing one or two methoxy substituents were deprotected in the presence of boron tribromide (1 M solution in dry DCM, 3 or 6 eq., respectively), which was added dropwise to the solution of the compound in dry DCM at $-78\text{ }^{\circ}\text{C}$. After 1 h of stirring at that temperature, the mixture was allowed to slowly warm up to r.t. and stirred until completion. The reaction was quenched by the addition of water and extracted with DCM (3 times). The combined organic extracts were dried over Na_2SO_4 , filtered, and the solvent was evaporated *in vacuo*. Purification was performed via flash column chromatography affording the desired product.

General procedure B for the synthesis of oxazinones: Adapting a procedure published by Steinhauser *et al.*,²⁷⁶ the amide (1 eq.) and the carboxylic acid (1.2 eq.) were suspended in xylenes (mixture of isomers). Dry pyridine was added and the mixture was heated to reflux. Thionyl chloride (2.2 eq.) was added dropwise over 1.5 h. Stirring under reflux was continued until TLC indicated consumption of the amide. The mixture was cooled to r.t. and volatiles were evaporated *in vacuo*. The remaining solid was resuspended in ethanol and glacial acetic acid. The mixture was brought to reflux and cooled to $0\text{ }^{\circ}\text{C}$. The crystalline solid was collected by suction filtration, washed with cold ethanol, and dried *in vacuo* yielding the desired product.

General Procedure C for the synthesis of 1,2,4-triazole derivatives: Following the procedure adapted from Patil *et al.*,²⁷⁷ the oxazinone (1 eq.) and hydrazinebenzoic acid (1.1 eq.) were suspended in methanol. The mixture was stirred under reflux until TLC indicated consumption of the starting material. The reaction mixture was

cooled to 0 °C resulting in the precipitation of the product, which was collected by suction filtration and purified via recrystallization from methanol.

General Procedure D for the synthesis of 1,2,4-triazole derivatives: In a variation of the procedure reported by Steinhauser *et al.*,²⁷⁶ the hydrazine or hydrazine hydrochloride (1.2 eq.) was suspended in ethanol and brought to reflux. The oxazinone (1 eq.) was added and the mixture was stirred at reflux until TLC showed consumption of the starting material. After cooling to r.t., an aqueous solution of HCl (2 M) was added dropwise, resulting in the formation of a precipitate, which was collected via suction filtration, washed with an aqueous solution of HCl (0.5 M), and dried *in vacuo* yielding the desired product. For compounds where precipitation was not feasible, the reaction mixture was evaporated to dryness and the desired product was purified via flash column chromatography followed by semi-preparative HPLC or recrystallization from methanol or 2-propanol.

General procedure E for the copper(I)-catalyzed alkyne-azide cycloaddition (CuAAC): Following the procedure adapted from Swyter *et al.*,²⁴⁸ the azide (1 eq.), **94a** (1–1.15 eq.), and TBTA (0.1 eq.) were suspended in *tert*-butanol, degassed with N₂ and subjected to sonication for 10 min. CuSO₄ (0.1–1.1 eq.) and sodium ascorbate (0.2 eq.) were dissolved in water and added to the reaction mixture, which was stirred at r.t. for 18 h. The reaction was quenched by the addition of water (5 mL) and either extracted with EtOAc, dried over Na₂SO₄, filtered, and evaporated to dryness or evaporated to dryness without an extraction step. Purification was performed via preparative TLC, reversed-phase flash column chromatography or semi-preparative HPLC. For **96c**, DMF was added to the solvent mixture to increase the solubility of the starting material.

General procedure F for the synthesis of thiazole derivatives: Thiazoles were synthesized via Hantzsch thiazole synthesis following the methodology published by Moreno *et al.*²⁶³ The α -brominated ketone* (1 eq.) and the thioamide (1.2–2 eq.) were dissolved in DMF and stirred at 65 °C until TLC showed consumption of the brominated ketone. Water was added and the mixture was extracted with EtOAc

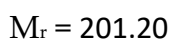
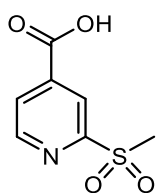
(3x20 mL). The combined organic extracts were washed with brine (3x20 mL), dried over Na₂SO₄, filtered, and evaporated to dryness. Purification was performed via flash column chromatography to afford the final compounds. *The proportions and reaction temperature were modified for compound 99d because of the susceptibility of the thioamide to decomposition.*

** In some cases, the α -brominated ketone contained some amount of non-brominated ketone from the previous step (as indicated in the respective protocol).*

General Procedure G for the synthesis of oxazole derivatives: Oxazoles were synthesized following the methodology published by Bailey *et al.*²⁶⁸ To a solution of the α -brominated ketone (1 eq.) and the carboxamide (1 eq.) in EtOAc AgSbF₆ (1.1 eq.) was added. The mixture was sonicated for 1 min and then heated to 50 °C–70 °C in a sealed tube in a microwave reactor until TLC showed consumption of the α -brominated ketone. After cooling to r.t., a saturated solution of NaHCO₃ was added and the product was extracted with EtOAc. The combined organic extracts were washed with brine, dried over Na₂SO₄, filtered, and evaporated to dryness. Purification was performed via flash column chromatography followed by recrystallization from 2-propanol or methanol.

6.2.7 Sulfones and Sulfoxides

2-(Methylsulfonyl)isonicotinic acid (**69a**)



To a suspension of 2-(methylthio)isonicotinic acid **70** in THF (1.5 mL) a solution of *meta*-chloroperoxybenzoic acid in THF (1.5 mL) was added. The reaction mixture was stirred at r.t. for 6 h and then quenched by the addition of a saturated solution of Na₂CO₃ (5 mL). THF was removed via evaporation *in vacuo*. The remaining solution was acidified with an aqueous solution of HCl (1 M), whereupon a white

precipitate was formed. The mixture was extracted with EtOAc (3x20 mL), dried over Na₂SO₄, filtered, and evaporated to dryness. Purification was performed via preparative TLC (DCM/methanol/acetic acid 95:5:0.1) yielding the desired product as a white solid.

Yield: 54 mg (87%)

R_f (DCM/Methanol/acetic acid 89.9:10:0.1) = 0.25

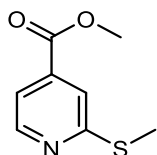
¹H-NMR (400 MHz, DMSO-*d*₆): δ (ppm) 14.24 (bs, 1H, COOH), 9.00 (dd, ³J = 4.8 Hz and ⁵J = 0.8 Hz, 1H, H₆), 8.34 (dd, ⁴J = 1.6 Hz and ⁵J = 0.8 Hz, 1H, H₃), 8.16 (dd, ³J = 4.9 Hz and ⁴J = 1.6 Hz, 1H, H₅), 3.34 (s, 3H, CH₃).

¹³C-NMR (101 MHz, DMSO-*d*₆): δ (ppm) 165.2 (COOH), 159.0 (C₂), 152.1 (C₆), 141.3 (C₄), 127.3 (C₅), 120.1 (C₃), 40.3 (CH₃).

HRMS (APCI positive): *m/z* 202.0168 [M+H]⁺, calcd for [C₇H₇NO₄S+H]⁺: *m/z* 202.0169

HPLC: *t_R* = 6.652 min (kinetex, 95.9%), *t_R* = 7.645 min (hydro-RP, 95.6%)

Methyl 2-(methylthio)isonicotinate (**71a**)



C₈H₉NO₂S

M_r = 183.23

To a suspension of 2-(methylthio)isonicotinic acid **70** (50 mg, 0.30 mmol, 1 eq.) in methanol (3 mL) concentrated sulphuric acid (200 μL, 3.6 mmol, 12 eq.) was added. The mixture was refluxed for 16 h. After cooling to r.t., the pH was adjusted to 8 by the addition of a saturated solution of NaHCO₃ and the mixture was extracted with EtOAc (3x15 mL). The combined organic extracts were dried over Na₂SO₄, filtered, and evaporated to dryness yielding the desired product as a brown oil, which was used in the next step without further purification.

Yield: 49 mg (88%)

R_f (CyHex/EtOAc 7:3) = 0.60

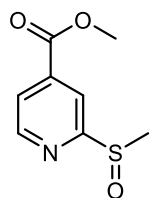
¹H-NMR (400 MHz, DMSO-*d*₆): δ (ppm) 8.63 (dd, ³*J* = 5.1 Hz and ⁵*J* = 0.9 Hz, 1H, H₆), 7.67 (dd, ⁴*J* = 1.5 Hz and ⁵*J* = 0.9 Hz, 1H, H₃), 7.52 (dd, ³*J* = 5.1 Hz and ⁴*J* = 1.5 Hz, 1H, H₅), 3.89 (s, 3H, OCH₃), 2.55 (s, 3H, SCH₃).

¹³C-NMR (101 MHz, DMSO-*d*₆): δ (ppm) 165.3 (*C*_{ester}), 161.4 (*C*₂), 150.9 (*C*₆), 137.6 (*C*₄), 120.1 (*C*₃), 118.4 (*C*₅), 53.3 (OCH₃), 13.3 (SCH₃).

MS (APCI positive): *m/z* 184.1 [M+H]⁺, calcd for [C₈H₉NO₂S+H]⁺: *m/z* 184.0

MS (APCI negative): *m/z* 168.0 [M-CH₃]⁻, calcd for [C₈H₉NO₂S-CH₃]⁻: *m/z* 168.0

Methyl 2-(methysulfinyl)isonicotinate (**74a**)



C₈H₉NO₃S

M_r = 199.22

In accordance to the published procedure by Khodaei et al.,²¹⁴ an aqueous solution of hydrogen peroxide (30%, 28 μ L, 0.21 mmol, 1.5 eq.) and trifluoromethanesulfonic anhydride (20 μ L, 0.14 mmol, 1 eq.) were added dropwise to a solution of **71a** (26 mg, 0.14 mmol, 1 eq.) in ethanol (1.4 mL) at 0 °C. The mixture was stirred for 16 h while slowly warming to r.t. Water was added and the mixture was extracted with DCM (3x15 mL). The combined organic extracts were washed with brine (15 mL), dried over Na₂SO₄ and evaporated to dryness yielding the desired product in sufficient purity as a white powder.

Yield: 24 mg (85%)

R_f (CyHex/EtOAc 8:2) = 0.60

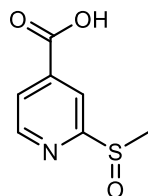
¹H-NMR (400 MHz, CDCl₃-*d*₁): δ (ppm) 8.78 (dd, ³*J* = 4.9 Hz and ⁵*J* = 0.8 Hz, 1H, H₆), 8.56 (dd, ⁴*J* = 1.6 Hz and ⁵*J* = 0.8 Hz, 1H, H₃), 7.95 (dd, ³*J* = 4.9 Hz and ⁴*J* = 1.6 Hz, 1H, H₅), 3.99 (s, 3H, OCH₃), 2.88 (s, 3H, SCH₃).

¹³C-NMR (101 MHz, CDCl₃-*d*₁): δ (ppm) 167.4 (*C*₂), 164.5 (*C*_{ester}), 150.4 (*C*₆), 139.7 (*C*₄), 123.9 (*C*₅), 118.7 (*C*₃), 53.0 (OCH₃), 41.3 (SCH₃).

MS (APCI positive): *m/z* 200.0 [M+H]⁺, calcd for [C₈H₉NO₃S+H]⁺: *m/z* 200.0

MS (APCI negative): m/z 184.1 $[M-CH_3]^-$, calcd for $[C_8H_9NO_3S-CH_3]^-$: m/z 184.0

2-(Methylsulfinyl)isonicotinic acid (**68a**)



$C_7H_7NO_3S$

$M_r = 185.20$

To a solution of **71** (22 mg, 0.11 mmol, 1 eq.) in THF (1 mL) an aqueous solution of LiOH (1 M, 550 μ L, 0.55 mmol, 5 eq.) was added at 0 °C. The mixture was stirred for 5 h while slowly warming to r.t., neutralized with an aqueous solution of HCl (0.5 M), and extracted with DCM (3x15 mL). The combined organic extracts were dried over Na_2SO_4 , filtered, and evaporated to dryness yielding the desired product as a pale-brown powder.

Yield: 20 mg (98%)

R_f (DCM/methanol/acetic acid 89.9:10:0.1) = 0.21

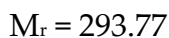
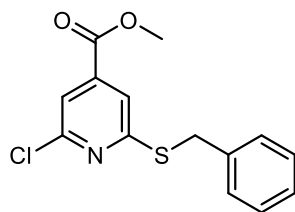
1H -NMR (400 MHz, DMSO- d_6): δ (ppm) 14.08 (s, 1H, OH), 8.89 (dd, $^3J = 4.9$ Hz and $^5J = 0.8$ Hz, 1H, H6), 8.28 (dd, $^4J = 1.6$ Hz and $^5J = 0.8$ Hz, 1H, H3), 7.96 (dd, $^3J = 4.9$ Hz and $^4J = 1.6$ Hz, 1H, H5), 2.84 (s, 3H, CH_3).

^{13}C -NMR (101 MHz, DMSO- d_6): δ (ppm) 167.8 (COOH), 165.8 (C2), 151.4 (C6), 141.0 (C4), 124.4 (C5), 118.2 (C3), 41.4 (CH_3).

HRMS (ESI positive): m/z 208.0040 (100%, $[M+Na]^+$), 186.0220 (50%, $[M+H]^+$), calcd for $[C_7H_7NO_3S+H]^+$: m/z 186.0219

HRMS (ESI negative): m/z 184.0077 $[M-H]^-$, calcd for $[C_7H_7NO_3S-H]^-$: m/z 184.0074

HPLC: $t_R = 6.111$ min (kinetex, 99.2%), $t_R = 8.076$ min (polar-RP, 96.9%)

Methyl 2-(benzylthio)-6-chloroisonicotinate (**71b**)

Following the reported procedure by Dally *et al.*,²¹⁶ phenylmethanethiol (47 μL , 0.49 mmol, 1 eq.) was added dropwise to a suspension of NaH (21 mg, 0.53 mmol, 1.1 eq.) in dry DMF (1.0 mL) at $-15\text{ }^{\circ}\text{C}$, followed by the dropwise addition of methyl 2,6-dichloroisonicotinate **72** (100 mg, 0.49 mmol, 1 eq.). The mixture was stirred for 16 h while slowly warming to r.t. The reaction mixture was quenched by the addition of water and extracted with diethyl ether (3x20 mL). The combined organic extracts were washed with brine (3x20 mL), dried over NaSO_4 , filtered, and evaporated to dryness. Purification was performed via flash column chromatography (CyHex/EtOAc 100:0–98:2) yielding the desired product as a pale-brown solid.

Yield: 89 mg (62%)

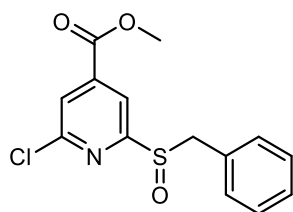
R_f (CyHex/EtOAc 8:2) = 0.70

¹H-NMR (400 MHz, CDCl_3 -*d*₁): δ (ppm) 7.62 (d, $^4J = 1.1\text{ Hz}$, 1H, H3), 7.52 (d, $^4J = 1.1\text{ Hz}$, 1H, H5), 7.45–7.40 (m, 2H, H2', H6'), 7.34–7.27 (m, 2H, H3', H5'), 7.28–7.20 (m, 1H, H4'), 4.43 (s, 2H, CH_2), 3.93 (s, 3H, CH_3).

¹³C-NMR (101 MHz, CDCl_3 -*d*₁): δ (ppm) 164.2 (C2), 161.0 (*C_{ester}*), 151.6 (C6), 139.8 (C4), 137.0 (C1'), 129.1 (2C, C3', C5'), 128.5 (2C, C2', C6'), 127.3 (C4'), 119.9 (C3 or C5), 118.8 (C3 or C5), 52.9 (CH_2), 34.8 (CH_3).

MS (APCI positive): m/z 293.9 $[\text{M}+\text{H}]^+$, calcd for $[\text{C}_{14}\text{H}_{12}^{35}\text{ClNO}_2\text{S}+\text{H}]^+$: m/z 294.0

MS (APCI negative): m/z 202.0 $[\text{M}-\text{tolyl}]^-$, calcd for $[\text{C}_{14}\text{H}_{12}^{35}\text{ClNO}_2\text{S}-\text{C}_7\text{H}_7]^-$: m/z 202.0

Methyl 2-(benzylsulfinyl)-6-chloroisonicotinate (**74a**)C₁₄H₁₂ClNO₃SM_r = 309.76

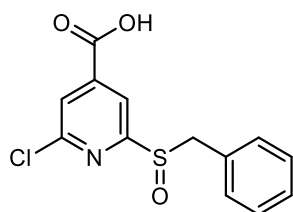
To a solution of **71b** (120 mg, 0.41 mmol, 1 eq.) in dry DCM (2 ml) *meta*-chloroperoxybenzoic acid (97 mg, 0.41 mmol, 1 eq.) was added at 0 °C. The mixture was stirred for 8 h while slowly warming to r.t. The reaction mixture was diluted with DCM (10 ml), washed with brine (3x10 ml), dried over Na₂SO₄, filtered and evaporated to dryness. Purification was performed via flash column chromatography (CyHex/EtOAc 95:5–50:50) followed by a second flash column chromatography run (DCM/methanol 95:5) yielding the desired product as a colourless oil.

Yield: 55 mg (43%)**R_f** (CyHex/EtOAc 7:3) = 0.15

¹H-NMR (400 MHz, CDCl₃-d₁): δ (ppm) 8.07 (d, ⁴J = 1.3 Hz, 1H, H₃), 7.91 (d, ⁴J = 1.3 Hz, 1H, H₅), 7.30–7.24 (m, 3H, H_{3'}, H_{4'}, H_{5'}), 7.09–7.05 (m, 2H, H_{2'}, H_{6'}), 4.40 (d, ²J = 13.2 Hz, 1H, H_{CH₂}), 4.11 (d, ²J = 13.2 Hz, 1H, H'_{CH₂}), 3.94 (s, 3H, CH₃).

¹³C-NMR (101 MHz, CDCl₃-d₁): δ (ppm) 166.1 (C₂), 163.3 (C_{ester}), 152.0 (C₆), 141.6 (C₄), 130.2 (2C, C_{2'}, C_{6'}), 128.7 (C_{1'}), 128.5 (2C, C_{3'}, C_{5'}), 128.4 (C_{4'}), 124.9 (C₃), 118.7 (C₅), 60.0 (CH₂), 53.2. (CH₃).

MS (APCI positive): *m/z* 309.8 [M+H]⁺, calcd for [C₁₄H₁₂³⁵ClNO₃S+H]⁺: *m/z* 310.0

2-(Benzylthio)-6-chloroisonicotinic acid (**68b**)C₁₃H₁₀ClNO₃SM_r = 295.74

6 Experimental

To a solution of **74b** (21 mg, 0.07 mmol, 1 eq.) in methanol (1 mL) an aqueous solution of LiOH (1 M, 1 mL, 1 mmol, 15 eq.) was added. The mixture was stirred for 4 h, then neutralized with an aqueous solution of HCl (1 M) and extracted with EtOAc (3x15 mL). The combined organic extracts were dried over Na₂SO₄, filtered, and evaporated to dryness yielding the desired product as a pale-brown powder.

Yield: 17 mg (85%)

R_f (DCM/methanol 9:1) = 0.15

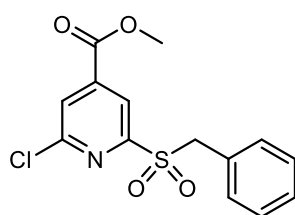
¹H-NMR (400 MHz, DMSO-*d*₆): δ (ppm) 12.11 (s, 1H, COOH), 7.95 (d, ⁴J = 1.3 Hz, 1H, H₃), 7.82 (d, ⁴J = 1.2 Hz, 1H, H₅), 7.31–7.21 (m, 3H, H_{3'}, H_{4'}, H_{5'}), 7.08–6.98 (m, 2H, H_{2'}, H_{6'}), 4.48 (d, ²J = 13.1 Hz, 1H, H_{CH₂}), 4.16 (d, ²J = 13.1 Hz, 1H, H'_{CH₂}).

¹³C-NMR (101 MHz, DMSO-*d*₆): δ (ppm) 166.2 (C₂), 164.5 (COOH), 151.4 (C₆), 130.8 (2C, C_{2'}, C_{6'}), 129.8 (C_{1'}), 128.6 (2C, C_{3'}, C_{5'}), 128.5 (C_{4'}), 125.2 (C₃), 118.8 (C₅), 59.5 (CH₂). The signal for C₄ is not visible in the spectrum.

HRMS (ESI negative): *m/z* 293.9997 [M-H]⁻, calcd for [C₁₃H₁₀³⁵ClNO₃S-H]⁻: *m/z* 293.9997

HPLC: *t_R* = 17.758 min (kinetex, 95.8%), *t_R* = 18.328 min (polar-RP, 95.6%)

Methyl 2-(benzylsulfonyl)-6-chloroisonicotinate (**75**)



C₁₄H₁₂ClNO₄S

M_r = 325.76

A solution of **71b** (13 mg, 0.04 mmol, 1 eq.) in EtOH (2 mL) was cooled to 0 °C. Hydrogen peroxide (30% aqueous solution, 11 μ L, 0.11 mmol, 2.5 eq) and trifluoromethanesulfonic anhydride (12 μ L, 0.09 mmol, 2 eq.) were added dropwise. The mixture was stirred for 16 h while slowly warming to r.t. The solvent was evaporated *in vacuo*. Purification was performed via flash column chromatography (CyHex/EtOAc 95:5–70:30) yielding the desired product as a white powder.

Yield: 7 mg (49%)

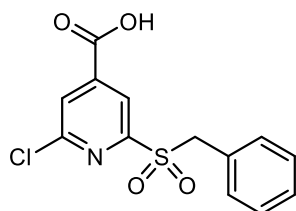
R_f (CyHex/EtOAc 7:3) = 0.24

$^1\text{H-NMR}$ (400 MHz, $\text{CDCl}_3\text{-}d_1$): δ (ppm) 8.26 (d, $^4J = 1.2$ Hz, 1H, H3), 8.07 (d, $^4J = 1.2$ Hz, 1H, H5), 7.33–7.22 (m, 5H, H_{phenyl}), 4.70 (s, 2H, CH_2), 3.96 (s, 3H, CH_3).

$^{13}\text{C-NMR}$ (101 MHz, $\text{CDCl}_3\text{-}d_1$): δ (ppm) 162.7 (C_{ester}), 157.5 (C_2), 152.8 (C_6), 142.0 (C_4), 131.1 (C_2 , C_2' , C_6'), 129.0 (C_1'), 128.8 (C_2 , C_3' , C_5'), 128.1 (C_4'), 126.6 (C_5), 120.6 (C_3), 58.0 (CH_2), 53.4 (CH_3).

MS (APCI positive): m/z 325.8 $[\text{M}+\text{H}]^+$, calcd for $[\text{C}_{14}\text{H}_{12}^{35}\text{ClNO}_4\text{S}+\text{H}]^+$: m/z 326.0

2-(Benzylsulfonyl)-6-chloroisonicotinic acid (**68b**)



$\text{C}_{13}\text{H}_{10}\text{ClNO}_4\text{S}$

$M_r = 311.74$

To a solution of **75** (7 mg, 0.02 mmol, 1 eq.) in methanol (0.5 mL) an aqueous solution of LiOH (1 M, 0.3 mL, 0.3 mmol, 15 eq.) was added. The mixture was stirred for 18 h, then neutralized with an aqueous solution of HCl (1 M) and extracted with EtOAc (3x15 mL). The combined organic extracts were dried over Na_2SO_4 , filtered, and evaporated to dryness. Purification was performed via flash column chromatography (DCM/methanol 99.5:0.5-98:2) yielding the desired product as a colourless semi-solid. *Compound purity was below 95%, but no further purification attempts were undertaken due to the low compound activity against KDM4A.*

Yield: 5 mg (75%)

R_f (DCM/methanol) = 0.10

$^1\text{H-NMR}$ (400 MHz, $\text{DMSO-}d_6$): δ (ppm) 12.00 (s, 1H, COOH), 8.13 (d, $^4J = 1.1$ Hz, 1H, H3), 8.08 (d, $^4J = 1.1$ Hz, 1H, H5), 7.36–7.30 (m, 3H, H_3' , H_4' , H_5'), 7.27–7.21 (m, 2H, H_2' , H_6'), 4.85 (s, 2H, CH_2).

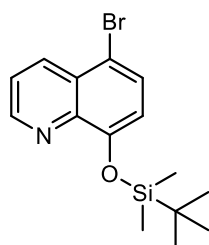
^{13}C -NMR (101 MHz, DMSO- d_6): δ (ppm) 163.8 (COOH), 156.9 (C2), 151.9 (C6), 131.7 (2C, C2', C6'), 129.0 (C1'), 128.9 (2C, C3', C5'), 128.5 (C4'), 127.8 (C5), 121.5 (C3), 58.1 (CH₂). The signal for C4 is not visible in the spectrum.

HRMS (ESI negative): m/z 309.9946 [M-H]⁻, calcd for [C₁₃H₁₀³⁵ClNO₄S-H]⁻: m/z 309.9946

HPLC: t_R = 18.333 min (kinetex, 90.4%), t_R = 18.114 min (polar-RP, 91.5%)

6.2.8 Boronic acids

5-Bromo-8-((tert-butyldimethylsilyl)oxy)quinoline (**78**)



C₁₅H₂₀BrNOSi

M_r = 338.32

Following the procedure published by Anderson *et al.*,²¹⁹ 5-Bromquinolin-8-ol **77** (500 mg, 2.23 mmol, 1 eq.), imidazole (228 mg, 3.35 mmol, 1.5 eq.) and *tert*-butyldimethyl chlorosilane **76** (1009 mg, 6.69 mmol, 3 eq.) were dissolved in anhydrous DCM (4 mL). The reaction mixture was stirred for 16 h at r.t., then diluted with DCM (20 mL), and washed with an aqueous solution of HCl (1 M, 20 mL) and water (20 mL). The organic extract was dried over Na₂SO₄, filtered, and concentrated *in vacuo* to afford a brown oil. Purification was performed via flash column chromatography (CyHex/EtOAc 99:1–95.5:4.5) yielding the desired product as a pink-coloured oil.

Yield: 596 mg (79%)

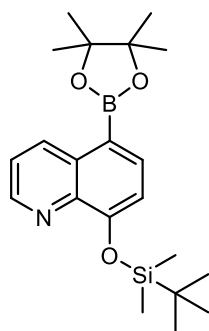
R_f (CyHex/EtOAc 8:2) = 0.80

^1H -NMR (400 MHz, CDCl₃- d_1): δ (ppm) 8.88 (dd, 3J = 4.1 Hz and 4J = 1.6 Hz, 1H, H2), 8.47 (dd, 3J = 8.6 Hz and 4J = 1.6 Hz, 1H, H4), 7.68 (d, 3J = 8.2 Hz, 1H, H6), 7.49 (dd, 3J = 8.6 Hz and 3J = 4.1 Hz, 1H, H3), 7.07 (d, 3J = 8.2 Hz, 1H, H7), 1.06 (s, 9H, (CH₃)_{*t*}-butyl), 0.26 (s, 6H, Si-CH₃).

^{13}C -NMR (101 MHz, CDCl_3 - d_1): δ (ppm) 152.76 (C8), 148.94 (C2), 142.67 (C8a), 135.40 (C4a), 130.41 (C4), 128.42 (C6), 122.25 (C3), 118.30 (C7), 112.27 (C5), 25.85 (3C, $(\text{CH}_3)_{t\text{-butyl}}$), 18.81 ($\text{Si}-\underline{\text{C}}-\text{C}_3$), -4.02 (2C, $\text{Si}-\text{CH}_3$).

GC-MS (EI positive): m/z 280 $[\text{M}-\text{C}_4\text{H}_9]^+$, calcd for $[\text{C}_{15}\text{H}_{20}^{79}\text{BrNOSi}-\text{C}_4\text{H}_9]^+$: m/z 280

8-((*Tert*-butyldimethylsilyl)oxy)-5-(4,4,5,5-tetramethyl-1,3,2-dioxaborolan-2-yl)quinoline (**79**)



$\text{C}_{21}\text{H}_{32}\text{BNO}_3\text{Si}$

$M_r = 385.39$

Following the procedure published by Babudri *et al.*,²⁷⁸ **78** (596 mg, 1.76 mmol, 1 eq.), pinacolborane (383 μL , 2.64 mmol, 1.5 eq.), Et_3N (733 μL , 5.28 mmol, 3 eq.) and $\text{Pd}(\text{dppf})\text{Cl}_2 \cdot \text{DCM}$ (43 mg, 0.05 mmol, 0.03 eq.) were dissolved in dry 1,4-dioxane (6 mL). The solution was stirred for 18 h at 80 $^\circ\text{C}$. After cooling to r.t., the mixture was poured into ice-water (5 mL) and extracted with cyclohexane (3x10 mL). The combined organic extracts were dried over Na_2SO_4 , filtered, and concentrated *in vacuo*. Purification was performed via flash column chromatography (CyHex/EtOAc 98:2–97:3) yielding the desired product as a brown oil.

Yield: 336 mg (49%)

R_f (CyHex/EtOAc 8:2) = 0.71

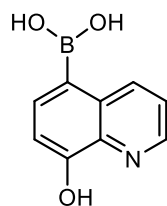
^1H -NMR (400 MHz, $\text{DMSO}-d_6$): δ (ppm) 9.00 (dd, $^3J = 8.6$ Hz and $^4J = 1.7$ Hz, 1H, H4), 8.88 (dd, $^3J = 4.1$ Hz and $^4J = 1.7$ Hz, 1H, H2), 7.96 (d, $^3J = 7.7$ Hz, 1H, H6), 7.59 (dd, $^3J = 8.6$ Hz and $^3J = 4.1$ Hz, 1H, H3), 7.21 (d, $^3J = 7.7$ Hz, 1H, H7), 1.36 (s, 12H, $(\text{CH}_3)_{pin}$), 1.02 (s, 9H, $(\text{CH}_3)_{t\text{-butyl}}$), 0.23 (s, 6H, $\text{Si}-\text{CH}_3$).

6 Experimental

¹³C-NMR (101 MHz, DMSO-*d*₆): δ (ppm) 155.7 (C8), 148.7 (C2), 141.5 (C8a), 137.7 (C4), 136.3 (2C, C4a, C6), 133.5 (C5), 122.5 (C3), 117.4 (C7), 83.9 (2C, O-C_{pin}), 26.2 (3C, (CH₃)_{*t*-butyl}), 25.1 (4C, (CH₃)_{*pin*}), 19.0 (Si-C-C₃), -3.4 (2C, Si-CH₃).

GC-MS (EI positive) m/z 328 [M-C₄H₉]⁺, calcd for [C₂₁H₃₂BNO₃Si-C₄H₉]⁺: m/z 328

(8-Hydroxyquinolin-5-yl)boronic acid (**80**)



C₉H₈BNO₃

M_r = 188.98

To a solution of **79** (12 mg, 0.04 mmol, 1 eq.) in acetone (0.5 mL) a solution of sodium periodate (28 mg, 0.13 mmol, 3 eq.) and ammonium acetate (9 mg, 0.11 mmol, 2.5 eq.) in water (0.5 mL) was added. The mixture was stirred for 8 h at r.t. and then evaporated to dryness. The brown residue was taken up in EtOAc, washed with brine (3x20 mL), dried over Na₂SO₄, filtered, and evaporated to dryness. Purification was performed via semi-preparative HPLC (water/ACN + 0.05% TFA, 0–4 min: 90:10, 4–20 min: 90:10–50:50) yielding a brown powder. *Compound purity was below 95%, but no further purification attempts were undertaken due to the low compound activity against KDM4A.*

Yield: 7 mg (84%)

R_f (reversed-phase; water/ACN 1:1) = 0.45

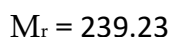
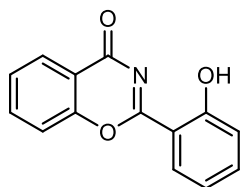
¹H-NMR (400 MHz, DMSO-*d*₆): δ (ppm) 9.05 (dd, ³J = 4.7 Hz and ⁴J = 1.8 Hz, 1H, H2), 8.38 (dd, ³J = 7.9 Hz and ⁴J = 1.8 Hz, 1H, H4), 8.18 (s, 1H, C-OH), 7.88 (dd, ³J = 7.9 Hz and ⁴J = 4.7 Hz, 1H, H3), 7.09 (d, ³J = 7.7 Hz, 1H, H6 or H7), 7.06 (d, ³J = 7.7 Hz, 1H, H6 or H7), 6.55 (s, 2H, B-OH). *Only compound signals are listed, the spectrum additionally shows unidentified impurities. No evaluable ¹³C spectrum could be obtained.*

MS (APCI positive): m/z 190.2 [M+H]⁺, calcd for [C₉H₈BNO₃+H]⁺: m/z 190.1

HPLC: t_R = 21.505 min (kinetex, 92.8%)

6.2.9 Triazoles

6.2.9.1 Precursors

2-(2-Hydroxyphenyl)-4*H*-benzo[e][1,3]oxazin-4-one (**88a**)

According to general procedure B, the title compound was synthesized using salicylamide **87a** (1.00 g, 7.29 mmol, 1 eq.), salicylic acid **86a** (1.21 g, 8.75 mmol, 1.2 eq.), dry pyridine (145 μL , 1.82 mmol, 0.3 eq.), thionyl chloride (1163 μL , 16.04 mmol, 2.2 eq.) and xylenes (1.5 mL). The reaction was complete after 2 h. Purification was performed using ethanol (4.4 mL) and glacial acetic acid (83 μL) yielding the desired product as a pale-yellow powder.

Yield: 980 mg (57%)

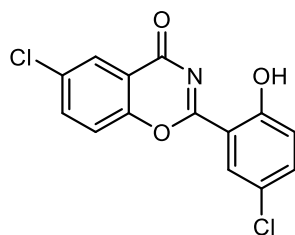
R_f (DCM/methanol 9:1) = 0.70

¹H-NMR (400 MHz, DMSO-*d*₆): δ (ppm) 12.95 (s, 1H, OH'), 8.21 (ddd, ³*J* = 7.7 Hz, ⁴*J* = 1.8 Hz and ⁵*J* = 0.8 Hz, 1H, H6'), 8.07 (dd, ³*J* = 7.9 Hz and ⁴*J* = 1.6 Hz, 1H, H5), 7.95 (ddd, ³*J* = 8.4 Hz, ³*J* = 7.3 Hz and ⁴*J* = 1.6 Hz, 1H, H7), 7.80 (dd, ³*J* = 8.4 Hz and ⁴*J* = 0.6 Hz, 1H, H8), 7.71–7.54 (m, 2H, H4', H6), 7.14–7.05 (m, 2H, H3', H5').

¹³C-NMR (101 MHz, DMSO-*d*₆): δ (ppm) 165.3 (C2), 163.9 (C4), 162.3 (C2'), 154.4 (C8a), 137.2 (C4'), 136.5 (C7), 129.5 (C6), 127.6 (C6'), 127.2 (C5), 120.0 (C5'), 118.4 (C3'), 118.3 (C4a), 117.9 (C8), 111.9 (C1').

MS (APCI positive): *m/z* 240.2 [M+H]⁺, calcd for [C₁₄H₉NO₃+H]⁺: *m/z* 240.1

MS (APCI negative): *m/z* 237.9 [M-H]⁻, calcd for [C₁₄H₉NO₃-H]⁻: *m/z* 238.1

6-Chloro-2-(5-chloro-2-hydroxyphenyl)-4*H*-benzo[e][1,3]oxazin-4-one (**88b**)C₁₄H₇Cl₂NO₃M_r = 308.11

According to general procedure B, the title compound was synthesized using 5-chlorosalicylamide **87b** (1.12 g, 6.07 mmol, 1 eq.), 5-chlorosalicylic acid **86b** (1.39 g, 8.04 mmol, 1.2 eq.), dry pyridine (414 μ L, 5.13 mmol, 0.9 eq.), thionyl chloride (1070 μ L, 14.75 mmol, 2.2 eq.) and xylenes (10.0 mL). The reaction was complete after 6 h. Purification was performed using ethanol (5.8 mL) and glacial acetic acid (70 μ L) yielding the desired product as a pale-yellow powder.

Yield: 1209 mg (59%)

R_f (CyHex/EtOAc 7:3) = 0.62

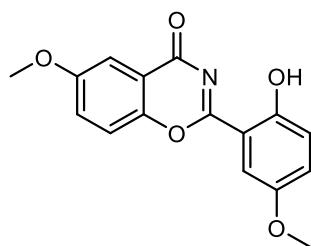
¹H-NMR (400 MHz, DMSO-*d*₆): δ (ppm) 12.53 (bs, 1H, OH'), 8.19 (dd, ⁴*J* = 2.6 Hz and ⁵*J* = 0.4 Hz, 1H, H5), 8.05 (dd, ⁴*J* = 2.7 Hz and ⁵*J* = 0.4 Hz, 1H, H6'), 7.78 (dd, ³*J* = 8.9 Hz and ⁴*J* = 2.6 Hz, 1H, H7), 7.53 (dd, ³*J* = 8.9 Hz and ⁵*J* = 0.4 Hz, 1H, H8), 7.50 (dd, ³*J* = 8.9 Hz and ⁴*J* = 2.7 Hz, 1H, H4'), 7.06 (dd, ³*J* = 8.9 Hz and ⁵*J* = 0.4 Hz, 1H, H3').

¹³C-NMR (101 MHz, DMSO-*d*₆): δ (ppm) 164.0 (C2), 162.4 (C4), 161.6 (C2'), 152.2 (C8a), 136.9 (C4'), 136.0 (C7), 133.2 (C4a), 127.5 (C6'), 127.4 (C5), 124.4 (C5'), 120.5 (C3'), 119.0 (C6), 118.6 (C8), 111.6 (C1').

MS (APCI positive): *m/z* 308.2 [M+H]⁺, calcd for [C₁₄H₇³⁵Cl₂NO₃+H]⁺: *m/z* 308.0

MS (APCI negative): *m/z* 306.2 [M-H]⁻, calcd for [C₁₄H₇³⁵Cl₂NO₃-H]⁻: *m/z* 306.0

2-(2-Hydroxy-5-methoxyphenyl)-6-methoxy-4*H*-benzo[e][1,3]oxazin-4-one
(**88c**)



$C_{16}H_{13}NO_5$

$M_r = 299.28$

According to general procedure B, the title compound was synthesized using 5-methoxysalicylamide **87c** (929 mg, 5.53 mmol, 1.2 eq.), 5-methoxysalicylic acid **86c** (770 mg, 4.61 mmol, 1 eq.), dry pyridine (56 μ L, 0.69 mmol, 0.15 eq.), thionyl chloride (735 μ L, 10.13 mmol, 2.2 eq.) and xylenes (2.9 mL). The reaction was complete after 3 h. Purification was modified as follows: after evaporation of the solvent, the crude was refluxed in ethanol (7.0 mL) and glacial acetic acid (500 μ L), cooled to r.t. and a pale-brown powder was filtered off. The filtrate was evaporated to dryness and purified via recrystallization from ethanol yielding the desired product as a pale-yellow powder.

Yield: 627 mg (45%)

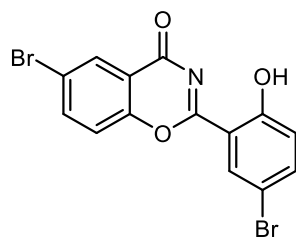
R_f (CyHex/EtOAc 7:3) = 0.27

1H -NMR (400 MHz, DMSO- d_6): δ (ppm) 12.55 (s, 1H, OH'), 7.84 (d, $^3J = 9.2$ Hz, 1H, H8), 7.64 (d, $^4J = 3.1$ Hz, 1H, H6'), 7.54 (dd, $^3J = 9.1$ Hz and $^4J = 3.2$ Hz, 1H, H7), 7.45 (d, $^4J = 3.1$ Hz, 1H, H5), 7.29 (dd, $^3J = 9.1$ Hz and $^4J = 3.2$ Hz, 1H, H4'), 7.04 (d, $^3J = 9.1$ Hz, 1H, H3'), 3.90 (s, 3H, CH₃), 3.84 (s, 3H, CH₃).

^{13}C -NMR (101 MHz, DMSO- d_6): δ (ppm) 164.7 (C2), 164.0 (C4), 158.1 (CO), 156.7 (CO), 152.4 (CO), 148.8 (C8a), 125.1 (C_{ar}), 124.8 (C_{ar}), 119.8 (C_{ar}), 119.5 (C_{ar}), 118.9 (C4a), 111.5 (C1'), 111.3 (C_{ar}), 107.6 (C_{ar}), 56.4 (CH₃), 56.2 (CH₃).

MS (ESI positive): m/z 300.1 [M+H]⁺, calcd for [C₁₆H₁₃NO₅+H]⁺: m/z 300.1

MS (ESI negative): m/z 298.0 [M-H]⁻, calcd for [C₁₆H₁₃NO₅-H]⁻: m/z 298.1

6-Bromo-2-(5-bromo-2-hydroxyphenyl)-4*H*-benzo[e][1,3]oxazin-4-one (**88d**)C₁₄H₇Br₂NO₃M_r = 397.02

According to general procedure B, the title compound was synthesized using 5-bromosalicylamide **87d** (2.00 g, 9.26 mmol, 1 eq.), 5-bromosalicylic acid **86d** (2.41 g, 1.11 mmol, 1.2 eq.), dry pyridine (1611 μ L, 20.37 mmol, 2.2 eq.), thionyl chloride (1477 μ L, 20.37 mmol, 2.2 eq.) and xylenes (20.0 mL). The reaction was complete after 5 h. Purification was performed using ethanol (14.0 mL) and glacial acetic acid (1.0 mL) yielding the desired product as a pale-yellow powder.

Yield: 1976 mg (54%)

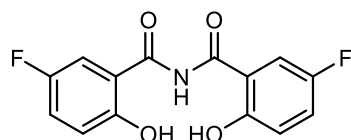
R_f (DCM/methanol 9:1) = 0.77

¹H-NMR (400 MHz, DMSO-*d*₆): δ (ppm) 12.85 (s, 1H, OH'), 8.37 (d, ⁴*J* = 2.5 Hz, 1H, H6'), 8.17–8.11 (m, 2H, H5, H7), 7.94–7.88 (m, 1H, H8), 7.80 (dd, ³*J* = 8.9 Hz and ⁴*J* = 2.6 Hz, 1H, H4'), 7.09 (d, ³*J* = 8.9 Hz, 1H, H3').

¹³C-NMR (101 MHz, DMSO-*d*₆): δ (ppm) 164.3 (C2), 162.8 (C4), 161.2 (C2'), 153.5 (C8a), 139.6 (C4'), 139.1 (C7), 131.4 (C4a), 129.1 (C6'), 120.9 (C3' or C5), 120.8 (C3' or C5), 119.9 (C6 or C8), 119.7 (C6 or C8), 113.8 (C5'), 111.0 (C1').

MS (ESI positive): *m/z* 395.9 [M+H]⁺, calcd for [C₁₄H₇⁷⁹Br₂NO₃+H]⁺: *m/z* 395.9

MS (ESI negative): *m/z* 393.9 [M-H]⁻, calcd for [C₁₄H₇⁷⁹Br₂NO₃-H]⁻: *m/z* 393.9

5-Fluoro-*N*-(5-fluoro-2-hydroxybenzoyl)-2-hydroxybenzamide (**88e**)C₁₄H₉F₂NO₄M_r = 293.23

In a variation of the procedure reported by Steinhäuser *et al.*,²⁷⁶ 5-fluorosalicylamide **87e** (594 mg, 3.83 mmol, 1.0 eq.) and 5-fluorosalicylic acid **86e** (658 mg, 4.21 mmol, 1.1 eq.) were suspended in xylenes (6.5 mL, mixture of isomers). Dry pyridine

(31 μ L, 0.38 mmol, 0.1 eq.) was added and the mixture was brought to reflux. Thionyl chloride (583 μ L, 8.04 mmol, 2.1 eq.) was added dropwise over 2 h under vigorous stirring. The mixture was refluxed for an additional hour and cooled to r.t., then volatiles were removed *in vacuo*. The remaining dark red residue was resuspended in methanol (4.0 mL) and glacial acetic acid (30 μ L). The mixture was brought to reflux. The insoluble solid material was collected by suction filtration, washed with hot methanol, and dried *in vacuo* yielding the desired product as a light brown powder.

Yield: 400 mg (32%)

R_f (CyHex/EtOAc/acetic acid 7:3:0.01) = 0.62

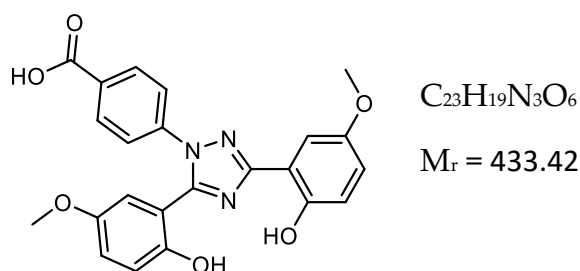
$^1\text{H-NMR}$ (400 MHz, DMSO- d_6): δ (ppm) 12.08 (br s, 1H, NH), 11.30 (br s, 2H, OH, OH'), 7.56 (dd, 3J = 9.5 Hz and 4J = 3.3 Hz, 2H, H6, H6'), 7.34 (ddd, 3J = 9.0 Hz, 3J = 7.8 Hz and 4J = 3.3 Hz, 2H, H4, H4'), 7.03 (dd, 3J = 9.0 Hz and 4J = 4.5 Hz, 2H, H3, H3').

$^{13}\text{C-NMR}$ (101 MHz, DMSO- d_6): δ (ppm) 163.5 (d, 4J = 2.4 Hz, 2C, CO, C'O), 155.7 (d, 1J = 235.7 Hz, 2C, C5, C5'), 153.3 (d, 4J = 1.6 Hz, 2C, C2, C2'), 121.6 (d, 2J = 23.4 Hz, 2C, C4, C4'), 120.4 (d, 3J = 6.6 Hz, 2C, C1, C1'), 119.0 (d, 3J = 7.5 Hz, 2C, C3, C3'), 116.5 (d, 2J = 24.4 Hz, 2C, C6, C6').

$^{19}\text{F-NMR}$ (376 MHz, DMSO- d_6): δ (ppm) -124.25–124.39 (m, 2F).

HRMS (ESI positive): m/z 316.0388 (100%, $[\text{M}+\text{Na}]^+$), 294.0570 (12%, $[\text{M}+\text{H}]^+$), calcd for $[\text{C}_{14}\text{H}_9\text{F}_2\text{NO}_4+\text{H}]^+$: m/z 294.0572

4-(3,5-Bis(2-hydroxy-5-methoxyphenyl)-1*H*-1,2,4-triazol-1-yl)benzoic acid (**90c**)



6 Experimental

According to general procedure C, the title compound was synthesized using **88c** (600 mg, 2.01 mmol, 1 eq.) and 4-hydrazinobenzoic acid **89a** (336 mg, 2.21 mmol, 1.1 eq.) in methanol (7.2 mL). The reaction was complete after 5 h. Recrystallization from methanol yielded the desired product as a pale-yellow powder.

Yield: 83 mg (10%)

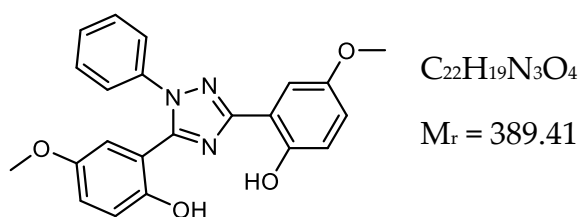
R_f (CyHex/EtOAc 7:3) = 0.51

¹H-NMR (400 MHz, DMSO-*d*₆): δ (ppm) 10.35 (s, 1H, OH'), 9.54 (s, 1H, OH), 8.03–7.98 (m, 2H, H3'', H5''), 7.61–7.56 (m, 2H, H2'', H6''), 7.55–7.52 (m, 1H, H6), 7.13 (d, ⁴*J* = 3.1 Hz, 1H, H6'), 7.03–6.97 (m, 3H, H3, H4, H4'), 6.79 (d, ³*J* = 9.0 Hz, 1H, H3'), 3.78 (s, 3H, CH₃), 3.73 (s, 3H, CH₃').

¹³C-NMR (101 MHz, DMSO-*d*₆): δ (ppm) 166.9 (COOH), 160.2 (C_c), 152.7 (C5), 152.4 (C5'), 152.4 (C_c), 150.8 (C2), 149.4 (C2'), 141.5 (C4''), 131.0 (C1''), 130.7 (2C, C3'', C5''), 123.8 (2C, C2'', C6''), 119.1 (C4'), 118.9 (C4), 118.5 (C3), 117.5 (C3'), 115.6 (C6'), 114.9 (C1'), 113.9 (C1), 110.2 (C6), 56.0 (CH₃'), 55.9 (CH₃).

MS (APCI negative): *m/z* 388.3 [M-CO₂H]⁻, calcd for [C₂₃H₁₉N₃O₆-CO₂H]⁻: *m/z* 388.1

2,2'-(1-Phenyl-1*H*-1,2,4-triazole-3,5-diyl)bis(4-methoxyphenol) (**90h**)



According to general procedure D, the title compound was synthesized using **88c** (285 mg, 4.61 mmol, 1 eq.) and phenylhydrazine hydrochloride **89b** (44 mg, 0.30 mmol, 1.2 eq.) in ethanol (8.3 mL). The reaction was complete after 3 h. Recrystallization from 2-propanol yielded the desired product as an ochre powder.

Yield: 33 mg (9%)

R_f (CyHex/EtOAc 1:1) = 0.63

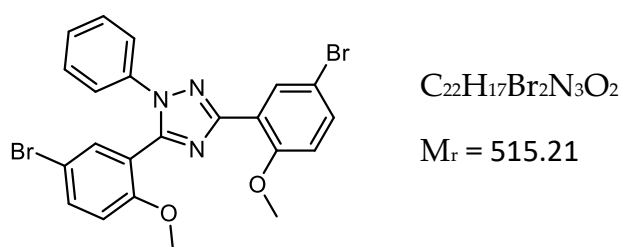
¹H-NMR (400 MHz, DMSO-*d*₆): δ (ppm) 9.45 (bs, 2H, OH), 7.52 (dd, $^4J = 2.5$ Hz and $^5J = 0.4$ Hz, 1H, H₆), 7.49–7.41 (m, 5H, H_{phenyl}), 7.04 (d, $^4J = 3.1$ Hz, 1H, H_{6'}), 7.01–6.94 (m, 3H, H₃, H₄, H_{4'}), 6.82 (d, $^3J = 8.9$ Hz, 1H, H_{3'}), 3.77 (s, 3H, CH₃), 3.68 (s, 3H, CH₃).

¹³C-NMR (101 MHz, DMSO-*d*₆): δ (ppm) 159.7 (C_c), 152.6 (CO), 152.2 (CO), 152.0 (C_c), 150.8 (CO), 149.7 (CO), 138.1 (C1''), 129.6 (2C, C3'', C5'', 129.2 (C4''), 124.3 (2C, C2'', C6''), 118.8 (C1 or C1'), 118.7 (C1 or C1'), 118.4 (C3, C4, C3' or C4'), 117.4 (C3, C4, C3' or C4'), 115.6 (C3, C4, C3' or C4'), 114.9 (C3, C4, C3' or C4'), 114.0 (C6'), 110.2 (C6), 55.9 (CH₃), 55.9 (CH₃).

MS (APCI positive): m/z 390.0 [M+H]⁺, calcd for [C₂₂H₁₉N₃O₄+H]⁺: m/z 390.1

MS (APCI negative): m/z 388.0 [M-H]⁻, calcd for [C₂₂H₁₉N₃O₄-H]⁻: m/z 388.1

3,5-Bis(5-bromo-2-methoxyphenyl)-1-phenyl-1*H*-1,2,4-triazole (**91**)



To a stirred solution of **90f** (730 mg, 1.50 mmol, 1 eq.) in dry acetone (13.7 mL), potassium carbonate (414 mg, 3.00 mmol, 2 eq.) and methyl iodide (187 μ L, 2.00 mmol, 2 eq.) were added. The mixture was stirred at 55 °C in a sealed vessel for 16 h. The reaction was cooled to r.t., quenched by the addition of water (5 mL), and the solvent was evaporated *in vacuo*. The residue was taken up in ethyl acetate (25 mL), washed with water and brine (15 mL each), dried over Na₂SO₄, and evaporated to dryness. Purification was performed via flash column chromatography (CyHex/EtOAc 95:5–50:50) yielding the desired product as a pale-yellow crystalline powder.

Yield: 237 mg (31%)

R_f (CyHex/EtOAc 7:3) = 0.29

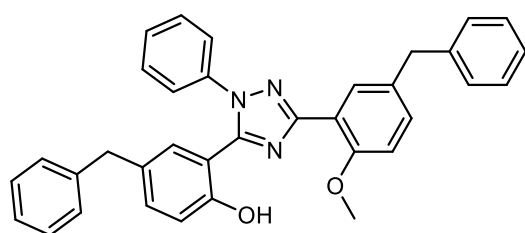
¹H-NMR (400 MHz, DMSO-*d*₆): δ (ppm) 8.01 (d, 4J = 2.7 Hz, 1H, H₆), 7.80 (d, 4J = 2.5 Hz, 1H, H_{6'}), 7.69 (dd, 3J = 8.9 Hz and 4J = 2.5 Hz, 1H, H_{4'}), 7.64 (dd, 3J = 8.9 Hz and 4J = 2.7 Hz, 1H, H₄), 7.49–7.40 (m, 3H, H_{2''}, H_{4''}, H_{6''}), 7.39–7.31 (m, 2H, H_{3''}, H_{5''}), 7.18 (d, 3J = 9.0 Hz, 1H, H₃), 7.01 (d, 3J = 9.0 Hz, 1H, H_{3'}), 3.86 (s, 3H, CH₃), 3.30 (s, 3H, CH₃).

¹³C-NMR (101 MHz, DMSO): δ (ppm) 158.7 (C_c), 156.9 (C₂), 156.0 (C_{2'}), 150.7 (C_e), 138.5 (C_{1''}), 135.1 (C_{4'}), 133.9 (C₄), 133.5 (C_{6'}), 132.8 (C₆), 129.5 (2C, C_{3''}, C_{5''}), 128.9 (C_{4''}), 123.9 (2C, C_{2''}, C_{6''}), 121.9 (C₅), 119.8 (C_{5'}), 115.2 (C_{1'}), 114.6 (C₁), 112.3 (C₃), 112.0 (C_{3'}), 56.5 (CH₃), 55.8 (CH₃).

MS (APCI positive): m/z 514.0 [M+H]⁺, calcd for [C₂₂H₁₇⁷⁹Br₂N₃O₂+H]⁺: m/z 514.0

MS (APCI negative): m/z 498.1 [M-CH₃]⁻, calcd for [C₂₂H₁₇⁷⁹Br₂N₃O₂-CH₃]⁻: m/z 498.0

4-Benzyl-2-(3-(5-benzyl-2-methoxyphenyl)-1-phenyl-1*H*-1,2,4-triazol-5-yl)phenol (**93**)



C₃₅H₂₉N₃O₂

M_r = 523.64

(*t*BuP)₃Pd₂I₂ **92** was prepared as described by Aufiero *et al.*²⁷⁹ by dissolving tri-*tert*-butylphosphine (255 mg, 1.26 mmol, 2 eq.) and tris(dibenzylideneacetone)-dipalladium(0) (288 mg, 0.32 mmol, 0.5 eq.) in dry THF (7.7 mL), stirring at r.t. for 2 h, addition of palladium(II) iodide (227 mg, 0.63 mmol, 1 eq) and 2 h of further stirring. Dry acetone (100 mL) was added and the resulting mixture was left to crystallize at -20 °C overnight. The Pd(I)-I-dimer **92** was collected by suction filtration as dark purple crystals and washed with acetone (25 mL). **Yield:** 379 mg (69.0%).

Following the procedure published by Kalvet *et al.*,²⁴⁴ **91** (50 mg, 0.10 mmol, 1 eq.) was dissolved in toluene (1.5 mL). (*t*BuP)₃Pd₂I₂ **92** (2 mg, 2.4 μ mol, 2.5%) and benzylmagnesium chloride (1.4 M solution in THF, 208 μ L, 0.30 mmol) were added

to the solution. The reaction was stirred for 15 min, quenched by the addition of a saturated solution of NH_4Cl , and filtered over a short pad of celite. After separation of the layers, the organic layer was evaporated to dryness. Purification was performed via flash column chromatography (CyHex/EtOAc 90:10–50:50) yielding the desired product as a white powder.

Yield: 21 mg (40%)

R_f (CyHex/EtOAc 7:3) = 0.66

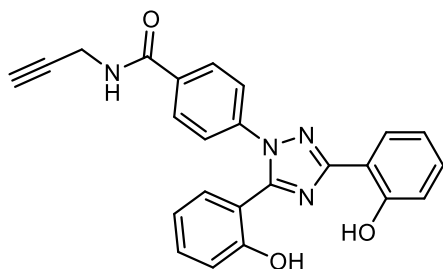
^1H -NMR (400 MHz, $\text{DMSO}-d_6$): δ (ppm) 10.23 (s, 1H, OH'), 7.67 (d, $^4J = 2.4$ Hz, 1H, H₆), 7.46–7.37 (m, 5H, H_{N-phenyl}), 7.34–7.23 (m, 7H, H_{ar}), 7.20–7.15 (m, 3H, H_{ar}), 7.15–7.10 (m, 4H, H_{ar}), 6.80 (d, $^3J = 8.3$ Hz, 1H, H_{3'}), 3.95 (s, 2H, CH₂), 3.81 (s, 3H, CH₃), 3.80 (s, 2H, CH₂').

^{13}C -NMR (101 MHz, $\text{DMSO}-d_6$): δ (ppm) 159.2 (C_c), 156.1 (C₂), 154.4 (C_{2'}), 152.1 (C_c), 142.0 (C₇), 141.8 (C_{7'}), 138.7 (C_{1''}), 133.6 (C_{4'}), 132.5 (C₅), 132.4 (C₄), 132.1 (C_{5'}), 131.0 (C_{6'}), 129.6 (2C, C_{3''}, C_{5''}), 129.1 (C_{4''}), 129.0 (2C, C₈, C₁₂), 128.9 (2C, C₉, C₁₁), 128.8 (2C, C_{8'}, C_{12'}), 128.8 (2C, C_{9'}, C_{11'}), 128.8 (C₆), 126.3 (2C, C₁₀, C_{10'}), 124.4 (2C, C_{2''}, C_{6''}), 116.7 (C_{3'}), 114.9 (C_{1'}), 114.8 (C₁), 112.9 (C₃), 56.2 (CH₃). The signals for CH₂ and CH₂' are overlaid by the solvent signal.

MS (APCI positive): m/z 523.7 $[\text{M}+\text{H}]^+$, calcd for $[\text{C}_{35}\text{H}_{29}\text{N}_3\text{O}_2+\text{H}]^+$: m/z 524.2

MS (APCI negative): m/z 522.8 $[\text{M}-\text{H}]^-$, calcd for $[\text{C}_{35}\text{H}_{29}\text{N}_3\text{O}_2-\text{H}]^-$: m/z 522.2

4-(3,5-Bis(2-hydroxyphenyl)-1H-1,2,4-triazol-1-yl)-N-(prop-2-yn-1-yl)benzamide (**94a**)



$\text{C}_{24}\text{H}_{18}\text{N}_4\text{O}_3$

$M_r = 410.43$

In accordance to the published procedure by Kaufmann *et. al.*,²⁴⁷ a solution of **54b** (2.00 g, 5.36 mmol, 1 eq.), EDCI (1.34 g, 6.96 mmol, 1.3 eq.), HOBT (1.07 g, 6.96 mmol,

6 Experimental

1.3 eq.) and *N*-methylmorpholine (1.7 mL, 13.40 mmol, 2.5 eq.) in dry DMF (10 mL) was stirred at 0 °C for 30 min. To this mixture, propargylamine (515 µL, 8.00 mmol, 1.5 eq.) was slowly added. After stirring for 5 h, the mixture was allowed to warm to r.t. and stirred at that temperature for further 16 h. After completion of the reaction, the solvent was evaporated *in vacuo*. The residue was taken up in EtOAc (50 mL), washed with a saturated solution of NaHCO₃ (50 mL) and a saturated solution of LiCl (3x20 mL), dried over Na₂SO₄, filtered, and evaporated to dryness. Purification was performed via flash column chromatography (CyHex/EtOAc 80:20–20:80) yielding the desired product as a light-brown powder.

Yield: 1.16 g (53%)

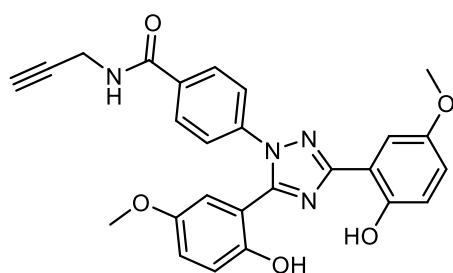
R_f (CyHex/EtOAc 1:1) = 0.57

¹H-NMR (400 MHz, DMSO-*d*₆): δ (ppm) 10.84 (s, 1H, OH), 10.05 (s, 1H, OH'), 9.05 (t, ³J = 5.5 Hz, 1H, NH), 8.06 (dd, ³J = 7.8 Hz and ⁴J = 1.7 Hz, 1H, H₆), 7.98–7.88 (m, 2H, H_{3''}, H_{5''}), 7.61–7.48 (m, 3H, H_{6'}, H_{2''}, H_{6''}), 7.45–7.34 (m, 2H, H₄, H_{4'}), 7.08–6.95 (m, 3H, H₃, H₅, H_{5'}), 6.87 (dd, ³J = 8.2 Hz and ⁴J = 1.0 Hz, 1H, H_{3'}), 4.07 (dd, ³J = 5.5 Hz and ⁴J = 2.5 Hz, 2H, CH₂), 3.15 (t, ⁴J = 2.5 Hz, 1H, CH).

¹³C-NMR (101 MHz, DMSO-*d*₆): δ (ppm) 165.3 (C_{amide}), 160.2 (C_e), 156.7 (C₂), 155.6 (C_{2'}), 152.4 (C_e), 140.5 (C_{1''}), 133.9 (C_{4'}), 132.9 (C₄), 131.8 (C_{6'}), 131.5 (C_{4''}), 128.7 (2C, C_{3''}, C_{5''}), 127.2 (C₆), 123.7 (2C, C_{2''}, C_{6''}), 120.1 (C₅), 119.8 (C_{5'}), 117.5 (C₃), 116.5 (C_{3'}), 114.8 (C_{1'}), 114.1 (C₁), 81.5 (C-CH), 73.4 (CH), 29.0 (CH₂).

HRMS (ESI negative): *m/z* 409.1307 [M-H]⁻, calcd for [C₂₄H₁₈N₄O₃-H]⁻: *m/z* 409.1306

4-(3,5-Bis(2-hydroxy-5-methoxyphenyl)-1*H*-1,2,4-triazol-1-yl)-*N*-(prop-2-yn-1-yl)benzamide (**94b**)



C₂₆H₂₂N₄O₅

M_r = 470.49

In accordance to the published procedure by Kaufmann *et. al.*,²⁴⁷ a solution of **90c** (480 mg, 1.11 mmol, 1 eq.), EDCI (276 mg, 1.44 mmol, 1.3 eq.), HOBt (220 mg, 1.44 mmol, 1.3 eq.) and *N*-methyilmorpholine (353 μ L, 2.77 mmol, 2.5 eq.) in dry DMF (5.1 mL) was stirred at 0 °C for 30 min. To this mixture, propargylamine (106 μ L, 1.66 mmol, 1.5 eq.) was slowly added at 0 °C. The mixture was allowed to warm to r.t. and was stirred at that temperature for further 16 h. After completion of the reaction, the solvent was evaporated *in vacuo*. Purification was performed via flash column chromatography (CyHex/EtOAc 75:25–40:60) yielding the desired product as an off-white powder.

Yield: 300 mg (58%)

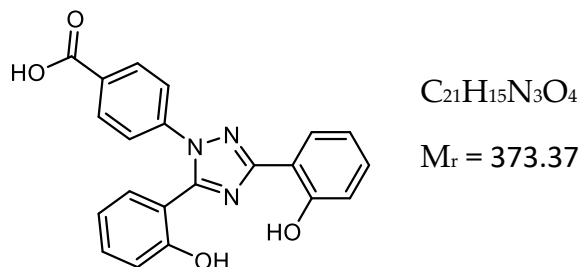
R_f (CyHex/EtOAc 1:1) = 0.34

¹H-NMR (400 MHz, DMSO-*d*₆): δ (ppm) 10.38 (s, 1H, OH), 9.54 (s, 1H, OH'), 9.05 (t, ³*J* = 5.6 Hz, 1H, NH), 7.99–7.86 (m, 2H, H3'', H5''), 7.61–7.55 (m, 2H, H2'', H6''), 7.54 (dd, ⁴*J* = 2.8 Hz and ⁵*J* = 0.8 Hz, 1H, H6), 7.12 (d, ⁴*J* = 3.2 Hz, 1H, H6'), 7.06–6.94 (m, 3H, H3, H4, H4'), 6.79 (d, ³*J* = 9.0 Hz, 1H, H3'), 4.07 (dd, ³*J* = 5.5 Hz and ⁴*J* = 2.5 Hz, 2H, CH₂), 3.78 (s, 3H, CH₃), 3.72 (s, 3H, CH₃'), 3.15 (t, ⁴*J* = 2.5 Hz, 1H, CH).

¹³C-NMR (101 MHz, DMSO-*d*₆): δ (ppm) 165.3 (*C*_{amide}), 160.1 (*C*_c), 152.6 (*C*₅), 152.4 (*C*_{5'}), 152.3 (*C*_c), 150.8 (*C*₂), 149.4 (*C*_{2'}), 140.4 (*C*_{4''}), 133.9 (*C*_{1''}), 128.7 (2*C*, *C*_{3''}, *C*_{5''}), 123.8 (2*C*, *C*_{2''}, *C*_{6''}), 119.0 (*C*_{4'}), 118.8 (*C*₄), 118.5 (*C*₃), 117.5 (*C*_{3'}), 115.6 (*C*_{6'}), 114.9 (*C*_{1'}), 114.0 (*C*₁), 110.2 (*C*₆), 81.5 (*C*-CH), 73.4 (CH), 56.0 (CH₃'), 55.9 (CH₃), 29.0 (CH₂).

HRMS (ESI positive): *m/z* 471.1665 [M+H]⁺, calcd for [C₂₆H₂₂N₄O₅+H]⁺: *m/z* 471.1663

6.2.9.2 Final compounds

4-(3,5-Bis(2-hydroxyphenyl)-1*H*-1,2,4-triazol-1-yl)benzoic acid (Deferasirox; **54**)

According to general procedure C, the title compound was synthesized using **88a** (2.00 g, 8.47 mmol, 1 eq.) and 4-hydrazinobenzoic acid (1.42 g, 9.31 mmol, 1.1 eq.) in methanol (30 mL). The reaction was complete after 2 h. Recrystallization from methanol yielded the desired product as pale-brown powder.

Yield: 1500 mg (47%)

R_f (CyHex/EtOAc/acetic acid 69.9:30:0.1) = 0.21

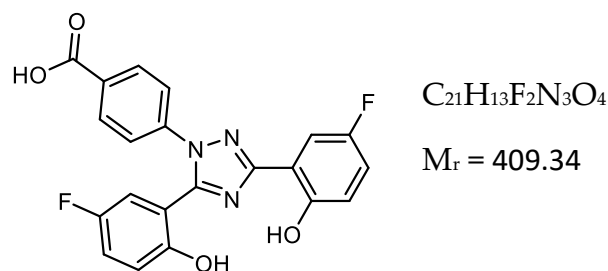
¹H-NMR (400 MHz, DMSO-*d*₆): δ (ppm) 13.19 (s, 1H, COOH), 10.81 (s, 1H, OH), 10.06 (s, 1H, OH'), 8.06 (dd, ³*J* = 7.8 Hz and ⁴*J* = 1.7 Hz, 1H, H6), 8.04–7.93 (m, 2H, H3'', H5''), 7.61–7.51 (m, 3H, H6', H2'', H6''), 7.45–7.33 (m, 2H, H4, H4'), 7.07–6.95 (m, 3H, H3, H5, H5'), 6.87 (dd, ³*J* = 8.4 Hz and ⁴*J* = 1.0 Hz, 1H, H3').

¹³C-NMR (101 MHz, DMSO-*d*₆): δ (ppm) 166.8 (COOH), 160.3 (C_c), 156.7 (C2), 155.6 (C2'), 152.4 (C_e), 141.6 (C1''), 133.0 (C4'), 131.9 (C4), 131.5 (C6'), 130.9 (C4''), 130.7 (2C, C3'', C5''), 127.2 (C6), 123.7 (2C, C2'', C6''), 120.1 (C5), 119.9 (C5'), 117.5 (C3), 116.5 (C3'), 114.8 (C1'), 114.0 (C1).

MS (APCI positive): *m/z* 374.2 [M+H]⁺, calcd for [C₂₁H₁₅N₃O₄+H]⁺: *m/z* 274.1

MS (APCI negative): *m/z* 372.2 [M-H]⁻, calcd for [C₂₁H₁₅N₃O₄-H]⁻: *m/z* 272.1

HPLC: *t_R* = 21.744 min (kinetex, 99.3%), *t_R* = 22.327 min (hydro-RP, 98.8%)

4-(3,5-Bis(5-fluoro-2-hydroxyphenyl)-1*H*-1,2,4-triazol-1-yl)benzoic acid (**90e**)

In a variation of the procedure reported by Patil *et al.*,²⁷⁷ **88e** (400 mg, 1.45 mmol, 1.0 eq.) and 4-hydrazinobenzoic acid (265 mg, 1.74 mmol, 1.2 eq.) were suspended in ethanol (5 mL). The mixture was refluxed for 8 h. Upon cooling to r.t., a light-brown solid material was formed. Precipitation was completed overnight in a refrigerator. The solid material was collected by suction filtration, washed with cold ethanol, and dried *in vacuo* yielding the desired product as a light-brown powder.

Yield: 75 mg (13%)

R_f (CyHex/EtOAc/acetic acid 1:1:0.01) = 0.20

¹H-NMR (400 MHz, DMSO-*d*₆): δ (ppm) 13.23 (bs, 1H, COOH), 10.51 (bs, 1H, OH), 10.05 (bs, 1H, OH'), 8.06–7.97 (m, 2H, H3'', H5''), 7.75 (dd, $^3J_{1-F} = 9.2$ Hz and $^4J_{1-4} = 3.2$ Hz, 1H, H6), 7.64–7.55 (m, 2H, H2'', H6''), 7.47 (dd, $^3J_{6'-F} = 8.7$ Hz and $^4J_{6'-4'} = 3.3$ Hz, 1H, H6'), 7.32–7.20 (m, 2H, H4, H4'), 7.07 (dd, $^3J_{3-4} = 9.1$ Hz and $^4J_{3-F} = 4.7$ Hz, 1H, H3), 6.85 (dd, $^3J_{3'-4'} = 9.1$ Hz and $^4J_{3'-F} = 4.6$ Hz, 1H, H3').

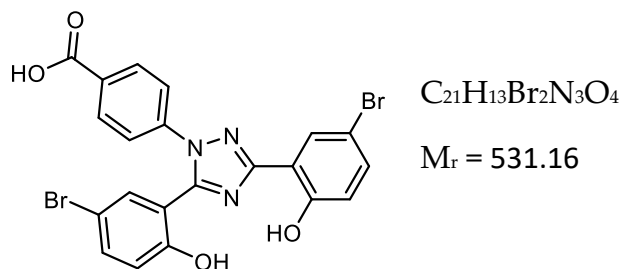
¹³C-NMR (101 MHz, DMSO-*d*₆): δ (ppm) 166.8 (COOH), 159.5 (d, $^4J = 2.6$ Hz, C_c), 155.8 (d, $^1J = 234.9$ Hz, C5), 155.4 (d, $^1J = 235.5$ Hz, C5'), 153.0 (d, $^4J = 1.6$ Hz, C2), 152.1 (d, $^4J = 1.4$ Hz, C2'), 151.6 (d, $^4J = 2.1$ Hz, C_e), 141.3 (C1''), 131.2 (C4''), 130.8 (2C, C3'', C5''), 123.9 (2C, C2'', C6''), 119.8 (d, $^2J = 22.7$ Hz, C4'), 119.0 (d, $^3J = 8.1$ Hz, C3), 118.8 (d, $^2J = 23.3$ Hz, C4), 117.8 (d, $^3J = 7.5$ Hz, C3'), 117.6 (d, $^2J = 17.5$ Hz, C6'), 115.3 (d, $^3J = 8.7$ Hz, C1'), 114.7 (d, $^3J = 8.3$ Hz, C1), 112.7 (d, $^2J = 24.7$ Hz, C6).

¹⁹F-NMR (376 MHz, DMSO-*d*₆): δ (ppm) -124.33–-124.41 (m, 1F), -124.86–-124.94 (m, 1F).

HRMS (ESI negative): m/z 408.0801 [M-H]⁻, calcd for [C₂₁H₁₃F₂N₃O₄-H]⁻: m/z 408.0801

HPLC: t_R = 22.551 min (kinetex, 99.8%), t_R = 23.025 min (polar-RP, 99.8%)

4-(3,5-Bis(5-bromo-2-hydroxyphenyl)-1*H*-1,2,4-triazol-1-yl)benzoic acid (90d)



According to general procedure C, the title compound was synthesized using **88d** (200 mg, 0.50 mmol, 1 eq.) and 4-hydrazinobenzoic acid (84 mg, 0.55 mmol, 1.1 eq.) in methanol (10.0 mL). The reaction was complete after 6 h. Recrystallization from methanol yielded the desired product as a pale-yellow powder.

Yield: 69 mg (26%)

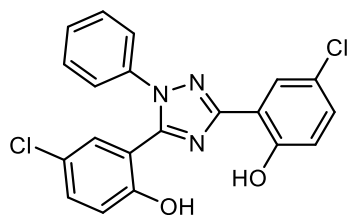
R_f (CyHex/EtOAc/acetic acid 7:3:0.01) = 0.12

1H -NMR (400 MHz, DMSO- d_6): δ (ppm) 13.20 (bs, 1H, COOH), 10.68 (bs, 1H, OH), 10.40 (bs, 1H, OH'), 8.12 (d, 4J = 2.6 Hz, 1H, H6), 8.04–8.00 (m, 2H, H3'', H5''), 7.79 (d, 4J = 2.6 Hz, 1H, H6'), 7.62–7.58 (m, 2H, H2'', H6''), 7.57 (dd, 3J = 8.8 Hz and 4J = 2.6 Hz, 1H, H4'), 7.54 (dd, 3J = 8.8 Hz and 4J = 2.6 Hz, 1H, H4), 7.04 (d, 3J = 8.8 Hz, 1H, H3), 6.82 (d, 3J = 8.8 Hz, 1H, H3').

^{13}C -NMR (101 MHz, DMSO- d_6): δ (ppm) 166.8 (COOH), 159.1 (C_e), 155.8 (C2), 155.0 (C2'), 151.3 (C_e), 141.4 (C1''), 135.6 (C4'), 134.3 (C4), 133.7 (C6'), 131.2 (C4''), 130.8 (2C, C3'', C5''), 129.4 (C6), 123.8 (2C, C2'', C6''), 120.0 (C3), 118.7 (C3'), 116.9 (C1'), 116.4 (C1), 111.1 (C5), 110.5 (C5').

HRMS (ESI negative): m/z 527.9203 [M-H] $^-$, calcd for [$C_{21}H_{13}^{79}Br_2N_3O_4$ -H] $^-$: m/z 527.9200

HPLC: t_R = 26.499 min (kinetex, 95.5%), t_R = 23.907 min (polar-RP, 95.5%)

2,2'-(1-Phenyl-1*H*-1,2,4-triazole-3,5-diyl)bis(4-chlorophenol) (**90b**) $C_{20}H_{13}Cl_2N_3O_2$ $M_r = 398.24$

According to general procedure D, the title compound was synthesized using **88b** (500 mg, 1.62 mmol, 1 eq.) and phenylhydrazine hydrochloride (282 mg, 1.95 mmol, 1.2 eq.) in ethanol (15.0 mL). The reaction was complete after 4 h. Recrystallization from methanol yielded the desired product as a white solid.

Yield: 114 mg (18%)

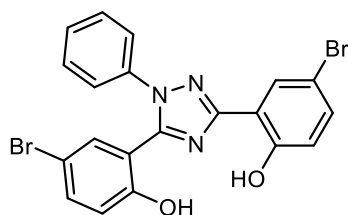
R_f (CyHex/EtOAc 7:3) = 0.32

1H -NMR (400 MHz, DMSO- d_6): δ 10.79 (s, 1H, OH), 10.41 (s, 1H, OH'), 7.99 (d, $^4J = 2.7$ Hz, 1H, H6), 7.61 (d, $^4J = 2.7$ Hz, 1H, H6'), 7.50–7.46 (m, 5H, H_{phenyl}), 7.42 (dd, $^3J = 8.8$ Hz and $^4J = 2.7$ Hz, 1H, H4'), 7.41 (dd, $^3J = 8.8$ Hz and $^4J = 2.7$ Hz, 1H, H4), 7.08 (d, $^3J = 8.8$ Hz, 1H, H3), 6.87 (d, $^3J = 8.8$ Hz, 1H, H3').

^{13}C -NMR (101 MHz, DMSO- d_6): δ (ppm) 158.9 (C_c), 155.4 (C_2), 154.8 (C_2'), 151.1 (C_e), 137.9 (C_1''), 132.5 (C_4'), 131.4 (C_4), 130.8 (C_6'), 129.7 (2C, C_3'' , C_5''), 129.3 (C_4''), 126.2 (C_6), 124.2 (2C, C_2'' , C_6''), 123.7 (C_5), 122.9 (C_5'), 119.5 (C_3), 118.2 (C_3'), 116.5 (C_1'), 115.8 (C_1).

HRMS (ESI positive): m/z 398.0461 $[M+H]^+$, calcd for $[C_{20}H_{13}^{35}Cl_2N_3O_2+H]^+$: m/z 398.0458

HPLC: $t_R = 28.555$ min (kinetex, 99.1%), $t_R = 28.816$ min (hydro-RP, 99.7%)

2,2'-(1-Phenyl-1*H*-1,2,4-triazole-3,5-diyl)bis(4-bromophenol) (**90f**) $C_{20}H_{13}Br_2N_3O_2$ $M_r = 487.15$

6 Experimental

According to general procedure D, the title compound was synthesized using **88d** (500 mg, 1.62 mmol, 1 eq.) and phenylhydrazine hydrochloride (44 mg, 0.30 mmol, 1.2 eq.) in ethanol (15.0 mL). The reaction was complete after 4 h. Recrystallization from methanol yielded the desired product as a white solid.

Yield: 41 mg (34%)

R_f (CyHex/EtOAc 7:3) = 0.54

¹H-NMR (400 MHz, DMSO-*d*₆): δ (ppm) 10.79 (s, 1H, OH), 10.42 (s, 1H, OH'), 8.12 (d, ⁴J = 2.5 Hz, 1H, H₆), 7.73 (d, ⁴J = 2.6 Hz, 1H, H_{6'}), 7.53 (dd, ³J = 8.8 Hz and ⁴J = 2.6 Hz, 1H, H_{4'}), 7.53 (dd, ³J = 8.8 Hz and ⁴J = 2.5 Hz, 1H, H₄), 7.54–7.44 (m, 5H, H_{phenyl}), 7.03 (d, ³J = 8.8 Hz, 1H, H₃), 6.82 (d, ³J = 8.8 Hz, 1H, H_{3'}).

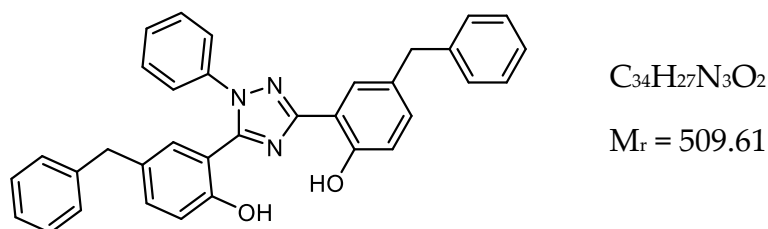
¹³C-NMR (101 MHz, DMSO): δ (ppm) 158.8 (C_e), 155.8 (C₂), 155.2 (C_{2'}), 151.0 (C_e), 137.9 (C_{1''}), 135.4 (C_{4'}), 134.2 (C₄), 133.6 (C_{6'}), 129.7 (2C, C_{3''}, C_{5''}), 129.3 (C_{4''}), 129.2 (C₆), 124.2 (2C, C_{2''}, C_{6''}), 119.9 (C₃), 118.6 (C_{3'}), 117.1 (C_{1'}), 116.4 (C₁), 111.1 (C₅), 110.3 (C_{5'}).

HRMS (ESI positive): *m/z* 485.9451 [M+H]⁺, calcd for [C₂₀H₁₃⁷⁹Br₂N₃O₂+H]⁺: *m/z* 485.9447

HRMS (ESI negative): *m/z* 483.9302 [M-H]⁻, calcd for [C₂₀H₁₃⁷⁹Br₂N₃O₂-H]⁻: *m/z* 483.9302

HPLC: *t_R* = 29.181 min (kinetex, 95.6%), *t_R* = 25.959 min (polar-RP, 95.4%)

2,2'-(1-Phenyl-1*H*-1,2,4-triazole-3,5-diyl)bis(4-benzylphenol) (**90n**)



According to general procedure A, **93** (12 mg, 0.02 mmol, 1 eq.) was solubilized in freshly distilled DCM (130 μ L). BBr₃ (1 M solution in dry DCM, 70 μ L, 0.07 mmol, 3 eq.) was added dropwise at -78 °C. Purification was performed via flash column chromatography (CyHex/EtOAc 95:5–80:20) followed by semi-preparative HPLC

(water/ACN + 0.05% TFA, 0–3 min: 10:90, 3–12 min: 10:90–0:100, 12–22 min: 0:100, 22–23 min: 0:100–10:90, 23–24 min: 10:90) yielding the product as a white powder.

Yield: 10 mg (86%)

R_f (CyHex/EtOAc 7:3) = 0.67

$^1\text{H-NMR}$ (400 MHz, DMSO- d_6): δ (ppm) 10.71 (s, 1H, OH), 9.93 (s, 1H, OH'), 7.88 (d, 4J = 2.3 Hz, 1H, H₆), 7.48–7.37 (m, 5H, H_{N-phenyl}), 7.32–7.12 (m, 13H, H₄, H_{4'}, H_{6'}, H_{phenyl}), 6.95 (d, 3J = 8.4 Hz, 1H, H₃), 6.80 (d, 3J = 8.4 Hz, 1H, H_{3'}), 3.95 (s, 2H, CH₂), 3.86 (s, 2H, CH_{2'}).

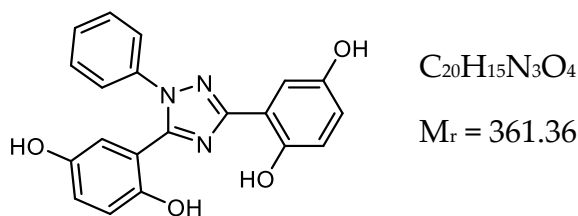
$^{13}\text{C-NMR}$ (101 MHz, DMSO- d_6): δ (ppm) 159.9 (C_e), 155.0 (C₂), 154.1 (C_{2'}), 152.1 (C_e), 142.1 (C₇), 141.8 (C_{7'}), 138.0 (C_{1''}), 133.0 (C_{4'}), 132.8 (C₅), 132.3 (C_{5'}), 132.2 (C₄), 131.3 (C_{6'}), 129.6 (2C, C_{3''}, C_{5''}), 129.1 (C_{4''}), 129.0 (2C, C₈, C₁₂), 128.9 (2C, C₉, C₁₁ or C_{9'}, C_{11'}), 128.8 (2C, C_{8'}, C_{12'}), 128.8 (2C, C₉, C₁₁ or C_{9'}, C_{11'}), 126.9 (C₆), 126.3 (2C, C₁₀, C_{10'}), 124.3 (2C, C_{2''}, C_{6''}), 117.5 (C₃), 116.6 (C_{3'}), 114.6 (C_{1'}), 114.0 (C₁), 40.5 (CH₂), 40.3 (CH_{2'}). The signals for CH₂ and CH_{2'} are overlaid by the solvent signal, but can be identified via the HSQC spectrum.

HRMS (ESI positive): m/z 510.2176 [M+H]⁺, calcd for [C₃₄H₂₇N₃O₂+H]⁺: m/z 510.2176

HRMS (ESI negative): m/z 508.2033 [M-H][−], calcd for [C₃₄H₂₇N₃O₂-H][−]: m/z 508.2031

HPLC: t_R = 31.350 min (kinetex, 96.4%), t_R = 27.790 min (polar-RP, 95.3%)

2,2'-(1-Phenyl-1H-1,2,4-triazole-3,5-diyl)bis(benzene-1,4-diol) (**90m**)



According to general procedure A, **90h** (20 mg, 0.05 mmol, 1 eq.) was solubilized in freshly distilled DCM (0.7 mL). BBr₃ (1 M solution in dry DCM, 308 μL , 0.31 mmol, 6 eq.) was added dropwise at -78°C . Purification was performed via flash column chromatography (DCM/methanol 99.5:0.5–90:10) yielding the desired product as a white powder.

Yield: 8 mg (43%)

R_f (CyHex/EtOAc 1:1) = 0.31

¹H-NMR (400 MHz, DMSO-*d*₆): δ (ppm) 10.29 (s, 1H, C2OH), 9.31 (s, 1H, C2'OH), 9.11 (bs, 1H, C5OH), 9.08 (bs, 1H, C5'OH), 7.52–7.39 (m, 6H, H₆, H_{phenyl}), 6.85 (dd, ³J = 8.8 Hz and ⁵J = 0.6 Hz, 1H, H₃), 6.83–6.76 (m, 3H, H₄, H_{4'}, H_{6'}), 6.69 (dd, ³J = 8.8 Hz and ⁵J = 0.4 Hz, 1H, H_{3'}).

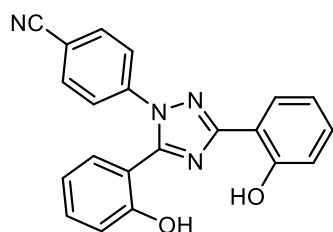
¹³C-NMR (101 MHz, DMSO-*d*₆): δ (ppm) 160.0 (C_c), 152.0 (C_e), 150.4 (COH), 150.1 (COH), 149.6 (COH), 148.3 (COH), 138.2 (C1''), 129.6 (2C, C3'', C5''), 128.9 (C4''), 124.0 (2C, C2'', C6''), 119.7 (C1 or C1'), 119.3 (C1 or C1'), 118.1 (C3, C4, C3' or C4'), 117.4 (C3, C4, C3' or C4'), 116.7 (C3, C4, C3' or C4'), 115.0 (C3, C4, C3' or C4'), 114.0 (C6'), 112.0 (C6).

HRMS (ESI positive): *m/z* 362.1133 [M+H]⁺, calcd for [C₂₀H₁₅N₃O₄+H]⁺: *m/z* 362.1135

HRMS (ESI negative): *m/z* 360.0991 [M-H]⁻, calcd for [C₂₀H₁₅N₃O₄-H]⁻: *m/z* 360.0990

HPLC: *t_R* = 17.900 min (kinetex, 99.1%), *t_R* = 18.466 min (hydro-RP, 99.3%)

4-(3,5-Bis(2-hydroxyphenyl)-1*H*-1,2,4-triazol-1-yl)benzonitrile (**90g**)



C₂₁H₁₄N₄O₂

M_r = 354.37

According to general procedure D, the title compound was synthesized using **88a** (250 mg, 1.05 mmol, 1 eq.) and 4-hydrazinylbenzonitrile (167 mg, 1.25 mmol, 1.2 eq.) in ethanol (4.5 mL). The reaction was complete after 3 h. After cooling to r.t., non-reacted 4-hydrazinylbenzonitrile was removed via filtration. The filtrate was evaporated to dryness and purified via flash column chromatography (DCM/methanol 99.5:0.5–96:4) followed by recrystallization from methanol yielding the desired product as a beige solid.

Yield: 59 mg (16%)

R_f (CyHex/EtOAc 7:3) = 0.21

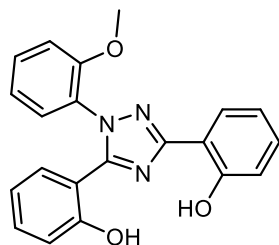
¹H-NMR (400 MHz, DMSO-*d*₆): δ (ppm) 10.71 (s, 1H, OH), 10.09 (s, 1H, OH'), 8.06 (dd, ³*J* = 7.8 Hz and ⁴*J* = 1.7 Hz, 1H, H₆), 8.06–7.91 (m, 2H, H_{3''}, H_{5''}), 7.67–7.63 (m, 2H, H_{2''}, H_{6''}), 7.60 (dd, ³*J* = 7.7 Hz and ⁴*J* = 1.8 Hz, 1H, H_{6'}), 7.42 (ddd, ³*J* = 8.3 Hz, ³*J* = 7.4 Hz and ⁴*J* = 1.8 Hz, 1H, H_{4'}), 7.39 (ddd, ³*J* = 8.4 Hz, ³*J* = 7.3 Hz and ⁴*J* = 1.7 Hz, 1H, H₄), 7.12–6.92 (m, 3H, H₃, H₅, H_{5'}), 6.88 (dd, ³*J* = 8.3 Hz and ⁴*J* = 1.0 Hz, 1H, H_{3'}).

¹³C-NMR (101 MHz, DMSO-*d*₆): δ (ppm) 160.5 (C_c), 156.7 (C₂), 155.4 (C_{2'}), 152.6 (C_c), 141.8 (C_{1''}), 133.9 (2C, C_{3''}, C_{5''}), 133.2 (C_{4'}), 132.0 (C₄), 131.6 (C_{6'}), 127.3 (C₆), 124.3 (2C, C_{2''}, C_{6''}), 120.1 (C₅), 120.0 (C_{5'}), 118.5 (CN), 117.5 (C₃), 116.6 (C_{3'}), 114.6 (C_{1'}), 114.0 (C₁), 111.4 (C_{4''}).

HRMS (ESI positive): *m/z* 355.1194 [M+H]⁺, calcd for [C₂₁H₁₄N₄O₂+H]⁺: *m/z* 355.1190

HPLC: *t_R* = 24.084 min (kinetex, 98.8%), *t_R* = 23.136 min (polar-RP, 99.2%)

2,2'-(1-(2-Methoxyphenyl)-1*H*-1,2,4-triazole-3,5-diyl)diphenol (**90i**)



C₂₁H₁₇N₃O₃

M_r = 359.39

According to general procedure D, the title compound was synthesized using 2-methoxyphenylhydrazine hydrochloride (438 mg, 2.51 mmol, 1.2 eq.) and **88a** (500 mg, 2.09 mmol, 1 eq.) in ethanol (18.0 mL). The reaction was complete after 5 h. Purification via flash column chromatography (DCM/methanol 99.9:0.1–97.5:2.5) followed by recrystallization from 2-propanol yielded the desired product as yellow needles.

Yield: 191 mg (25%)

R_f (DCM/methanol 98:2) = 0.80

¹H-NMR (400 MHz, DMSO-*d*₆): δ (ppm) 10.97 (s, 1H, OH), 10.21 (s, 1H, OH'), 8.02–7.98 (m, 1H, H₆), 7.55–7.43 (m, 2H, H_{4''}, H_{6''}), 7.36 (ddd, ³*J* = 8.4 Hz, ³*J* = 7.6 Hz and

$^4J = 1.4$ Hz, 1H, H4), 7.31–7.22 (m, 2H, H4', H6'), 7.15 (dd, $^3J = 8.5$ Hz and $^4J = 1.1$ Hz, 1H, H3''), 7.10–7.05 (m, 1H, H5''), 7.04–6.96 (m, 2H, H3, H5), 6.89–6.85 (m, 1H, H3'), 6.87–6.78 (m, 1H, H5'), 3.58 (s, 3H, CH₃).

^{13}C -NMR (101 MHz, DMSO-*d*₆): δ (ppm) 159.8 (C_c), 156.6 (C2), 156.1 (C2'), 154.1 (C2''), 153.8 (C_e), 132.3 (C4'), 131.8 (C4''), 131.6 (C4), 130.4 (C6'), 128.7 (C6''), 127.0 (C6), 126.6 (C1''), 121.0 (C5''), 120.0 (C5), 119.1 (C5'), 117.4 (C3), 116.5 (C3'), 114.4 (C1'), 114.3 (C1), 113.1 (C3), 56.0 (CH₃).

HRMS (ESI positive): m/z 360.1343 [M+H]⁺, calcd for [C₂₁H₁₇N₃O₃+H]⁺: m/z 360.1343

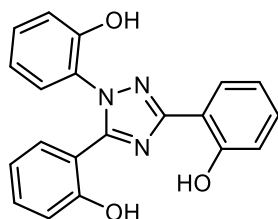
HRMS (ESI negative): m/z 358.1194 [M-H]⁻, calcd for [C₂₁H₁₇N₃O₃-H]⁻: m/z 358.1197

HPLC: $t_R = 26.121$ min (kinetex, 99.9%), $t_R = 26.587$ min (hydro-RP, 99.1%)

2,2',2''-(1*H*-1,2,4-Triazole-1,3,5-triyl)triphenol (**90i**)

C₂₀H₁₅N₃O₃

M_r = 345.36



According to general procedure A, **90i** (180 mg, 0.50 mmol, 1 eq.) was solubilized in freshly distilled DCM (2.8 mL). BBr₃ (1 M solution in dry DCM, 3.0 mL, 1.50 mmol, 3 eq.) was added dropwise at -78 °C. Purification was performed via flash column chromatography (DCM/methanol 99.5:0.5–90:10) yielding the desired product as a light-yellow powder.

Yield: 68 mg (39%)

R_f (CyHex/EtOAc 7:3) = 0.46

^1H -NMR (400 MHz, DMSO-*d*₆): δ (ppm) 10.95 (s, 1H, OH), 10.37 (bs, 1H, OH), 10.16 (bs, 1H, OH), 8.00 (ddd, $^3J = 7.8$ Hz, $^4J = 1.7$ Hz and $^5J = 0.4$ Hz, 1H, H6), 7.41 (dd, $^3J = 7.8$ Hz and $^4J = 1.7$ Hz, 1H, H6''), 7.39–7.23 (m, 4H, H4, H4', H4'', H6'), 7.05–6.87 (m, 5H, H3, H3', H3'', H5, H5''), 6.80 (ddd, $^3J = 7.7$ Hz, $^3J = 7.3$ Hz and $^4J = 1.1$ Hz, 1H, H5').

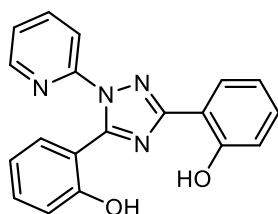
^{13}C -NMR (101 MHz, DMSO- d_6): δ (ppm) 159.5 (C_e), 156.6 (C_2), 156.3 (C_2'), 153.5 (C_e), 153.0 (C_2''), 132.3 (C_4'), 131.5 (C_4''), 131.5 (C_4), 130.2 (C_6'), 128.9 (C_6''), 127.1 (C_6), 125.4 (C_1''), 120.0 (C_5''), 119.5 (C_5), 119.1 (C_5'), 117.3 (C_3), 117.1 (C_3''), 116.7 (C_3'), 114.5 (C_1'), 114.3 (C_1).

HRMS (ESI positive): m/z 346.1184 $[\text{M}+\text{H}]^+$, calcd for $[\text{C}_{20}\text{H}_{15}\text{N}_3\text{O}_3+\text{H}]^+$: m/z 346.1186

HRMS (ESI negative): m/z $[\text{M}-\text{H}]^-$, calcd for $[\text{C}_{20}\text{H}_{15}\text{N}_3\text{O}_3-\text{H}]^-$: m/z 344.1041

HPLC: t_R = 23.729 min (kinetex, 97.6%), t_R = 22.701 min (polar-RP, 98.0%)

2,2'-(1-(Pyridin-2-yl)-1*H*-1,2,4-triazole-3,5-diyl)diphenol (**90j**)



$\text{C}_{19}\text{H}_{14}\text{N}_4\text{O}_2$

$M_r = 330.35$

According to general procedure D, the title compound was synthesized using **88a** (500 mg, 2.09 mmol, 1 eq.) and 2-hydrazinopyridine (363 mg, 2.51 mmol, 1.2 eq.) in ethanol (18.0 mL). The reaction was complete after 6 h. Purification via flash column chromatography (DCM/methanol 99.5:0.5–95:5) followed by semi-preparative HPLC ($\text{H}_2\text{O}/\text{ACN}$ 50:50 + 0.05% TFA) yielded the desired product as a white solid.

Isolated Yield: 7 mg (1%)

R_f (DCM/methanol 98:2) = 0.76

^1H -NMR (400 MHz, DMSO- d_6): δ (ppm) 10.85 (s, 1H, OH), 9.90 (s, 1H, OH'), 8.36 (ddd, $^3J = 4.9$ Hz, $^4J = 1.9$ Hz and $^5J = 1.0$ Hz, 1H, H_6''), 8.10–8.04 (m, 2H, H_6 , H_4''), 7.80 (dt, $^3J = 8.1$ Hz, $^4J = 1.0$ Hz and $^5J = 1.0$ Hz, 1H, H_3''), 7.57 (dd, $^3J = 7.5$ Hz and $^4J = 1.7$ Hz, 1H, H_6'), 7.48 (ddd, $^3J = 7.5$ Hz, $^3J = 4.9$ Hz and $^5J = 1.0$ Hz, 1H, H_5''), 7.42–7.32 (m, 2H, H_4 , H_4'), 7.06–6.99 (m, 2H, H_3 , H_5), 6.97 (td, $^3J = 7.5$ Hz, $^3J = 7.5$ Hz and $^4J = 1.0$ Hz, 1H, H_5'), 6.82 (dd, $^3J = 8.3$ Hz and $^4J = 1.0$ Hz, 1H, H_3').

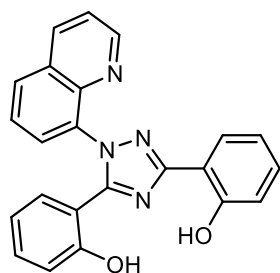
^{13}C -NMR (101 MHz, DMSO- d_6): δ (ppm) 160.0 (C_e), 156.8 (C_2), 155.4 (C_2'), 152.4 (C_e), 151.0 (C_2''), 148.6 (C_6''), 139.7 (C_4''), 132.4 (C_4'), 131.9 (C_4), 131.0 (C_6'), 127.2

(C6), 124.5 (C5''), 120.1 (C5), 119.5 (C5'), 118.2 (C3''), 117.5 (C3), 116.1 (C3'), 115.9 (C1'), 114.1 (C1).

HRMS (ESI positive): m/z 331.1190 $[M+H]^+$, calcd for $[C_{19}H_{14}N_4O_2+H]^+$: m/z 331.1190

HPLC: t_R = 22.230 min (kinetex, 95.3%), t_R = 22.025 min (hydro-RP, 96.4%)

2,2'-(1-(Quinolin-8-yl)-1*H*-1,2,4-triazole-3,5-diyl)diphenol (90k**)**



$C_{23}H_{16}N_4O_2$

$M_r = 380.41$

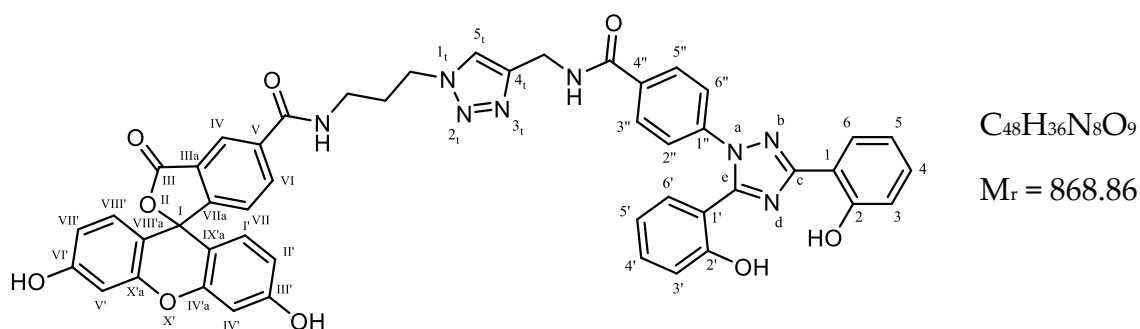
According to general procedure D, the title compound was synthesized using **88a** (250 mg, 1.05 mmol, 1 eq.) and 8-hydrazinoquinoline dihydrochloride hydrate (314 mg, 1.25 mmol, 1.2 eq.) in ethanol (9.2 mL). The reaction was complete after 16 h. Purification via flash column chromatography (CyHex/EtOAc 95:5–50:50) followed by recrystallization from 2-propanol yielded the desired product as a brown solid.

Yield: 42 mg (11%)

R_f (CyHex/EtOAc 7:3) = 0.40

1H -NMR (400 MHz, DMSO- d_6): δ (ppm) 10.99 (bs, 1H, OH), 10.21 (bs, 1H, OH'), 8.80 (dd, $^3J = 4.2$ Hz and $^4J = 1.7$ Hz, 1H, H2''), 8.48 (dd, $^3J = 8.4$ Hz and $^4J = 1.7$ Hz, 1H, H4''), 8.20 (dd, $^3J = 8.3$ Hz and $^4J = 1.4$ Hz, 1H, H5''), 8.08 (dd, $^3J = 7.4$ Hz and $^4J = 1.4$ Hz, 1H, H7''), 8.02 (dd, $^3J = 7.8$ Hz and $^4J = 1.7$ Hz, 1H, H6), 7.77 (dd, $^3J = 8.3$ Hz and $^4J = 7.4$ Hz, 1H, H6''), 7.58 (dd, $^3J = 8.3$ Hz and $^4J = 4.2$ Hz, 1H, H3''), 7.37 (ddd, $^3J = 8.3$ Hz, $^3J = 7.2$ Hz and $^4J = 1.7$ Hz, 1H, H4), 7.22 (dd, $^3J = 7.5$ Hz and $^4J = 1.8$ Hz, 1H, H6'), 7.15 (ddd, $^3J = 8.3$ Hz, $^3J = 7.5$ Hz and $^4J = 1.8$ Hz, 1H, H4'), 7.04 (dd, $^3J = 8.3$ Hz and $^4J = 1.1$ Hz, 1H, H3), 7.00 (ddd, $^3J = 7.8$ Hz, $^3J = 7.4$ Hz and $^4J = 1.1$ Hz, 1H, H5), 6.73 (dd, $^3J = 8.3$ Hz and $^4J = 1.1$ Hz, 1H, H3'), 6.67 (td, $^3J = 7.5$ Hz, $^3J = 7.5$ Hz and $^4J = 1.1$ Hz, 1H, H5').

N-(3-(4-((4-(3,5-Bis(2-hydroxyphenyl)-1*H*-1,2,4-triazol-1-yl)benzamido)methyl)-1*H*-1,2,3-triazol-1-yl)propyl)-3',6'-dihydroxy-3-oxo-3*H*-spiro[isobenzofuran-1,9'-xanthene]-5-carboxamide (**96a**)



The title compound was synthesized following general procedure E using **94a** (12.5 mg, 30 μ mol, 1 eq.), 6-FAM azide **95a** (14.0 mg, 30 μ mol, 1 eq.), TBTA (1.7 mg, 3 μ mol, 0.1 eq.), CuSO₄ (0.5 mg, 3 μ mol, 0.1 eq.) and sodium ascorbate (1.2 mg, 6 μ mol, 0.2 eq.). *Tert*-butanol and water (0.25 mL each) were used as solvents. After 18 h of stirring, water (5 mL) was added and the mixture was extracted with EtOAc (3x15 mL). The combined organic extracts were dried over Na₂SO₄, filtered, and evaporated to dryness. Purification was performed via reversed-phase flash column chromatography (H₂O/ACN/TFA 60:40:0.1–50:50:0.1) yielding the desired product as a yellow powder.

Yield: 5 mg (18%)

$$R_f \text{ (reversed-phase; H}_2\text{O/ACN 1:1)} = 0.42$$

¹H-NMR (400 MHz, DMSO-*d*₆): δ (ppm) 10.83 (s, 1H, OH), 10.17 (s, 2H, OH_{flu}), 10.07 (s, 1H, OH'), 9.16 (t, ³J = 5.7 Hz, 1H, NH_{deferasirox}), 8.92 (t, ³J = 5.5 Hz, 1H, NH_{flu}), 8.50–

6 Experimental

8.45 (m, 1H, H_{IV}), 8.24 (dd, ³J = 8.1 Hz and ⁴J = 1.6 Hz, 1H, H_{VI}), 8.09–8.01 (m, 2H, H₆, H_{5^{triazole}}), 7.97–7.92 (m, 2H, H_{3''}, H_{5''}), 7.58–7.49 (m, 3H, H_{6'}, H_{2''}, H_{6''}), 7.43–7.33 (m, 3H, H₄, H_{4'}, H_{VII}), 7.07–6.93 (m, 3H, H₃, H₅, H_{5'}), 6.86 (dd, ³J = 8.3 Hz and ⁴J = 1.0 Hz, 1H, H_{3'}), 6.70 (d, ⁴J = 2.2 Hz, 2H, H_{IV'}, H_{V'}), 6.61–6.53 (m, 4H, H_{I'}, H_{II'}, H_{VIII'}, H_{VIII'}), 4.52 (d, ³J = 5.6 Hz, 2H, C_{4^{triazole}}-CH₂), 4.44 (t, ³J = 7.0 Hz, 2H, N_{triazole}-CH₂), 3.34 (q, ³J = 6.4 Hz, 2H, NH-CH₂-CH₂), 2.11 (p, ³J = 7.0 Hz, 2H, NH-CH₂-CH₂).

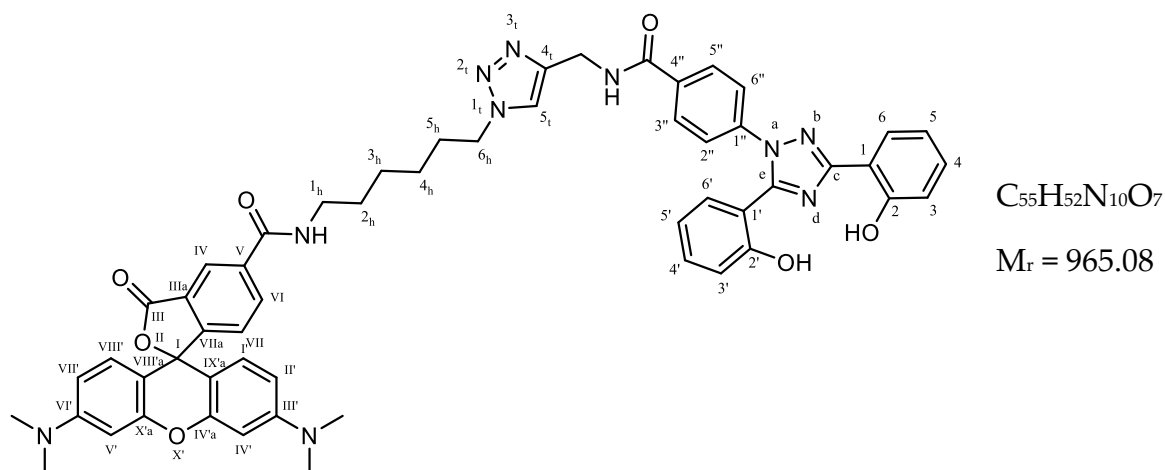
¹³C-NMR (101 MHz, DMSO-*d*₆): δ (ppm) 168.6 (C_{III}), 165.4 (C_{amide}), 165.2 (C_{amide}), 160.2 (C_c), 160.0 (2C, C_{III'}, C_{IV'}), 156.7 (C₂), 155.6 (C_{2'}), 152.3 (C_e), 152.2 (3C, C_{VIIa}, C_{IV'a}, C_{X'a}), 142.4 (C_{4^{triazole}}), 140.3 (C_{1''}), 136.5 (C_{VI}), 134.3 (C_{4'}), 132.9 (C₄), 131.9 (C_{6'}), 131.5 (C_{4''}), 129.6 (2C, C_{I'}, C_{VIII'}), 128.7 (2C, C_{3''}, C_{5''}), 127.2 (C₆), 126.8 (C_{VII}), 125.2 (C_{5^{triazole}}), 124.7 (C_{IV}), 123.6 (2C, C_{2''}, C_{6''}), 120.6 (C₅), 120.1 (C_{5'}), 117.5 (C₃), 116.5 (C_{3'}), 114.8 (C_{1'}), 114.1 (C₁), 113.1 (2C, C_{II'}, C_{VIII'}), 109.5 (2C, C_{VIII'a}, C_{IX'a}), 102.7 (2C, C_{IV'}, C_{V'}), 47.7 (N_{triazole}-CH₂), 47.0 (C_{4^{triazole}}-CH₂), 37.2 (NH-CH₂-CH₂), 27.4 (NH-CH₂-CH₂). Due to the low signal intensity, C_I, C_{IIIa} and C_V could not be identified in the spectrum.

HRMS (ESI positive): *m/z* 869.2665 [M+H]⁺, calcd for [C₄₈H₃₆N₈O₉+H]⁺: *m/z* 869.2678

HRMS (ESI negative): *m/z* 867.2534 [M-H]⁻, calcd for [C₄₈H₃₆N₈O₉-H]⁻: *m/z* 867.2532

HPLC: *t*_R = 20.675 min (kinetex, 98.3%), *t*_R = 21.973 min (polar-RP, 95.6%)

N-(6-(4-((4-(3,5-Bis(2-hydroxyphenyl)-1*H*-1,2,4-triazol-1-yl)benzamido)methyl)-1*H*-1,2,3-triazol-1-yl)hexyl)-3',6'-bis(dimethylamino)-3-oxo-3*H*-spiro[isobenzofuran-1,9'-xanthene]-5-carboxamide (**96b**)



The title compound was synthesized following general procedure E using 5-TAMRA azide **95b** (10.3 mg, 19 μ mol, 1 eq.), **94a** (9.0 mg, 20 μ mol, 1.15 eq.), TBTA (1.0 mg, 2 μ mol, 0.1 eq.), CuSO₄ (0.5 mg, 3 μ mol, 0.1 eq.) and sodium ascorbate (1.2 mg, 6 μ mol, 0.2 eq.). *Tert*-butanol and water (0.25 mL each) were used as solvents. After 18 h of stirring, water (5 mL) was added and the mixture was evaporated to dryness. Purification was performed via preparative TLC (Silica 0.5 mm, Merck; DCM/methanol/acetic acid 89.5:10:0.5) followed by semi-preparative HPLC (H₂O/ACN + 0.05% TFA, 0–4 min: 50:50, 4–10 min: 50:50–0:100, 10–20 min: 0:100) yielding the desired product as a pink powder.

Isolated Yield: 3.5 mg (20%)

R_f (reversed-phase; H₂O/ACN 1:1) = 0.45

¹H-NMR (400 MHz, DMSO-*d*₆): δ (ppm) 10.82 (s, 1H, OH), 10.09 (s, 1H, OH'), 9.14 (t, ³J = 5.7 Hz, 1H, NH_{deferasirox}), 8.88 (t, ³J = 5.6 Hz, 1H, NH_{TAMRA}), 8.68 (d, ⁴J = 1.8 Hz, 1H, H_{IV}), 8.29 (dd, ³J = 8.0 Hz and ⁴J = 1.8 Hz, 1H, H_{VI}), 8.03 (dd, ³J = 7.8 Hz and ⁴J = 1.7 Hz, 1H, H₆), 8.00 (s, 1H, H₅_{triazole}), 7.96–7.91 (m, 2H, H₃'', H₅''), 7.57 (d, ³J = 7.9 Hz, 1H, H_{VII}), 7.55–7.49 (m, 3H, H₆', H₂'', H₆''), 7.41–7.34 (m, 2H, H₄, H₄'), 7.10–6.92 (m, 9H, H₃, H₅, H₅', H_I', H_{III}', H_{IV}', H_V', H_{VII}', H_{VIII}'), 6.90–6.84 (m, 1H, H₃'), 4.51 (d, ³J = 5.6 Hz, 2H, C₄_{triazole}-CH₂), 4.34 (t, ³J = 7.0 Hz, 2H, (CH₂)₆_{hexyl}), 3.32 (dd, ³J = 13.3 Hz and ³J = 7.0 Hz, 2H, (CH₂)₁_{hexyl}), 3.26 (s, 12H, CH₃), 1.83 (dt, ³J = 11.9 Hz and ³J = 5.5 Hz, 2H, (CH₂)₅_{hexyl}), 1.56 (dt, ³J = 14.5 Hz and ³J = 7.2 Hz, 2H, (CH₂)₂_{hexyl}), 1.42–1.26 (m, 4H, (CH₂)₃_{hexyl}, (CH₂)₄_{hexyl}). Two small singlets appear at 7.3 Hz and 7.1 Hz, which can be attributed to the dication protonated at the amino groups.

¹³C-NMR (101 MHz, DMSO-*d*₆): δ (ppm) 166.4 (C_{III}), 165.4 (C_{amide}), 164.9 (C_{amide}), 160.2 (C_c), 158.5 (2C, C_{IV'a}, C_{X'a}), 158.5 (2C, C_{III'}, C_{VI'}), 156.7 (C₂), 155.6 (C_{2'}), 152.3 (C_e), 145.2 (C_{VIIa}), 141.9 (C₄_{triazole}), 140.3 (C₁''), 136.5 (C_{VI}), 134.3 (C_{4'}), 132.9 (C₄), 131.8 (C_{6'}), 131.5 (C_{4''}), 128.7 (2C, C₃'', C₅''), 127.1 (C₆), 125.4 (C_{VII}), 125.2 (C₅_{triazole}), 123.6 (2C, C₂'', C_{6''}), 123.3 (C_{IV}), 120.6 (C₅), 120.1 (C_{5'}), 119.8 (2C, C_{II'}, C_{VII'}), 117.4 (C₃), 116.5 (C_{3'}), 114.8 (C_{1'}), 114.0 (C₁), 107.4 (2C, C_{VIII'a}, C_{IX'a}), 96.7 (2C, C_{IV'}, C_{V'}), 83.8 (C_I), 55.3 (4C, CH₃), 49.6 (C₆_{hexyl}), 40.9 (C₁_{hexyl}), 35.4 (C₄_{triazole}-CH₂), 30.1 (C_{hexyl}), 29.2 (C_{hexyl}), 26.3

6 Experimental

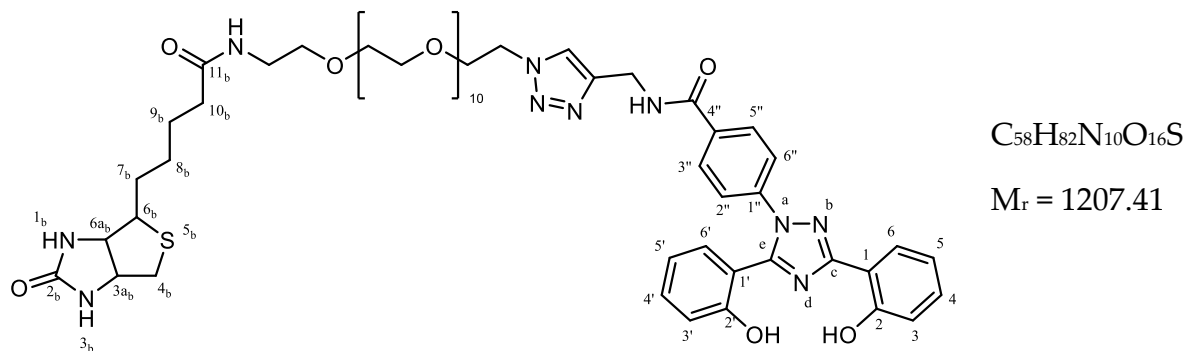
(C_{hexyl}), 26.0 (C_{hexyl}). Due to the low signal intensity, C_{IIIa} and C_{V} could not be identified in the spectrum.

HRMS (ESI positive): m/z 965.4092 [$M+H$] $^+$, calcd for [$C_{55}H_{52}N_{10}O+H$] $^+$: m/z 965.4093

HRMS (ESI negative): m/z 963.3943 [$M-H$] $^-$, calcd for [$C_{55}H_{52}N_{10}O-H$] $^-$: m/z 963.3948

HPLC: t_R = 20.132 min (kinetex, 98.6%), t_R = 23.704 min (polar-RP, 98.9%)

4-(3,5-Bis(2-hydroxyphenyl)-1*H*-1,2,4-triazol-1-yl)-*N*-((1-(37-oxo-41-(2-oxohexahydro-1*H*-thieno[3,4-*d*]imidazol-4-yl)-3,6,9,12,15,18,21,24,27,30,33-undecaoxa-36-azahentetracontyl)-1*H*-1,2,3-triazol-4-yl)methyl)benzamide (**96c**)



Following general procedure E the title compound was synthesized using Biotin-PEG₁₁-Azide (26.5 mg, 33 μ mol, 1 eq.), **94a** (15.0 mg, 37 μ mol, 1.1 eq.), TBTA (1.7 mg, 3 μ mol, 0.1 eq.), CuSO₄ (5.8 mg, 37 μ mol, 1.1 eq.) and sodium ascorbate (1.3 mg, 7 μ mol, 0.2 eq.). *Tert*-butanol, DMF, and water (0.25 mL each) were used as solvents. Purification was performed via reversed-phase column chromatography (H₂O/ACN 90:10–10:90) followed by semi-preparative HPLC (H₂O/ACN + 0.05% TFA, 0–4 min: 50:50, 4–10 min: 50:50–0:100, 10–20 min: 0:100) yielding a slightly yellow semi-solid.

Yield: 6 mg (15%)

R_f (reversed-phase; H₂O/ACN 1:1) = 0.45

¹H-NMR (400 MHz, DMSO-*d*₆): δ (ppm) 10.83 (s, 1H, OH), 10.05 (s, 1H, OH'), 9.13 (t, 3J = 5.8 Hz, 1H, NH_{deferasirox}), 8.05 (dd, 3J = 7.8 Hz and 4J = 1.7 Hz, 1H, H₆), 7.98–7.90 (m, 3H, H_{3''}, H_{5''}, H_{5triazole}), 7.84 (t, 3J = 5.3 Hz, 1H, NH_{biot-amide}), 7.57–7.49 (m, 3H, H_{6'}, H_{2''}, H_{6''}), 7.44–7.34 (m, 2H, H₄, H_{4'}), 7.07–6.94 (m, 3H, H₃, H₅, H_{5'}), 6.89–6.84 (m,

1H, H3'), 6.43 (s, 1H, NH1_{biot}), 6.36 (s, 1H, NH3_{biot}), 4.54–4.46 (m, 4H, C4_{triazole}-CH₂, N_{triazole}-CH₂), 4.34–4.27 (m, 1H, (CH₂)_{3biot}), 4.13 (s, 1H, (CH₂)_{6biot}), 3.80 (t, ³J = 5.2 Hz, 2H, N_{triazole}-CH₂-CH₂-O), 3.56–3.42 (m, 40H, (CH₂)_{PEG}), 3.39 (t, ³J = 5.9 Hz, 2H, NH-CH₂-CH₂-O), 3.18 (q, ³J = 5.8 Hz, 2H, NH-CH₂-CH₂-O), 3.09 (s, 1H, (CH₂)_{6biot}), 2.82 (dd, ³J = 12.3 Hz and ³J = 5.2 Hz, 1H, H4_{biot}), 2.64–2.54 (m, 1H, H4'_{biot}), 2.07 (dd, ³J = 7.9 Hz and ³J = 7.2 Hz, 2H, (CH₂)_{10biot}), 1.49 (s, 4H, (CH₂)_{8biot}, (CH₂)_{9biot}), 1.35–1.27 (m, 2H, (CH₂)_{7biot}).

Due to the low sample amount no ¹³C-NMR spectrum was recorded.

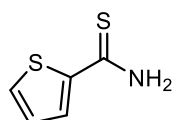
HRMS (ESI positive): *m/z* 1229.5529 (100%, [M+Na]⁺), 1207.5726 (38%, [M+H]⁺), calcd for [C₅₈H₈₂N₁₀O₁₆S+H]⁺: *m/z* 1207.5704

HPLC: *t_R* = 18.108 min (kinetex, 95.1%), *t_R* = 20.397 min (polar-RP, 96.4%)

6.2.10 Thiazoles

6.2.10.1 Precursors

Thiophene-2-carbothioamide (**98a**)



C₅H₅NS₂

M_r = 143.22

According to the published procedure by Li *et. al.*,²⁵⁵ Lawesson's reagent (191 mg, 0.47 mmol, 0.6 eq.) was added to a solution of thiophene-2-carboxamide **100** (100 mg, 0.79 mmol, 1 eq.) in THF (2 mL). The mixture was refluxed for 4 h and then evaporated to dryness. The residue was dissolved in EtOAc (10 mL), washed with a 5% solution of NaHCO₃ (15 mL) and brine (3x15 mL), dried over Na₂SO₄, filtered, and evaporated to dryness. Purification was performed via flash column chromatography (CyHex/EtOAc 90:10–0:100) yielding the desired product as a yellow solid.

Yield: 87 mg (77%)

R_f (CyHex/EtOAc 7:3) = 0.26

¹H-NMR (400 MHz, CDCl₃-d₁): δ (ppm) 7.57 (dd, ³*J* = 5.1 Hz and ⁴*J* = 1.2 Hz, 1H, H5), 7.51 (dd, ³*J* = 3.8 Hz and ⁴*J* = 1.2 Hz, 1H, H3), 7.37 (bs, 2H, NH₂), 7.10 (dd, ³*J* = 5.1 Hz and ³*J* = 3.8 Hz, 1H, H4).

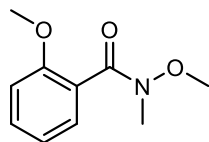
¹³C-NMR (101 MHz, CDCl₃-d₁): δ (ppm) 192.1 (C_{thioamide}), 144.6 (C2), 133.9 (C5), 128.3 (C4), 126.8 (C3).

MS (APCI positive): *m/z* 126.9 [M-NH₂]⁺, calcd for [C₅H₅NS₂-NH₂]⁺: *m/z* 127.0

MS (APCI negative): *m/z* 142.2 [M-H]⁻, calcd for [C₅H₅NS₂-H]⁻: *m/z* 142.0

6.2.10.1.1 Weinreb amides

N,2-Dimethoxy-*N*-methylbenzamide (**104a**)



C₁₀H₁₃NO₃

M_r = 195.22

According to the published procedure by Yamazaki *et al.*,²⁸⁰ *N,O*-dimethylhydroxylamine hydrochloride (1.20 g, 11.9 mmol, 1.1 eq.), triethylamine (1.67 mL, 11.9 mmol, 1.1 eq.) and EDCI (2.29 g, 11.9 mmol, 1.1 eq.) were added to a solution of 2-methoxybenzoic acid **105a** (1.50 g, 10.9 mmol, 1 eq.) in DMF (17 mL). After stirring for 18 h at r.t., the solvent was removed *in vacuo*. The residue was dissolved in EtOAc, washed with 0.5% citric acid, a saturated solution of NaHCO₃ and brine (20 mL each), dried over Na₂SO₄, and evaporated to dryness yielding the desired product as a colourless oil.

Yield: 2.06 g (97%)

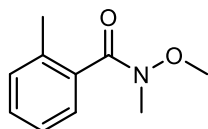
¹H-NMR (400 MHz, DMSO-*d*₆): δ (ppm) 7.40 (td, ³*J* = 8.1 Hz, ³*J* = 7.5 Hz and ⁴*J* = 1.8 Hz, 1H, H4), 7.22 (dd, ³*J* = 7.4 Hz and ⁴*J* = 1.8 Hz, 1H, H6), 7.08 (d, ³*J* = 8.1 Hz, 1H, H3), 6.98 (td, ³*J* = 7.5 Hz, ³*J* = 7.4 Hz and ⁴*J* = 1.0 Hz, 1H, H5), 3.79 (s, 3H, COCH₃), 3.44 (bs, 3H, NOCH₃), 3.20 (bs, 3H, NCH₃).

¹³C-NMR (101 MHz, DMSO-*d*₆): δ (ppm) 168.5 (C_{amide}), 155.6 (C2), 130.8 (C4), 127.5 (C6), 125.7 (C1), 120.5 (C5), 111.8 (C3), 61.0 (COCH₃), 55.9 (NOCH₃), 32.2 (NCH₃).

R_f (DCM/methanol 92:8) = 0.69

MS (APCI positive): m/z 196.1 $[M+H]^+$, calcd for $[C_{10}H_{13}NO_3+H]^+$: m/z 196.1

***N*-Methoxy-*N*,2-dimethylbenzamide (**106b**)**



$C_{10}H_{13}NO_2$

$M_r = 179.22$

According to the published procedure by Kumar *et. al.*,²⁸¹ DMF (3 μ L, 0.04 mmol, 0.5 mol%) was added to a suspension of 2-methylbenzoic acid **105b** (1.00 g, 7.34 mmol, 1 eq.) in dry DCM (10 mL) at 0 °C. Oxalyl chloride (8.81 mL, 8.81 mmol, 1.2 eq.) was added dropwise. After stirring at r.t. for 1 h, the reaction was concentrated *in vacuo* yielding 2-methylbenzoyl chloride as a yellow oil.

To a suspension of *N,O*-dimethylhydroxylamine hydrochloride (1.07 g, 11.02 mmol, 1.5 eq.) in dry DCM (10 mL) triethylamine (2.05 mL, 14.69 mmol, 2 eq.) was added dropwise at 0 °C. The reaction mixture was stirred at 0 °C for 10 min, followed by the dropwise addition of a solution of the acid chloride in dry DCM (5 mL). The reaction mixture was allowed to warm to r.t., stirred for 14 h and then quenched with water (25 mL). The product was extracted with DCM (2x25 mL). The combined organic extracts were washed with brine (3x25 mL), dried over Na_2SO_4 , and evaporated to dryness. Purification via flash column chromatography (CyHex/EtOAc 65:35–20:80) yielded the desired product as white crystals.

Yield: 1.06 g (81%)

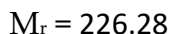
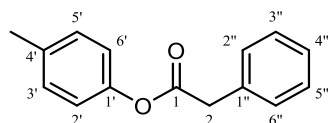
R_f (CyHex/EtOAc 3:7) = 0.60

1H -NMR (400 MHz, DMSO- d_6): δ (ppm) 7.35–7.30 (m, 1H, H₆), 7.28–7.21 (m, 3H, H_{ar}), 3.46 (s, 3H, OCH₃), 3.23 (s, 3H, NCH₃), 2.23 (s, 3H, (CH₃)_{ar}).

^{13}C -NMR (101 MHz, DMSO- d_6): δ (ppm) 136.1 (C1), 134.4 (C2), 130.3 (C3 or C4), 129.3 (C3 or C4), 126.3 (C5), 125.8 (C6), 61.1 (OCH₃), 32.5 (weak, NCH₃), 19.1 ((CH₃)_{ar}). The amide carbon is not visible in the spectrum.

MS (APCI positive): m/z 180.1 $[M+H]^+$, calcd for $[C_{10}H_{13}NO_2+H]^+$: m/z 180.1

6.2.10.1.2 Ester

p-Tolyl 2-phenylacetate (**102**)

In a modification of the published procedure by Shaye *et. al.*,²⁸² a solution of 4-methylphenol (2.00 g, 18.5 mmol, 1 eq.) in dry DCM (7.5 mL) was slowly added to a solution of phenylacetic acid (2.47 g, 20.3 mmol, 1.1 eq.) and DCI (4.39 g, 21.3 mmol, 1.2 eq.) in dry DCM (20 mL) at 0 °C. The mixture was stirred for 18 h while slowly warming to r.t. The formed solid was filtered off and the organic solution was evaporated to dryness. Purification was performed via flash column chromatography (CyHex/EtOAc 95:5–85:15) yielding the desired product as white crystals.

Yield: 3.56 g (85%)

R_f (CyHex/EtOAc 7:3) = 0.68

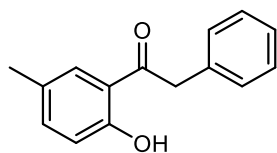
¹H-NMR (400 MHz, DMSO-*d*₆): δ (ppm) 7.41–7.34 (m, 4H, H_{phenyl}), 7.34–7.27 (m, 1H, H_{phenyl}), 7.24–7.19 (m, 2H, H3', H5'), 7.03–6.97 (m, 2H, H2', H6'), 3.95 (s, 2H, CH₂), 2.30 (s, 3H, CH₃).

¹³C-NMR (101 MHz, DMSO-*d*₆): δ (ppm) 170.6 (C_{ketone}), 148.7 (C1'), 135.4 (C4'), 134.4 (C1''), 130.3 (2C, C_{ar}), 129.9 (2C, C_{ar}), 128.9 (2C, C_{ar}), 127.4 (C4''), 121.8 (2C, C2', C6'), 20.8 (CH₃). The CH₂ signal overlaps with the solvent signal.

MS (APCI positive): *m/z* 109.0 (100%, [M-phenylacetyl]⁺), 227.1 (3%, [M+H]⁺), calcd for [C₁₅H₁₄O₂+H]⁺: *m/z* 227.1

MS (APCI negative): *m/z* 225.1 [M-H]⁻, calcd for [C₁₅H₁₄O₂-H]⁻: *m/z* 225.1

6.2.10.1.3 Ketones

1-(2-Hydroxy-5-methylphenyl)-2-phenylethan-1-one (**101a**) $\text{C}_{15}\text{H}_{14}\text{O}_2$ $M_r = 226.28$

In accordance with the published procedure by Ortar *et. al.*²⁵⁷ **102** (5.27 g, 23.29 mmol, 1 eq.) was heated to 100 °C to give a clear melt. To this, AlCl_3 (3.11 g, 34.94 mmol, 1.5 eq.) was slowly added resulting in a strong evolution of gas and a colour change to dark brown. The mixture was stirred at 100 °C for 16 h. The reaction was quenched with water (50 mL) and extracted with EtOAc (3x60 mL). The combined organic extracts were washed with brine (15 mL), dried over NaSO_4 , filtered, and evaporated to dryness. Purification via flash column chromatography (CyHex/EtOAc 100:0–95:5) followed by recrystallisation from 2-propanol yielded the desired product as light-yellow needles.

Yield: 3.11 g (59%)

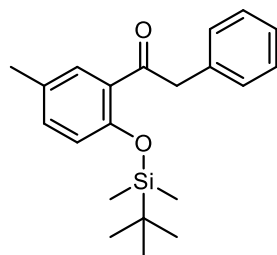
R_f (CyHex/2-propanol 9:1) = 0.70

^1H -NMR (400 MHz, $\text{DMSO}-d_6$): δ (ppm) 11.65 (s, 1H, OH'), 7.84 (dd, $^4J = 2.3$ Hz and $^5J = 1.0$ Hz, 1H, H6'), 7.39–7.27 (m, 6H, H4', H_{phenyl}), 6.89 (d, $^3J = 8.4$ Hz, 1H, H3'), 4.44 (s, 2H, CH₂), 2.29 (s, 3H, CH₃).

^{13}C -NMR (101 MHz, $\text{DMSO}-d_6$): δ (ppm) 204.1 (C_{ketone}), 159.2 (C2'), 137.4 (C4'), 135.3 (C1''), 131.1 (C5'), 130.2 (2C, C2'', C6'' or C3'', C5''), 128.7 (2C, C2'', C6'' or C3'', C5''), 128.3 (C4''), 127.0 (C6'), 120.2 (C1'), 118.0 (C3'), 45.7 (CH₂), 20.4 (CH₃).

MS (APCI positive): m/z 227.1 $[\text{M}+\text{H}]^+$, calcd for $[\text{C}_{15}\text{H}_{14}\text{O}_2+\text{H}]^+$: m/z 227.1

MS (APCI negative): m/z 225.2 $[\text{M}-\text{H}]^-$, calcd for $[\text{C}_{15}\text{H}_{14}\text{O}_2-\text{H}]^-$: m/z 225.1

1-(2-((*Tert*-butyldimethylsilyl)oxy)-5-methylphenyl)-2-phenylethan-1-one
(**101b**)C₂₁H₂₈O₂SiM_r = 340.54

To a solution of **101a** (173 mg, 0.76 mmol, 1 eq.) in dry DCM (3.0 mL), dry triethylamine (160 μ L, 1.15 mmol, 1.1 eq.) and *tert*-butyldimethylsilyl chloride (346 mg, 2.29 mmol, 3 eq.) were added. The mixture was stirred at r.t. for 0.5 h and then refluxed for 16 h. The solvent was evaporated *in vacuo* and the residue was taken up in diethyl ether. The remaining solid was filtered off and the filtrate was concentrated *in vacuo*. Purification was performed via flash column chromatography (CyHex/EtOAc 100:0–70:30) yielding the desired product as a slightly brown oil.

Yield: 243 mg (93%)

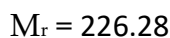
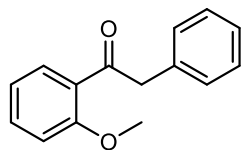
R_f (CyHex/EtOAc 8:2) = 0.77

¹H-NMR (400 MHz, DMSO-*d*₆): δ (ppm) 7.31–7.27 (m, 3H, H_{ar}), 7.25–7.21 (m, 2H, H_{ar}), 7.19–7.15 (m, 2H, H_{ar}), 6.88 (d, ³J = 8.3 Hz, 1H, H3'), 4.27 (s, 2H, CH₂), 2.24 (s, 3H, (CH₃)_{ar}), 0.96 (s, 9H, (CH₃)_{*t*-butyl}), 0.23 (s, 6H, Si-CH₃).

¹³C-NMR (101 MHz, DMSO-*d*₆): δ (ppm) 200.6 (C_{ketone}), 151.5 (C2'), 135.2 (C1''), 133.7 (C4'), 131.1 (C5'), 130.6 (C6'), 130.1 (2C, C2'', C6'' or C3'', C5''), 130.0 (C4''), 128.7 (2C, C2'', C6'' or C3'', C5''), 126.9 (C1'), 120.6 (C3'), 49.4 (CH₂), 26.1 (3C, (CH₃)_{*t*-butyl}), 20.3 ((CH₃)_{ar}), 18.5 (Si-C-C₃), -3.9 (2C, Si-CH₃).

MS (APCI positive): *m/z* 341.2 [M+H]⁺, calcd for [C₂₁H₂₈O₂Si+H]⁺: *m/z* 341.2

MS (APCI negative): *m/z* 239.2 [M-H]⁻, calcd for [C₂₁H₂₈O₂Si-H]⁻: *m/z* 239.2

1-(2-Methoxyphenyl)-2-phenylethan-1-one (**101c**)

Following the procedure published by Mc Laughlin *et al.*,²⁵⁸ benzylmagnesium chloride (1.4 M solution in THF, 10.98 mL, 15.37 mmol, 1.5 eq.) was added dropwise to a solution of *N*,2-dimethoxy-*N*-methylbenzamide (2.00 g, 10.25 mmol, 1 eq.) in dry THF (12.5 mL) over 30 min at 0 °C. The mixture was stirred at 0 °C for 1 h, then warmed to r.t. and stirred at that temperature for 20 h. The reaction was quenched by the addition of an aqueous solution of HCl (1 M, 15 mL), concentrated *in vacuo* to a volume of approximately 10 mL and extracted with EtOAc (3x20 mL). The combined organic extracts were dried over Na₂SO₄, filtered, and evaporated to dryness. Purification via flash column chromatography (CyHex/EtOAc 96:4–88:12) yielded the desired product as a slightly yellow oil.

Yield: 1.80 g (78%)

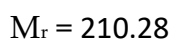
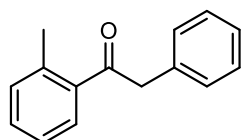
R_f (CyHex/EtOAc 8:2) = 0.40

¹H-NMR (400 MHz, DMSO-*d*₆): δ (ppm) 7.56–7.50 (m, 2H, H4', H6'), 7.32–7.27 (m, 2H, H3', H_{phenyl}), 7.25–7.15 (m, 4H, H_{phenyl}), 7.04–6.99 (m, 1H, H5'), 4.26 (s, 2H, CH₂), 3.91 (s, 3H, CH₃).

¹³C-NMR (101 MHz, DMSO-*d*₆): δ (ppm) 200.1 (C_{ketone}), 158.4 (C2'), 135.7 (C1''), 134.1 (C4') 130.1 (2C, C2'', C6'' or C3'', C5''), 130.0 (C6'), 128.6 (2C, C2'', C6'' or C3'', C5''), 128.3 (C4''), 126.8 (C1'), 120.9 (C5'), 112.8 (C3'), 56.1 (CH₃), 49.8 (CH₂).

MS (APCI positive): *m/z* 227.1 [M+H]⁺, calcd for [C₁₅H₁₄O₂+H]⁺: *m/z* 227.1

MS (APCI negative): *m/z* 225.1 [M-H]⁻, calcd for [C₁₅H₁₄O₂-H]⁻: *m/z* 225.1

2-Phenyl-1-(*o*-tolyl)ethan-1-one (**101d**)

6 Experimental

To a solution of **106b** (1.06 g, 5.93 mmol, 1 eq.) in dry THF (3 mL) benzylmagnesium chloride (1.4 M in THF, 4.66 mL, 6.52 mmol, 1.1 eq.) was added dropwise over 1 h at $-78\text{ }^{\circ}\text{C}$. The mixture was allowed to warm to r.t. and was stirred at that temperature for 5 h. The reaction was quenched by the addition of a saturated solution of NH_4Cl (20 mL). The aqueous phase was extracted with EtOAc (3x40 mL). The combined organic extracts were washed with brine (40 mL), dried over Na_2SO_4 , filtered, and evaporated to dryness. Purification via flash column chromatography (CyHex/EtOAc 96:4–89:11) yielded the desired product as a colourless oil.

Yield: 814 mg (65%)

R_f (CyHex/2-propanol 9:1) = 0.69

$^1\text{H-NMR}$ (400 MHz, CDCl_3 - d_1): δ (ppm) 7.73 (dd, $^3J = 7.7\text{ Hz}$ and $^4J = 1.4\text{ Hz}$, 1H, $\text{H}_{6'}$), 7.40–7.21 (m, 9H, H_{ar}), 4.22 (s, 2H, CH_2), 2.45 (s, 3H, CH_3).

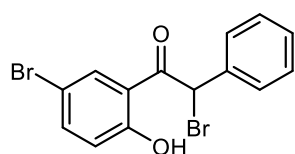
$^{13}\text{C-NMR}$ (101 MHz, CDCl_3 - d_1): δ (ppm) 201.4 (C_{ketone}), 138.5 ($\text{C}2'$), 137.5 ($\text{C}1'$), 134.4 ($\text{C}1''$), 131.9 ($\text{C}4'$), 131.3 ($\text{C}3'$), 129.5 (2C, $\text{C}2''$, $\text{C}6''$ or $\text{C}3''$, $\text{C}5''$), 128.6 ($\text{C}4''$), 128.6 (2C, $\text{C}2''$, $\text{C}6''$ or $\text{C}3''$, $\text{C}5''$), 126.8 ($\text{C}6'$), 125.5 ($\text{C}5'$), 48.4 (CH_2), 21.2 (CH_3).

GC-MS (EI positive): m/z 119 (100%, $[\text{M-tolyl}]^+$), 210 (15%, $[\text{M}]^+$), calcd for $[\text{C}_{15}\text{H}_{14}\text{O}]^+$: m/z 210

MS (APCI negative): m/z 209.5 $[\text{M-H}]^-$, calcd for $[\text{C}_{15}\text{H}_{14}\text{O-H}]^-$: m/z 209.1

6.2.10.1.4 Brominated ketones

2-Bromo-1-(5-bromo-2-hydroxyphenyl)-2-phenylethan-1-one (**97d**)



$\text{C}_{14}\text{H}_{10}\text{Br}_2\text{O}_2$

$M_r = 370.04$

To a solution of 1-(2-hydroxyphenyl)-2-phenylethan-1-one **101e** (200 mg, 0.94 mmol, 1 eq.) in 1.0 mL dioxane, Br_2 (97 μL , 1.88 mmol, 2 eq.) was slowly added via syringe. The mixture was stirred at r.t. for 4.5 h. EtOAc (5 mL) was added and the mixture was washed with a saturated solution of $\text{Na}_2\text{S}_2\text{O}_3$ (5 mL) and water (15 mL), dried over Na_2SO_4 , filtered, and evaporated to dryness. Purification was

performed via recrystallization from ethanol yielding the desired product as yellow crystals.

Yield: 63 mg (18%)

R_f (CyHex/EtOAc 7:3) = 0.70

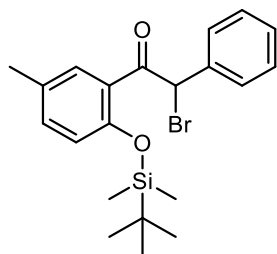
^1H -NMR (400 MHz, DMSO- d_6): δ (ppm) 11.79 (s, 1H, OH'), 7.91 (d, 4J = 2.4 Hz, 1H, H6'), 7.59–7.53 (m, 3H, H4', H_{phenyl}), 7.45–7.38 (m, 3H, H_{phenyl}), 6.93 (d, 3J = 8.9 Hz, 1H, H3'), 6.31 (s, 1H, CHBr).

^{13}C -NMR (101 MHz, DMSO- d_6): δ (ppm) 191.0 (C_{ketone}), 157.7 (C2'), 135.1 (C4'), 129.9 (C1''), 127.4 (C6'), 124.8 (C4''), 124.4 (2C, C2'', C6'' or C3'', C5''), 124.3 (2C, C2'', C6'' or C3'', C5''), 116.3 (C3'), 113.1 (C1'), 106.0 (C5'), 44.1 (C2).

MS (APCI positive): m/z 369.2 [M+H]⁺, calcd for [C₁₄H₁₀⁷⁹Br₂O₂+H]⁺: m/z 368.9

MS (APCI negative): m/z 367.1 [M-H]⁻, calcd for [C₁₄H₁₀⁷⁹Br₂O₂-H]⁻: m/z 366.9

2-Bromo-1-(2-((*tert*-butyldimethylsilyl)oxy)-5-methylphenyl)-2-phenylethan-1-one (**97a**)



C₂₁H₂₇BrO₂Si

M_r = 419.43

Following the procedure adapted from Guan *et. al.*,²⁶² *N*-bromosuccinimide (140 mg, 0.78 mmol, 1.1 eq.) and *p*-toluenesulfonic acid (8 mg, 0.07 mmol, 0.1 eq.) were added to a solution of **101b** (243 mg, 0.71 mmol, 1 eq.) in DCM (1.6 mL). The mixture was heated to 80 °C under μW -irradiation for 45 min. The mixture was cooled to r.t., diluted with DCM (15 mL), washed with a saturated solution of NaHCO₃ (15 mL) and brine (15 mL), dried over Na₂SO₄, filtered, and evaporated to dryness. Purification was performed via flash column chromatography (CyHex/EtOAc 99:1–97:3) yielding the desired product as a slightly yellow oil.

Yield: 228 mg (76%)

R_f (CyHex/2-propanol 9:1) = 0.72

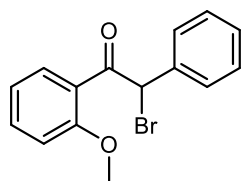
$^1\text{H-NMR}$ (400 MHz, DMSO- d_6): δ (ppm) 7.42–7.31 (m, 6H, H_{phenyl} , $\text{H6}'$), 7.22 (ddd, $^3J_{4'-3'} = 8.3$ Hz, $^4J_{4'-6'} = 2.4$ Hz and $^4J_{4'-\text{CH}_3} = 0.8$ Hz, 1H, $\text{H4}'$), 6.85 (d, $^3J = 8.3$ Hz, 1H, $\text{H3}'$), 6.78 (s, 1H, CHBr), 2.21 (dd, $^4J = 0.8$ Hz and $^4J = 0.7$ Hz, 3H, $(\text{CH}_3)_{\text{ar}}$), 0.98 (s, 9H, $(\text{CH}_3)_{\text{t-butyl}}$), 0.26 (s, 3H, Si- CH_3), 0.21 (s, 3H, Si- CH_3).

$^{13}\text{C-NMR}$ (101 MHz, DMSO- d_6): δ (ppm) 193.8 (C_{ketone}), 151.5 ($\text{C2}'$), 136.3 ($\text{C1}''$), 134.5 ($\text{C4}'$), 130.8 ($\text{C5}'$), 130.5 ($\text{C6}'$), 129.4 (2C, $\text{C2}''$, $\text{C6}''$ or $\text{C3}''$, $\text{C5}''$), 129.4 ($\text{C4}''$), 129.3 (2C, $\text{C2}''$, $\text{C6}''$ or $\text{C3}''$, $\text{C5}''$), 128.3 ($\text{C1}'$), 120.4 ($\text{C3}'$), 55.9 (CBr), 26.1 (3C, $(\text{CH}_3)_{\text{t-butyl}}$), 20.2 ($(\text{CH}_3)_{\text{ar}}$), 18.5 (Si- $\text{C}-\text{C}_3$), -3.8 (Si- CH_3), -3.9 (Si- CH_3).

MS (APCI positive): m/z 419.3 $[\text{M}+\text{H}]^+$, calcd for $[\text{C}_{21}\text{H}_{27}^{79}\text{BrO}_2\text{Si}+\text{H}]^+$: m/z 419.1

MS (APCI negative): m/z 417.3 $[\text{M}-\text{H}]^-$, calcd for $[\text{C}_{21}\text{H}_{27}^{79}\text{BrO}_2\text{Si}-\text{H}]^-$: m/z 417.1

2-Bromo-1-(2-methoxyphenyl)-2-phenylethan-1-one (**97b**)



$\text{C}_{15}\text{H}_{13}\text{BrO}_2$

$M_r = 305.17$

Following the procedure adapted from Guan *et. al.*,²⁶² *N*-bromosuccinimide (1023 mg, 5.73 mmol, 1.1 eq.) and *p*-toluenesulfonic acid (248 mg, 1.30 mmol, 0.3 eq.) were added to a solution of **101c** (1178 mg, 5.21 mmol, 1 eq.) in DCM (16.6 mL). The mixture was heated to 80 °C under μW -irradiation for 2 h. The mixture was cooled to r.t., diluted with DCM (15 mL), washed with a saturated solution of NaHCO_3 (15 mL) and brine (15 mL), dried over Na_2SO_4 , filtered, and evaporated to dryness. Purification was performed via flash column chromatography (CyHex/EtOAc 97:3–93:7) followed by recrystallization from 2-propanol yielding the desired product as a white crystalline powder, which contained traces of the starting material.

Yield: 650 mg (41%)

R_f (CyHex/EtOAc 7:3) = 0.55

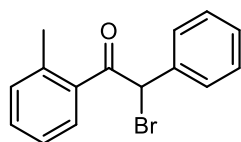
¹H-NMR (400 MHz, DMSO-*d*₆): δ (ppm) 7.71 (dd, $^3J = 7.7$ Hz and $^4J = 1.9$ Hz, 1H, H6'), 7.52–7.41 (m, 3H, H4', H_{phenyl}), 7.38–7.25 (m, 3H, H_{phenyl}), 7.00 (td, $^3J = 7.7$ Hz, $^3J = 7.7$ Hz and $^4J = 0.9$ Hz, 1H, H5'), 6.93 (dd, $^3J = 8.5$ Hz and $^4J = 0.9$ Hz, 1H, H3'), 6.59 (s, 1H, CHBr), 3.90 (s, 3H, CH₃).

¹³C-NMR (101 MHz, DMSO-*d*₆): δ (ppm) 193.7 (C_{ketone}), 157.8 (C2'), 136.3 (C1''), 134.1 (C4'), 131.7 (C6'), 129.3 (2C, C2'', C6'' or C3'', C5''), 128.7 (C4''), 128.6 (2C, C2'', C6'' or C3'', C5''), 125.8 (C1'), 121.0 (C5'), 111.5 (C3'), 55.5 (CH₃), 55.2 (CH₂).

MS (APCI positive): m/z 305.1 [M+H]⁺, calcd for [C₁₅H₁₃⁷⁹BrO₂+H]⁺: m/z 305.0

MS (APCI negative): m/z 302.9 [M-H]⁻, calcd for [C₁₅H₁₃⁷⁹BrO₂-H]⁻: m/z 303.0

2-Bromo-2-phenyl-1-(*o*-tolyl)ethan-1-one (**97c**)



C₁₅H₁₃BrO

M_r = 289.17

Bromine (39 μ L, 0.76 mmol, 1.1 eq.) was added dropwise to a solution of **101d** (145 mg, 0.69 mmol, 1 eq.) in acetic acid (0.5 mL). The mixture was stirred at 80 °C for 18 h and then evaporated to dryness. The residue was purified via flash column chromatography (CyHex/EtOAc 97:3–95:5) yielding the product as a yellowish oil, which contained 15% of the starting material (as determined by NMR) and was used for the next step without further purification.

Yield: 158 mg of a mixture of starting material and product (ratio 15:85)

Calculated product **Yield:** 147 mg (74%)

R_f (CyHex/2-propanol 9:1) = 0.75

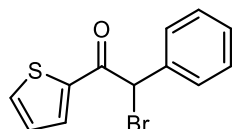
¹H-NMR (400 MHz, CDCl₃-*d*₁): δ (ppm) 7.61–7.57 (m, 1H, H6'), 7.55–7.48 (m, 2H, H_{phenyl}), 7.40–7.32 (m, 4H, H5', H_{phenyl}), 7.26–7.22 (m, 2H, H3', H4'), 6.22 (s, 1H, CHBr), 2.44 (s, 3H, CH₃).

¹³C-NMR (101 MHz, CDCl₃-*d*₁): δ (ppm) 194.4 (C_{ketone}), 139.0 (C2'), 135.7 (C1'), 135.5 (C1''), 131.9 (C4'), 131.7 (C3'), 129.1 (2C, C2'', C6'' or C3'', C5''), 129.1 (C4''), 128.9 (2C, C2'', C6'' or C3'', C5''), 127.8 (C6'), 125.6 (C5'), 53.4 (CHBr), 20.9 (CH₃).

GC-MS (EI positive): m/z 119 (100%, $[M-(\alpha\text{-bromotolyl})]^+$), 197 (80%, $[M\text{-tolyl}]^+$), calcd for $[C_{15}H_{13}^{79}\text{BrO-C}_7\text{H}_7]^+$: m/z 197

MS (APCI positive): m/z 207.7 (100%, $[C_{15}H_{12}O]^+$), 289.0 (17%, $[M+H]^+$), calcd for $[C_{15}H_{13}^{79}\text{BrO+H}]^+$: m/z 289.0

2-Bromo-2-phenyl-1-(thiophen-2-yl)ethan-1-one (**97e**)



$C_{12}H_9BrOS$

$M_r = 281.17$

Trimethylphenylammonium tribromide (372 mg, 0.99 mmol, 1 eq.) and AIBN (38 mg, 0.20 mmol, 0.2 eq.) were added to a solution of 2-phenyl-1-(2-thienyl)ethanone **101f** (200 mg, 0.99 mmol, 1 eq.) in toluene (3.4 mL). The reaction mixture was heated to 60 °C under μW -irradiation for 1 h. After cooling to r.t., the mixture was diluted with EtOAc (50 mL), washed with a saturated solution of $\text{Na}_2\text{S}_2\text{O}_3$ (20 mL) and brine (20 mL), dried over Na_2SO_4 , filtered, and evaporated to dryness. Purification via flash column chromatography (CyHex/EtOAc 98:2–95:5) yielded the desired product as a brown oil, which contained 9% of the starting material (as determined by NMR) and was used for the next step without further purification.

Yield: 234 mg of a mixture of starting material and product (ratio 9:91)

Calculated product **Yield:** 213 mg (79%)

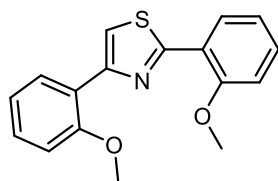
R_f (CyHex/EtOAc 8:2) = 0.56

$^1\text{H-NMR}$ (400 MHz, $\text{DMSO-}d_6$): δ (ppm) 7.77 (dd, $^3J = 3.9$ Hz and $^4J = 1.1$ Hz, 1H, $\text{H5}'$), 7.69 (dd, $^3J = 5.0$ Hz and $^4J = 1.1$ Hz, 1H, $\text{H3}'$), 7.63–7.50 (m, 2H, H_{phenyl}), 7.43–7.28 (m, 3H, H_{phenyl}), 7.12 (dd, $^3J = 5.0$ Hz and $^3J = 3.9$ Hz, 1H, $\text{H3}'$), 6.21 (s, 1H, CHBr).

$^{13}\text{C-NMR}$ (101 MHz, $\text{DMSO-}d_6$): δ (ppm) 184.1 (C_{ketone}), 140.5 ($\text{C2}'$), 135.8 ($\text{C1}''$), 135.2 ($\text{C3}'$ or $\text{C5}'$), 133.3 ($\text{C3}'$ or $\text{C5}'$), 129.2 ($\text{C4}''$), 129.0 (C2 , $\text{C2}''$, $\text{C6}''$ or $\text{C3}''$, $\text{C5}''$), 128.9 (C2 , $\text{C2}''$, $\text{C6}''$ or $\text{C3}''$, $\text{C5}''$), 128.3 ($\text{C4}'$), 51.3 (CBr).

GC-MS (EI positive) m/z 280 $[M]^+$, calcd for $[C_{12}H_9^{79}\text{BrOS}]^+$: m/z 280

6.2.10.1.5 Protected thiazoles

2,4-Bis(2-methoxyphenyl)thiazole (**107a**)C₁₇H₁₅NO₂SM_r = 297.37

2-Methoxythiobenzamide **98b** (100 mg, 0.60 mmol, 1.2 eq.) and 2-bromo-2'-methoxy-acetophenone **97g** (114 mg, 0.50 mmol, 1.2 eq.) were dissolved in dry ethanol (15 mL). The mixture was stirred under reflux for 6 h. The solvent was evaporated *in vacuo*. The remaining solid was dissolved in DCM (20 mL), washed with brine (3x15 mL), dried over Na₂SO₄, filtered, and evaporated to dryness. Purification was performed via recrystallization from methanol yielding the product as slightly yellow crystals.

Yield: 96 mg (64%)

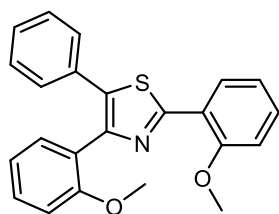
R_f (CyHex/EtOAc 7:3) = 0.72

¹H-NMR (400 MHz, CDCl₃-d₁): δ (ppm) 8.61 (dd, ³J = 7.8 Hz and ⁴J = 1.7 Hz, 1H, H6'), 8.46 (dd, ³J = 7.7 Hz and ⁴J = 1.8 Hz, 1H, H6), 8.02 (s, 1H, H_a), 7.41 (ddd, ³J = 8.3 Hz, ³J = 7.3 Hz and ⁴J = 1.8 Hz, 1H, H4), 7.32 (ddd, ³J = 8.2 Hz, ³J = 7.3 Hz and ⁴J = 1.8 Hz, 1H, H4'), 7.15–7.09 (m, 2H, H3 and H3'), 7.07–7.00 (m, 2H, H5 and H5'), 4.05 (s, 3H, CH₃), 3.98 (s, 3H, CH₃).

¹³C-NMR (101 MHz, CDCl₃-d₁): δ (ppm) 160.0 (C_c), 156.8 (C2 or C2'), 156.4 (C2 or C2'), 149.4 (C_e), 130.6 (C4 or C4'), 130.2 (C4 or C4'), 128.8 (2C, C6, C6'), 123.1 (C1 or C1'), 122.1 (C1 or C1'), 121.0 (C5 or C5'), 120.8 (C5 or C5'), 118.3 (C_a), 111.3 (C3 or C3'), 111.0 (C3 or C3'), 55.6 (CH₃), 55.4 (CH₃).

MS (APCI positive): *m/z* 298.2 [M+H]⁺, calcd for [C₁₇H₁₅NO₂S+H]⁺: *m/z* 298.1

MS (APCI negative) *m/z* 282.3 [M-CH₃]⁻, calcd for [C₁₇H₁₅NO₂S-CH₃]⁻: *m/z* 282.1

2,4-Bis(2-methoxyphenyl)-5-phenylthiazole (**107e**)C₂₃H₁₉NO₂SM_r = 373.47

According to general procedure F, the title compound was synthesized using **97b** (191 mg, 0.63 mmol, 1 eq.) and 2-methoxythiobenzamide **98b** (209 mg, 1.25 mmol, 2 eq) in DMF (2.4 mL). The reaction was complete after 3 h. Purification via flash column chromatography (CyHex/EtOAc 99:1–72:18) yielded the desired product as a white powder.

Yield: 41 mg (18%)

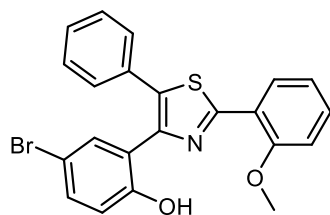
R_f (CyHex/EtOAc 8:2) = 0.65

¹H-NMR (400 MHz, CDCl₃-d₁): δ (ppm) 8.51 (dd, ³J = 7.8 Hz and ⁴J = 1.7 Hz, 1H, H6), 7.57 (dd, ³J = 7.5 Hz and ⁴J = 1.8 Hz, 1H, H6'), 7.39 (ddd, ³J = 8.3 Hz, ³J = 7.3 Hz and ⁴J = 1.8 Hz, 1H, H4'), 7.39–7.28 (m, 3H, H4, H2'', H6''), 7.29–7.16 (m, 3H, H3'', H4'', H5''), 7.08 (ddd, ³J = 7.8 Hz, ³J = 7.3 Hz and ⁴J = 1.1 Hz, 1H, H5), 7.09–6.98 (m, 2H, H3, H5'), 6.86 (dd, ³J = 8.3 Hz and ⁴J = 1.0 Hz, 1H, H3'), 4.06 (s, 3H, CH₃), 3.41 (s, 3H, CH₃').

¹³C-NMR (101 MHz, CDCl₃-d₁): δ (ppm) 155.0 (C_c), 152.2 (C2'), 151.6 (C2), 140.7 (C_e), 130.5 (C_a), 128.2 (C1''), 127.1 (C6'), 126.1 (C4), 125.1 (C4'), 123.9 (C6), 123.5 (2C, C2'', C6''), 123.3 (2C, C3'', C5''), 122.7 (C4''), 119.0* (C1), 116.7* (C1'), 116.4 (C5), 116.0 (C5'), 106.7 (C3'), 106.5 (C3), 50.9 (CH₃), 50.3 (CH₃').

MS (APCI positive): *m/z* 373.9 [M+H]⁺, calcd for [H]⁺: *m/z* 374.1

MS (APCI negative): *m/z* 358.1 [M-CH₃]⁻, calcd for [C₂₃H₁₉NO₂S-CH₃]⁻: *m/z* 358.1

4-Bromo-2-(2-(2-methoxyphenyl)-5-phenylthiazol-4-yl)phenol (**107c**)C₂₂H₁₆BrNO₂SM_r = 438.34

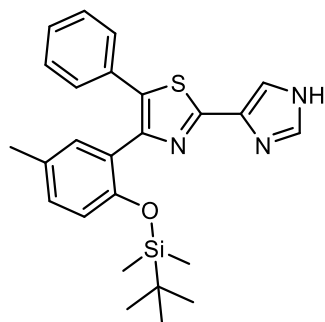
According to general procedure F, the title compound was synthesized using **97d** (50 mg, 0.17 mmol, 1 eq.) and 2-methoxythiobenzamide **98b** (35 mg, 0.21 mmol, 1.2 eq.) in 1.5 mL DMF. The reaction was complete after 4 h. Purification via flash column chromatography (CyHex/EtOAc 93:7–40:60) yielded the desired product as a white powder.

Yield: 41 mg (55%)

R_f (CyHex/EtOAc 7:3) = 0.65

¹H-NMR (400 MHz, DMSO-*d*₆): δ (ppm) 11.91 (s, 1H, OH'), 8.27 (dd, ³J = 7.8 Hz and ⁴J = 1.6 Hz, 1H, H₆), 7.51–7.45 (m, 6H, H₄, H_{phenyl}), 7.25 (dd, ³J = 8.5 Hz and ⁴J = 2.5 Hz, 1H, H_{4'}), 7.23 (dd, ⁴J = 2.5 Hz and ⁵J = 0.5 Hz, 1H, H_{6'}), 7.14 (ddd, ³J = 7.8 Hz, ³J = 7.4 Hz and ⁴J = 1.0 Hz, 1H, H₅), 7.08 (dd, ³J = 8.4 Hz and ⁴J = 1.0 Hz, 1H, H₃), 6.95 (dd, ³J = 8.5 Hz and ⁵J = 0.5 Hz, 1H, H_{3'}), 4.06 (s, 3H, CH₃).

¹³C-NMR (101 MHz, DMSO-*d*₆): δ (ppm) 160.0 (C_c), 156.5 (C₂), 155.7 (C_{2'}), 144.0 (C_c), 134.6 (C_{1''}), 132.2 (C_{6'}), 131.6 (C_{4'}), 131.4 (C_a), 130.8 (C₄), 129.7 (2C, C_{2''}, C_{6''} or C_{3''}, C_{5''}), 129.1 (2C, C_{2''}, C_{6''} or C_{3''}, C_{5''}), 128.9 (C_{4''}), 127.6 (C₆), 121.2 (C₅), 120.6 (C_{1'}), 119.8 (C₁), 119.4 (C_{3'}), 111.5 (C₃), 110.4 (C_{5'}), 55.6 (CH₃).

4-(2-((*Tert*-butyldimethylsilyl)oxy)-5-methylphenyl)-2-(1*H*-imidazol-4-yl)-5-phenylthiazole (**107b**)C₂₅H₂₉N₃OSSiM_r = 447.67

According to general procedure F, the title compound was synthesized using **97a** (200 mg, 0.48 mmol, 1 eq.) and 1*H*-imidazole-4-carbothioamide (73 mg, 0.57 mmol, 1.2 eq.) in DMF (2.6 mL). The reaction was complete after 5 h. In contrast to the other derivatives, cleavage of the protecting group was not observed under these conditions. Purification via flash column chromatography (DCM/methanol 98:2–90:10) yielded the desired product as a brownish-yellow oil.

Yield: 160 mg (75%)

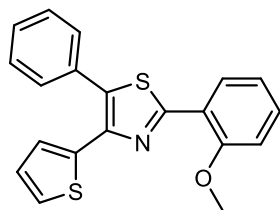
R_f (DCM/methanol 9:1) = 0.53

¹H-NMR (400 MHz, CDCl₃-*d*₁): δ (ppm) 7.57 (d, ³*J* = 1.1 Hz, 1H, H₂), 7.34–7.27 (m, 3H, H₄, H₂'', H₆''), 7.26–7.19 (m, 3H, H₃'', H₄'', H₅''), 7.15 (dd, ⁴*J* = 2.4 Hz and ⁴*J* = 0.7 Hz, 1H, H₆'), 7.07 (ddd, ³*J* = 8.2 Hz, ⁴*J*_{4'-6'} = 2.4 Hz and ⁴*J*_{4'-CH₃} = 0.7 Hz, 1H, H₄'), 6.76 (d, ³*J* = 8.3 Hz, 1H, H₃'), 2.25 (t, ⁴*J* = 0.7 Hz, 3H, (CH₃)_{ar}), 0.67 (s, 9H, (CH₃)_{*t*-butyl}), -0.06 (s, 6H, Si-CH₃). *The NH group is not visible in the spectrum.*

¹³C-NMR (101 MHz, CDCl₃-*d*₁): δ (ppm) 151.4 (2C, C_c, C_e), 147.6 (C₂'), 136.2 (C₂), 133.4 (C₁''), 132.0 (C_a), 132.0 (C₄'), 130.6 (C₅'), 130.4 (C₆'), 128.4 (2C, C₂'', C₆'' or C₃'', C₅''), 128.1 (2C, C₂'', C₆'' or C₃'', C₅''), 127.4 (C₄''), 126.8 (C₁'), 125.2 (C₅), 120.6 (C₄), 119.8 (C₃'), 25.3 (2C, (CH₃)_{*t*-butyl}), 20.4 ((CH₃)_{ar}), 17.8 (Si-C-C₃), -4.7 (2C, Si-CH₃).

MS (APCI positive): *m/z* 448.4 [M+H]⁺, calcd for [C₂₅H₂₉N₃OSSi+H]⁺: *m/z* 448.2

MS (ESI negative): *m/z* 446.2 [M-H]⁻, calcd for [C₂₅H₂₉N₃OSSi-H]⁻: *m/z* 446.2

2-(2-Methoxyphenyl)-5-phenyl-4-(thiophen-2-yl)thiazole (**107d**)C₂₀H₁₅NOS₂M_r = 349.47

According to general procedure F, the title compound was synthesized using **97e** (210 mg, 0.74 mmol, 1 eq.) and 2-methoxythiobenzamide **98b** (250 mg, 1.49 mmol, 2 eq.) in DMF (5.0 mL). The reaction was complete after 3 h. Purification via flash column chromatography (CyHex/EtOAc 95:5–85:15) yielded the desired product as a slightly yellow solid.

Yield: 215 mg (82%)

R_f (CyHex/EtOAc 8:2) = 0.70

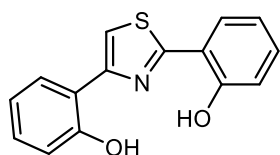
¹H-NMR (400 MHz, DMSO-*d*₆): δ (ppm) 8.36 (dd, ³*J* = 7.9 Hz and ⁴*J* = 1.8 Hz, 1H, H₆), 7.59–7.45 (m, 7H, H₄, H_{5'}, H_{phenyl}), 7.29 (dd, ³*J* = 8.5 Hz and ³*J* = 1.1 Hz, 1H, H₃), 7.18 (ddd, ³*J* = 7.9 Hz, ³*J* = 7.3 Hz and ⁴*J* = 1.1 Hz, 1H, H₅), 7.02 (dd, ³*J* = 3.7 Hz and ⁴*J* = 1.2 Hz, 1H, H_{3'}), 6.99 (dd, ³*J* = 5.0 Hz and ³*J* = 3.7 Hz, 1H, H_{4'}), 4.03 (s, 3H, CH₃).

¹³C-NMR (101 MHz, DMSO-*d*₆): δ (ppm) 159.3 (C_c), 156.6 (C₂), 143.0 (C_e), 138.0 (C_{1''}), 131.9 (C₄), 131.8 (C_a), 131.4 (C_{2'}), 130.3 (2C, C_{2''}, C_{6''} or C_{3''}, C_{5''}), 129.5 (2C, C_{2''}, C_{6''} or C_{3''}, C_{5''}), 129.4 (C_{4''}), 128.0 (C_{4'}), 127.6 (C₆), 126.9 (C_{5'}), 125.6 (C_{3'}), 121.5 (C₅), 121.1 (C₁), 112.7 (C₃), 56.4 (CH₃).

MS (APCI positive): *m/z* 350.3 [M+H]⁺, calcd for [C₂₀H₁₅NOS₂+H]⁺: *m/z* 350.1

MS (APCI negative): *m/z* 334.2 [M-CH₃]⁻, calcd for [C₂₀H₁₅NOS₂-CH₃]⁻: *m/z* 334.0

6.2.10.2 Final compounds

2,2'-(Thiazole-2,4-diyl)diphenol (**99c**)C₁₅H₁₁NO₂SM_r = 269.32

6 Experimental

According to general procedure A, **107a** (150 mg, 0.50 mmol, 1 eq.) was solubilized in freshly distilled DCM (3 mL). BBr₃ (1 M solution in dry DCM, 3.0 mL, 0.30 mmol, 6 eq.) was added dropwise at -78 °C. After completion of the reaction and work-up, purification was performed via flash column chromatography (DCM/methanol 99:1–90:10) yielding the desired product as a slightly yellow powder.

Yield: 120 mg (88%)

R_f (CyHex/EtOAc 8:2) = 0.35

¹H-NMR (400 MHz, DMSO-*d*₆): δ (ppm) 11.46 (s, 1H, OH), 11.09 (s, 1H, OH'), 8.23 (s, 1H, H_a), 8.11 (dd, ³J = 7.9 Hz and ⁴J = 1.7 Hz, 1H, H₆), 8.04 (dd, ³J = 7.8 Hz and ⁴J = 1.7 Hz, 1H, H_{6'}), 7.36 (ddd, ³J = 8.3 Hz, ³J = 7.2 Hz and ⁴J = 1.7 Hz, 1H, H₄), 7.23 (ddd, ³J = 8.2 Hz, ³J = 7.2 Hz and ⁴J = 1.7 Hz, 1H, H_{4'}), 7.07 (dd, ³J = 8.3 Hz and ⁴J = 1.1 Hz, 1H, H₃), 7.04–6.97 (m, 2H, H_{3'}, H₅), 6.99–6.90 (m, 1H, H_{5'}).

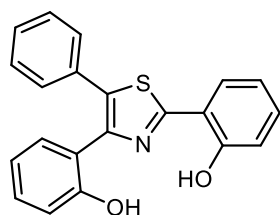
¹³C-NMR (101 MHz, DMSO-*d*₆): δ (ppm) 162.6 (C_c), 155.6 (C_{2'}), 155.6 (C₂), 150.8 (C_e), 131.7 (C₄), 129.7 (C_{4'}), 128.4 (C₆), 127.6 (C_{6'}), 120.1 (C₅), 119.8 (C_{5'}), 119.4 (C_{1'}), 119.0 (C₁), 117.1 (C₃), 117.0 (C_a), 116.6 (C_{3'}).

HRMS (ESI positive): *m/z* 270.0585 [M+H]⁺, calcd for [C₁₅H₁₁NO₂S+H]⁺: *m/z* 270.0583

HRMS (ESI negative): *m/z* 268.0439 [M-H]⁻, calcd for [C₁₅H₁₁NO₂S-H]⁻: *m/z* 268.0438

HPLC: *t_R* = 24.219 min (kinetex, 99.0%), *t_R* = 22.957 min (polar-RP, 98.5%)

2,2'-(5-Phenylthiazole-2,4-diyl)diphenol (**99b**)



C₂₁H₁₅NO₂S

M_r = 345.42

According to general procedure A, **107e** (31 mg, 0.08 mmol, 1 eq.) was solubilized in freshly distilled DCM (3.0 mL). BBr₃ (1 M solution in dry DCM, 0.50 mL, 0.50 mmol, 6 eq.) was added dropwise at -78 °C. After completion of the reaction and work-up, purification was performed via flash column chromatography (CyHex/EtOAc 95:5–30:70) yielding the desired product as a slightly yellow solid.

Yield: 14 mg (49%)

R_f (CyHex/EtOAc 8:2) = 0.48

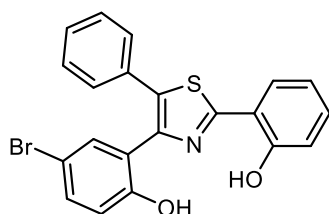
¹H-NMR (400 MHz, DMSO-*d*₆): δ (ppm) 11.46 (s, 1H, OH), 9.80 (s, 1H, OH'), 8.04 (dd, ³*J* = 7.9 Hz and ⁴*J* = 1.7 Hz, 1H, H6), 7.44–7.26 (m, 6H, H4, H_{phenyl}), 7.28–7.17 (m, 2H, H4', H6'), 7.06 (dd, ³*J* = 8.3 Hz and ⁴*J* = 1.1 Hz, 1H, H3), 6.99 (td, ³*J* = 7.9 Hz, ³*J* = 7.3 Hz and ⁴*J* = 1.1 Hz, 1H, H5), 6.91 (dd, ³*J* = 8.1 Hz and ⁴*J* = 1.1 Hz, 1H, H3'), 6.81 (td, ³*J* = 7.4 Hz, ³*J* = 7.4 Hz and ⁴*J* = 1.1 Hz, 1H, H5').

¹³C-NMR (101 MHz, DMSO-*d*₆): δ (ppm) 161.4 (C_e), 155.9 (C2'), 155.7 (C2), 146.5 (C_e), 133.8 (C_a), 132.3 (C1''), 131.7 (C4), 131.2 (C4'), 130.2 (C6'), 129.2 (2C, C2'', C6'' or C3'', C5''), 128.6 (2C, C2'', C6'' or C3'', C5''), 128.3 (C4''), 127.5 (C6), 122.0 (C1'), 120.1 (C5), 119.3 (C5'), 118.9 (C1), 117.1 (C3), 116.6 (C3').

HRMS (ESI negative): *m/z* 344.0749 [M-H]⁻, calcd for [C₂₁H₁₅NO₂S-[-H]]: *m/z* 344.0751

HPLC: *t_R* = 26.997 min (kinetex, 97.7%), *t_R* = 24.893 min (polar-RP, 97.0%)

4-Bromo-2-(2-(2-hydroxyphenyl)-5-phenylthiazol-4-yl)phenol (**99a**)



C₂₁H₁₄BrNO₂S

M_r = 424.31

According to general procedure A, **107c** (27 mg, 0.06 mmol, 1 eq.) was solubilized in freshly distilled DCM (1.0 mL). BBr₃ (1 M solution in dry DCM, 180 μ L, 0.18 mmol, 3 eq.) was added dropwise at -78 °C. After completion of the reaction and work-up, purification was performed via flash column chromatography (CyHex/EtOAc 90:10–60:40) yielding the desired product as a white powder.

Yield: 8 mg (31%)

R_f (CyHex/EtOAc 7:3) = 0.45

¹H-NMR (DMSO-*d*₆, 400 MHz): δ (ppm) 11.34 (s, 1H, OH'), 10.05 (s, 1H, OH), 8.08 (dd, ³*J* = 7.9 Hz and ⁴*J* = 1.7 Hz, 1H, H6), 7.42–7.32 (m, 8H, H4, H4', H6', H_{phenyl}), 7.06

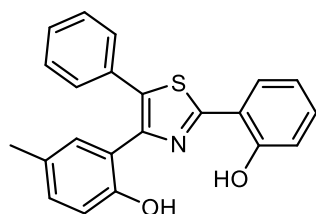
(dd, $^3J = 8.3$ Hz and $^4J = 1.1$ Hz, 1H, H3), 6.98 (ddd, $^3J = 7.9$ Hz, $^3J = 7.4$ Hz and $^4J = 1.1$ Hz, 1H, H5), 6.88–6.83 (m, 1H, H3').

^{13}C -NMR (101 MHz, DMSO- d_6): δ (ppm) 161.2 (C_c), 155.5 (C_2), 155.2 (C_2'), 144.9 (C_e), 134.7 (C_1''), 133.4 (C_6'), 132.7 (C_4'), 132.2 (C_a), 131.7 (C_4), 129.2 (2C, C_2'' , C_6'' or C_3'' , C_5''), 128.5 (2C, C_2'' , C_6'' or C_3'' , C_5''), 127.5 (C_6), 124.7 (C_1'), 120.1 (C_5), 119.2 (C_1), 118.7 (C_3'), 117.0 (C_3), 110.1 (C_5').

HRMS (ESI negative): m/z 421.9852 [$\text{M}-\text{H}$] $^-$, calcd for [$\text{C}_{21}\text{H}_{14}^{79}\text{BrNO}_2\text{S}-\text{H}$] $^-$: m/z 421.9856

HPLC: $t_R = 28.605$ min (kinetex, 98.3%), $t_R = 28.651$ min (hydro-RP, 98.9%)

2-(2-(2-Hydroxyphenyl)-5-phenylthiazol-4-yl)-4-methylphenol (**99g**)



$\text{C}_{22}\text{H}_{17}\text{NO}_2\text{S}$

$M_r = 359.44$

According to general procedure F, the title compound was synthesized using **97a** (228 mg, 0.42 mmol, 1 eq.) and 2-hydroxybenzothioamide (100 mg, 0.65 mmol, 1.2 eq.) in DMF (1.8 mL). The reaction was complete after 6 h. Purification via flash column chromatography (CyHex/EtOAc 93:7–80:20) yielded the desired product as a yellow solid.

Yield: 78 mg (40%)

R_f (CyHex/EtOAc 8:2) = 0.37

^1H -NMR (DMSO- d_6 , 400 MHz): δ (ppm) 11.44 (bs, 1H, OH), 9.50 (bs, 1H, OH'), 8.04 (dd, $^3J = 7.9$ Hz and $^4J = 1.7$ Hz, 1H, H6), 7.39–7.30 (m, 6H, H4, H_{phenyl}), 7.07–7.02 (m, 3H, H3, H4', H6'), 6.98 (ddd, $^3J = 8.2$ Hz, $^3J = 7.2$ Hz and $^4J = 1.1$ Hz, 1H, H5), 6.81–6.78 (m, 1H, H3'), 2.17 (s, 3H, CH_3).

^{13}C -NMR (101 MHz, DMSO- d_6): δ (ppm) 161.3 (C_c), 155.7 (C_2'), 153.5 (C_2), 146.6 (C_e), 133.7 (C_1''), 132.4 (C_a), 131.7 (C_4), 131.4 (C_6'), 130.7 (C_4'), 129.1 (2C, C_2'' , C_6'')

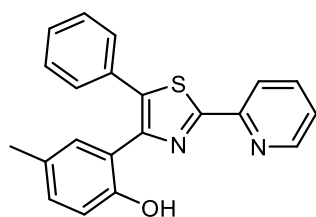
or C3'', C5''), 128.5 (2C, C2'', C6'' or C3'', C5''), 128.3 (C4''), 127.7 (C5'), 127.5 (C6), 121.7 (C1'), 120.0 (C5), 118.9 (C1), 117.1 (C3), 116.4 (C3'), 20.4 (CH₃).

HRMS (ESI positive): m/z 360.1057 [M+H]⁺, calcd for [C₂₂H₁₇NO₂S+H]⁺: m/z 360.1053

HRMS (ESI negative): m/z 358.0908 [M-H]⁻, calcd for [C₂₂H₁₇NO₂S-H]⁻: m/z 358.0907

HPLC: t_R = 28.252 min (kinetex, 99.8%), t_R = 25.242 min (polar-RP, 99.8%)

4-Methyl-2-(5-phenyl-2-(pyridin-2-yl)thiazol-4-yl)phenol (**99d**)



C₂₁H₁₆N₂OS

M_r = 344.43

In a variation of general procedure F, the reaction was carried out at r.t. instead of 65 °C to avoid decomposition of the thioamide. The title compound was synthesized using **97a** (146 mg, 0.35 mmol, 1 eq.) and pyridine-2-carbothioamide (63 mg, 0.45 mmol, 1.3 eq.) in DMF (2.0 mL). The reaction was complete after 18 h. Purification via flash column chromatography (CyHex/EtOAc 90:10–87:13) followed by reversed-phase flash column chromatography (water/ACN 50:50–0:100) yielded the desired product as a yellow solid.

Yield: 14 mg (12%)

R_f (CyHex/EtOAc 7:3) = 0.53

¹H-NMR (400 MHz, DMSO-*d*₆): δ (ppm) 9.26 (s, 1H, OH'), 8.67 (ddd, ³ J = 4.8 Hz, ⁴ J = 1.7 Hz and ⁵ J = 1.0 Hz, 1H, H3), 8.13 (dt, ³ J = 7.7 Hz, ⁴ J = 1.0 Hz and ⁵ J = 1.0 Hz, 1H, H6), 7.98 (td, ³ J = 7.7 Hz, ³ J = 7.7 Hz and ⁴ J = 1.7 Hz, 1H, H5), 7.52 (ddd, ³ J = 7.7 Hz, ³ J = 4.8 Hz and ⁴ J = 1.0 Hz, 1H, H4), 7.40–7.30 (m, 5H, H_{phenyl}), 7.11–7.08 (m, 1H, H6), 7.05 (ddd, ³ J = 8.2 Hz, ⁴ $J_{6'-4'}$ = 2.3, and ⁴ $J_{6'-CH_3}$ = 0.8 Hz, 1H, H6'), 6.77 (d, ³ J = 8.2 Hz, 1H, H3'), 2.21 (t, ⁴ J = 0.8 Hz, 3H, CH₃).

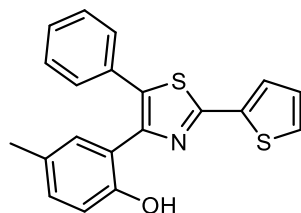
¹³C-NMR (101 MHz, DMSO-*d*₆): δ (ppm) 165.4 (C_c), 153.3 (C2'), 150.9 (C2), 150.2 (C6), 149.3 (C_e), 138.2 (C4), 136.6 (C1''), 132.5 (C_a), 131.7 (C6'), 130.7 (C4'), 129.1 (2C,

C2'', C6'' or C3'', C5''), 128.5 (C4''), 128.3 (2C, C2'', C6'' or C3'', C5''), 127.7 (C5'), 125.5 (C5), 122.4 (C1'), 119.3 (C3), 116.2 (C3'), 20.4 (CH₃).

HRMS (ESI positive): m/z 345.1059 [M+H]⁺, calcd for [C₂₁H₁₆N₂OS+H]⁺: m/z 345.1056

HPLC: t_R = 28.359 min (kinetex, 96.5%), t_R = 25.124 min (polar-RP, 95.4%)

4-Methyl-2-(5-phenyl-2-(thiophen-2-yl)thiazol-4-yl)phenol (**99f**)



C₂₀H₁₅NOS₂

M_r = 349.47

According to general procedure F, the title compound was synthesized using **97a** (65 mg, 0.16 mmol, 1 eq.) and thiophene-2-carbothioamide (27 mg, 0.19 mmol, 1.2 eq.) in DMF (1.0 mL). The reaction was complete after 18 h. Purification via flash column chromatography (CyHex/EtOAc 80:20–70:30) followed by reversed-phase flash column chromatography (water/ACN 50:50–0:100) yielded the final product as a yellow solid.

Yield: 16 mg (30%)

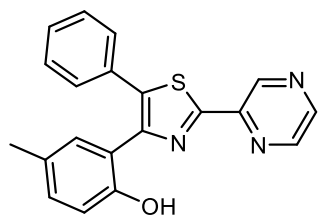
R_f (CyHex/EtOAc 7:3) = 0.68

¹H-NMR (400 MHz, DMSO-*d*₆): δ (ppm) 9.29 (s, 1H, OH'), 7.75 (dd, ³*J* = 5.1 Hz and ⁴*J* = 1.2 Hz, 1H, H5), 7.71 (dd, ³*J* = 3.7 Hz and ⁴*J* = 1.2 Hz, 1H, H3), 7.36–7.26 (m, 5H, H_{phenyl}), 7.21 (dd, ³*J* = 5.1 Hz and ³*J* = 3.7 Hz, 1H, H4), 7.07–7.01 (m, 2H, H4', H6'), 6.77 (d, ³*J* = 8.8 Hz, 1H, H3'), 2.20 (s, 3H, CH₃).

¹³C-NMR (101 MHz, DMSO-*d*₆): δ (ppm) 158.0 (C_c), 153.4 (C2'), 148.3 (C_c), 136.8 (C1''), 133.5 (C_a), 132.1 (C2), 131.6 (C6'), 130.8 (C4'), 129.4 (C4), 129.1 (2C, C2'', C6'' or C3'', C5''), 129.0 (C5), 128.4 (C4''), 128.2 (2C, C2'', C6'' or C3'', C5''), 127.8 (C5'), 127.7 (C3), 122.0 (C1'), 116.2 (C3'), 20.4 (CH₃).

HRMS (ESI positive): m/z 350.0667 [M+H]⁺, calcd for [C₂₀H₁₅NOS₂+H]⁺: m/z 350.0668

HPLC: t_R = 30.080 min (kinetex, 99.8%), t_R = 26.392 min (polar-RP, 99.5%)

4-Methyl-2-(5-phenyl-2-(pyrazin-2-yl)thiazol-4-yl)phenol (**99k**)C₂₀H₁₅N₃OSM_r = 345.42

According to general procedure F, the title compound was synthesized using **97a** (42 mg, 0.10 mmol, 1 eq.) and pyrazine-2-thiocarboxamide (17 mg, 0.12 mmol, 1.2 eq.) in DMF (0.4 mL). The reaction was complete after 18 h. Purification via flash column chromatography (CyHex/EtOAc, 85:15–80:20) yielded the final product as a yellow solid.

Yield: 3 mg (9%)

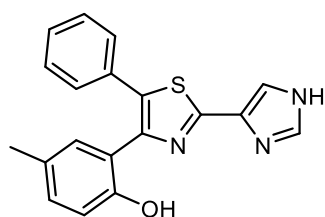
R_f (CyHex/EtOAc 7:3) = 0.45

¹H-NMR (400 MHz, DMSO-*d*₆): δ (ppm) 9.32 (d, ⁴*J* = 1.5 Hz, 1H, H₆), 9.26 (s, 1H, OH'), 8.77 (d, ³*J* = 2.6 Hz, 1H, H₃), 8.75 (dd, ³*J* = 2.6 Hz and ⁴*J* = 1.5 Hz, 1H, H₅), 7.42–7.29 (m, 5H, H_{phenyl}), 7.11 (dd, ⁴*J*_{6'-4'} = 2.3 Hz and ⁴*J*_{6'-CH₃} = 0.8 Hz, 1H, H_{6'}), 7.06 (ddd, ³*J* = 8.2 Hz, ⁴*J*_{4'-6'} = 2.3 Hz and ⁴*J*_{4'-CH₃} = 0.8 Hz, 1H, H_{4'}), 6.78 (d, ³*J* = 8.2 Hz, 1H, H_{3'}), 2.22 (bs, 3H, CH₃).

¹³C-NMR (101 MHz, DMSO-*d*₆): δ (ppm) 162.7 (C_c), 153.4 (C_{2'}), 150.0 (C_e), 146.3 (C₂), 146.1 (C₃), 145.0 (C₆), 140.7 (C₅), 137.7 (C_{1''}), 132.1 (C_a), 131.7 (C_{6'}), 130.9 (C_{4'}), 129.2 (2C, C_{2''}, C_{6''} or C_{3''}, C_{5''}), 128.7 (C_{4''}), 128.3 (2C, C_{2''}, C_{6''} or C_{3''}, C_{5''}), 127.8 (C_{5'}), 122.1 (C_{1'}), 116.2 (C_{3'}), 20.4 (CH₃).

HRMS (ESI positive): *m/z* 346.1005 [M+H]⁺, calcd for [C₂₀H₁₅N₃OS+H]⁺; *m/z* 346.1009

HPLC: *t_R* = 14.774 min (kinetex, 95.1%), *t_R* = 24.617 min (polar-RP, 97.3%)

2-(2-(1H-imidazol-4-yl)-5-phenylthiazol-4-yl)-4-methylphenol (**99e**)C₁₉H₁₅N₃OSM_r = 333.41

6 Experimental

To a solution of **107b** (150 mg, 0.34 mmol, 1 eq.) in dry THF (1.6 mL) TBAF (1 M solution in THF, 500 μ L, 0.50 mmol, 1.5 eq.) was added at 0 °C. The solution was stirred for 2 h while slowly warming to r.t. The solvent was evaporated *in vacuo*. Purification via flash column chromatography (DCM/methanol 99.5:0.5–92:8) followed by semi-preparative HPLC (water/ACN + 0.05% TFA, 0–4 min: 50:50, 4–20 min: 50:50–20:80) yielded the final product as an off-white solid.

Yield: 17 mg (15%)

R_f (CyHex/EtOAc 7:3) = 0.61

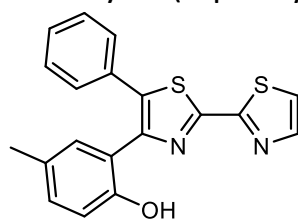
¹H-NMR (400 MHz, DMSO-*d*₆): δ (ppm) δ 9.40 (bs, 1H, OH'), 8.24 (s, 1H, H₂), 7.97 (s, 1H, H₄), 7.37–7.28 (m, 5H, H_{phenyl}), 7.07–6.99 (m, 2H, H_{4'}, H_{6'}), 6.80–6.73 (m, 1H, H_{3'}), 2.17 (s, 3H, CH₃). The NH group is not visible in the spectrum.

¹³C-NMR (101 MHz, DMSO-*d*₆): δ (ppm) 153.4 (2C, C_c, C_e), 148.1 (C_{2'}), 137.0 (C₂), 132.3 (C_{1''}), 131.5 (C_{6'}), 130.6 (C_{4'}), 129.1 (2C, C_{2''}, C_{6''} or C_{3''}, C_{5''}), 128.3 (2C, C_{2''}, C_{6''} or C_{3''}, C_{5''}), 128.3 (C_{4''}), 127.6 (C_{5'}), 125.2 (C₅), 122.0 (C_{1'}), 120.6 (C₄), 116.3 (C_{3'}), 20.4 (CH₃).

HRMS (ESI positive): m/z 334.1011 [M+H]⁺, calcd for [C₁₉H₁₅N₃OS+H]⁺: m/z 334.1009

HPLC: t_R = 17.306 min (kinetex, >99.9%), t_R = 18.676 min (polar-RP, 99.9%)

4-Methyl-2-(5-phenyl-[2,2'-bithiazol]-4-yl)phenol (**99I**)



C₁₉H₁₄N₂OS₂

M_r = 350.45

According to general procedure F, the title compound was synthesized using **97a** (300 mg, 0.72 mmol, 1 eq.) and 2-thiazolecarbothioamide (124 mg, 0.86 mmol, 1.2 eq.) in DMF (2.8 mL). The reaction was complete after 5 h. Purification via flash column chromatography (CyHex/EtOAc 80:20–65:35) followed by reversed-phase

flash column chromatography (ACN/methanol 90:10) yielded the final product as a yellow solid.

Yield: 27 mg (11%)

R_f (CyHex/EtOAc 8:2) = 0.45

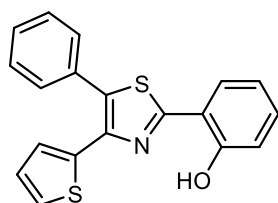
$^1\text{H-NMR}$ (400 MHz, DMSO- d_6): δ (ppm) 9.30 (s, 1H, OH'), 8.06 (d, 3J = 3.2 Hz, 1H, H4), 8.00 (d, 3J = 3.2 Hz, 1H, H5), 7.45–7.33 (m, 5H, H_{phenyl}), 7.15–7.06 (m, 2H, H4', H6'), 6.81 (d, 3J = 8.1 Hz, 1H, H3'), 2.25 (d, 4J = 0.7 Hz, 3H, CH₃).

$^{13}\text{C-NMR}$ (101 MHz, DMSO- d_6): δ (ppm) 161.0 (C2), 157.7 (C_c), 153.3 (C2'), 149.3 (C_e), 144.6 (C4), 136.4 (C1''), 131.8 (C_a), 131.7 (C6'), 130.9 (C4'), 129.2 (2C, C2'', C6'' or C3'', C5''), 128.8 (C4''), 128.3 (2C, C2'', C6'' or C3'', C5''), 127.9 (C5'), 123.2 (C5), 121.9 (C1'), 116.2 (C3'), 20.4 (CH₃).

HRMS (ESI positive): m/z 351.0625 [M+H]⁺, calcd for [C₁₉H₁₄N₂OS₂+H]⁺: m/z 351.0620

HPLC: t_R = 27.310 min (kinetex, 97.6%), t_R = 24.785 min (polar-RP, 98.7%)

2-(5-Phenyl-4-(thiophen-2-yl)thiazol-2-yl)phenol (**99h**)



C₁₉H₁₃NOS₂

M_r = 335.44

According to general procedure A, **107d** (200 mg, 0.57 mmol, 1 eq.) was solubilized in freshly distilled DCM (7.0 mL). BBr₃ (1 M solution in dry DCM, 1.72 mL, 1.72 mmol, 3 eq.) was added dropwise at -78 °C. After completion of the reaction and work-up, purification was performed via flash column chromatography (CyHex/EtOAc 99:1–97.5:2.5) followed by recrystallization from methanol yielding the desired product as light-yellow needles.

Yield: 30 mg (16%)

R_f (CyHex/EtOAc 8:2) = 0.72

¹H-NMR (400 MHz, DMSO-*d*₆): δ (ppm) 11.25 (s, 1H, OH), 8.20 (dd, $^3J = 7.9$ Hz and $^4J = 1.6$ Hz, 1H, H6), 7.59–7.48 (m, 6H, H5', H_{phenyl}), 7.36 (dt, $^3J = 8.0$ Hz, $^4J = 1.6$ Hz and $^5J = 0.9$ Hz, 1H, H4), 7.07 (d, $^3J = 8.2$ Hz, 1H, H3), 7.05–6.97 (m, 3H, H5, H3', H4').

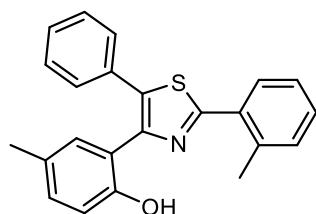
¹³C-NMR (101 MHz, DMSO-*d*₆): δ (ppm) 161.2 (C_c), 155.5 (C2), 142.7 (C_e), 137.8 (C2'), 131.8 (C4) 131.4 (C1'), 131.3 (C_a), 130.3 (2C, C2'', C6'' or C3'', C5''), 129.5 (2C, C2'', C6'' or C3'', C5''), 129.4 (C4''), 128.0 (C4'), 127.6 (C6), 126.9 (C5'), 125.7 (C3'), 120.0 (C5), 119.2 (C1), 116.9 (C3).

HRMS (ESI positive): m/z 336.0505 [M+H]⁺, calcd for [C₁₉H₁₃NOS₂+H]⁺: m/z 336.0511

HRMS (ESI negative): m/z 334.0367 [M-H]⁻, calcd for [C₁₉H₁₃NOS₂-H]⁻: m/z 334.0366

HPLC: $t_R = 31.005$ min (kinetex, 99.8%), $t_R = 27.115$ min (polar-RP, 99.8%)

4-Methyl-2-(5-phenyl-2-(*o*-tolyl)thiazol-4-yl)phenol (**99j**)



C₂₃H₁₉NOS

M_r = 357.47

According to general procedure F, the title compound was synthesized using **97a** (272 mg, 0.65 mmol, 1 eq.) and 2-methylthiobenzamide (118 mg, 0.78 mmol, 1.2 eq.) in DMF (2.0 mL). The reaction was complete after 18 h. Purification via flash column chromatography (CyHex/DCM 85:15–80:20) yielded the final product as a yellow solid.

Yield: 175 mg (76%)

R_f (CyHex/EtOAc 7:3) = 0.69

¹H-NMR (400 MHz, DMSO-*d*₆): δ (ppm) 9.38 (s, 1H, OH'), 7.87–7.79 (m, 1H, H6), 7.42–7.30 (m, 8H, H3, H4, H5, H_{phenyl}), 7.10–7.06 (m, 1H, H6'), 7.03 (ddd, $^3J = 8.1$ Hz, $^4J_{4'-6'} = 2.3$ Hz and $^4J_{4'-CH3} = 0.8$ Hz, 1H, H4'), 6.77 (d, $^3J = 8.2$ Hz, 1H, H3'), 2.63 (s, 3H, CH₃), 2.18 (s, 3H, CH₃').

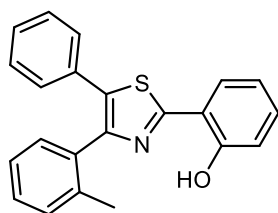
¹³C-NMR (101 MHz, DMSO-*d*₆): δ (ppm) 164.0 (C_c), 153.4 (C2'), 148.1 (C_e), 136.2 (C1''), 134.6 (C_a), 132.4 (C1), 132.3 (C2), 132.1 (C3), 131.5 (C6'), 130.6 (C4'), 130.1 (C4),

129.8 (C6), 129.1 (2C, C2'', C6'' or C3'', C5''), 128.4 (2C, C2'', C6'' or C3'', C5''), 128.4 (C4''), 127.7 (C5'), 126.9 (C5), 122.0 (C1'), 116.3 (C3'), 21.7 (CH₃), 20.5 (CH₃').

HRMS (ESI positive): m/z 358.1256 [M+H]⁺, calcd for [C₂₃H₁₉NOS+H]⁺: m/z 358.1260

HPLC: t_R = 31.923 min (kinetex, 96.7%), t_R = 27.105 min (polar-RP, 98.7%)

2-(5-Phenyl-4-(*o*-tolyl)thiazol-2-yl)phenol (**99i**)



C₂₂H₁₇NOS

M_r = 343.44

To a solution of **97c** (164 mg, 0.57 mmol, 1 eq.) in ethanol 2-hydroxythiobenzamide (104 mg, 0.68 mmol, 1.2 eq.) and copper acetate (23 mg, 0.11 mmol, 0.2 eq.) were added. The mixture was stirred at r.t. for 20 h. An orange solid was filtered off and discarded. The filtrate was evaporated to dryness. The residue was taken up in EtOAc (15 mL), washed with a diluted aqueous ammonia solution (15 mL) and brine (15 mL), dried over Na₂SO₄, filtered, and evaporated to dryness. Purification via flash column chromatography (CyHex/DCM 90:10–70:30) followed by recrystallisation from methanol yielded the final product as a yellow solid.

Yield: 24 mg (12%)

R_f (CyHex/EtOAc 7:3) = 0.79

¹H-NMR (400 MHz, DMSO-*d*₆): δ (ppm) 11.32 (s, 1H, OH), 8.10 (dd, ³ J = 7.9 Hz and ⁴ J = 1.7 Hz, 1H, H6), 7.37–7.22 (m, 10H, H4, H_{phenyl}, H_{tolyl}), 7.06 (dd, ³ J = 8.3 Hz and ⁴ J = 1.1 Hz, 1H, H3), 6.97 (ddd, ³ J = 7.9 Hz, ³ J = 7.2 Hz and ⁴ J = 1.1 Hz, 1H, H5), 2.09 (s, 3H, CH₃).

¹³C-NMR (101 MHz, DMSO-*d*₆): δ (ppm) 161.1 (C_c), 155.6 (C2), 149.2 (C_e), 136.9 (C2'), 135.4 (C1''), 133.8 (C_a), 131.9 (C1'), 131.6 (C4), 130.8 (C3'), 130.7 (C4'), 129.3 (2C, C2'', C6'' or C3'', C5''), 128.8 (C4''), 128.6 (2C, C2'', C6'' or C3'', C5''), 128.3 (C6'), 127.6 (C5), 126.3 (C5'), 120.0 (C6), 119.4 (C1), 117.0 (C3), 20.0 (CH₃).

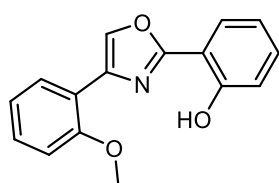
HRMS (ESI positive): m/z 344.1104 [M+H]⁺, calcd for [C₂₂H₁₇NOS]⁺: m/z 344.1104

HPLC: t_R = 31.569 min (kinetex, 95.4%), t_R = 27.255 min (polar-RP, 96.8%)

6.2.11 Oxazoles

6.2.11.1 Protected oxazoles

2-(4-(2-Methoxyphenyl)oxazol-2-yl)phenol (**108c**)



$C_{16}H_{13}NO_3$

$M_r = 267.28$

According to general procedure G, the title compound was synthesized using 2-bromo-2'-methoxyacetophenone (300 mg, 1.31 mmol, 1 eq.), salicylamide (180 mg, 1.31 mmol, 1 eq.) and $AgSbF_6$ (495 mg, 1.44 mmol, 1.1 eq.) in EtOAc (2.6 mL). The reaction was performed at 65 °C under μW -irradiation for 2 h. Purification via flash column chromatography (CyHex/EtOAc 95:5–50:50) followed by recrystallization from 2-propanol yielded the desired product as light-yellow crystals.

Yield: 33 mg (9%)

R_f (CyHex/EtOAc 7:3) = 0.72

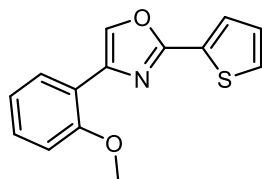
1H -NMR (400 MHz, DMSO- d_6): δ (ppm) 11.09 (s, 1H, OH), 8.58 (s, 1H, H_a), 8.02 (dd, 3J = 7.7 Hz and 4J = 1.7 Hz, 1H, H6'), 7.89 (dd, 3J = 7.9 Hz and 4J = 1.7 Hz, 1H, H6), 7.46 (ddd, 3J = 8.5 Hz, 3J = 7.5 Hz and 4J = 1.7 Hz, 1H, H4), 7.40 (ddd, 3J = 8.3 Hz, 3J = 7.5 Hz and 4J = 1.7 Hz, 1H, H4'), 7.18 (dd, 3J = 8.3 Hz and 4J = 1.0 Hz, 1H, H3'), 7.15–7.09 (m, 2H, H3, H5'), 7.05 (ddd, 3J = 8.5 Hz, 3J = 7.9 Hz and 4J = 1.1 Hz, 1H, H5), 3.98 (s, 3H, CH₃).

^{13}C -NMR (101 MHz, DMSO- d_6): δ (ppm) 160.0 (C_c), 156.8 (C_2), 156.6 (C_2'), 137.2 (C_a), 135.3 (C_e), 133.2 (C_4), 129.8 (C_4'), 127.4 (C_6'), 126.9 (C_6), 121.2 (C_5), 120.3 (C_5'), 118.5 (C_1'), 117.4 (C_3), 111.7 (C_3'), 111.2 (C_1), 56.0 (CH₃).

MS (ESI positive): m/z 268.3 [$M+H$]⁺, calcd for [$C_{16}H_{13}NO_3+H$]⁺: m/z 268.1

MS (ESI negative): m/z 266.3 [$M-H$]⁻, calcd for [$C_{16}H_{13}NO_3-H$]⁻: m/z 266.1

HPLC: t_R = 23.166 min (kinetex, 96.8%), t_R = 29.231 min (hydro-RP, 97.5%)

4-(2-Methoxyphenyl)-2-(thiophen-2-yl)oxazole (**108a**) $\text{C}_{14}\text{H}_{11}\text{NO}_2\text{S}$ $M_r = 257.31$

According to general procedure G, the title compound was synthesized using 2-bromo-2'-methoxyacetophenone (50 mg, 0.22 mmol, 1 eq.), thiophene-2-carboxamide **100** (28 mg, 0.22 mmol, 1 eq.) and AgSbF_6 (83 mg, 0.24 mmol, 1.1 eq.) in EtOAc (0.9 mL). The reaction was performed at 70 °C under μW -irradiation for 1.5 h. Purification via flash column chromatography (CyHex/EtOAc 95:5–60:40) followed by recrystallization from 2-propanol yielded the desired product as light-yellow crystals.

Yield: 6 mg (11%)

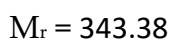
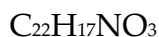
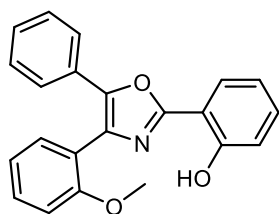
R_f (CyHex/EtOAc 8:2) = 0.65

^1H -NMR (400 MHz, $\text{DMSO}-d_6$): δ (ppm) 8.45 (s, 1H, H_a), 8.05 (dd, $^3J = 7.5$ Hz and $^4J = 1.8$ Hz, 1H, $\text{H}_{6'}$), 7.84 (dd, $^3J = 5.0$ Hz and $^4J = 1.2$ Hz, 1H, H_5), 7.78 (dd, $^3J = 3.7$ Hz and $^4J = 1.2$ Hz, 1H, H_3), 7.36 (ddd, $^3J = 8.4$ Hz, $^3J = 7.5$ Hz and $^4J = 1.8$ Hz, 1H, $\text{H}_{4'}$), 7.26 (dd, $^3J = 5.0$ Hz and $^3J = 3.7$ Hz, 1H, H_4), 7.15 (dd, $^3J = 8.4$ Hz and $^4J = 1.1$ Hz, 1H, $\text{H}_{3'}$), 7.09 (td, $^3J = 7.5$ Hz, $^3J = 7.5$ Hz and $^4J = 1.1$ Hz, 1H, $\text{H}_{5'}$), 3.96 (s, 3H, CH_3).

^{13}C -NMR (101 MHz, $\text{DMSO}-d_6$): δ (ppm) 156.6 ($\text{C}_{2'}$), 156.5 (C_c), 137.5 (C_a), 136.8 (C_e), 130.2 (C_5), 129.5 ($\text{C}_{4'}$), 129.4 (C_2), 129.0 (C_4), 128.7 (C_3), 127.5 ($\text{C}_{6'}$), 121.0 ($\text{C}_{5'}$), 119.3 ($\text{C}_{1'}$), 111.6 ($\text{C}_{3'}$), 55.9 (CH_3).

MS (APCI positive): m/z 258.1 $[\text{M}+\text{H}]^+$, calcd for $[\text{C}_{14}\text{H}_{11}\text{NO}_2\text{S}+\text{H}]^+$: m/z 258.1

MS (APCI negative): m/z 256.0 $[\text{M}-\text{H}]^-$, calcd for $[\text{C}_{14}\text{H}_{11}\text{NO}_2\text{S}-\text{H}]^-$: m/z 256.0

2-(4-(2-Methoxyphenyl)-5-phenyloxazol-2-yl)phenol (**108b**)

According to general procedure G, the title compound was synthesized using **97b** (200 mg, 0.66 mmol, 1 eq.), salicylamide (90 mg, 0.66 mmol, 1 eq.) and AgSbF_6 (248 mg, 0.72 mmol, 1.1 eq) in EtOAc (1.0 mL). The reaction was performed at 60 °C under μW -irradiation for 4 h. Purification via flash column chromatography (CyHex/EtOAc 99:1–80:20) followed by recrystallization from 2-propanol yielded the desired product as a white solid.

Yield: 35 mg (16%)

R_f (CyHex/EtOAc 8:2) = 0.68

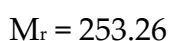
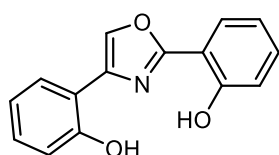
^1H -NMR (400 MHz, $\text{DMSO}-d_6$): δ (ppm) 10.95 (s, 1H, OH), 8.04 (dd, $^3J = 7.9$ Hz and $^4J = 1.6$ Hz, 1H, H6), 7.55–7.49 (m, 4H, H4', H6', H2'', H6''), 7.49–7.36 (m, 4H, H4, H3'', H4'', H5''), 7.21–7.17 (m, 1H, H3'), 7.15–7.05 (m, 3H, H3, H5, H5'), 3.62 (s, 3H, CH_3).

^{13}C -NMR (101 MHz, $\text{DMSO}-d_6$): δ (ppm) 159.2 (C_c), 157.2 (C_2), 156.8 (C_2'), 145.4 (C_a), 133.1 (C_4), 131.5 (C_e), 131.4 (C_6'), 131.3 (C_4'), 129.1 (2C, C_3'' , C_5''), 129.0 (C_4''), 128.3 (C_1''), 126.9 (C_6), 125.4 (2C, C_2'' , C_6''), 121.2 (C_5'), 120.5 (C_1'), 120.3 (C_5), 117.3 (C_3), 112.3 (C_3'), 111.1 (C_1), 55.7 (CH_3).

MS (APCI positive): m/z 344.2 $[\text{M}+\text{H}]^+$, calcd for $[\text{C}_{22}\text{H}_{17}\text{NO}_3+\text{H}]^+$: m/z 344.1

MS (APCI negative): m/z 342.2 $[\text{M}-\text{H}]^-$, calcd for $[\text{C}_{22}\text{H}_{17}\text{NO}_3-\text{H}]^-$: m/z 342.1

6.2.11.2 Final compounds

2,2'-(Oxazole-2,4-diyl)diphenol (**109c**)

According to general procedure A, 108c (20 mg, 0.07 mmol, 1 eq.) was solubilized in freshly distilled DCM (0.5 mL). BBr₃ (1 M solution in dry DCM, 225 µL, 0.22 mmol, 3 eq.) was added dropwise at -78 °C. After completion of the reaction, the mixture was worked up yielding the desired product as a white powder without further purification.

Yield: 19 mg (100%)

R_f (CyHex/EtOAc 7:3) = 0.46

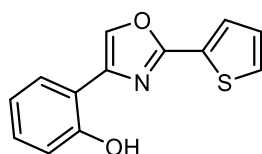
¹H-NMR (400 MHz, DMSO-*d*₆): δ (ppm) 11.16 (s, 1H, OH), 10.60 (s, 1H, OH'), 8.50 (s, 1H, H_a), 7.91 (dd, ³J = 7.6 Hz and ⁴J = 1.7 Hz, 1H, H6'), 7.88 (dd, ³J = 7.9 Hz and ⁴J = 1.7 Hz, 1H, H6), 7.46 (ddd, ³J = 8.3 Hz, ³J = 7.3 Hz and ⁴J = 1.7 Hz, 1H, H4), 7.22 (ddd, ³J = 8.3 Hz, ³J = 7.3 Hz and ⁴J = 1.7 Hz, 1H, H4'), 7.10 (dd, ³J = 8.3 Hz and ⁴J = 1.1 Hz, 1H, H3), 7.05 (ddd, ³J = 7.9 Hz, ³J = 7.3 Hz and ⁴J = 1.1 Hz, 1H, H5), 6.99 (dd, ³J = 8.3 Hz and ⁴J = 1.1 Hz, 1H, H3'), 6.97 (ddd, ³J = 7.6 Hz, ³J = 7.3 Hz and ⁴J = 1.1 Hz, 1H, H5').

¹³C-NMR (101 MHz, DMSO-*d*₆): δ (ppm) 159.9 (C_c), 156.7 (C2), 155.1 (C2'), 136.6 (C_a), 135.9 (C_e), 133.2 (C4), 129.5 (C4'), 127.3 (C6'), 126.8 (C6), 120.3 (C5), 119.9 (C5'), 117.4 (C3), 116.8 (C1'), 116.0 (C3'), 111.2 (C1).

HRMS (ESI negative): *m/z* 252.0667 [M-H]⁻, calcd for [C₁₅H₁₁NO₃-H]⁻: *m/z* 252.0666

HPLC: *t_R* = 23.745 min (kinetex, 96.5%), *t_R* = 22.485 min (polar-RP, 97.5%)

2-(2-(Thiophen-2-yl)oxazol-4-yl)phenol (**109a**)



C₁₃H₉NO₂S

M_r = 243.28

According to general procedure G, the title compound was synthesized using thiophene-2-carboxamide **100** (100 mg, 0.46 mmol, 1 eq.), salicylamide **87a** (59 mg, 0.46 mmol, 1 eq.) and AgSbF₆ (176 mg, 0.51 mmol, 1.1 eq.) in EtOAc (1.8 mL). The reaction was performed at 50 °C under µW-irradiation for 5 h. Purification via flash

column chromatography (CyHex/EtOAc 95:5–60:40) followed by recrystallization from 2-propanol yielded the final product as light-brown crystals.

Yield: 12 mg (11%)

R_f (CyHex/EtOAc 8:2) = 0.49

¹H-NMR (400 MHz, DMSO-*d*₆): δ (ppm) 10.39 (s, 1H, OH'), 8.40 (s, 1H, H_a), 7.95 (dd, ³*J* = 7.5 Hz and ⁴*J* = 1.7 Hz, 1H, H6'), 7.82 (dd, ³*J* = 5.0 Hz and ⁴*J* = 1.2 Hz, 1H, H5), 7.77 (dd, ³*J* = 3.7 Hz and ⁴*J* = 1.2 Hz, 1H, H3), 7.25 (dd, ³*J* = 5.0 Hz and ³*J* = 3.7 Hz, 1H, H4), 7.19 (ddd, ³*J* = 8.1 Hz, ³*J* = 7.5 Hz and ⁴*J* = 1.7 Hz, 1H, H4'), 6.97 (dd, ³*J* = 8.1 Hz and ⁴*J* = 1.2 Hz, 1H, H3'), 6.93 (td, ³*J* = 7.5 Hz and ⁴*J* = 1.2 Hz, 1H, H5').

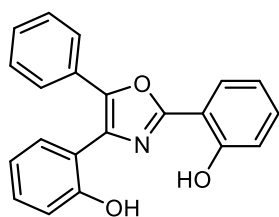
¹³C-NMR (101 MHz, DMSO-*d*₆): δ (ppm) 156.4 (C_c), 155.0 (C2'), 137.5 (C_e), 137.0 (C_a), 130.1 (C5), 129.4 (C2), 129.2 (C4'), 129.0 (C4), 128.6 (C3), 127.5 (C6'), 119.6 (C5'), 117.6 (C1'), 115.9 (C3').

HRMS (ESI positive): *m/z* 244.0424 [M+H]⁺, calcd for [C₁₃H₉NO₂S+H]⁺: *m/z* 244.0427

HRMS (ESI negative): *m/z* 242.0284 [M-H]⁻, calcd for [C₁₃H₉NO₂S-H]⁻: *m/z* 242.0281

HPLC: *t_R* = 23.178 min (kinetex, 98.4%), *t_R* = 24.124 min (hydro-RP, 99.8%)

2,2'-(5-Phenylloxazole-2,4-diyl)diphenol (**109b**)



C₂₁H₁₅NO₃

M_r = 329.36

According to general procedure A, **108b** (25 mg, 0.07 mmol, 1 eq.) was solubilized in freshly distilled DCM (0.5 mL). BBr₃ (1 M solution in dry DCM, 220 μ L, 0.22 mmol, 3 eq.) was added dropwise at -78 °C. After completion of the reaction and work-up, purification was performed via flash column chromatography (CyHex/EtOAc 95:5–80:20) yielding the desired product as a white powder.

Yield: 18 mg (75%)

R_f (CyHex/EtOAc 8:2) = 0.48

¹H-NMR (400 MHz, DMSO-*d*₆): δ (ppm) 11.02 (s, 1H, OH), 9.79 (s, 1H, OH'), 8.06 (dd, ³*J* = 8.1 Hz and ⁴*J* = 1.7 Hz, 1H, H₆), 7.63–7.55 (m, 2H, H₂'', H₆''), 7.52–7.40 (m, 4H, H₄, H₄', H₃'', H₅''), 7.40–7.31 (m, 2H, H₄', H₄''), 7.13–7.04 (m, 2H, H₃, H₅), 7.00 (dd, ³*J* = 8.2 and ⁴*J* = 1.1 Hz, 1H, H₃'), 6.96 (td, ³*J* = 7.4 Hz, ³*J* = 7.4 Hz and ⁴*J* = 1.1 Hz, 1H, H₅').

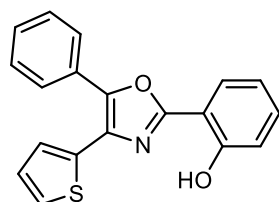
¹³C-NMR (101 MHz, DMSO-*d*₆): δ (ppm) 159.1 (C_c), 156.9 (C₂), 155.8 (C₂'), 145.2 (C_a), 133.1 (C₄), 131.9 (C_e), 131.3 (C₄'), 131.0 (C₁''), 129.1 (2C, C₃'', C₅''), 128.9 (C₄''), 128.3 (C₆'), 126.8 (C₆), 125.4 (2C, C₂'', C₆''), 120.3 (C₅), 119.8 (C₅'), 118.7 (C₁'), 117.3 (C₃), 116.6 (C₃'), 111.1 (C₁).

HRMS (ESI positive): *m/z* 330.1126 [M+H]⁺, calcd for [C₂₁H₁₅NO₃+H]⁺: *m/z* 330.1125

HRMS (ESI negative): *m/z* 328.0979 [M-H]⁻, calcd for [C₂₁H₁₅NO₃-H]⁻: *m/z* 328.0979

HPLC: *t_R* = 27.074 min (kinetex, 99.7%), *t_R* = 27.250 min (polar-RP, 99.9%)

2-(5-Phenyl-4-(thiophen-2-yl)oxazol-2-yl)phenol (**109d**)



C₁₉H₁₃NO₂S

M_r = 319.38

According to general procedure G, the title compound was synthesized using **97e** (200 mg, 0.71 mmol, 1 eq.), salicylamide (98 mg, 0.71 mmol, 1 eq.) and AgSbF₆ (269 mg, 0.78 mmol, 1.1 eq.) in EtOAc (1.0 mL). The reaction was performed at 60 °C under μ W-irradiation for 4 h. Purification via flash column chromatography (CyHex/EtOAc 99:1–94:6) followed by recrystallization from methanol yielded the final product as white needles.

Yield: 34 mg (15%)

R_f (CyHex/EtOAc 8:2) = 0.72

¹H-NMR (400 MHz, DMSO-*d*₆): δ (ppm) 10.75 (s, 1H, OH), 7.96 (dd, ³*J* = 7.9 Hz and ⁴*J* = 1.7 Hz, 1H, H₆), 7.87 – 7.79 (m, 2H, H₂'', H₆''), 7.69 (dd, ³*J* = 5.1 Hz and ⁴*J* = 1.2 Hz, 1H, H₅'), 7.62 – 7.43 (m, 5H, H₄, H₃', H₃'', H₄'', H₅''), 7.18 (dd, ³*J* = 5.1 Hz and

6 Experimental

$^3J = 3.6$ Hz, 1H, H4'), 7.13 – 7.09 (m, 1H, H3), 7.07 (ddd, $^3J = 7.9$ Hz, $^3J = 7.3$ Hz and $^4J = 1.1$ Hz, 1H, H5).

^{13}C -NMR (101 MHz, DMSO-*d*₆): δ (ppm) 159.7 (C_e), 156.8 (C2), 144.2 (C_a), 133.4 (C4), 132.9 (C2'), 130.1 (C4''), 129.5 (2C, C3'', C5''), 129.5 (C1''), 129.3 (C_e), 128.5 (C4'), 127.7 (C6), 127.7 (C5'), 127.5 (2C, C2'', C6''), 126.7 (C3'), 120.3 (C5), 117.5 (C3), 111.1 (C1).

HRMS (ESI positive): m/z 320.0739 [M+H]⁺, calcd for [C₁₉H₁₃NO₂S+H]⁺: m/z 320.0740

HRMS (ESI negative): m/z 318.0592 [M-H]⁻, calcd for [C₁₉H₁₃NO₂S-H]⁻: m/z 318.0594

HPLC: $t_R = 30.381$ min (kinetex, 99.6%), $t_R = 26.791$ min (polar-RP, 99.7%)

References

1. Cavalli, G.; Heard, E. Advances in epigenetics link genetics to the environment and disease. *Nature* **2019**, 571, 489-499.
2. Russo, V. E. A.; Martienssen, R. A.; Riggs, A. D. *Epigenetic Mechanisms of Gene Regulation*. Cold Spring Harbor Laboratory Press: Plainview, N.Y., 1996; Vol. 32.
3. Wei, J. W.; Huang, K.; Yang, C.; Kang, C. S. Non-coding RNAs as regulators in epigenetics (Review). *Oncol Rep* **2017**, 37, 3-9.
4. Breiling, A.; Lyko, F. Epigenetic regulatory functions of DNA modifications: 5-methylcytosine and beyond. *Epigenetics Chromatin* **2015**, 8, 24-24.
5. Greenberg, M. V. C.; Bourc'his, D. The diverse roles of DNA methylation in mammalian development and disease. *Nat Rev Mol Cell Biol* **2019**, 20, 590-607.
6. Lister, R.; Pelizzola, M.; Dowen, R. H.; Hawkins, R. D.; Hon, G.; Tonti-Filippini, J.; Nery, J. R.; Lee, L.; Ye, Z.; Ngo, Q.-M.; Edsall, L.; Antosiewicz-Bourget, J.; Stewart, R.; Ruotti, V.; Millar, A. H.; Thomson, J. A.; Ren, B.; Ecker, J. R. Human DNA methylomes at base resolution show widespread epigenomic differences. *Nature* **2009**, 462, 315-322.
7. Wu, X.; Zhang, Y. TET-mediated active DNA demethylation: mechanism, function and beyond. *Nat Rev Genet* **2017**, 18, 517-534.
8. Kitsera, N.; Allgayer, J.; Parsa, E.; Geier, N.; Rossa, M.; Carell, T.; Khobta, A. Functional impacts of 5-hydroxymethylcytosine, 5-formylcytosine, and 5-carboxycytosine at a single hemi-modified CpG dinucleotide in a gene promoter. *Nucleic Acids Res* **2017**, 45, 11033-11042.
9. Hahn, M. A.; Qiu, R.; Wu, X.; Li, A. X.; Zhang, H.; Wang, J.; Jui, J.; Jin, S.-G.; Jiang, Y.; Pfeifer, G. P.; Lu, Q. Dynamics of 5-hydroxymethylcytosine and chromatin marks in Mammalian neurogenesis. *Cell Reports* **2013**, 3, 291-300.
10. Wen, L.; Tang, F. Genomic distribution and possible functions of DNA hydroxymethylation in the brain. *Genomics* **2014**, 104, 341-346.
11. Xiao, C.-L.; Zhu, S.; He, M.; Chen, D.; Zhang, Q.; Chen, Y.; Yu, G.; Liu, J.; Xie, S.-Q.; Luo, F.; Liang, Z.; Wang, D.-P.; Bo, X.-C.; Gu, X.-F.; Wang, K.; Yan, G.-R. N6-Methyladenine DNA Modification in the Human Genome. *Mol Cell* **2018**, 71, 306-318.e7.
12. Kumar, S.; Chinnusamy, V.; Mohapatra, T. Epigenetics of Modified DNA Bases: 5-Methylcytosine and Beyond. *Front Genet* **2018**, 9, 640-640.
13. Douvlataniotis, K.; Bensberg, M.; Lentini, A.; Gylemo, B.; Nestor, C. E. No evidence for DNA N (6)-methyladenine in mammals. *Sci Adv* **2020**, 6, 3335.
14. Bannister, A. J.; Kouzarides, T. Regulation of chromatin by histone modifications. *Cell Res* **2011**, 21, 381-395.
15. Hebbes, T. R.; Thorne, A. W.; Crane-Robinson, C. A direct link between core histone acetylation and transcriptionally active chromatin. *EMBO J* **1988**, 7, 1395-402.

16. Zhang, Y.; Reinberg, D. Transcription regulation by histone methylation: interplay between different covalent modifications of the core histone tails. *Genes Dev* **2001**, *15*, 2343-2360.
17. Lee, J. J.; Murphy, G. F.; Lian, C. G. Melanoma epigenetics: novel mechanisms, markers, and medicines. *Lab Invest* **2014**, *94*, 822-838.
18. Musselman, C. A.; Khorasanizadeh, S.; Kutateladze, T. G. Towards understanding methyllysine readout. *Biochim Biophys Acta Gene Regul Mech* **2014**, *1839*, 686-693.
19. Hyun, K.; Jeon, J.; Park, K.; Kim, J. Writing, erasing and reading histone lysine methylations. *Exp Mol Med* **2017**, *49*, e324.
20. Ninova, M.; Fejes Tóth, K.; Aravin, A. A. The control of gene expression and cell identity by H3K9 trimethylation. *Development* **2019**, *146*, dev181180.
21. Ferrari, Karin J.; Scelfo, A.; Jammula, S.; Cuomo, A.; Barozzi, I.; Stützer, A.; Fischle, W.; Bonaldi, T.; Pasini, D. Polycomb-Dependent H3K27me1 and H3K27me2 Regulate Active Transcription and Enhancer Fidelity. *Mol Cell* **2014**, *53*, 49-62.
22. Wagner, E. J.; Carpenter, P. B. Understanding the language of Lys36 methylation at histone H3. *Nat Rev Mol Cell Biol* **2012**, *13*, 115-126.
23. Arrowsmith, C. H.; Bountra, C.; Fish, P. V.; Lee, K.; Schapira, M. Epigenetic protein families: a new frontier for drug discovery. *Nat Rev Drug Discov* **2012**, *11*, 384-400.
24. Ghasemi, S. Cancer's epigenetic drugs: where are they in the cancer medicines? *Pharmacogenomics J* **2019**, *20*, 367-379.
25. Hoy, S. M. Tazemetostat: First Approval. *Drugs* **2020**, *80*, 513-521.
26. Shi, Y.; Lan, F.; Matson, C.; Mulligan, P.; Whetstine, J. R.; Cole, P. A.; Casero, R. A.; Shi, Y. Histone Demethylation Mediated by the Nuclear Amine Oxidase Homolog LSD1. *Cell* **2004**, *119*, 941-953.
27. Tsukada, Y.-i.; Fang, J.; Erdjument-Bromage, H.; Warren, M. E.; Borchers, C. H.; Tempst, P.; Zhang, Y. Histone demethylation by a family of JmjC domain-containing proteins. *Nature* **2006**, *439*, 811-816.
28. Lu, T.; Jackson, M. W.; Wang, B.; Yang, M.; Chance, M. R.; Miyagi, M.; Gudkov, A. V.; Stark, G. R. Regulation of NF-kappaB by NSD1/FBXL11-dependent reversible lysine methylation of p65. *Proc Natl Acad Sci USA* **2010**, *107*, 46-51.
29. Stavropoulos, P.; Blobel, G.; Hoelz, A. Crystal structure and mechanism of human lysine-specific demethylase-1. *Nat Struct Mol Biol* **2006**, *13*, 626-632.
30. Zhang, Q.; Qi, S.; Xu, M.; Yu, L.; Tao, Y.; Deng, Z.; Wu, W.; Li, J.; Chen, Z.; Wong, J. Structure-function analysis reveals a novel mechanism for regulation of histone demethylase LSD2/AOF1/KDM1b. *Cell Res* **2013**, *23*, 225-241.
31. Shi, Y.; Sawada, J.-i.; Sui, G.; Affar, E. B.; Whetstine, J. R.; Lan, F.; Ogawa, H.; Po-Shan Luke, M.; Nakatani, Y.; Shi, Y. Coordinated histone modifications mediated by a CtBP co-repressor complex. *Nature* **2003**, *422*, 735-738.
32. Wang, Y.; Zhang, H.; Chen, Y.; Sun, Y.; Yang, F.; Yu, W.; Liang, J.; Sun, L.; Yang, X.; Shi, L.; Li, R.; Li, Y.; Zhang, Y.; Li, Q.; Yi, X.; Shang, Y. LSD1 is a subunit of the NuRD complex and targets the metastasis programs in breast cancer. *Cell* **2009**, *138*, 660-672.

33. Metzger, E.; Wissmann, M.; Yin, N.; Müller, J. M.; Schneider, R.; Peters, A. H. F. M.; Günther, T.; Buettner, R.; Schüle, R. LSD1 demethylates repressive histone marks to promote androgen-receptor-dependent transcription. *Nature* **2005**, 437, 436-439.
34. Perillo, B.; Ombra, M. N.; Bertoni, A.; Cuozzo, C.; Sacchetti, S.; Sasso, A.; Chiariotti, L.; Malorni, A.; Abbondanza, C.; Avvedimento, E. V. DNA oxidation as triggered by H3K9me2 demethylation drives estrogen-induced gene expression. *Science* **2008**, 319, 202-206.
35. Carnesecchi, J.; Cerutti, C.; Vanacker, J. M.; Forcet, C. ERRalpha protein is stabilized by LSD1 in a demethylation-independent manner. *PLoS One* **2017**, 12, e0188871.
36. Lan, H.; Tan, M.; Zhang, Q.; Yang, F.; Wang, S.; Li, H.; Xiong, X.; Sun, Y. LSD1 destabilizes FBXW7 and abrogates FBXW7 functions independent of its demethylase activity. *Proc Natl Acad Sci USA* **2019**, 116, 12311-12320.
37. Sehrawat, A.; Gao, L.; Wang, Y.; Bankhead, A.; McWeeney, S. K.; King, C. J.; Schwartzman, J.; Urrutia, J.; Bisson, W. H.; Coleman, D. J.; Joshi, S. K.; Kim, D.-H.; Sampson, D. A.; Weinmann, S.; Kallakury, B. V. S.; Berry, D. L.; Haque, R.; Van Den Eeden, S. K.; Sharma, S.; Bearss, J.; Beer, T. M.; Thomas, G. V.; Heiser, L. M.; Alumkal, J. J. LSD1 activates a lethal prostate cancer gene network independently of its demethylase function. *Proc Natl Acad Sci USA* **2018**, 115, E4179-E4188.
38. Fang, R.; Barbera, A. J.; Xu, Y.; Rutenberg, M.; Leonor, T.; Bi, Q.; Lan, F.; Mei, P.; Yuan, G.-C.; Lian, C.; Peng, J.; Cheng, D.; Sui, G.; Kaiser, U. B.; Shi, Y.; Shi, Y. G. Human LSD2/KDM1b/AOF1 regulates gene transcription by modulating intragenic H3K4me2 methylation. *Mol Cell* **2010**, 39, 222-233.
39. Majello, B.; Gorini, F.; Sacca, C. D.; Amente, S. Expanding the Role of the Histone Lysine-Specific Demethylase LSD1 in Cancer. *Cancers (Basel)* **2019**, 11, 324-338.
40. Chen, L.; Vasilatos, S. N.; Qin, Y.; Katz, T. A.; Cao, C.; Wu, H.; Tasdemir, N.; Levine, K. M.; Oesterreich, S.; Davidson, N. E.; Huang, Y. Functional characterization of lysine-specific demethylase 2 (LSD2/KDM1B) in breast cancer progression. *Oncotarget* **2017**, 8, 81737-81753.
41. Cao, L. L.; Du, C.; Liu, H.; Pei, L.; Qin, L.; Jia, M.; Wang, H. Lysine-specific demethylase 2A expression is associated with cell growth and cyclin D1 expression in colorectal adenocarcinoma. *Int J Biol Markers* **2018**, 1724600818764069.
42. Kim, D.; Nam, H. J.; Lee, W.; Yim, H. Y.; Ahn, J.-Y.; Park, S. W.; Shin, H.-J. R.; Yu, R.; Won, K.-J.; Bae, J.-S.; Kim, K. I.; Baek, S. H. PKCα-LSD1-NF-κB-Signaling Cascade Is Crucial for Epigenetic Control of the Inflammatory Response. *Mol Cell* **2018**, 69, 398-411.e6.
43. Maes, T.; Mascaro, C.; Ortega, A.; Lunardi, S.; Ciceri, F.; Somervaille, T. C.; Buesa, C. KDM1 histone lysine demethylases as targets for treatments of oncological and neurodegenerative disease. *Epigenomics* **2015**, 7, 609-626.
44. Liang, Y.; Vogel, J. L.; Narayanan, A.; Peng, H.; Kristie, T. M. Inhibition of the histone demethylase LSD1 blocks alpha-herpesvirus lytic replication and reactivation from latency. *Nat Med* **2009**, 15, 1312-1317.

45. Chen, Y.; Yang, Y.; Wang, F.; Wan, K.; Yamane, K.; Zhang, Y.; Lei, M. Crystal structure of human histone lysine-specific demethylase 1 (LSD1). *Proc Natl Acad Sci USA* **2006**, *103*, 13956-13961.
46. Klose, R. J.; Kallin, E. M.; Zhang, Y. JmjC-domain-containing proteins and histone demethylation. *Nat Rev Genet* **2006**, *7*, 715-727.
47. Walport, L. J.; Hopkinson, R. J.; Chowdhury, R.; Schiller, R.; Ge, W.; Kawamura, A.; Schofield, C. J. Arginine demethylation is catalysed by a subset of JmjC histone lysine demethylases. *Nat Commun* **2016**, *7*, 11974-11974.
48. Chen, Z.; Zang, J.; Whetstine, J.; Hong, X.; Davrazou, F.; Kutateladze, T. G.; Simpson, M.; Mao, Q.; Pan, C.-H.; Dai, S.; Hagman, J.; Hansen, K.; Shi, Y.; Zhang, G. Structural Insights into Histone Demethylation by JMJD2 Family Members. *Cell* **2006**, *125*, 691-702.
49. Aik, W.; McDonough, M. A.; Thalhammer, A.; Chowdhury, R.; Schofield, C. J. Role of the jelly-roll fold in substrate binding by 2-oxoglutarate oxygenases. *Curr Opin Struct Biol* **2012**, *22*, 691-700.
50. Pilka, E. S.; James, T.; Lisztwan, J. H. Structural definitions of Jumonji family demethylase selectivity. *Drug Discov Today* **2015**, *20*, 743-749.
51. Cascella, B.; Lee, S. G.; Singh, S.; Jez, J. M.; Mirica, L. M. The small molecule JIB-04 disrupts O₂ binding in the Fe-dependent histone demethylase KDM4A/JMJD2A. *Chem Commun* **2017**, *53*, 2174-2177.
52. Arifuzzaman, S.; Khatun, M. R.; Khatun, R. Emerging of lysine demethylases (KDMs): From pathophysiological insights to novel therapeutic opportunities. *Biomed Pharmacother* **2020**, *129*, 110392-110412.
53. Levin, M.; Stark, M.; Assaraf, Y. G. The JmjN domain as a dimerization interface and a targeted inhibitor of KDM4 demethylase activity. *Oncotarget* **2018**, *9*, 16861-16882.
54. Bhushan, B.; Erdmann, A.; Zhang, Y.; Belle, R.; Johansson, C.; Oppermann, U.; Hopkinson, R. J.; Schofield, C. J.; Kawamura, A. Investigations on small molecule inhibitors targeting the histone H3K4 tri-methyllysine binding PHD-finger of JmjC histone demethylases. *Bioorg Med Chem* **2018**, *26*, 2984-2991.
55. Johansson, C.; Tumber, A.; Che, K.; Cain, P.; Nowak, R.; Gileadi, C.; Oppermann, U. The roles of Jumonji-type oxygenases in human disease. *Epigenomics* **2014**, *6*, 89-120.
56. Horton, J. R.; Engstrom, A.; Zoeller, E. L.; Liu, X.; Shanks, J. R.; Zhang, X.; Johns, M. A.; Vertino, P. M.; Fu, H.; Cheng, X. Characterization of a Linked Jumonji Domain of the KDM5/JARID1 Family of Histone H3 Lysine 4 Demethylases. *J Biol Chem* **2016**, *291*, 2631-2646.
57. Lohse, B.; Helgstrand, C.; Kristensen, J. B. L.; Leurs, U.; Cloos, P. A. C.; Kristensen, J. L.; Clausen, R. P. Posttranslational modifications of the histone 3 tail and their impact on the activity of histone lysine demethylases in vitro. *PloS One* **2013**, *8*, e67653-e67653.
58. Hillringhaus, L.; Yue, W. W.; Rose, N. R.; Ng, S. S.; Gileadi, C.; Loenarz, C.; Bello, S. H.; Bray, J. E.; Schofield, C. J.; Oppermann, U. Structural and evolutionary basis for the dual substrate selectivity of human KDM4 histone demethylase family. *J Biol Chem* **2011**, *286*, 41616-41625.

59. Singh, W.; Quinn, D.; Moody, T. S.; Huang, M. Reaction Mechanism of Histone Demethylation in α KG-dependent Non-Heme Iron Enzymes. *J Phys Chem B* **2019**, *123*, 7801-7811.
60. Cortopassi, W. A.; Simion, R.; Honsby, C. E.; França, T. C. C.; Paton, R. S. Dioxygen Binding in the Active Site of Histone Demethylase JMJD2A and the Role of the Protein Environment. *Chem Eur J* **2015**, *21*, 18983-18992.
61. Kooistra, S. M.; Helin, K. Molecular mechanisms and potential functions of histone demethylases. *Nat Rev Mol Cell Biol* **2012**, *13*, 297-311.
62. Pedersen, M. T.; Helin, K. Histone demethylases in development and disease. *Trends Cell Biol* **2010**, *20*, 662-671.
63. Nottke, A.; Colaiácovo, M. P.; Shi, Y. Developmental roles of the histone lysine demethylases. *Development* **2009**, *136*, 879-889.
64. Black, J. C.; Van Rechem, C.; Whetstine, J. R. Histone lysine methylation dynamics: establishment, regulation, and biological impact. *Mol Cell* **2012**, *48*, 491-507.
65. Dimitrova, E.; Turberfield, A. H.; Klose, R. J. Histone demethylases in chromatin biology and beyond. *EMBO Rep* **2015**, *16*, 1620-1639.
66. Kuroki, S.; Akiyoshi, M.; Tokura, M.; Miyachi, H.; Nakai, Y.; Kimura, H.; Shinkai, Y.; Tachibana, M. JMJD1C, a JmjC domain-containing protein, is required for long-term maintenance of male germ cells in mice. *Biol Reprod* **2013**, *89*, 93, 1-9.
67. Okada, Y.; Scott, G.; Ray, M. K.; Mishina, Y.; Zhang, Y. Histone demethylase JHDM2A is critical for Tnp1 and Prm1 transcription and spermatogenesis. *Nature* **2007**, *450*, 119-123.
68. Sankar, A.; Lerdrup, M.; Manaf, A.; Johansen, J. V.; Gonzalez, J. M.; Borup, R.; Blanshard, R.; Klungland, A.; Hansen, K.; Andersen, C. Y.; Dahl, J. A.; Helin, K.; Hoffmann, E. R. KDM4A regulates the maternal-to-zygotic transition by protecting broad H3K4me3 domains from H3K9me3 invasion in oocytes. *Nat Cell Biol* **2020**, *22*, 380-388.
69. Blackledge, N. P.; Klose, R. CpG island chromatin. *Epigenetics* **2011**, *6*, 147-152.
70. Agger, K.; Cloos, P. A.; Christensen, J.; Pasini, D.; Rose, S.; Rappsilber, J.; Issaeva, I.; Canaani, E.; Salcini, A. E.; Helin, K. UTX and JMJD3 are histone H3K27 demethylases involved in HOX gene regulation and development. *Nature* **2007**, *449*, 731-734.
71. Fueyo, R.; García, M. A.; Martínez-Balbás, M. A. Jumonji family histone demethylases in neural development. *Cell Tissue Res* **2015**, *359*, 87-98.
72. Tang, G. B.; Zeng, Y. Q.; Liu, P. P.; Mi, T. W.; Zhang, S. F.; Dai, S. K.; Tang, Q. Y.; Yang, L.; Xu, Y. J.; Yan, H. L.; Du, H. Z.; Teng, Z. Q.; Zhou, F. Q.; Liu, C. M. The Histone H3K27 Demethylase UTX Regulates Synaptic Plasticity and Cognitive Behaviors in Mice. *Front Mol Neurosci* **2017**, *10*, 267, 1-22.
73. Strobl-Mazzulla, P. H.; Sauka-Spengler, T.; Bronner-Fraser, M. Histone demethylase JmjD2A regulates neural crest specification. *Dev Cell* **2010**, *19*, 460-468.
74. Cascante, A.; Klum, S.; Biswas, M.; Antolin-Fontes, B.; Barnabé-Heider, F.; Hermanson, O. Gene-specific methylation control of H3K9 and H3K36 on

- neurotrophic BDNF versus astroglial GFAP genes by KDM4A/C regulates neural stem cell differentiation. *J Mol Biol* **2014**, 426, 3467-3477.
75. Pathak, S. S.; Maitra, S.; Chakravarty, S.; Kumar, A. Histone Lysine Demethylases of JMJD2 or KDM4 Family are Important Epigenetic Regulators in Reward Circuitry in the Etiopathology of Depression. *Neuropsychopharmacology* **2017**, 42, 854-863.
76. Kang, C.; Saso, K.; Ota, K.; Kawazu, M.; Ueda, T.; Okada, H. JMJD2B/KDM4B inactivation in adipose tissues accelerates obesity and systemic metabolic abnormalities. *Genes Cells* **2018**, 23, 767-777.
77. Qi, Q.; Wang, Y.; Wang, X.; Yang, J.; Xie, Y.; Zhou, J.; Li, X.; Wang, B. Histone demethylase KDM4A regulates adipogenic and osteogenic differentiation via epigenetic regulation of C/EBPalpha and canonical Wnt signaling. *Cell Mol Life Sci* **2019**, 77, 2407-2421.
78. Rondinelli, B.; Schwerer, H.; Antonini, E.; Gaviraghi, M.; Lupi, A.; Frenquelli, M.; Cittaro, D.; Segalla, S.; Lemaitre, J. M.; Tonon, G. H3K4me3 demethylation by the histone demethylase KDM5C/JARID1C promotes DNA replication origin firing. *Nucleic Acids Res* **2015**, 43, 2560-2574.
79. Cornett, E. M.; Ferry, L.; Defossez, P.-A.; Rothbart, S. B. Lysine Methylation Regulators Moonlighting outside the Epigenome. *Mol Cell* **2019**, 75, 1092-1101.
80. Salminen, A.; Kauppinen, A.; Hiltunen, M.; Kaarniranta, K. Krebs cycle intermediates regulate DNA and histone methylation: Epigenetic impact on the aging process. *Ageing Res Rev* **2014**, 16, 45-65.
81. Butler, J. S.; Koutelou, E.; Schibler, A. C.; Dent, S. Y. R. Histone-modifying enzymes: regulators of developmental decisions and drivers of human disease. *Epigenomics* **2012**, 4, 163-177.
82. Morera, L.; Lübbert, M.; Jung, M. Targeting histone methyltransferases and demethylases in clinical trials for cancer therapy. *Clin Epigenetics* **2016**, 8, 57, 1-16.
83. Neganova, M. E.; Klochkov, S. G.; Aleksandrova, Y. R.; Aliev, G. Histone modifications in epigenetic regulation of cancer: perspectives and achieved progress. *Semin Cancer Biol* **2020**, in press.
84. Janardhan, A.; Kathera, C.; Darsi, A.; Ali, W.; He, L.; Yang, Y.; Luo, L.; Guo, Z. Prominent role of histone lysine demethylases in cancer epigenetics and therapy. *Oncotarget* **2018**, 9, 34429-34448.
85. McCabe, M. T.; Mohammad, H. P.; Barbash, O.; Kruger, R. G. Targeting Histone Methylation in Cancer. *Cancer J* **2017**, 23, 292-301.
86. Park, S. Y.; Park, J. W.; Chun, Y. S. Jumonji histone demethylases as emerging therapeutic targets. *Pharmacol Res* **2016**, 105, 146-151.
87. Hu, F.; Li, H.; Liu, L.; Xu, F.; Lai, S.; Luo, X.; Hu, J.; Yang, X. Histone demethylase KDM4D promotes gastrointestinal stromal tumor progression through HIF1 β /VEGFA signalling. *Mol Cancer* **2018**, 17, 107.
88. Liu, J.; Murali, T.; Yu, T.; Liu, C.; Sivakumaran, T. A.; Moseley, H. N. B.; Zhulin, I. B.; Weiss, H. L.; Durbin, E. B.; Ellingson, S. R.; Liu, J.; Huang, B.; Hallahan, B. J.; Horbinski, C. M.; Hodges, K.; Napier, D. L.; Bocklage, T.; Mueller, J.; Vanderford, N. L.; Fardo, D. W.; Wang, C.; Arnold, S. M. Characterization of Squamous Cell

- Lung Cancers from Appalachian Kentucky. *Cancer Epidemiol Biomarkers Prev* **2019**, 28, 348-356.
89. Patani, N.; Jiang, W.; Newbold, R.; Mokbel, K. Histone-modifier Gene Expression Profiles Are Associated with Pathological and Clinical Outcomes in Human Breast Cancer. *Anticancer Res* **2011**, 31, 4115-4125.
 90. Neele, A. E.; Gijbels, M. J. J.; van der Velden, S.; Hoeksema, M. A.; Boshuizen, M. C. S.; Prange, K. H. M.; Chen, H. J.; Van den Bossche, J.; van Roomen, C.; Shami, A.; Levels, J. H. M.; Kroon, J.; Lucas, T.; Dimmeler, S.; Lutgens, E.; de Winther, M. P. J. Myeloid Kdm6b deficiency results in advanced atherosclerosis. *Atherosclerosis* **2018**, 275, 156-165.
 91. Wang, H. J.; Pochampalli, M.; Wang, L. Y.; Zou, J. X.; Li, P. S.; Hsu, S. C.; Wang, B. J.; Huang, S. H.; Yang, P.; Yang, J. C.; Chu, C. Y.; Hsieh, C. L.; Sung, S. Y.; Li, C. F.; Tepper, C. G.; Ann, D. K.; Gao, A. C.; Evans, C. P.; Izumiya, Y.; Chuu, C. P.; Wang, W. C.; Chen, H. W.; Kung, H. J. KDM8/JMJD5 as a dual coactivator of AR and PKM2 integrates AR/EZH2 network and tumor metabolism in CRPC. *Oncogene* **2019**, 38, 17-32.
 92. Shin, S.; Janknecht, R. Activation of androgen receptor by histone demethylases JMJD2A and JMJD2D. *Biochem Biophys Res Commun* **2007**, 359, 742-746.
 93. Berry, W. L.; Shin, S.; Lightfoot, S. A.; Janknecht, R. Oncogenic features of the JMJD2A histone demethylase in breast cancer. *Int J Oncol* **2012**, 41, 1701-1706.
 94. Qiu, M. T.; Fan, Q.; Zhu, Z.; Kwan, S. Y.; Chen, L.; Chen, J. H.; Ying, Z. L.; Zhou, Y.; Gu, W.; Wang, L. H.; Cheng, W. W.; Zeng, J.; Wan, X. P.; Mok, S. C.; Wong, K. K.; Bao, W. KDM4B and KDM4A promote endometrial cancer progression by regulating androgen receptor, c-myc, and p27kip1. *Oncotarget* **2015**, 6, 31702-31720.
 95. Duan, L.; Rai, G.; Roggero, C.; Zhang, Q.-J.; Wei, Q.; Ma, S. H.; Zhou, Y.; Santoyo, J.; Martinez, E. D.; Xiao, G.; Raj, G. V.; Jadhav, A.; Simeonov, A.; Maloney, D. J.; Rizo, J.; Hsieh, J.-T.; Liu, Z.-P. KDM4/JMJD2 Histone Demethylase Inhibitors Block Prostate Tumor Growth by Suppressing the Expression of AR and BMYB-Regulated Genes. *Chem Biol* **2015**, 22, 1185-1196.
 96. Metzger, E.; Stepputtis, S. S.; Strietz, J.; Preca, B. T.; Urban, S.; Willmann, D.; Allen, A.; Zenk, F.; Iovino, N.; Bronsert, P.; Proske, A.; Follo, M.; Boerries, M.; Stickeler, E.; Xu, J.; Wallace, M. B.; Stafford, J. A.; Kanouni, T.; Maurer, J.; Schüle, R. KDM4 Inhibition Targets Breast Cancer Stem-like Cells. *Cancer Res* **2017**, 77, 5900-5912.
 97. Kim, T. D.; Jin, F.; Shin, S.; Oh, S.; Lightfoot, S. A.; Grande, J. P.; Johnson, A. J.; van Deursen, J. M.; Wren, J. D.; Janknecht, R. Histone demethylase JMJD2A drives prostate tumorigenesis through transcription factor ETV1. *J Clin Invest* **2016**, 126, 706-720.
 98. Wang, F.; Li, Y.; Shan, F.; Zhang, Q.; Wang, L.; Sheng, B.; Cheng, G. Upregulation of JMJD2A promotes migration and invasion in bladder cancer through regulation of SLUG. *Oncol Rep* **2019**, 42, 1431-1440.
 99. Li, Y.; Wang, Y.; Xie, Z.; Hu, H. JMJD2A facilitates growth and inhibits apoptosis of cervical cancer cells by downregulating tumor suppressor miR-491-5p. *Mol Med Rep* **2019**, 19, 2489-2496.

100. Kim, T.-D.; Shin, S.; Berry, W. L.; Oh, S.; Janknecht, R. The JMJD2A demethylase regulates apoptosis and proliferation in colon cancer cells. *J Cell Biochem* **2012**, *113*, 1368-1376.
101. Hu, C.-E.; Liu, Y.-C.; Zhang, H.-D.; Huang, G.-J. JMJD2A predicts prognosis and regulates cell growth in human gastric cancer. *Biochem Biophys Res Commun* **2014**, *449*, 1-7.
102. An, J.; Xu, J.; Li, J.; Jia, S.; Li, X.; Lu, Y.; Yang, Y.; Lin, Z.; Xin, X.; Wu, M.; Zheng, Q.; Pu, H.; Gui, X.; Li, T.; Lu, D. HistoneH3 demethylase JMJD2A promotes growth of liver cancer cells through up-regulating miR372. *Oncotarget* **2017**, *8*, 49093-49109.
103. Soini, Y.; Kosma, V. M.; Pirinen, R. KDM4A, KDM4B and KDM4C in non-small cell lung cancer. *Int J Clin Exp Pathol* **2015**, *8*, 12922-12928.
104. Su, Y.; Yu, Q. H.; Wang, X. Y.; Yu, L. P.; Wang, Z. F.; Cao, Y. C.; Li, J. D. JMJD2A promotes the Warburg effect and nasopharyngeal carcinoma progression by transactivating LDHA expression. *BMC Cancer* **2017**, *17*, 477, 1-13.
105. Wang, B.; Fan, X.; Ma, C.; Lei, H.; Long, Q.; Chai, Y. Downregulation of KDM4A Suppresses the Survival of Glioma Cells by Promoting Autophagy. *J Mol Neurosci* **2016**, *60*, 137-144.
106. Guerra-Calderas, L.; Gonzalez-Barrios, R.; Herrera, L. A.; Cantu de Leon, D.; Soto-Reyes, E. The role of the histone demethylase KDM4A in cancer. *Cancer Genet* **2015**, *208*, 215-224.
107. Neault, M.; Mallette, Frédérick A.; Richard, S. miR-137 Modulates a Tumor Suppressor Network-Inducing Senescence in Pancreatic Cancer Cells. *Cell Rep* **2016**, *14*, 1966-1978.
108. Boila, L. D.; Chatterjee, S. S.; Banerjee, D.; Sengupta, A. KDM6 and KDM4 histone lysine demethylases emerge as molecular therapeutic targets in human acute myeloid leukemia. *Exp Hematol* **2018**, *58*, 44-51.
109. Filiú-Braga, L. D. C.; Serejo, T. R. T.; Lucena-Araujo, A. R.; Neves, F. A. R.; de Carvalho, J. L.; Rego, E. M.; Saldanha-Araujo, F. Unraveling KDM4 histone demethylase expression and its association with adverse cytogenetic findings in chronic lymphocytic leukemia. *Med Oncol* **2018**, *36*, 3.
110. Kauffman, E. C.; Robinson, B. D.; Downes, M. J.; Powell, L. G.; Lee, M. M.; Scherr, D. S.; Gudas, L. J.; Mongan, N. P. Role of androgen receptor and associated lysine-demethylase coregulators, LSD1 and JMJD2A, in localized and advanced human bladder cancer. *Mol Carcinog* **2011**, *50*, 931-944.
111. Lee, D. H.; Kim, G. W.; Jeon, Y. H.; Yoo, J.; Lee, S. W.; Kwon, S. H. Advances in histone demethylase KDM4 as cancer therapeutic targets. *Faseb J* **2020**, *34*, 3461-3484.
112. Zhang, Q.-J.; Chen, H.-Z.; Wang, L.; Liu, D.-P.; Hill, J. A.; Liu, Z.-P. The histone trimethyllysine demethylase JMJD2A promotes cardiac hypertrophy in response to hypertrophic stimuli in mice. *J Clin Invest* **2011**, *121*, 2447-2456.
113. Chakravarty, S.; Jhelum, P.; Bhat, U. A.; Rajan, W. D.; Maitra, S.; Pathak, S. S.; Patel, A. B.; Kumar, A. Insights into the epigenetic mechanisms involving histone lysine methylation and demethylation in ischemia induced damage and repair has therapeutic implication. *Biochim Biophys Acta Mol Basis Dis* **2017**, *1863*, 152-164.

114. Wang, X.; Wang, S.; Yao, G.; Yu, D.; Chen, K.; Tong, Q.; Ye, L.; Wu, C.; Sun, Y.; Li, H.; Hermann, D. M.; Doeppner, T. R.; Jin, F.; Dai, Y.; Wu, J. Identification of the histone lysine demethylase KDM4A/JMJD2A as a novel epigenetic target in M1 macrophage polarization induced by oxidized LDL. *Oncotarget* **2017**, *8*, 114442-114456.
115. Kong, M.; Wu, J.; Fan, Z.; Chen, B.; Wu, T.; Xu, Y. The histone demethylase Kdm4 suppresses activation of hepatic stellate cell by inducing MiR-29 transcription. *Biochem Biophys Res Commun* **2019**, *514*, 16-23.
116. Young, J. I.; Züchner, S.; Wang, G. Regulation of the Epigenome by Vitamin C. *Annu Rev Nutr* **2015**, *35*, 545-564.
117. Couture, J.-F.; Collazo, E.; Ortiz-Tello, P. A.; Brunzelle, J. S.; Trievel, R. C. Specificity and mechanism of JMJD2A, a trimethyllysine-specific histone demethylase. *Nat Struct Mol Biol* **2007**, *14*, 689-695.
118. Leurs, U.; Lohse, B.; Rand, K. D.; Ming, S.; Riise, E. S.; Cole, P. A.; Kristensen, J. L.; Clausen, R. P. Substrate- and cofactor-independent inhibition of histone demethylase KDM4C. *ACS Chem Biol* **2014**, *9*, 2131-2138.
119. Sakurai, M.; Rose, N. R.; Schultz, L.; Quinn, A. M.; Jadhav, A.; Ng, S. S.; Oppermann, U.; Schofield, C. J.; Simeonov, A. A miniaturized screen for inhibitors of Jumonji histone demethylases. *Mol Biosyst* **2010**, *6*, 357-364.
120. Roatsch, M. *Assays and Inhibitors for JumonjiC Domain-Containing Histone Demethylases as Epigenetic Regulators*. Dissertation. Albert-Ludwigs-Universität, Freiburg im Breisgau, **2016**.
121. Li, Q.; Sritharathikhun, P.; Motomizu, S. Development of novel reagent for Hantzsch reaction for the determination of formaldehyde by spectrophotometry and fluorometry. *Anal Sci* **2007**, *23*, 413-417.
122. Liu, L.-J.; Lu, L.; Zhong, H.-J.; He, B.; Kwong, D. W. J.; Ma, D.-L.; Leung, C.-H. An Iridium(III) Complex Inhibits JMJD2 Activities and Acts as a Potential Epigenetic Modulator. *J Med Chem* **2015**, *58*, 6697-6703.
123. Quesenberry, M. S.; Lee, Y. C. A rapid formaldehyde assay using purpald reagent: application under periodation conditions. *Anal Biochem* **1996**, *234*, 50-55.
124. Wang, Y.; Deng, X.; Liu, J.; Tang, H.; Jiang, J. Surface enhanced Raman scattering based sensitive detection of histone demethylase activity using a formaldehyde-selective reactive probe. *Chem Commun* **2013**, *49*, 8489-8491.
125. Nielsen, A. L.; Kristensen, L. H.; Stephansen, K. B.; Kristensen, J. B. L.; Helgstrand, C.; Lees, M.; Cloos, P.; Helin, K.; Gajhede, M.; Olsen, L. Identification of catechols as histone-lysine demethylase inhibitors. *FEBS Lett* **2012**, *586*, 1190-1194.
126. Kawamura, A.; Tumber, A.; Rose, N. R.; King, O. N. F.; Daniel, M.; Oppermann, U.; Heightman, T. D.; Schofield, C. Development of homogeneous luminescence assays for histone demethylase catalysis and binding. *Anal Biochem* **2010**, *404*, 86-93.
127. PerkinElmer, AlphaLISA and AlphaScreen No-wash Assays. <https://www.perkinelmer.com/de/lab-products-and-services/application-support-knowledgebase/alphalisa-alphascreen-no-wash-assays/alphalisa-alphascreen-no-wash-assays>

- washassays-main.html#AlphaLISAAlphaScreenno-washassays-Assayprinciple* (accessed January 15, 2020).
128. Rose, N. R.; Woon, E. C. Y.; Tumber, A.; Walport, L. J.; Chowdhury, R.; Li, X. S.; King, O. N. F.; Lejeune, C.; Ng, S. S.; Krojer, T.; Chan, M. C.; Rydzik, A. M.; Hopkinson, R. J.; Che, K. H.; Daniel, M.; Strain-Damerell, C.; Gileadi, C.; Kochan, G.; Leung, I. K. H.; Dunford, J.; Yeoh, K. K.; Ratcliffe, P. J.; Burgess-Brown, N.; von Delft, F.; Muller, S.; Marsden, B.; Brennan, P. E.; McDonough, M. A.; Oppermann, U.; Klose, R. J.; Schofield, C. J.; Kawamura, A. Plant growth regulator daminozide is a selective inhibitor of human KDM2/7 histone demethylases. *J Med Chem* **2012**, *55*, 6639-6643.
129. Kawamura, A.; Munzel, M.; Kojima, T.; Yapp, C.; Bhushan, B.; Goto, Y.; Tumber, A.; Katoh, T.; King, O. N.; Passioura, T.; Walport, L. J.; Hatch, S. B.; Madden, S.; Muller, S.; Brennan, P. E.; Chowdhury, R.; Hopkinson, R. J.; Suga, H.; Schofield, C. J. Highly selective inhibition of histone demethylases by de novo macrocyclic peptides. *Nat Commun* **2017**, *8*, 14773, 1-10.
130. PerkinElmer, Alpha Epigenetic Assays. <https://www.perkinelmer.com/de/lab-products-and-services/application-support-knowledgebase/alphalisa-alphascreen-no-wash-assays/alpha-epigenetic-assays.html> (accessed January 17, 2020).
131. Zheng, J. Spectroscopy-Based Quantitative Fluorescence Resonance Energy Transfer Analysis. In *Ion Channels: Methods and Protocols*, Stockand, J. D.; Shapiro, M. S., Eds. Humana Press: Totowa, NJ, **2006**; pp 65-77.
132. Hauser, A.-T.; Roatsch, M.; Schulz-Fincke, J.; Robaa, D.; Sippl, W.; Jung, M. Chapter 18 - Discovery of Histone Demethylase Inhibitors. In *Epigenetic Technological Applications*, Zheng, Y. G., Ed. Academic Press: Boston, **2015**; pp 397-424.
133. PerkinElmer, LANCE and LANCE Ultra TR-FRET Assays. <https://www.perkinelmer.com/de/lab-products-and-services/application-support-knowledgebase/lance/lance-lance-ultra-tr-fret-assays.html#LANCEandLANCEUltraTR-FRETassays-Assayprinciple> (accessed January 17, 2020).
134. Gauthier, N.; Caron, M.; Pedro, L.; Arcand, M.; Blouin, J.; Labonté, A.; Normand, C.; Paquet, V.; Rodenbrock, A.; Roy, M.; Rouleau, N.; Beaudet, L.; Padrós, J.; Rodriguez-Suarez, R. Development of homogeneous nonradioactive methyltransferase and demethylase assays targeting histone H3 lysine 4. *J Biomol Screen* **2012**, *17*, 49-58.
135. PerkinElmer, LANCE Ultra Europium-anti-tri-methyl-Histone H3 Lysine 27 (H3K27me3) Antibody. <https://www.perkinelmer.com/de/product/eu-anti-tri-methyl-h3-k27me3-10-ug-trf0407-d> (accessed January 17, 2020).
136. PerkinElmer, DELFIA Time-Resolved Fluorescence Assays. <https://www.perkinelmer.com/de/lab-products-and-services/application-support-knowledgebase/delfia/delfia-trf-assays.html> (accessed January 17, 2020).
137. Luo, X.; Liu, Y.; Kubicek, S.; Myllyharju, J.; Tumber, A.; Ng, S.; Che, K. H.; Podoll, J.; Heightman, T. D.; Oppermann, U.; Schreiber, S. L.; Wang, X. A selective inhibitor and probe of the cellular functions of Jumonji C domain-containing histone demethylases. *J Am Chem Soc* **2011**, *133*, 9451-9456.

138. Williams, S. T.; Walport, L. J.; Hopkinson, R. J.; Madden, S. K.; Chowdhury, R.; Schofield, C. J.; Kawamura, A. Studies on the catalytic domains of multiple JmjC oxygenases using peptide substrates. *Epigenetics* **2014**, *9*, 1596-1603.
139. Hutchinson, S. E.; Leveridge, M. V.; Heathcote, M. L.; Francis, P.; Williams, L.; Gee, M.; Munoz-Muriedas, J.; Leavens, B.; Shillings, A.; Jones, E.; Homes, P.; Baddeley, S.; Chung, C.-w.; Bridges, A.; Argyrou, A. Enabling Lead Discovery for Histone Lysine Demethylases by High-Throughput RapidFire Mass Spectrometry. *J Biomol Screen* **2012**, *17*, 39-48.
140. Leveridge, M.; Buxton, R.; Argyrou, A.; Francis, P.; Leavens, B.; West, A.; Rees, M.; Hardwicke, P.; Bridges, A.; Ratcliffe, S.; Chung, C.-w. Demonstrating Enhanced Throughput of RapidFire Mass Spectrometry through Multiplexing Using the JmjD2d Demethylase as a Model System. *J Biomol Screen* **2014**, *19*, 278-286.
141. Wigle, T. J.; Swinger, K. K.; Campbell, J. E.; Scholle, M. D.; Sherrill, J.; Admirand, E. A.; Boriack-Sjodin, P. A.; Kuntz, K. W.; Chesworth, R.; Moyer, M. P.; Scott, M. P.; Copeland, R. A. A High-Throughput Mass Spectrometry Assay Coupled with Redox Activity Testing Reduces Artifacts and False Positives in Lysine Demethylase Screening. *J Biomol Screen* **2015**, *20*, 810-20.
142. Yu, W.; Eram, M. S.; Hajian, T.; Szykowska, A.; Burgess-Brown, N.; Vedadi, M.; Brown, P. J. A scintillation proximity assay for histone demethylases. *Anal Biochem* **2014**, *463*, 54-60.
143. Rossi, A. M.; Taylor, C. W. Analysis of protein-ligand interactions by fluorescence polarization. *Nat Protoc* **2011**, *6*, 365-87.
144. Xu, W.; Podoll, J. D.; Dong, X.; Tumber, A.; Oppermann, U.; Wang, X. Quantitative analysis of histone demethylase probes using fluorescence polarization. *J Med Chem* **2013**, *56*, 5198-5202.
145. Wang, W.; Marholz, L. J.; Wang, X. Novel Scaffolds of Cell-Active Histone Demethylase Inhibitors Identified from High-Throughput Screening. *J Biomol Screen* **2015**, *20*, 821-827.
146. Rose, N. R.; Woon, E. C. Y.; Kingham, G. L.; King, O. N. F.; Mecinović, J.; Clifton, I. J.; Ng, S. S.; Talib-Hardy, J.; Oppermann, U.; McDonough, M. A.; Schofield, C. J. Selective inhibitors of the JMJD2 histone demethylases: combined nondenaturing mass spectrometric screening and crystallographic approaches. *J Med Chem* **2010**, *53*, 1810-1818.
147. Hoffmann, I.; Roatsch, M.; Schmitt, M. L.; Carlino, L.; Pippel, M.; Sippl, W.; Jung, M. The role of histone demethylases in cancer therapy. *Mol Oncol* **2012**, *6*, 683-703.
148. Thinnes, C. C.; England, K. S.; Kawamura, A.; Chowdhury, R.; Schofield, C. J.; Hopkinson, R. J. Targeting histone lysine demethylases — Progress, challenges, and the future. *Biochim Biophys Acta Gene Regul Mech* **2014**, *1839*, 1416-1432.
149. McGrath, J.; Trojer, P. Targeting histone lysine methylation in cancer. *Pharmacol Ther* **2015**, *150*, 1-22.
150. Lohse, B.; Kristensen, J. L.; Kristensen, L. H.; Agger, K.; Helin, K.; Gajhede, M.; Clausen, R. P. Inhibitors of histone demethylases. *Bioorg Med Chem* **2011**, *19*, 3625-3636.

151. Wang, Z.; Patel, D. J. Small molecule epigenetic inhibitors targeted to histone lysine methyltransferases and demethylases. *Q Rev Biophys* **2013**, *46*, 349-373.
152. Maes, T.; Carceller, E.; Salas, J.; Ortega, A.; Buesa, C. Advances in the development of histone lysine demethylase inhibitors. *Curr Opin Pharmacol* **2015**, *23*, 52-60.
153. McAllister, T. E.; England, K. S.; Hopkinson, R. J.; Brennan, P. E.; Kawamura, A.; Schofield, C. J. Recent Progress in Histone Demethylase Inhibitors. *J Med Chem* **2016**, *59*, 1308-1329.
154. Jambhekar, A.; Anastas, J. N.; Shi, Y. Histone Lysine Demethylase Inhibitors. *Cold Spring Harb Perspect Med* **2017**, *7*, 1-25.
155. Kaniskan, H. U.; Martini, M. L.; Jin, J. Inhibitors of Protein Methyltransferases and Demethylases. *Chem Rev* **2018**, *118*, 989-1068.
156. Hatch, S. B.; Yapp, C.; Montenegro, R. C.; Savitsky, P.; Gamble, V.; Tumber, A.; Ruda, G. F.; Bavetsias, V.; Fedorov, O.; Atrash, B.; Raynaud, F.; Lanigan, R.; Carmichael, L.; Tomlin, K.; Burke, R.; Westaway, S. M.; Brown, J. A.; Prinjha, R. K.; Martinez, E. D.; Oppermann, U.; Schofield, C. J.; Bountra, C.; Kawamura, A.; Blagg, J.; Brennan, P. E.; Rossanese, O.; Muller, S. Assessing histone demethylase inhibitors in cells: lessons learned. *Epigenetics Chromatin* **2017**, *10*, 9, 1-17.
157. Ballatore, C.; Hury, D. M.; Smith, A. B., 3rd. Carboxylic acid (bio)isosteres in drug design. *ChemMedChem* **2013**, *8*, 385-395.
158. Rautio, J.; Kumpulainen, H.; Heimbach, T.; Oliyai, R.; Oh, D.; Järvinen, T.; Savolainen, J. Prodrugs: design and clinical applications. *Nat Rev Drug Discov* **2008**, *7*, 255-270.
159. Hamada, Y. Recent progress in prodrug design strategies based on generally applicable modifications. *Bioorg Med Chem Lett* **2017**, *27*, 1627-1632.
160. Kristensen, L. H.; Nielsen, A. L.; Helgstrand, C.; Lees, M.; Cloos, P.; Kastrop, J. S.; Helin, K.; Olsen, L.; Gajhede, M. Studies of H3K4me3 demethylation by KDM5B/Jarid1B/PLU1 reveals strong substrate recognition in vitro and identifies 2,4-pyridine-dicarboxylic acid as an in vitro and in cell inhibitor. *FEBS J* **2012**, *279*, 1905-1914.
161. Nie, Z.; Stafford, J. A.; Veal, J. M.; Wallace, M. B. Histone Demethylase Inhibitors. *Patent* WO(2014/089364), **2014**, 1-294.
162. Roatsch, M.; Robaa, D.; Pippel, M.; Nettleship, J. E.; Reddivari, Y.; Bird, L. E.; Hoffmann, I.; Franz, H.; Owens, R. J.; Schüle, R.; Flaig, R.; Sippl, W.; Jung, M. Substituted 2-(2-aminopyrimidin-4-yl)pyridine-4-carboxylates as potent inhibitors of JumonjiC domain-containing histone demethylases. *Future Med Chem* **2016**, *8*, 1553-1571.
163. Kruidenier, L.; Chung, C.-w.; Cheng, Z.; Liddle, J.; Che, K.; Joberty, G.; Bantscheff, M.; Bountra, C.; Bridges, A.; Diallo, H.; Eberhard, D.; Hutchinson, S.; Jones, E.; Katso, R.; Leveridge, M.; Mander, P. K.; Mosley, J.; Ramirez-Molina, C.; Rowland, P.; Schofield, C. J.; Sheppard, R. J.; Smith, J. E.; Swales, C.; Tanner, R.; Thomas, P.; Tumber, A.; Drewes, G.; Oppermann, U.; Patel, D. J.; Lee, K.; Wilson, D. M. A selective jumonji H3K27 demethylase inhibitor modulates the proinflammatory macrophage response. *Nature* **2012**, *488*, 404-408.

164. Thinnes, C. C.; Tumber, A.; Yapp, C.; Scozzafava, G.; Yeh, T.; Chan, M. C.; Tran, T. A.; Hsu, K.; Tarhonskaya, H.; Walport, L. J.; Wilkins, S. E.; Martinez, E. D.; Müller, S.; Pugh, C. W.; Ratcliffe, P. J.; Brennan, P. E.; Kawamura, A.; Schofield, C. J. Betti reaction enables efficient synthesis of 8-hydroxyquinoline inhibitors of 2-oxoglutarate oxygenases. *Chem Commun* **2015**, 51, 15458-15461.
165. Hamada, S.; Suzuki, T.; Mino, K.; Koseki, K.; Oehme, F.; Flamme, I.; Ozasa, H.; Itoh, Y.; Ogasawara, D.; Komaarashi, H.; Kato, A.; Tsumoto, H.; Nakagawa, H.; Hasegawa, M.; Sasaki, R.; Mizukami, T.; Miyata, N. Design, Synthesis, Enzyme-Inhibitory Activity, and Effect on Human Cancer Cells of a Novel Series of Jumonji Domain-Containing Protein 2 Histone Demethylase Inhibitors. *J Med Chem* **2010**, 53, 5629-5638.
166. Patani, G. A.; LaVoie, E. J. Bioisosterism: A Rational Approach in Drug Design. *Chem Rev* **1996**, 96, 3147-3176.
167. Rüger, N.; Roatsch, M.; Emmrich, T.; Franz, H.; Schüle, R.; Jung, M.; Link, A. Tetrazolylhydrazides as Selective Fragment-Like Inhibitors of the JumonjiC-Domain-Containing Histone Demethylase KDM4A. *ChemMedChem* **2015**, 10, 1875-1883.
168. Roatsch, M.; Hoffmann, I.; Abboud, M. I.; Hancock, R. L.; Tarhonskaya, H.; Hsu, K.-F.; Wilkins, S. E.; Yeh, T.-L.; Lippl, K.; Serrer, K.; Moneke, I.; Ahrens, T. D.; Robaa, D.; Wenzler, S.; Barthes, N. P. F.; Franz, H.; Sippl, W.; Lassmann, S.; Diederichs, S.; Schleicher, E.; Schofield, C. J.; Kawamura, A.; Schüle, R.; Jung, M. The Clinically Used Iron Chelator Deferasirox Is an Inhibitor of Epigenetic JumonjiC Domain-Containing Histone Demethylases. *ACS Chem Biol* **2019**, 14, 1737-1750.
169. Al-Qahtani, K.; Jabeen, B.; Sekirnik, R.; Riaz, N.; Claridge, T. D. W.; Schofield, C. J.; McCullagh, J. S. O. The broad spectrum 2-oxoglutarate oxygenase inhibitor N-oxalylglycine is present in rhubarb and spinach leaves. *Phytochemistry* **2015**, 117, 456-461.
170. Rose, N. R.; Ng, S. S.; Mecinović, J.; Liénard, B. M. R.; Bello, S. H.; Sun, Z.; McDonough, M. A.; Oppermann, U.; Schofield, C. J. Inhibitor Scaffolds for 2-Oxoglutarate-Dependent Histone Lysine Demethylases. *J Med Chem* **2008**, 51, 7053-7056.
171. Hopkinson, R. J.; Tumber, A.; Yapp, C.; Chowdhury, R.; Aik, W.; Che, K. H.; Li, X. S.; Kristensen, J. B. L.; King, O. N. F.; Chan, M. C.; Yeoh, K. K.; Choi, H.; Walport, L. J.; Thinnes, C. C.; Bush, J. T.; Lejeune, C.; Rydzik, A. M.; Rose, N. R.; Bagg, E. A.; McDonough, M. A.; Krojer, T. J.; Yue, W. W.; Ng, S. S.; Olsen, L.; Brennan, P. E.; Oppermann, U.; Müller, S.; Klose, R. J.; Ratcliffe, P. J.; Schofield, C. J.; Kawamura, A. 5-Carboxy-8-hydroxyquinoline is a broad spectrum 2-oxoglutarate oxygenase inhibitor which causes iron translocation. *Chem Sci* **2013**, 4, 3110-3117.
172. Binó, L.; Kučera, J.; Štefková, K.; Švihálková Šindlerová, L.; Lánová, M.; Kudová, J.; Kubala, L.; Pacherník, J. The stabilization of hypoxia inducible factor modulates differentiation status and inhibits the proliferation of mouse embryonic stem cells. *Chem Biol Interact* **2016**, 244, 204-214.

173. Hamada, S.; Kim, T.-D.; Suzuki, T.; Itoh, Y.; Tsumoto, H.; Nakagawa, H.; Janknecht, R.; Miyata, N. Synthesis and activity of N-oxalylglycine and its derivatives as Jumonji C-domain-containing histone lysine demethylase inhibitors. *Bioorg Med Chem Lett* **2009**, *19*, 2852-2855.
174. Tarhonskaya, H.; Nowak, R. P.; Johansson, C.; Szykowska, A.; Tumber, A.; Hancock, R. L.; Lang, P.; Flashman, E.; Oppermann, U.; Schofield, C. J.; Kawamura, A. Studies on the Interaction of the Histone Demethylase KDM5B with Tricarboxylic Acid Cycle Intermediates. *J Mol Biol* **2017**, *429*, 2895-2906.
175. Xu, W.; Yang, H.; Liu, Y.; Yang, Y.; Wang, P.; Kim, S.-H.; Ito, S.; Yang, C.; Wang, P.; Xiao, M.-T.; Liu, L.-x.; Jiang, W.-q.; Liu, J.; Zhang, J.-y.; Wang, B.; Frye, S.; Zhang, Y.; Xu, Y.-h.; Lei, Q.-y.; Guan, K.-L.; Zhao, S.-m.; Xiong, Y. Oncometabolite 2-Hydroxyglutarate Is a Competitive Inhibitor of α -Ketoglutarate-Dependent Dioxygenases. *Cancer Cell* **2011**, *19*, 17-30.
176. Thalhammer, A.; Mecinović, J.; Loenarz, C.; Tumber, A.; Rose, N. R.; Heightman, T. D.; Schofield, C. J. Inhibition of the histone demethylase JMJD2E by 3-substituted pyridine 2,4-dicarboxylates. *Org Biomol Chem* **2011**, *9*, 127-135.
177. Korczynska, M.; Le, D. D.; Younger, N.; Gregori-Puigjane, E.; Tumber, A.; Krojer, T.; Velupillai, S.; Gileadi, C.; Nowak, R. P.; Iwasa, E.; Pollock, S. B.; Ortiz Torres, I.; Oppermann, U.; Shoichet, B. K.; Fujimori, D. G. Docking and Linking of Fragments To Discover Jumonji Histone Demethylase Inhibitors. *J Med Chem* **2016**, *59*, 1580-98.
178. Tumber, A.; Nuzzi, A.; Hookway, E. S.; Hatch, S. B.; Velupillai, S.; Johansson, C.; Kawamura, A.; Savitsky, P.; Yapp, C.; Szykowska, A.; Wu, N.; Bountra, C.; Strain-Damerell, C.; Burgess-Brown, N. A.; Ruda, G. F.; Fedorov, O.; Munro, S.; England, K. S.; Nowak, R. P.; Schofield, C. J.; La Thangue, N. B.; Pawlyn, C.; Davies, F.; Morgan, G.; Athanasou, N.; Müller, S.; Oppermann, U.; Brennan, P. E. Potent and Selective KDM5 Inhibitor Stops Cellular Demethylation of H3K4me3 at Transcription Start Sites and Proliferation of MM1S Myeloma Cells. *Cell Chem Biol* **2017**, *24*, 371-380.
179. Westaway, S. M.; Preston, A. G.; Barker, M. D.; Brown, F.; Brown, J. A.; Campbell, M.; Chung, C. W.; Diallo, H.; Douault, C.; Drewes, G.; Eagle, R.; Gordon, L.; Haslam, C.; Hayhow, T. G.; Humphreys, P. G.; Joberty, G.; Katso, R.; Kruidenier, L.; Leveridge, M.; Liddle, J.; Mosley, J.; Muelbaier, M.; Randle, R.; Rioja, I.; Rueger, A.; Seal, G. A.; Sheppard, R. J.; Singh, O.; Taylor, J.; Thomas, P.; Thomson, D.; Wilson, D. M.; Lee, K.; Prinjha, R. K. Cell Penetrant Inhibitors of the KDM4 and KDM5 Families of Histone Lysine Demethylases. 1. 3-Amino-4-pyridine Carboxylate Derivatives. *J Med Chem* **2016**, *59*, 1357-1369.
180. Westaway, S. M.; Preston, A. G.; Barker, M. D.; Brown, F.; Brown, J. A.; Campbell, M.; Chung, C. W.; Drewes, G.; Eagle, R.; Garton, N.; Gordon, L.; Haslam, C.; Hayhow, T. G.; Humphreys, P. G.; Joberty, G.; Katso, R.; Kruidenier, L.; Leveridge, M.; Pemberton, M.; Rioja, I.; Seal, G. A.; Shipley, T.; Singh, O.; Suckling, C. J.; Taylor, J.; Thomas, P.; Wilson, D. M.; Lee, K.; Prinjha, R. K. Cell Penetrant Inhibitors of the KDM4 and KDM5 Families of Histone Lysine Demethylases. 2. Pyrido[3,4-d]pyrimidin-4(3H)-one Derivatives. *J Med Chem* **2016**, *59*, 1370-1387.

181. Chang, K.-H.; King, O. N. F.; Tumber, A.; Woon, E. C. Y.; Heightman, T. D.; McDonough, M. A.; Schofield, C. J.; Rose, N. R. Inhibition of histone demethylases by 4-carboxy-2,2'-bipyridyl compounds. *ChemMedChem* **2011**, 6, 759-764.
182. England, K. S.; Tumber, A.; Krojer, T.; Scozzafava, G.; Ng, S. S.; Daniel, M.; Szykowska, A.; Che, K.; von Delft, F.; Burgess-Brown, N. A.; Kawamura, A.; Schofield, C. J.; Brennan, P. E. Optimisation of a triazolopyridine based histone demethylase inhibitor yields a potent and selective KDM2A (FBXL11) inhibitor. *MedChemComm* **2014**, 5, 1879-1886.
183. Chin, Y.-W.; Han, S.-Y. KDM4 histone demethylase inhibitors for anti-cancer agents: a patent review. *Expert Opin Ther Pat* **2015**, 25, 135-144.
184. Bavetsias, V.; Lanigan, R. M.; Ruda, G. F.; Atrash, B.; McLaughlin, M. G.; Tumber, A.; Mok, N. Y.; Le Bihan, Y. V.; Dempster, S.; Boxall, K. J.; Jeganathan, F.; Hatch, S. B.; Savitsky, P.; Velupillai, S.; Krojer, T.; England, K. S.; Sejberg, J.; Thai, C.; Donovan, A.; Pal, A.; Scozzafava, G.; Bennett, J. M.; Kawamura, A.; Johansson, C.; Szykowska, A.; Gileadi, C.; Burgess-Brown, N. A.; von Delft, F.; Oppermann, U.; Walters, Z.; Shipley, J.; Raynaud, F. I.; Westaway, S. M.; Prinjha, R. K.; Fedorov, O.; Burke, R.; Schofield, C. J.; Westwood, I. M.; Bountra, C.; Muller, S.; van Montfort, R. L.; Brennan, P. E.; Blagg, J. 8-Substituted Pyrido[3,4-d]pyrimidin-4(3H)-one Derivatives As Potent, Cell Permeable, KDM4 (JMJD2) and KDM5 (JARID1) Histone Lysine Demethylase Inhibitors. *J Med Chem* **2016**, 59, 1388-409.
185. Heinemann, B.; Nielsen, J. M.; Hudlebusch, H. R.; Lees, M. J.; Larsen, D. V.; Boesen, T.; Labelle, M.; Gerlach, L.-O.; Birk, P.; Helin, K. Inhibition of demethylases by GSK-J1/J4. *Nature* **2014**, 514, E1-E2.
186. Hu, J.; Wang, X.; Chen, L.; Huang, M.; Tang, W.; Zuo, J.; Liu, Y. C.; Shi, Z.; Liu, R.; Shen, J.; Xiong, B. Design and discovery of new pyrimidine coupled nitrogen aromatic rings as chelating groups of JMJD3 inhibitors. *Bioorg Med Chem Lett* **2016**, 26, 721-725.
187. Rotili, D.; Altun, M.; Kawamura, A.; Wolf, A.; Fischer, R.; Leung, I. K. H.; Mackeen, M. M.; Tian, Y.-M.; Ratcliffe, P. J.; Mai, A.; Kessler, B. M.; Schofield, C. J. A photoreactive small-molecule probe for 2-oxoglutarate oxygenases. *Chem Biol* **2011**, 18, 642-654.
188. Rotili, D.; Tomassi, S.; Conte, M.; Benedetti, R.; Tortorici, M.; Ciossani, G.; Valente, S.; Marrocco, B.; Labella, D.; Novellino, E.; Mattevi, A.; Altucci, L.; Tumber, A.; Yapp, C.; King, O. N.; Hopkinson, R. J.; Kawamura, A.; Schofield, C. J.; Mai, A. Pan-histone demethylase inhibitors simultaneously targeting Jumonji C and lysine-specific demethylases display high anticancer activities. *J Med Chem* **2014**, 57, 42-55.
189. Suzuki, T.; Ozasa, H.; Itoh, Y.; Zhan, P.; Sawada, H.; Mino, K.; Walport, L.; Ohkubo, R.; Kawamura, A.; Yonezawa, M.; Tsukada, Y.; Tumber, A.; Nakagawa, H.; Hasegawa, M.; Sasaki, R.; Mizukami, T.; Schofield, C. J.; Miyata, N. Identification of the KDM2/7 histone lysine demethylase subfamily inhibitor and its antiproliferative activity. *J Med Chem* **2013**, 56, 7222-7231.

190. Itoh, Y.; Sawada, H.; Suzuki, M.; Tojo, T.; Sasaki, R.; Hasegawa, M.; Mizukami, T.; Suzuki, T. Identification of Jumonji AT-Rich Interactive Domain 1A Inhibitors and Their Effect on Cancer Cells. *ACS Med Chem Lett* **2015**, *6*, 665-670.
191. Morera, L.; Roatsch, M.; Fürst, M. C.; Hoffmann, I.; Senger, J.; Hau, M.; Franz, H.; Schüle, R.; Heinrich, M. R.; Jung, M. 4-Biphenylalanine- and 3-Phenyltyrosine-Derived Hydroxamic Acids as Inhibitors of the JumonjiC-Domain-Containing Histone Demethylase KDM4A. *ChemMedChem* **2016**, *11*, 2063-2083.
192. Leurs, U.; Clausen, R. P.; Kristensen, J. L.; Lohse, B. Inhibitor scaffold for the histone lysine demethylase KDM4C (JMJD2C). *Bioorg Med Chem Lett* **2012**, *22*, 5811-5813.
193. Kim, S.-H.; Kwon, S. H.; Park, S.-H.; Lee, J. K.; Bang, H.-S.; Nam, S.-J.; Kwon, H. C.; Shin, J.; Oh, D.-C. Tripartin, a Histone Demethylase Inhibitor from a Bacterium Associated with a Dung Beetle Larva. *Org Lett* **2013**, *15*, 1834-1837.
194. Guillade, L.; Sarno, F.; Tarhonskaya, H.; Nebbioso, A.; Alvarez, S.; Kawamura, A.; Schofield, C. J.; Altucci, L.; de Lera, A. R. Synthesis and Biological Evaluation of Tripartin, a Putative KDM4 Natural Product Inhibitor, and 1-Dichloromethylinden-1-ol Analogs. *ChemMedChem* **2018**, *13*, 1949-1956.
195. Khodaverdian, V.; Tapadar, S.; MacDonald, I. A.; Xu, Y.; Ho, P. Y.; Bridges, A.; Rajpurohit, P.; Sanghani, B. A.; Fan, Y.; Thangaraju, M.; Hathaway, N. A.; Oyelere, A. K. Deferiprone: Pan-selective Histone Lysine Demethylase Inhibition Activity and Structure Activity Relationship Study. *Sci Rep* **2019**, *9*, 4802, 1-17.
196. Gehling, V. S.; Bellon, S. F.; Harmange, J. C.; LeBlanc, Y.; Poy, F.; Odate, S.; Buker, S.; Lan, F.; Arora, S.; Williamson, K. E.; Sandy, P.; Cummings, R. T.; Bailey, C. M.; Bergeron, L.; Mao, W.; Gustafson, A.; Liu, Y.; VanderPorten, E.; Audia, J. E.; Trojer, P.; Albrecht, B. K. Identification of potent, selective KDM5 inhibitors. *Bioorg Med Chem Lett* **2016**, *26*, 4350-4354.
197. Vinogradova, M.; Gehling, V. S.; Gustafson, A.; Arora, S.; Tindell, C. A.; Wilson, C.; Williamson, K. E.; Guler, G. D.; Gangurde, P.; Manieri, W.; Busby, J.; Flynn, E. M.; Lan, F.; Kim, H. J.; Odate, S.; Cochran, A. G.; Liu, Y.; Wongchenko, M.; Yang, Y.; Cheung, T. K.; Maile, T. M.; Lau, T.; Costa, M.; Hegde, G. V.; Jackson, E.; Pitti, R.; Arnott, D.; Bailey, C.; Bellon, S.; Cummings, R. T.; Albrecht, B. K.; Harmange, J. C.; Kiefer, J. R.; Trojer, P.; Classon, M. An inhibitor of KDM5 demethylases reduces survival of drug-tolerant cancer cells. *Nat Chem Biol* **2016**, *12*, 531-538.
198. Wang, L.; Chang, J.; Varghese, D.; Dellinger, M.; Kumar, S.; Best, A. M.; Ruiz, J.; Bruick, R.; Peña-Llopis, S.; Xu, J.; Babinski, D. J.; Frantz, D. E.; Brekken, R. A.; Quinn, A. M.; Simeonov, A.; Easmon, J.; Martinez, E. D. A small molecule modulates Jumonji histone demethylase activity and selectively inhibits cancer growth. *Nat Commun* **2013**, *4*, 2035-2035.
199. Chu, C.-H.; Wang, L.-Y.; Hsu, K.-C.; Chen, C.-C.; Cheng, H.-H.; Wang, S.-M.; Wu, C.-M.; Chen, T.-J.; Li, L.-T.; Liu, R.; Hung, C.-L.; Yang, J.-M.; Kung, H.-J.; Wang, W.-C. KDM4B as a target for prostate cancer: structural analysis and selective inhibition by a novel inhibitor. *J Med Chem* **2014**, *57*, 5975-5985.

200. Upadhyay, A. K.; Rotili, D.; Han, J. W.; Hu, R.; Chang, Y.; Labella, D.; Zhang, X.; Yoon, Y.-S.; Mai, A.; Cheng, X. An analog of BIX-01294 selectively inhibits a family of histone H3 lysine 9 Jumonji demethylases. *J Mol Biol* **2012**, 416, 319-327.
201. Saleta, V.-R.; Miranda, W.; Catherine, R.; Adam, C.; Srikannathasan, V.; Martin, P.; Henry, L.; James E., D.; Kilian, H.; Matthew B., R.; Jim, V.; Marie-Laetitia, T.; Sarah, B.; Benedikt M., K.; James, B.; Oleg, F.; Florence, R.; Adam, D.; Julian, B.; Vassilios, B.; Udo, O.; Akane, K.; Paul, B. Design, Synthesis and Characterization of Covalent KDM5 Inhibitors. *Angew Chem Int Ed* **2019**, 58, 515-519.
202. Lohse, B.; Nielsen, A. L.; Kristensen, J. B. L.; Helgstrand, C.; Cloos, P. A. C.; Olsen, L.; Gajhede, M.; Clausen, R. P.; Kristensen, J. L. Targeting Histone Lysine Demethylases by Truncating the Histone 3 Tail to Obtain Selective Substrate-Based Inhibitors. *Angew Chem Int Ed* **2011**, 50, 9100-9103.
203. Woon, E. C. Y.; Tumber, A.; Kawamura, A.; Hillringhaus, L.; Ge, W.; Rose, N. R.; Ma, J. H. Y.; Chan, M. C.; Walport, L. J.; Che, K. H.; Ng, S. S.; Marsden, B. D.; Oppermann, U.; McDonough, M. A.; Schofield, C. J. Linking of 2-Oxoglutarate and Substrate Binding Sites Enables Potent and Highly Selective Inhibition of JmJc Histone Demethylases. *Angew Chem Int Edit* **2012**, 51, 1631-1634.
204. Sekirnik, R.; Rose, N. R.; Thalhammer, A.; Seden, P. T.; Mecinovic, J.; Schofield, C. J. Inhibition of the histone lysine demethylase JMJD2A by ejection of structural Zn(ii). *Chem Commun* **2009**, 6376-6378.
205. Schofield, C. J.; Rose, N.; Sekirnik, R. Jmjd2 demethylase inhibitors. *Patent WO(2011/030108)*, **2011**, 1-63.
206. Day, J. A.; Cohen, S. M. Investigating the Selectivity of Metalloenzyme Inhibitors. *J Med Chem* **2013**, 56, 7997-8007.
207. Chen, Y.; Cohen, S. M. Investigating the Selectivity of Metalloenzyme Inhibitors in the Presence of Competing Metalloproteins. *ChemMedChem* **2015**, 10, 1733-1738.
208. King, O. N.; Li, X. S.; Sakurai, M.; Kawamura, A.; Rose, N. R.; Ng, S. S.; Quinn, A. M.; Rai, G.; Mott, B. T.; Beswick, P.; Klose, R. J.; Oppermann, U.; Jadhav, A.; Heightman, T. D.; Maloney, D. J.; Schofield, C. J.; Simeonov, A. Quantitative high-throughput screening identifies 8-hydroxyquinolines as cell-active histone demethylase inhibitors. *PLoS One* **2010**, 5, e15535.
209. Hong, B.-T.; Cheng, Y.-S. E.; Cheng, T.-J.; Fang, J.-M. Boronate, trifluoroborate, sulfone, sulfinic acid and sulfonate congeners of oseltamivir carboxylic acid: Synthesis and anti-influenza activity. *Eur J Med Chem* **2019**, 163, 710-721.
210. Herr, R. J. 5-Substituted-1H-tetrazoles as carboxylic acid isosteres: medicinal chemistry and synthetic methods. *Bioorg Med Chem* **2002**, 10, 3379-3393.
211. Romeo, R.; Pier Giovanni, B.; Vincent, R.; Maria Dora, C.; Carlota Lopez, C.; Olga, C.-L.; Delia, P.; Francesca, F.; Mojgan Aghazadeh, T.; Jan, B.; Ernest, H. Synthesis and Biological Evaluation of 2-amino-3-(3,4,5-trimethoxyphenylsulfonyl)-5-aryl thiophenes as a New Class of Antitubulin Agents. *Med Chem* **2007**, 3, 507-512.
212. Sipos, G.; Drinkel, E. E.; Dorta, R. The emergence of sulfoxides as efficient ligands in transition metal catalysis. *Chem Soc Rev* **2015**, 44, 3834-3860.

213. Furukawa, N.; Ogawa, S.; Kawai, T.; Oae, S. ipso-Substitution of a sulphinyl or sulphonyl group attached to pyridine rings and its application for the synthesis of macrocycles. *J Chem Soc Perkin 1* **1984**, 1839-1845.
214. Khodaei, M. M.; Bahrami, K.; Karimi, A. H₂O₂/Tf₂O System: An Efficient Oxidizing Reagent for Selective Oxidation of Sulfanes. *Synthesis* **2008**, 2008, 1682-1684.
215. Komsta, Z.; Barbasiewicz, M.; Małkosza, M. Diastereoselective Synthesis of Tetrahydrofurans from Aryl 3-Chloropropylsulfoxides and Aldehydes. *J Org Chem* **2010**, 75, 3251-3259.
216. Dally, R. D. S., Timothy Alan; Bender, David Michael; Rojo Garcia, Maria Isabel Preparation of acylated 2-amino-1-(pyrrolidin-2-yl)ethanols and derivatives as BACE inhibitors for treating Alzheimer's. *Patent*, WO 2005108358, **2005**, 1-198.
217. Fernandes, G. F. S.; Denny, W. A.; Dos Santos, J. L. Boron in drug design: Recent advances in the development of new therapeutic agents. *Eur J Med Chem* **2019**, 179, 791-804.
218. Cox, P. A.; Leach, A. G.; Campbell, A. D.; Lloyd-Jones, G. C. Protodeboronation of Heteroaromatic, Vinyl, and Cyclopropyl Boronic Acids: pH-Rate Profiles, Autocatalysis, and Disproportionation. *J Am Chem Soc* **2016**, 138, 9145-9157.
219. Anderson, D. W.; Cotton, G. J.; Hay, A. M.; Armstrong, P. W.; Wilson, I. Purification tags of synthetic peptides and proteins. *Patent*, WO2011114099A1, **2011**, 1-27.
220. Coutts, S. J.; Adams, J.; Krolkowski, D.; Snow, R. J. Two efficient methods for the cleavage of pinanediol boronate esters yielding the free boronic acids. *Tetrahedron Lett* **1994**, 35, 5109-5112.
221. Hall, D. G. *Boronic Acids: Preparation and Applications in Organic Synthesis and Medicine*. Wiley-VCH-Verlag: Weinheim, **2005**.
222. Fassauer, G. M. *Modulatoren epigenetischer Regulationsmechanismen: Medizinische Chemie neuer KDM4-Inhibitoren und Methodenentwicklung zur SFC-MS-Analytik von Ketaminmetaboliten*. Dissertation. Universität Greifswald, **2018**.
223. Saeki, I.; Yamamoto, N.; Yamasaki, T.; Takami, T.; Maeda, M.; Fujisawa, K.; Iwamoto, T.; Matsumoto, T.; Hidaka, I.; Ishikawa, T.; Uchida, K.; Tani, K.; Sakaida, I. Effects of an oral iron chelator, deferasirox, on advanced hepatocellular carcinoma. *World J Gastroenterol* **2016**, 22, 8967-8977.
224. Greene, C. J.; Sharma, N. J.; Fiorica, P. N.; Forrester, E.; Smith, G. J.; Gross, K. W.; Kauffman, E. C. Suppressive effects of iron chelation in clear cell renal cell carcinoma and their dependency on VHL inactivation. *Free Radic Biol Med* **2019**, 133, 295-309.
225. Ford, S. J.; Obeidy, P.; Lovejoy, D. B.; Bedford, M.; Nichols, L.; Chadwick, C.; Tucker, O.; Lui, G. Y.; Kalinowski, D. S.; Jansson, P. J.; Iqbal, T. H.; Alderson, D.; Richardson, D. R.; Tselepis, C. Deferasirox (ICL670A) effectively inhibits oesophageal cancer growth in vitro and in vivo. *Br J Pharmacol* **2013**, 168, 1316-1328.
226. Choi, J. H.; Kim, J. S.; Won, Y. W.; Uhm, J.; Park, B. B.; Lee, Y. Y. The potential of deferasirox as a novel therapeutic modality in gastric cancer. *World J Surg Oncol* **2016**, 14, 77.

227. Kamihara, Y.; Takada, K.; Sato, T.; Kawano, Y.; Murase, K.; Arihara, Y.; Kikuchi, S.; Hayasaka, N.; Usami, M.; Iyama, S.; Miyanishi, K.; Sato, Y.; Kobune, M.; Kato, J. The iron chelator deferasirox induces apoptosis by targeting oncogenic Pyk2/ β -catenin signaling in human multiple myeloma. *Oncotarget* **2016**, *7*, 64330-64341.
228. Messa, E.; Carturan, S.; Maffè, C.; Pautasso, M.; Bracco, E.; Roetto, A.; Messa, F.; Arruga, F.; Defilippi, I.; Rosso, V.; Zanone, C.; Rotolo, A.; Greco, E.; Pellegrino, R. M.; Alberti, D.; Saglio, G.; Cilloni, D. Deferasirox is a powerful NF-kappaB inhibitor in myelodysplastic cells and in leukemia cell lines acting independently from cell iron deprivation by chelation and reactive oxygen species scavenging. *Haematologica* **2010**, *95*, 1308-1316.
229. Ohyashiki, J. H.; Kobayashi, C.; Hamamura, R.; Okabe, S.; Tauchi, T.; Ohyashiki, K. The oral iron chelator deferasirox represses signaling through the mTOR in myeloid leukemia cells by enhancing expression of REDD1. *Cancer Sci* **2009**, *100*, 970-977.
230. Bedford, M. R.; Ford, S. J.; Horniblow, R. D.; Iqbal, T. H.; Tselepis, C. Iron chelation in the treatment of cancer: a new role for deferasirox? *J Clin Pharmacol* **2013**, *53*, 885-891.
231. Tury, S.; Assayag, F.; Bonin, F.; Chateau-Joubert, S.; Servely, J. L.; Vacher, S.; Becette, V.; Caly, M.; Rapinat, A.; Gentien, D.; de la Grange, P.; Schnitzler, A.; Lallemand, F.; Marangoni, E.; Bieche, I.; Callens, C. The iron chelator deferasirox synergises with chemotherapy to treat triple-negative breast cancers. *J Pathol* **2018**, *246*, 103-114.
232. Shinoda, S.; Kaino, S.; Amano, S.; Harima, H.; Matsumoto, T.; Fujisawa, K.; Takami, T.; Yamamoto, N.; Yamasaki, T.; Sakaida, I. Deferasirox, an oral iron chelator, with gemcitabine synergistically inhibits pancreatic cancer cell growth in vitro and in vivo. *Oncotarget* **2018**, *9*, 28434-28444.
233. Shneine, J.; Alaraji, Y. Chemistry of 1, 2, 4-Triazole: A Review Article. *Int J Sci Res* **2016**, *5*, 1411-1423.
234. Ji Ram, V.; Sethi, A.; Nath, M.; Pratap, R. Chapter 5 - Five-Membered Heterocycles. In *The Chemistry of Heterocycles*, Ji Ram, V.; Sethi, A.; Nath, M.; Pratap, R., Eds. Elsevier, Amsterdam, **2019**; pp 149-478.
235. Keri, R. S.; Patil, S. A.; Budagumpi, S.; Nagaraja, B. M. Triazole: A Promising Antitubercular Agent. *Chem Biol Drug Des* **2015**, *86*, 410-423.
236. Patil, R. S. C., K.; Neela, P. K.; Pradhan, N. S.; Valgeirsson, J. Substantially pure Deferasirox and process for the preparation thereof. *Patent*, WO2009/147529 A1, **2009**, 1-25.
237. Steinhauser, S.; Heinz, U.; Bartholomä, M.; Weyhermüller, T.; Nick, H.; Hegetschweiler, K. Complex Formation of ICL670 and Related Ligands with FeIII and FeII. *Eur J Inorg Chem* **2004**, *2004*, 4177-4192.
238. Brunetti, H.; Lüthi, C. E. Die Synthese von asymmetrisch substituierten o-Hydroxyphenyl-s-triazinen. *Helv Chim Acta* **1972**, *55*, 1566-1595.
239. Lattmann, R.; Acklin, P. Preparation of 3,5-bishydroxyphenyl-1,2,4-triazoles as pharmaceutical chelators. *Patent*, US6465504, **2002**, 1-16.
240. Lattmann, R.; Acklin, P. Preparation of substituted 3,5-diphenyl-1,2,4-triazoles as pharmaceutical metal chelators. *Patent*, WO9749395, **1997**, 1-44.

241. Staben, S. T.; Blaquiere, N. Four-component synthesis of fully substituted 1,2,4-triazoles. *Angew Chem Int Ed* **2010**, *49*, 325-328.
242. Tselepis, C.; Fossey, J. S.; Byravan, R. Iron complexing agent and uses thereof in the treatment and prevention of colorectal cancer. *Patent*, WO2015079244, **2015**, 1-37.
243. Aufiero, M.; Scattolin, T.; Proutière, F.; Schoenebeck, F. Air-Stable Dinuclear Iodine-Bridged Pd(I) Complex - Catalyst, Precursor, or Parasite? The Additive Decides. Systematic Nucleophile-Activity Study and Application as Precatalyst in Cross-Coupling. *Organometallics* **2015**, *34*, 5191-5195.
244. Kalvet, I.; Magnin, G.; Schoenebeck, F. Rapid Room-Temperature, Chemoselective Csp²-Csp² Coupling of Poly(pseudo)halogenated Arenes Enabled by Palladium(I) Catalysis in Air. *Angew Chem Int Ed* **2017**, *56*, 1581-1585.
245. Kolb, H. C.; Finn, M. G.; Sharpless, K. B. Click Chemistry: Diverse Chemical Function from a Few Good Reactions. *Angew Chem Int Ed* **2001**, *40*, 2004-2021.
246. Rostovtsev, V. V.; Green, L. G.; Fokin, V. V.; Sharpless, K. B. A Stepwise Huisgen Cycloaddition Process: Copper(I)-Catalyzed Regioselective "Ligation" of Azides and Terminal Alkynes. *Angew Chem Int Ed* **2002**, *41*, 2596-2599.
247. Kaufmann, T.; Gokmen, M. T.; Rinnen, S.; Arlinghaus, H. F.; Du Prez, F.; Ravoo, B. J. Bifunctional Janus beads made by "sandwich" microcontact printing using click chemistry. *J Mater Chem* **2012**, *22*, 6190-6199.
248. Swyter, S.; Schiedel, M.; Monaldi, D.; Szunyogh, S.; Lehotzky, A.; Rumpf, T.; Ovádi, J.; Sippl, W.; Jung, M. New chemical tools for probing activity and inhibition of the NAD(+)-dependent lysine deacylase sirtuin 2. *Philos Trans R Soc Lond B Biol Sci* **2018**, *373*, 20170083, 1-13.
249. Begtrup, M.; Elguero, J.; Faure, R.; Camps, P.; Estopá, C.; Ilavský, D.; Fruchier, A.; Marzin, C.; de Mendoza, J. Effect of N-substituents on the ¹³C NMR parameters of azoles. *Magn Reson Chem* **1988**, *26*, 134-151.
250. Ayati, A.; Emami, S.; Asadipour, A.; Shafiee, A.; Foroumadi, A. Recent applications of 1,3-thiazole core structure in the identification of new lead compounds and drug discovery. *Eur J Med Chem* **2015**, *97*, 699-718.
251. Hantzsch, A.; Weber, J. H. Ueber Verbindungen des Thiazols (Pyridins der Thiophenreihe). *Chem Ber* **1887**, *20*, 3118-3132.
252. Wang, Z. Hantzsch Thiazole Synthesis. In *Comprehensive Organic Name Reactions and Reagents*, John Wiley & Sons, Inc.: Hoboken, **2010**; pp 1330-1334.
253. Carter, J. S.; Rogier, D. J.; Graneto, M. J.; Seibert, K.; Koboldt, C. M.; Yan, Z.; Talley, J. J. Design and synthesis of sulfonyl-substituted 4,5-diarylthiazoles as selective cyclooxygenase-2 inhibitors. *Bioorg Med Chem Lett* **1999**, *9*, 1167-1170.
254. Aoyama, T.; Takido, T.; Kodomari, M. One-Pot Synthesis of Benzo[b]thiophenes and Naphtho[2,1-b]thiophenes in the Presence of Acidic and Basic Supported Reagents. *Synlett* **2005**, 2005, 2739-2742.
255. Li, Z.; Qiu, Q.; Xu, X.; Wang, X.; Jiao, L.; Su, X.; Pan, M.; Huang, W.; Qian, H. Design, synthesis and Structure-activity relationship studies of new thiazole-based free fatty acid receptor 1 agonists for the treatment of type 2 diabetes. *Eur J Med Chem* **2016**, *113*, 246-257.

256. Jesberger, M.; Davis, T. P.; Barner, L. Applications of Lawesson's Reagent in Organic and Organometallic Syntheses. *Synthesis* **2003**, 2003, 1929-1958.
257. Ortar, G.; Schiano Moriello, A.; Morera, E.; Nalli, M.; Di Marzo, V.; De Petrocellis, L. 3-Ylidenephthalides as a new class of transient receptor potential channel TRPA1 and TRPM8 modulators. *Bioorg Med Chem Lett* **2013**, 23, 5614-5618.
258. McLaughlin, G.; Morris, N.; Kavanagh, P. V.; Power, J. D.; O'Brien, J.; Talbot, B.; Elliott, S. P.; Wallach, J.; Hoang, K.; Morris, H.; Brandt, S. D. Test purchase, synthesis, and characterization of 2-methoxydiphenidine (MXP) and differentiation from its meta- and para-substituted isomers. *Drug Test Anal* **2016**, 8, 98-109.
259. Hanaya, K.; Muramatsu, T.; Hasegawa, E. A convenient synthesis of 2-phenyl-3-benzo[b]furanone and 3-phenyl-2-benzo[b]furanones. *Chem Ind (London)* **1990**, 23, 802.
260. King, L. C.; Ostrum, G. K. Selective Bromination with Copper(II) Bromide. *J Org Chem* **1964**, 29, 3459-3461.
261. Uchil, V.; Joshi, V. Montmorillonite K10 — AlCl₃ Catalyzed Enolization: A Bifunctional System for Selective Bromination of Hydroxyacetophenones. *Cheminform* **2003**, 34.
262. Guan, X.-Y.; Al-Misba'a, Z.; Huang, K.-W. Efficient and selective α -bromination of carbonyl compounds with N-bromosuccinimide under microwave. *Arab J Chem* **2015**, 8, 892-896.
263. Moreno, I.; Tellitu, I.; Domínguez, E.; SanMartín, R. A Simple Route to New Phenanthro- and Phenanthroid-Fused Thiazoles by a PIFA-Mediated (Hetero)biaryl Coupling Reaction. *Eur J Org Chem* **2002**, 2126-2135.
264. Blümlein, F. O. Einwirkung von Bromacetophenon auf Säureamide. *Chem Ber* **1884**, 17, 2578-2581.
265. Lewy, M. Ueber die Einwirkung von Säureamiden auf Bromacetophenon. *Chem Ber* **1887**, 20, 2576-2580.
266. Ritson, D. J.; Spiteri, C.; Moses, J. E. A silver-mediated one-step synthesis of oxazoles. *J Org Chem* **2011**, 76, 3519-22.
267. Spiteri, C.; Ritson, D. J.; Awaad, A.; Moses, J. E. Silver mediated one-step synthesis of oxazoles from α -haloketones. *J Saudi Chem Soc* **2011**, 15, 375-378.
268. Bailey, J. L.; Sudini, R. R. Synthesis of 2,4- and 2,4,5-substituted oxazoles via a silver triflate mediated cyclization. *Tetrahedron Lett* **2014**, 55, 3674-3677.
269. Hoffmann, I. Zelluläre Charakterisierung neuer Hemmstoffe der Jumonji C-Domäne-enhaltenden Demethylasen. Albert-Ludwigs-Universität, Freiburg, 2015.
270. Shimada, Y.; Imamura, M.; Wagata, T.; Yamaguchi, N.; Tobe, T. Characterization of 21 newly established esophageal cancer cell lines. *Cancer* **1992**, 69, 277-84.
271. Yang, Z. Q.; Imoto, I.; Fukuda, Y.; Pimkhaokham, A.; Shimada, Y.; Imamura, M.; Sugano, S.; Nakamura, Y.; Inazawa, J. Identification of a novel gene, GASC1, within an amplicon at 9p23-24 frequently detected in esophageal cancer cell lines. *Cancer Res* **2000**, 60, 4735-9.
272. Barltrop, J. A.; Owen, T. C.; Cory, A. H.; Cory, J. G. 5-(3-carboxymethoxyphenyl)-2-(4,5-dimethylthiazolyl)-3-(4-sulfophenyl)tetrazolium, inner salt (MTS) and related

- analogs of 3-(4,5-dimethylthiazolyl)-2,5-diphenyltetrazolium bromide (MTT) reducing to purple water-soluble formazans As cell-viability indicators. *Bioorg Med Chem Lett* **1991**, 1, 611-614.
273. Whetstine, J. R.; Nottke, A.; Lan, F.; Huarte, M.; Smolikov, S.; Chen, Z.; Spooner, E.; Li, E.; Zhang, G.; Colaiacovo, M.; Shi, Y. Reversal of histone lysine trimethylation by the JMJD2 family of histone demethylases. *Cell* **2006**, 125, 467-81.
274. Ng, S. S.; Kavanagh, K. L.; McDonough, M. A.; Butler, D.; Pilka, E. S.; Lienard, B. M. R.; Bray, J. E.; Savitsky, P.; Gileadi, O.; von Delft, F.; Rose, N. R.; Offer, J.; Scheinost, J. C.; Borowski, T.; Sundstrom, M.; Schofield, C. J.; Oppermann, U. Crystal structures of histone demethylase JMJD2A reveal basis for substrate specificity. *Nature* **2007**, 448, 87-91.
275. Prinz, H. Hill coefficients, dose-response curves and allosteric mechanisms. *J Chem Biol* **2009**, 3, 37-44.
276. Steinhäuser, S.; Heinz, U.; Bartholomä, M.; Weyhermüller, T.; Nick, H.; Hegetschweiler, K. Complex Formation of ICL670 and Related Ligands with FeIII and FeII. *Eur J Inorg Chem* **2004**, 2004, 4177-4192.
277. Patil, R. S. C., K.; Neela, P. K.; Pradhan, N. S.; Valgeirsson, J. Substantially pure Deferasirox and process for the preparation thereof. *Patent* US20110171138A1, **2009**, 1-9.
278. Babudri, F.; Cardone, A.; Cioffi, C. T.; Farinola, G. M.; Naso, F.; Ragni, R. A Straightforward Methodology for the Introduction of Aryl and Vinyl Substituents in the 5 or 7 Position of 8-Hydroxyquinoline. *Synthesis* **2006**, 2006, 1325-1332.
279. Aufiero, M.; Sperger, T.; Tsang, A. S.; Schoenebeck, F. Highly Efficient C-SeCF₃ Coupling of Aryl Iodides Enabled by an Air-Stable Dinuclear Pd(I) Catalyst. *Angew Chem Int Ed* **2015**, 54, 10322-6.
280. Yamazaki, Y.; Sumikura, M.; Masuda, Y.; Hayashi, Y.; Yasui, H.; Kiso, Y.; Chinen, T.; Usui, T.; Yakushiji, F.; Potts, B.; Neuteboom, S.; Palladino, M.; Lloyd, G. K.; Hayashi, Y. Synthesis and structure-activity relationships of benzophenone-bearing diketopiperazine-type anti-microtubule agents. *Bioorg Med Chem* **2012**, 20, 4279-89.
281. Kumar, G. D.; Chavarria, G. E.; Charlton-Sevcik, A. K.; Arispe, W. M.; MacDonough, M. T.; Strecker, T. E.; Chen, S.-E.; Siim, B. G.; Chaplin, D. J.; Trawick, M. L.; Pinney, K. G. Design, synthesis, and biological evaluation of potent thiosemicarbazone based cathepsin L inhibitors. *Bioorg Med Chem Lett* **2010**, 20, 1415-1419.
282. Shaye, N. A.; Benoit, D. M.; Chavda, S.; Coulbeck, E.; Dingjan, M.; Eames, J.; Yohannes, Y. Resolution of pentafluorophenyl 2-phenylpropanoate using combinations of quasi-enantiomeric oxazolidin-2-ones. *Tetrahedron Asymmetry* **2011**, 22, 413-438

Appendix

A. Abbreviations

6-FAM azide 6-Carboxyfluorescein azide **95a**

2-OG 2-oxoglutarate (α -ketoglutarate)

2,4-PDCA pyridine-2,4-dicarboxylic acid

5-TAMRA azide 5-carboxamido-(6-azidohexanyl)tetramethylrhodamine **95b**

ADD ATRX-DNMT3-DNMT3L (Alpha Thalassemia/Mental Retardation
Syndrome X-Linked-DNA methyltransferase3-DNA methyltransferase3L;
methyl reader domain)

ACN acetonitrile

AIBN azobisisobutyronitrile

AOL amine oxidase-like

AML acute myeloid leukaemia

APCI atmospheric pressure chemical ionization

AR androgen receptor

ASAP® atmospheric solids analysis probe (Advion)

BAH bromo adjacent homology (methyl reader domain)

BDNF brain-derived neurotrophic factor

BSA bovine serum albumin

CD chromodomain (methyl reader domain)

CDI *N,N'*-dicyclohexylcarbodiimide

CLL chronic lymphocytic leukaemia

COSY $^1\text{H}, ^1\text{H}$ -correlation spectroscopy

DCD double chromodomain (methyl reader domain)

DMF dimethyl formamide

EtOAc ethyl acetate

DCC dicyclohexylcarbodiimide

DCM dichloromethane

DMSO	dimethyl sulfoxide
DNA	deoxyribonucleic acid
DNMT	DNA methyltransferase
DMSO-d ₆	perdeuterated dimethyl sulfoxide
EDCI	1-ethyl-3-(3-dimethylaminopropyl)carbodiimide hydrochloride
EDTA	ethylenediaminetetraacetic acid
ERR α	estrogen-related receptor α
ELISA	enzyme-linked immunosorbent assay
ESI	electrospray ionization
ER	estrogen receptor
FBXW7	F-box/WD repeat-containing protein 7
FDH	formaldehyde dehydrogenase
FHL1	four-and-a-half LIM domains 1
FI	Fluorescence intensity
FRET	fluorescence (or Förster) resonance energy transfer
GC	gas chromatography
GFAP	glial fibrillary acidic protein
GI50	concentration at which 50% inhibition of cell growth is observed
HEAT domain	Huntingtin-elongation factor 3-protein phosphatase 2A-Target of rapamycin 1 domain (methyl reader domain)
H3K9me ₃	histone H3 trimethylated at lysine residue 9
HDAC	histone deacetylase
HEPES	2-[4-(2-hydroxyethyl)piperazin-1-yl] ethanesulfonic acid
HMBC	¹ H, ¹³ C-heteronuclear multiple bond correlation
HOBT	1-hydroxybenzotriazole hydrate
HPLC	high-performance liquid chromatography
HSQC	¹ H, ¹³ C-heteronuclear single quantum coherence
HRMS	high-resolution mass spectrometry
HTS	high-throughput screening

IC ₅₀	concentration at which 50% inhibition is observed
JARID	Jumonji, AT-rich interactive domain
JMJC	JumonjiC domain
JMJC demethylase	JumonjiC domain-containing histone demethylase
KAT	lysine acetyltransferase
KDAC	lysine deacetylase
KDM	lysine demethylase
KMT	lysine methyltransferase
K _i	inhibition constant
λ_{abs}	absorption wavelength
λ_{em}	emission wavelength
λ_{ex}	excitation wavelength
LANCE [®]	lanthanide chelate excite (assay technology by Perkin Elmer)
LDL	low-density lipoprotein
LRMS	low-resolution mass spectrometry
LSD1	lysine-specific demethylase 1
LRR	leucine-rich repeat domain
MALDI	matrix-assisted laser desorption ionization
MBT	malignant brain tumour (methyl reader domain)
MS	mass spectrometry
mTOR	mammalian target of rapamycin
NAD ⁺	oxidized form of nicotinamide adenine dinucleotide
NADH	reduced form of nicotinamide adenine dinucleotide
NF κ B	nuclear factor kappa-light-chain-enhancer of activated B cells
n. i.	no inhibition
NMR	nuclear magnetic resonance
NOG	N-oxalyl glycine
n. t.	not tested
Pd(dppf)Cl ₂	[1,1'-Bis(diphenylphosphino)ferrocene]dichloropalladium(II)

PHD	plant homeodomain (methyl reader domain)
ppm	parts per million
PRMT	protein arginine methyl transferase
PTSA	<i>para</i> -toluenesulfonic acid
PWWP domain	proline-tryptophan-tryptophan-proline domain (methyl reader domain)
RB1	retinoblastoma protein 1
RDM	arginine demethylase
RNA	ribonucleic acid
RP	reversed phase
r.t.	room temperature
SAR	structure-activity relationship
SDS-PAGE	sodium dodecylsulfate polyacrylamide gel electrophoresis
SERS	surface enhanced Raman scattering
Snail2	Snail Family Transcriptional Repressor 2
Sox	SRY-related HMG-box (sex-determining region Y-related high mobility group box)
SPR	surface plasmon resonance
SWIRM domain	Swi3p, Rsc8p and Moira domain (binding domain of LSDs)
TAMRA	tetramethylrhodamine
TBAF	tetrabutylammonium fluoride
TBTA	tris(benzyltriazolylmethyl)amine
TET	ten-eleven translocation
TFA	trifluoroacetic acid
TfO ₂	triflic anhydride (trifluoromethanesulfonic anhydride)
THF	tetrahydrofuran
TLC	thin-layer chromatography
TPR	tetratricopeptide domain
TRF	time-resolved fluorescence

TTD tandem tudor domain (methyl reader domain)

UV ultraviolet light

WD40 tryptophan-aspartic acid domain (methyl reader domain)

zf-CW zinc finger-cysteine tryptophan (methyl reader domain)

B. List of Compound Synonyms

All chemical compounds that were tested for their inhibition against KDM4A are numbered consecutively in the text. This tables give a summary of the lab codes for compounds obtained from collaboration partners and of synthesised compounds, as well as the trivial names of precursors.

67a	NBT61	84l	GF058	99e	SWE179
67b	MPB18	84m	GF055b	99f	SWE133
67c	NBT78	85a	AA027	99g	SWE122
67d	NBT67i	85b	AA046	99h	SWE223
67e	NBT41	85c	AA028	99i	SWE164
67f	RK6	85d	AA036	99j	SWE154
67g	RK11	85e	AA039	99k	SWE155
67h	RK13	85f	AA026	99l	SWE198
67i	NBT66	85g	AA040	100	thiophene-2-carboxamide
67j	NBT81	85h	AA031	101a	SWE111
67k	MPB09	86a	salicylic acid	101b	SWE120
67l	NBT58	86b	4-chlorosalicylic acid	101c	SWE177
67m	NBT70	86c	4-methoxy-salicylic acid	101d	SWE157
67n	RK9	86d	4-bromosalicylic acid	101e	1-(2-hydroxy-phenyl)-2-phenylethan-1-one
67o	MPB11	86e	4-fluorosalicylic acid	101f	2-phenyl-1-(2-thienyl)ethanone

67p	NBT35	87a	salicylamide	101g	2-phenyl- benzofuran- 3(2H)-one
67q	NBT83	87b	4-chloro- salicylamide	102	SWE110
67r	NBT87	87c	4-bromo- salicylamide	103	4-methylphenol
67s	NBT86	87d	4-methoxy- salicylamide	104	phenylacetic acid
67t	MPB10	87e	4-fluoro- salicylamide	105a	2-methoxy- benzoic acid
67u	MPB15	88a	SWE20a	105b	2-methylbenzoic acid
67v	MPB13	88b	SWE57	106a	SWE159
68a	SWE88	88c	SWE134	106b	SWE143
68b	SWE117	88d	SWE55	107a	SWE24
69a	SWE56	88e	SWE147	107b	SWE178
69b	SWE230	89a	4-hydrazino- benzoic acid	107c	SWE69
70	2-(methylthio)- isonicotinic acid	89b	phenylhydrazine hydrochloride	107d	SWE220
71a	SWE68	89c	4-hydrazinyl- benzonitrile	107e	SWE227
71b	SWE99	89d	2-methoxy- phenylhydrazine hydrochloride	108a	SWE166
72a	SWE70	89e	2-hydrazino- pyridine	108b	SWE181
72b	SWE116	89f	8-hydrazino- quinoline dihydrochloride	108c	SWE184
73	methyl 2,6- dichloro- isonicotinate	90a	SWE20b	109a	SWE169

74	phenylmethane-thiol	90b	SWE58	109b	SWE217
75	SWE229	90c	SWE138	109c	SWE191
76	<i>tert</i> -butyl-dimethyl chlorosilane	90d	SWE66	109d	SWE222
77	5-bromquinolin-8-ol	90e	SWE150	110a	NBT286
78	SWE126	90f	SWE61	110b	NBT243
79	SWE128	90g	SWE203	110c	NBT296
80	SWE136	90h	SWE173	110d	NBT291
81a	PZ005	90i	SWE186	110e	NBT264
81b	PZ012	90j	SWE185	110f	MOS02
81c	PZ014	90k	SWE189	110g	NBT261
81d	PZ011	90l	SWE188	110h	MTH01
81e	PZ034	90m	SWE176	111a	NBT203
81f	PZ020	90n	SWE216	111b	MOS01
81g	PZ002	90o	MR04	111c	MOS06
81h	PZ007	90p	MR23	111d	NBT479
81i	PZ025	90q	NBT511	111e	NBT135
81j	PZ003	90r	NBT512	111f	MOS09
81k	PZ027	90s	NBT513	111g	MOS11
81l	PZ015	90t	NBT331	111h	NBT509
81m	PZ016	91	SWE211	111i	NBT510
81n	PZ010	92	SWE192	111j	MOS08
81o	PZ024	93	SWE215	111k	MOS14
81p	PZ030	94a	SWE109	111l	NBT280
81q	PZ028	94b	SWE140	111m	NBT314
81r	PZ041	95a	6-FAM azide	111n	MTH04
81s	PZ036	95b	5-TAMRA-azide	111o	NBT245
81t	PZ018	96a	SWE153	111p	NBT271
81u	PZ039	96b	SWE163	111q	MOS13
82	GF55b COOH	96c	SWE165	111r	NBT283
83a	GF028	97a	SWE121	111s	NBT288

83b	GF026	97b	SWE180	111t	MOS15
84a	PZ51	97c	SWE161	111u	NBT248
84b	GF036	97d	SWE65	111v	NBT332
84c	GF067c	97e	SWE199	111w	MOS16
84d	GF062	97f	SWE71	111x	NBT247
84e	GF068	97g	2-bromo-2'- methoxy- acetophenone	111y	NBT282
84f	GF066	98a	SWE103	112a	pyNS3
84g	GF069	98b	2-methoxy- thiobenzamide	112b	quNS6
84h	GF052	99a	SWE75	112c	quNS3
84i	GF049	99b	SWE228	112d	pyNSe3
84j	GF046	99c	SWE74	112e	phNSe3
84k	GF053	99d	SWE131	112f	quNS9

C. List of Publications

Certain parts of this thesis work have previously been published in scientific journals and presented at conferences according to the following list.

- Published Original Articles
 - Roatsch, M.; Hoffmann, I.; Abboud, M. I.; Hancock, R. L.; Tarhonskaya, H.; Hsu, K.-F.; Wilkins, S. E.; Yeh, T.-L.; Lippl, K.; Serrer, K.; Moneke, I.; Ahrens, T. D.; Robaa, D.; Wenzler, S.; Barthes, N. P. F.; Franz, H.; Sippl, W.; Lassmann, S.; Diederichs, S.; Schleicher, E.; Schofield, C. J.; Kawamura, A.; Schüle, R.; Jung, M. The Clinically Used Iron Chelator Deferasirox Is an Inhibitor of Epigenetic JumonjiC Domain-Containing Histone Demethylases. *ACS Chem Biol* **2019**, 14, 1737-1750.
- Original Articles in Preparation
 - Barthes, N. P. F.; Wenzler, S.; Spiske, M.; Ngo, V.; Schmidtkunz, K.; Robaa, D.; Schüle, R.; Hein, L.; Sippl, W.; Jung, M. Design, synthesis and biological evaluation of 1,2,4-Triazole, Thiazole, Pyrazole & Imidazole analogs of Deferasirox as inhibitors of the JumonjiC-Domain-Containing Histone Demethylase KDM4A. *currently in preparation*

- Poster Presentations

- M. Roatsch, S. Wenzler, R. L. Hancock, H. Tarhonskaya, M. I. Abboud, K.-F. Hsu, S. E. Wilkins, K. Serrer, T. D. Ahrens, D. Robaa, R. Schüle, W. Sippl, S. Laßmann, E. Schleicher, C. J. Schofield, A. Kawamura, M. Jung, Deferasirox derivatives as Inhibitors of JumonjiC Domain-Containing Histone Demethylases. Epigenetics 2017, September 7, 2017; Windlesham, United Kingdom. (selected for short talk)
- S. Wenzler, M. Roatsch, R. L. Hancock, H. Tarhonskaya, M. Abboud, K.-F. Hsu, S. Wilkins, K. Serrer, D. Robaa, E. Metzger, R. Schüle, W. Sippl, E. Schleicher, C. J. Schofield, A. Kawamura, M. Jung, Synthesis and Biological Activity of Inhibitors for JumonjiC-domain containing Histone Demethylases. Albert-Ludwigs-Universität, July 13, 2018; Freiburg, Germany.
- N. P. F. Barthes,* S. Wenzler,* M. Spiske, K. Schmidtkunz, D. Robaa, V. Ngo, R. Schüle, W. Sippl, L. Hein, M. Jung, Synthesis and biological evaluation of imidazole and pyrazole analogs of Deferasirox targeting KDM4A demethylase. RICT2019, July 03-05,2019; Nantes, France. (poster prize)
- N. P. F. Barthes,* S. Wenzler,* M. Spiske, K. Schmidtkunz, V. Ngo, D. Robaa, R. Schüle, W. Sippl, L. Hein, M. Jung, Synthesis and Biological Evaluation of derivatives of Deferasirox as Inhibitors for JumonjiC-domain containing Histone Demethylases. DPhG Annual meeting 2019, September 01-04, 2019; Heidelberg, Germany.